SYNTHESIS AND COORDINATION CHEMISTRY OF DITOPIC LIGANDS CAPABLE OF COORDINATING METAL IONS AND INTERACTING WITH ANIONS.

University of HUDDERSFIELD

Joshua Higginson

A thesis submitted to the University of Huddersfield in partial fulfilment of the requirements for the degree of Doctor of Philosophy.

Department of Chemical and Biological Sciences

The University of Huddersfield

April 2015

Copyright statement

i. The author of this thesis (including any appendices and/or schedules to this thesis) owns any copyright in it ("Copyright") and he has given the University of Huddersfield the right to use such copyright for any administrative, promotional, educational and/or teaching purposes.

ii. Copies of this thesis, either in full or in extracts, may be made only in accordance with the regulations of the University of Huddersfield Library. Details of these regulations may be obtained from the Librarian. This page must form part of any such copies made.

iii. The ownership of any patents, designs, trademarks and any and all other intellectual property rights except for the Copyright (the "Intellectual Property Rights") and any reproductions of copyright works, for example graphs and tables ("Reproductions"), which may be described in this thesis, may not be owned by the author and may be owned by third parties. Such Intellectual Property Rights and Reproductions cannot and must not be available for use without the prior written permission of the owner(S) of the relevant Intellectual Property Rights and/or Reproductions.

Contents:

List of Abbreviations:

DMF -	Dimethyl Formaldehyde
DCM -	Dichloromethane
TMS-CN -	Trimethylsilyl cyanide
[L] -	Ligand
b -	Singlet
d -	Doublet
dd -	Doublet of doublets
t -	Triplet
dt -	Doublet of triplets
m -	Multiplet
Py -	Pyridyl
Tz -	Thiazole
RT -	Room temperature
Å -	Angstroms
***m/z* -**	mass/charge
MHz -	Megahertz
Hz -	Hertz
δ -	Delta (chemical shift)
g -	Gram
mg -	Milligrams
mL -	Millilitre
mmol -	Millimoles
mol -	Moles
M -	Molar
(aq) -	Aqueous
***J* -**	Coupling Constant

***d*-DMSO -** Deuterated dimethylsulphoxide

***mCPBA* -** *meta*-chloroperoxybenzoic acid

TLC - Thin Layer Chromatography

MS - Mass Spectrometry

ESI-MS - Electrospray ionisation mass spectrometry

^{1}H NMR - Proton, Nuclear Magnetic Resonance

^{13}C NMR - Carbon, Nuclear Magnetic Resonance

Acknowledgements

Firstly I would like to dedicate this thesis to my close friends and family, who without their continuous love and support none of this would have been possible. Secondly I would like to acknowledge the endless hours of commitment and support Prof. Craig Rice has given me over the past four years and Dr. Lindsay Harding who has worked tirelessly with me throughout my doctorate. Without this opportunity and their guidance none of the work shown herein would have been remotely possible.

And lastly to all of the friends and colleagues past and present at the University of Huddersfield, without your daily encouragement and friendship it wouldn't have been worthwhile.

"Between childhood, boyhood, adolescence &

Manhood (maturity) there should be sharp lines drawn with;

Tests, deaths, feats, rites, stories, songs & judgements."

-Jim Morrison (1943-1971).

Abstract:

The aim of this research was to synthesise a series of novel organic multidentate ligands which contain *N*-donor domains for the coordination of metal ions and amide or amine hydrogen atoms which are capable of interaction with anions. It was envisaged that incorporation of these two binding units would produce a system where the metal ions would control the ability of the ligand to interact with anions or *vice versa*.

Ligand 1 contains a tetradentate *N*-donor domain formed by a central bipyridine, two thaizole units and two amide units attached in the 4,4'-position of the bipyridine unit. Reaction of this with divalent metal ions results in a mono-nuclear complex where the metal is bound by the *N*-donor atoms and the amides interact with a variety of anions. Reaction with monovalent metal ions results in the formation of a dinuclear double helicate with the metal again coordinated by the *N*-donor domains and the anions interacting with the amide hydrogen atoms. This results in a polymeric assembly in the solid state.

Ligand 2 contains an identical tetradentate domain comprised of the same *N*-donor units; however the single amides in the 4,4'-position have been removed and a diamide attached in the 3,3'-position of the bipyridine unit. Reaction of **[L^2]** with divalent cations results in a similar mono-nuclear species. The metal centre is coordinated by the *N*-donor atoms and one of the acetyl units from two adjoining ligands with the counter ions undergoing interactions with the diamide hydrogen atoms. Coordination of the same ligand with a monovalent cation resulted in a di-nuclear double helicate, each metal centre is fulfilled by the *N*-donor atoms of the ligand strand and the hydrogen atoms of the diamide units interact with anions. This too results in a polymeric assembly in the solid state.

Ligands 3 and 4 contain the iso-structural tetradentate *N*-donor domain seen in **[L^1]** and **[L^2]** but their functionality in the 3,3'-position differ. Ligand 3 contains a urea group while ligand 4 has a single amide group attatched to an indole unit. Coordination of **[L^3]** and a divalent metal ion results in the formation of a mono-nuclear species with the metal ion bound by the central bipyridine and the *N*-donor of two thaizole units. Furthermore each of the urea groups in the 3,3'-position undergo favourable interactions with the perchlorate counter ions. A solid state structure of Ligand 4 was only successful with a monovalent cation resulting in the formation of a dinuclear double stranded species. Each metal centre exhibits

a distorted trigonal planar geometry through coordination with a pyridine and thiazole ring of one strand and a single thiazole ring of another. The indole and amide of each ligand strand undergo two sets of interactions; anion interactions through the amide and indole hydrogen atoms as well as complementary intermolecular interactions between the indole N···H units of one ligand and the carbonyl C···O units of another complex. Both **[L^3]** and **[L^4]** exhibit long range order through favourable anion-NH interactions however **[L^4]** also displays complimentary indole / acetyl interactions to develop a larger aggregate species.

In all these cases the resultant complex is *independent* upon which anion is used. However, this is not the case with ligand 5. Reaction of **[L^5]** with $Cu(BF_4)_2$ or $Cu(ClO_4)_2$ gave a dinuclear double helicate with a cleft within the helicate assembly in which an anion is bound. However, reaction of this with half an equivalent of either sulphate (SO_4^{2-}) or dihydrogen phosphate ($H_2PO_4^-$) results in the formation of a different dinuclear double helicate whereby the cleft is occupied by either a dihydrogen phosphate or sulphate anion which bridges the metal centres. Further addition of sulphate results in no change of the ESI-MS indicating the dinuclear double helicate persist however addition of one equivalent of di-hydrogen phosphate leads to the formation of a pentanuclear circular helicate. Each metal centre is coordinated by the pyridine and thiazole units of two different ligand strands and a single Cu···O interaction from one of the dihydrogen phosphates.

The inclusion of three dihydrogen phosphates into the centre of the assembly as well as a series of phosphate-ligand and phosphate-phosphate interactions leads to the dimerization of the structure with another set of phosphates from a second assembly.

Further reaction of this dinuclear species with one equivalent of $(Bu_4N)NO_3$ resulted in the formation of a hexanuclear circular *meso*-helicate (or mesocate). In this structure each *N*-donor domain of a thiazole and pyridine ring coordinate two different Cu^{2+} metal centres. Each metal centre exhibits a distorted octahedral arrangement with two ligand strands completing 4 of its 6 coordination sites, the remaining sites are occupied by two *O*-donors of a nitrate anion. In addition an amine of each ligand strand points into the centre of the complex creating a cavity capable of hosting two nitrate anions.

Ligand 6 is made up of the same bis-bidentate donors as ligand 5 with the addition of a nitrogen atom into the central phenyl spacer. On reaction of **[L^6]** with a divalent metal ion

(e.g. Cu(II)) a simple mono-nuclear structure is observed. Although a mono-nuclear assembly is expected, it is interesting that even a simple change in the ligand strand can have a dramatic affect on the self-assembly process. When a central 1,3-phenylene spacer is employed (i.e. **[L^5]**) a dinuclear double helicate is formed, however, when a 1,3-pyridine unit is contained within the ligand strand (i.e. **[L^6]**) a simple mono-nuclear species is produced.

1. Chapter 1 Introduction:

1.0 Supramolecular Chemistry

Over the past 5 decades supramolecular chemistry has grown rapidly as a research subject and in recent years cemented itself as a core branch of chemistry yielding some fascinating and innovative results. It can be thought of as chemistry beyond the molecule and has been defined as "components held together reversibly by intermolecular forces", not by covalent bonds.[1,2] Metallosupramolecular chemistry is heavily reliant on all disciplines, for example extensive organic chemistry knowledge is required for ligand synthesis, whilst the thermodynamics and kinetics of reactions have a strong basis in physical chemistry and like all areas of research high quality characterisation is equally important. [1,2]

The first discoveries in this area weren't until the late 1960s – 1970s when Lehn and co-workers synthesised a series of macrocyclic ligands capable of forming supramolecular complexes with metal ions.[3a-3b] Due to their outstanding work in the field Jean-Marie Lehn along with his fellow co-workers C. J. Pedersen and D. J. Cram received the 1987 Nobel Prize for their achievements in the field of supramolecular chemistry.[2] Decades later their efforts and results that followed are still referenced and discussed to this day.[3-5]

Their discoveries have led to an increase in research activity and development of new supramolecular architectures. What was once an area devoted to the synthesis of large macrocyclic ligands capable of binding a range of metal cations for coordination with different guest species is now a vast and immensely diverse area of research. Many groups still adopt the host-guest motif which is fundamental to the nature of this chemistry, whilst simultaneously pursuing many other design principles in order to expand and improve upon the original coordination chemistry principles, taking advantage of a large range of intramolecular interactions.

1.1 Supramolecular Interactions

In order for these large supramolecular complexes to form there has to be some form of interaction, which by definition are non-covalent in nature. In fact, there are many forms of interactions that can take place, the most commonly used form being hydrogen bonding due to its large degree of directionality. These non-covalent interactions are relatively weak (2 - 300 kJ mol^{-1} as opposed to 150 - 450 kJ mol^{-1} for covalent bonds); however, when numerous hydrogen bonds are used together they result in a very stable assembly.[2,6] There are many forms of non-covalent interactions most of which have been listed below along with their relative strengths (Fig. 1):

Interaction	**Strength (kJ mol^{-1})**
Ion – Ion	200 – 300
Ion – Dipole	50 - 200
Dipole – Dipole	5 – 50
Hydrogen bonding	4 -120
π – π stacking	0 – 50
Van der Waals	< 5, but varies depending on surface area
Hydrophobic	Related to solvent – solvent interaction energy

Fig.1: Table of supramolecular interactions and their relative strengths.[2]

As interactions can be both positively and negatively charged (attractive and repulsive) it is important to note that design also plays a crucial role in the formation, there must be a complimentary arrangement of binding sites in order for the most thermodynamically stable species to form.

1.2 Electrostatic Interactions

1.2.1 Ion–ion interactions

Electrostatic interactions that occur between positively charged cations (i.e. sodium, Na^+) and negatively charged anions (i.e. chloride, Cl^-) are termed ion-ion interactions.[2] The positively charged sodium has lost an electron and so must share one with the negatively charged chloride, this interaction is more ionic in nature and not a true covalent bond although they are comparable in energy; due to the opposite charges a large electronegativity difference exists between the two atoms thus an ionic bond is formed. Take for example Fig. 2 where positively charged sodium ions have converged with negatively charged chloride ions resulting in a NaCl lattice.[1]

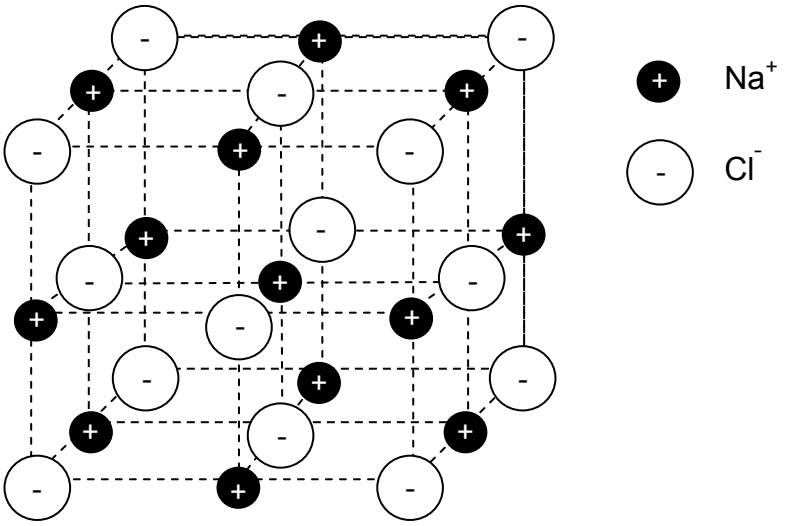

Fig.2: NaCl lattice formed via ionic bonding.

1.2.2 Ion–dipole interactions

Whereas ion–ion interactions are non-directional, ion–dipole interactions must be suitably aligned with each other so that optimal binding is achieved.[1,2] Due to their high electrostatic affinity for one another they have become a useful tool in supramolecular chemistry for achieving strong bonds. One such example of this type of interaction is Pedersen's discovery of the crown ethers and related compounds, shown in Fig. 3.

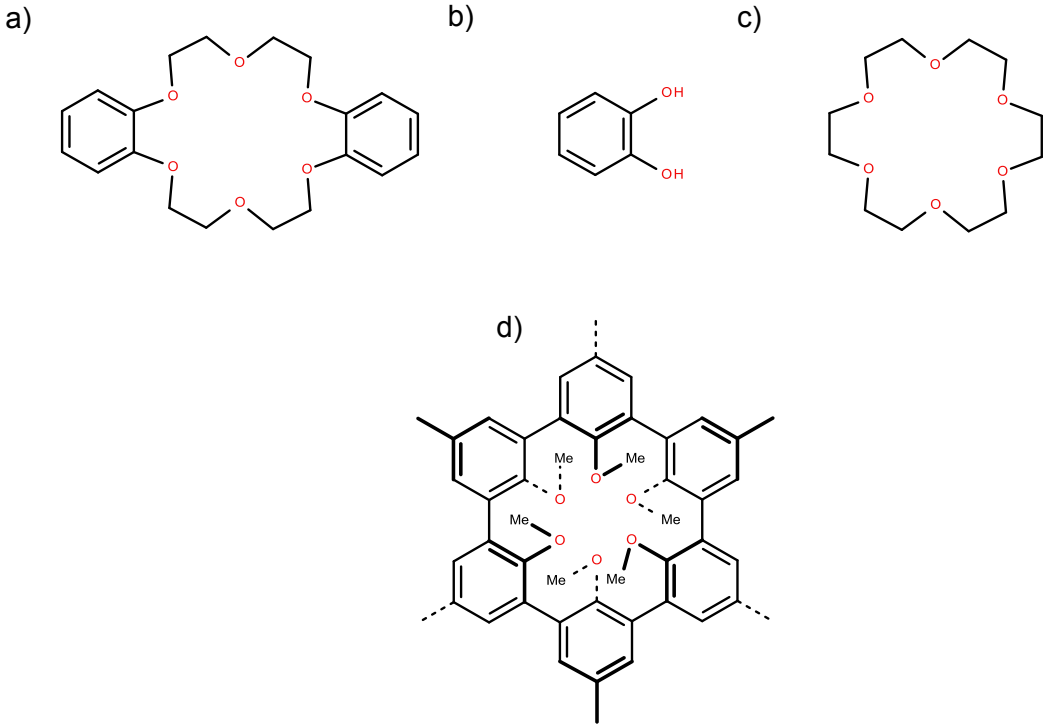

Fig. 3: a) Dibenzo[18]crown-6 b) Catechol, c) [18]Crown-6 d) Best known example of a spherand.[2]

In his early career Pedersen worked on the prevention of oxidative degradation of petroleum products and rubber through trace amounts of metal-ion impurities (copper and vanadium). It was at DuPont where he developed a series of ligands (Fig. 3) capable of detecting trace metals and upon binding, converted them into inactive compounds which later led to them being called 'metal deactivators'.[2,6]

This series of ligands are termed 'crown ethers' due to their crown like conformation in the solid state (Fig. 4d). Crown ethers predominantly contain carbon and oxygen atoms which then make up the macrocycle, depending on the size of the macrocycle this allows a number of positively charged guest species (usually metal cations) to be held within the cavity by electrostatic ion-dipole interactions between the alkali metal cation and the oxygen donor atoms.[1] A number of factors such as the cavity size, cationic radius and stability effect the overall strength of the complex; the better the cations fit for the pocket the stronger the complex.[1]

An example of 'optimal spatial fit' can be seen in Fig. 4 which shows Frensdorff's work on the stability of various crown ethers with different sized cations. Frensdorff found

that the [18]crown-6 (Fig. 4b) forms the most stable complex with potassium whereas the larger [21]crown-7 (Fig. 4c) prefers the larger caesium ion.[1,6]

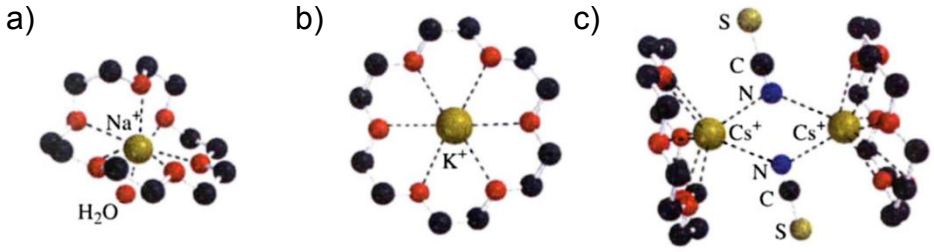

Fig. 4: Ion – Dipole interactions between oxygen atoms, Na^+, K^+ and Cs^+.[6]

1.2.3 Dipole–dipole interactions

Dipole–dipole interactions involve the association of one dipole (separated positive and negative charge) with another. A dipole occurs when there is unequal sharing of electrons between atoms; this form of interaction can be useful for bringing molecules into alignment.[2] One example of this form of interaction is that between carbonyl functional groups, for example in acetone (Fig. 5).[1, 7]

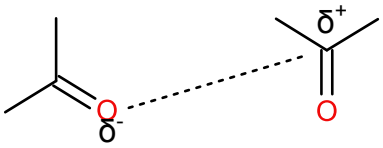

Fig. 5: The dipole–dipole interaction between two carbonyl groups.[1]

1.2.4 Hydrogen bonding

A hydrogen bond can be defined as the interaction between a 'hydrogen atom attached to an electronegative atom' and an 'electronegative atom that possesses a lone pair of electrons'.[7, 8] This is exemplified in the bonding between water molecules (Fig. 6).

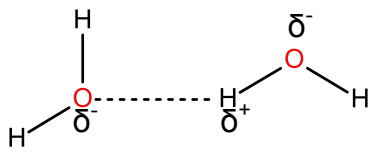

Fig. 6: The formation of a hydrogen bond between two water molecules.[7]

There are many ways in which a hydrogen bond can be utilized in chemistry; in supramolecular chemistry they are generally thought of as the most important non-covalent interaction. This is due to their ability to exhibit a high level of directionality whilst still maintaining strength. The strongest hydrogen bonds involve the first row elements such as oxygen (O) or nitrogen (N).[2, 8] The most well-known example of a self-assembled system containing multiple hydrogen bonds is in the DNA double helix.

A DNA helix is made up of two anti-parallel strands which undergo weak hydrogen bonding between complimentary base pairs (adenine/thymine and guanine/cytosine). Each base pair will recognise and bind exclusively with its complimentary partner foregoing all other conformations (Fig.7).[9, 10]

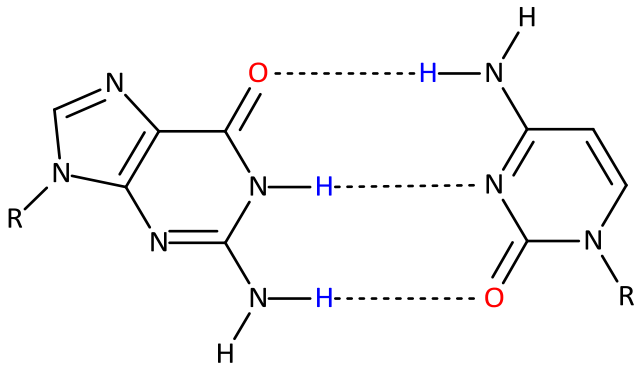

Fig.7: Hydrogen bonding between two base pairs guanine and cytosine.

1.2.5 π – π Stacking

π-π stacking interactions are weak interactions (around 0-50 kJ mol^{-1}) that occur between aromatic systems. There are two forms of π-π interactions: 'face-to-face' and 'face-to-edge' (Fig. 8a & b).[2]

A face-to-face interaction is where the centre of one aromatic ring interacts with the corner of another (Fig. 8a), whereas a face-to-edge interaction is where the hydrogen atom from one aromatic ring lies perpendicular to the face / centre of another aromatic ring (Fig. 8b).[2]

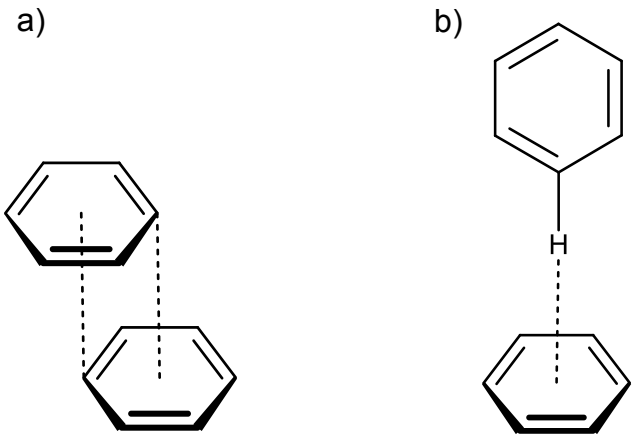

Fig. 7: a) Face-to-face arrangement, b) Face-to-edge arrangement.

These π-π interactions take place when a negatively charged π-electron cloud of one conjugated system comes into contact with the positively charged σ-framework of another molecule.[2]

1.3 Host-guest chemistry

Host-guest chemistry and supramolecular chemistry are synonymous in the fact they both rely on forces other than covalent bonds to assemble an overall structure which is both complimentary and stable for both the host and the guest.

Host molecules are defined as "molecules or ions whose binding sites converge in the complex". Common examples of such hosts are; crown ethers (Fig. 3), cyclodextrins and calixarenes (Fig. 9a & b). Similarly, guest species are defined as "any molecule or ion whose binding sites diverge in the complex".[2, 11,]

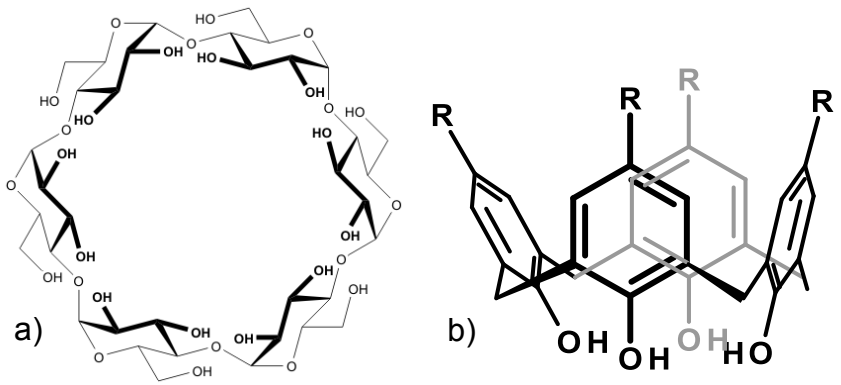

Fig.9: a) Structure of an alpha-cyclodextrin[11], b) structure of a calixarene.

There are many types of host-guest assemblies; *e.g.* induced fit (enzymes and their substrates) being the most common.[12] However, in order to gather an understanding of host-guest chemistry one must first look back to 1894 where Emil Fischer first described the 'lock and key principle'.[2,12] Fischer illustrated host-guest chemistry by using the 'lock and key principle' which was to become his most famous work.[13]

It describes the catalytic activity of enzymes in the formation of an end product. The substrate (guest/key) is defined as the compound which is undergoing reaction, this fits perfectly into the recognition pocket (host/lock) provided on the surface of the enzyme. Once combined the substrate is held tightly and undergoes the reaction which leads to the formation of the product (Fig. 10).

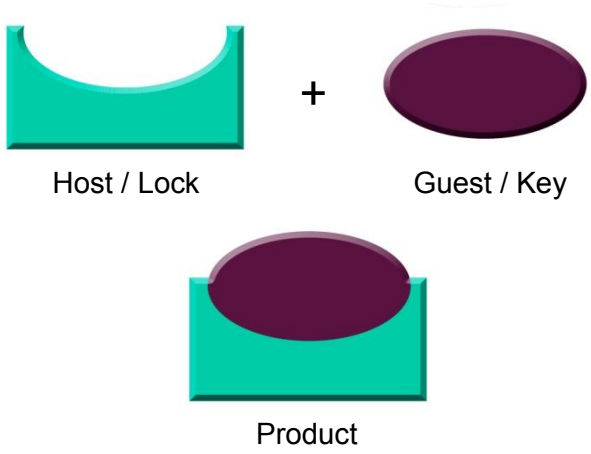

Fig. 10: Emil Fischer's lock and key principle.

Supramolecular chemists have attempted to mimic the lock and key principle in the form of host-guest chemistry, designing molecules capable of self recognition with complimentary molecules to form complexes.

1.4 Self–Assembly

Self assembly plays a large role in supramolecular chemistry and has been explored by many chemists. It is the process whereby large and often complex molecular species are spontaneously formed from small sub-units; these sub-units contain enough inherent molecular 'information' that they can spontaneously assemble into large super-molecules or architectures (Fig. 11).[2]

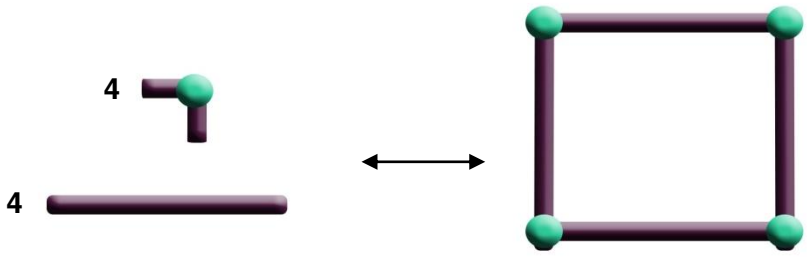

Fig. 11: A diagram to depict the formation of a self-assembled square.

A true self-assembled species must be kinetically favourable as well as being reversible and reproducible; for example, if conditions of the system are changed and the overall structure becomes unattached then reverting back to the original conditions should result in the previous outcome without any change or forced induction. The reversible nature of these structures along with their ability to correct mistakes during assembly is what makes this area of chemistry so complex.

These structures are held together by non-covalent interactions, many of which have been discussed above. The importance of these interactions is that they are reversible and will readily form and re-form into a number of complexes until the most thermodynamically favoured species is found.[2]

Less biological and more synthetic forms of self-assembly rely on the ability of the chemist to design molecules containing complimentary functionalities that will assemble under the correct conditions to give the desired species.[2] The outcome relies solely on the inherent information programmed within the molecules; the chemist uses their knowledge of complimentary sequences to design the components accordingly.

By far the most popular and in this case the most important series of interactions for self-assembly purposes are those between metal ions and ligands; this is due to their large degree of directionality and the chemist's ability to predict the metal ions' coordination environment. Combining this knowledge with a rigid ligand that has a sufficient arrangement of binding domains will result in a predictable self-assembly.

1.5 Metallosupramolecular Chemistry

The area of metallosupramolecular chemistry involves self-assembly processes which use a combination of bridging organic ligands alongside metal ions to synthesise well defined, organised, supramolecular complexes. The metal and ligand components have encoded or 'pre-programmed' information both spatial and directional that leads to the formation of a single product (the most thermodynamically stable species), usually in high yield.[14,15,16]

This inbuilt information pre-organizes the components into a single aggregated structure; the resulting complex is formed once all the possible structures have been explored and the most favourable one is found. The self-assembly process is reversible and can undergo many permutations before the final product is formed.[14,15]

The best examples of metallosupramolecular species are racks, grids, ladders and cages, all having different inbuilt information which allows the formation of these unique structures.

1.5.1 Racks

The simplest of these architectures is the rack which is made up of a single linear multidentate (polytopic) ligand that can be split into a number of different binding domains, once coordinated to a metal ion the structure is often completed by a second set of ligands with similar binding motifs.[2] The polytopic ligand acts as a back bone allowing the metal ion to adjoin the monotopic ligands in a rack-like arrangement (Fig. 12).[2]

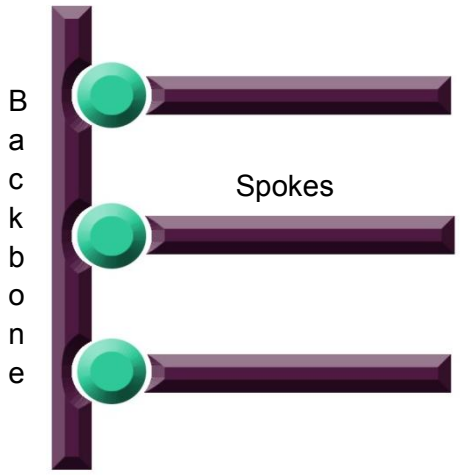

Fig. 12: [3] – Rack structure.

The naming of racks depends on the number of adjoining ligand strands or 'spokes', the rack in Fig. 12 would be called a [3]-rack due the fact it has three spokes lying horizontally against the perpendicular backbone.

A true example of a rack structure is shown in Fig. 13c.[17] A polydentate ligand comprising a central pyrimidine ring bridging two bipyridyl units is used as a backbone (Fig. 13a), effectively creating two bis-terdentate binding domains. When mixed with an octahedral metal ion such as Ru^{2+} each bis-terdentate domain occupies three of the six coordination sites, this allows the other three to be taken up by the second ligand or 'spoke'.[2,17] In this case the ligand acting as the spokes is a terpyridine unit (Fig. 13b). Due to the overall positive charge brought about through formation of the complex; they require a series of counter ions to be present; these counter ions must be weakly coordinating (BF_4^- or PF_6^-) so that they do not occupy the first coordination sphere of the metal ion and compete with the ligand for coordination of the metal centre.[2]

Successful formation of a rack structure requires the ligands to be capable of both binding the same metal ion, whether that be octahedral or tetrahedral; as well as contain binding sites to fulfil the metal ions' coordination sites.[2]

In the rack structure in Fig. 13 the terpyridine units satisfied the ruthenium's preference for a six coordinate geometry by lying at right-angles to one another along the pyrimidine/bipyridyl backbone.

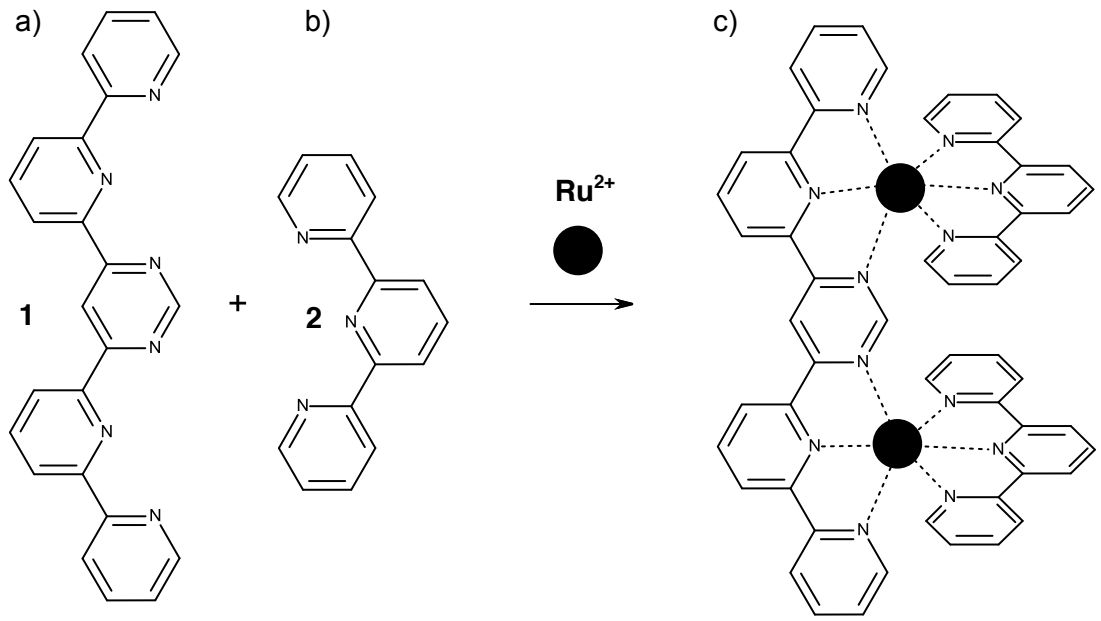

Fig. 13: a) L^1 Pyrimidine/bipyridyl backbone b) L^2 terpyridine unit c) Ru^{2+} [2] – rack.

1.5.2 Grids

In a recent review Lehn *et al.* define a grid as a structure "comprising of two-dimensional arrays of metal ions connecting a set of organic ligands in a perpendicular arrangement".[16] The formation of these grid-like architectures requires arrangement instructions brought about by the coordination geometry of the metal ion and the arrangement of the ligand's coordination sites.

The ligand strands must have multiple binding domains being either bidentate (the presence of two binding domains) or tridentate (the presence of three binding domains). The chosen metal ion must have a suitable coordination geometry (tetrahedral or octahedral) so that it may act as a metal centre.

The molecular grid can be made up of square or rectangular matrix arrays of metal centres:

- Square grids [a x a] are based around metal ions with tetrahedral coordination geometries (*e.g.* Cu^+ and Ag^+) and ligands with complimentary binding sites. They are formed using an even number of the same metal ions and ligands as shown in Fig. 14a.[16]

- Rectangular arrays [a x b] have also been made using the coordination geometries of both octahedral (Cu^{2+} and Zn^{2+}) and tetrahedral metal ions, however a rectangular arrangement requires a mixture of different ligands [a x b] (Fig. 14b).[16]

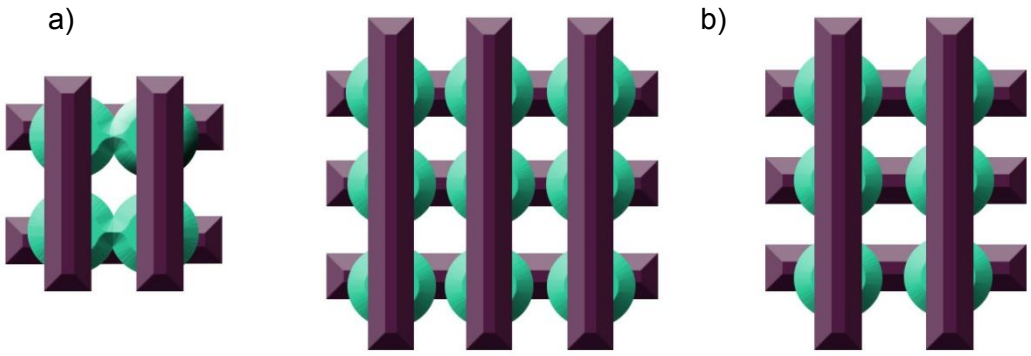

Fig. 14: a) Square grid architectures [2 x2] & [3x3], b) Rectangular grid architecture [2 x3].

The formation of a grid-like structure over any other is dictated by both the ligand and the metal which have to overcome a number of constraints, including steric hindrance as well as enthalpic and entropic effects. The ligand and metal ion must be complimentary to each other and in the correct stoichiometry to avoid the formation of competing structures. A mix of different metals and ligands could result in a plethora of different stable species; however, with the correct stoichiometry and a carefully designed system the programmed formation of these grid complexes can be accomplished.[16,18,19]

One of the first published grids was by Lehn *et al.* who reported the formation of a [2 x 2] metal ion array using tetrahedral coordination and four ditopic ligands.[16,18,19] When the bis(pyridyl)pyridazine ligand is mixed in a 1:1 stoichiometry with a tetrahedral metal ion, either Cu^{+} or Ag^{+}, it self-assembles, with each metal centre coordinated by two *N*-donor domains from two ligand strands (Fig. 15).[16]

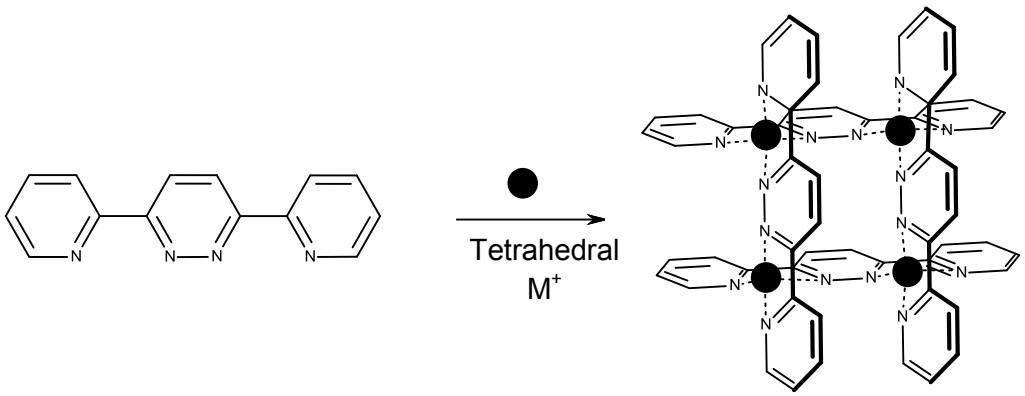

Fig. 15: Coordination of bis(pyridyl)pyridazine with a tetrahedral metal ion.

1.5.3 Ladders

Ladders, although different, share similarities with both racks and grids; like grids they predominantly result from the complexation of linear ligands with tetrahedral metal ions and can have varying forms depending on the system's pre-organization. However, the only difference between ladders and racks is the inclusion of a further polytopic ligand that acts as a second backbone. Instead of capped spokes, ditopic ligands are used which form rungs. The ladder architecture contains two linear polytopic ligands in the form of [2n]L (2 = number of backbones, n = number of rungs, L = ladder).[2]

Lehn and co-workers prepared a series of ligands (Fig. 16a & 16b) capable of forming tetranuclear [2 x 2]L (Fig. 16c) and hexanuclear [2 x 3]L (Fig. 16d) ladder complexes when mixed with a tetrahedral metal ion in varying stoichiometries.[20] The self-assembly of the ladder occurs in three main stages: i) recognition occurs between the components, ii) the components then undergo a growth phase by linking to one another, iii) finally termination of the complex, by saturation of the binding sites.[20]

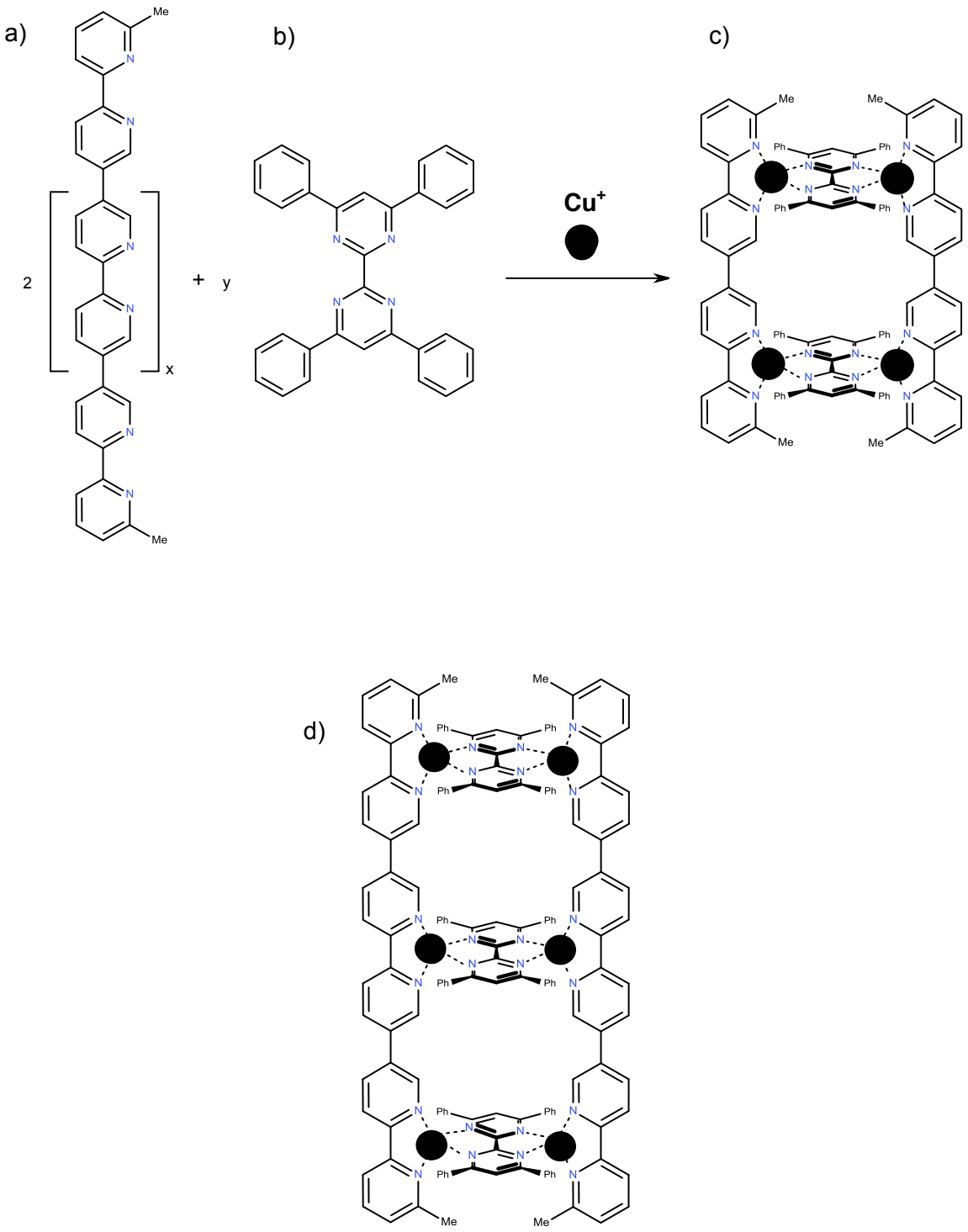

Fig. 16: a) Hexadentate backbone b) 2, 2'-bipyrimidine-based ligands or rungs c) [2x2]-ladder complex d) [2x3]-ladder complex.

1.5.4 Cages

The formation of a cage complex over any other structure requires stringent planning and more 'building blocks' than similar structures.[22] The reason for this is that a cage is a very complex structure which consequently requires a larger amount of pre-organisation and overall stability. There are many ways to form these three-dimensional species but most if not all require rigid ligands with a linear geometry to act as scaffolding for the formation.[8]

Increasing the functionality of the ligand and therefore the number of carbon atoms in the cage makes the formation of the overall structure more difficult; each functional group within the ligand strand must act as a potential binding site capable of providing more strength to the formation of the overall structure.[21]

Transition metal-based complexes are often free from restrictions due to the larger variety of metals with suitable coordination numbers. This allows the design of these cages to be much more complex and larger in size whilst still maintaining conformational rigidity.[21] There are many factors that can induce the formation of a cage: ligand design[2,22], metal coordination[23], guest templation[21,24-26] and stoichiometry[2] to name but a few. All however share the idea that it is 'pre-organisation' that drives formation.

Fujita *et al.* showed one of the only guest-induced cage formations.[24-26] When two equivalents of the tritopic ligand 1,3,5-tris(4-pyridylmethyl)-benzene (Fig. 17a) are combined with three equivalents of ethylene-diamine palladium dinitrate (Fig. 17b) in the presence of sodium 4-methoxyphenylacetate the resulting structure is a cage-like complex that is trigonal prismatic in shape (Fig. 17c).[24]

Furthermore various anionic guests with a hydrophobic moiety have been shown to induce the formation of a cage (Fig. 17d), this is due to their comparable size and shape to the complexes cavity. Larger species such as (1-naphthyl)acetate (Fig. 17e) negatively decrease the yield of the overall complex, as it is thought that they are too large to reside within the cavity.[24]

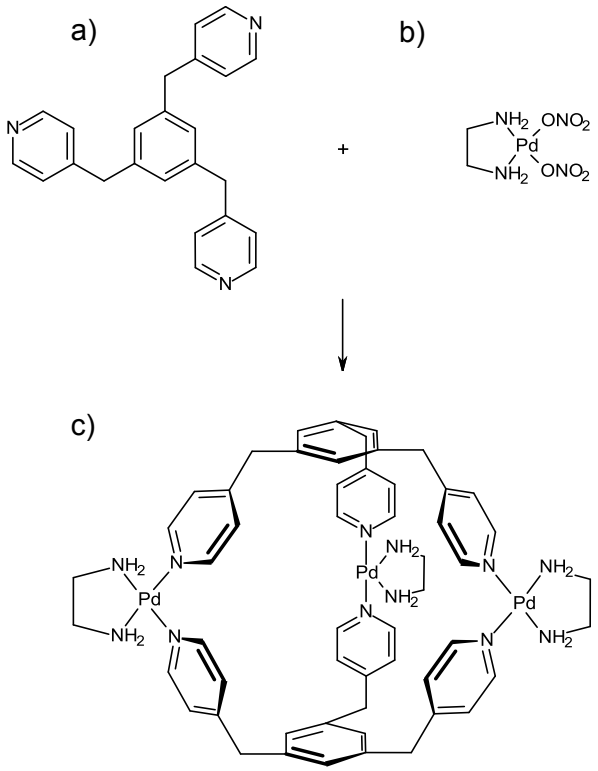

Fig. 17: a) 1,3,5-tris(4-pyridylmethyl)-benzene, b) ethylene-diaminepalladium dinitrate, c) guest-induced cage complex, guest omitted for clarity.

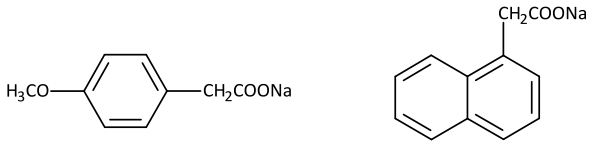

d) 4-Methoxyphenylacetic acid *e) (1-naphthyl)acetate.*

1.6 Helicates

One area of metallosupramolecular chemistry that has been the source of increased attention over the years is the design of polynuclear helicates. These multi-stranded multinuclear metal complexes form by wrapping linear ligand strands around a central metal ion (or ions) with a suitable coordination geometry (Fig. 18).[27]

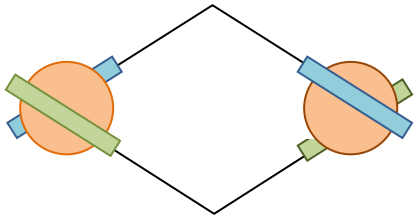

Fig. 18: Diagram depicting the overall structure of a multinuclear helicate.

Helicates are a constant source of research for supramolecular chemists and often form by self-assembly, they consist of two or more multidentate ligand strands which become partitioned into distinct metal binding domains. Each site then binds to a separate metal cation rather than chelating a single metal centre. This usually arises from the ligands' inability to coordinate a single metal centre due to geometric constraints.

The ligands wrap around the metal centres in an over and under fashion giving rise to the term helicate, they can orientate in one of two possible directions (clockwise or counter-clockwise) which is known as 'helicity', a special form of chirality.[2,28]

1.6.1 Nomenclature

Due to the many permutations these helical species can adopt, naming them can become complex. So that each helicate architecture can be distinguished a series of categorisation steps can be followed.[28]

Number of metal ions:

Initially it is the number of metal ions within the structure that are characterized *e.g.* 1 = mononuclear, 2 = dinuclear, 3 = trinuclear *etc*. This indicates how many metal centres make up the complex.[2,29]

Number of ligand strands:

The number of ligand strands can be calculated by the number of ligands directly coordinated to the metal centres, *e.g.* 2 (*double* helicate), 3 (*triple* helicate) or the lesser known 4-stranded (*quadruple* helicate).[2,23]

Nature and orientation of the strands:

The nature and conformation of the ligand strands is also of importance. A helicate made up of the same type of ligand can be termed 'homoleptic' whilst helicates made up of different strands are 'heteroleptic' (Fig. 19c).[1,8,23]

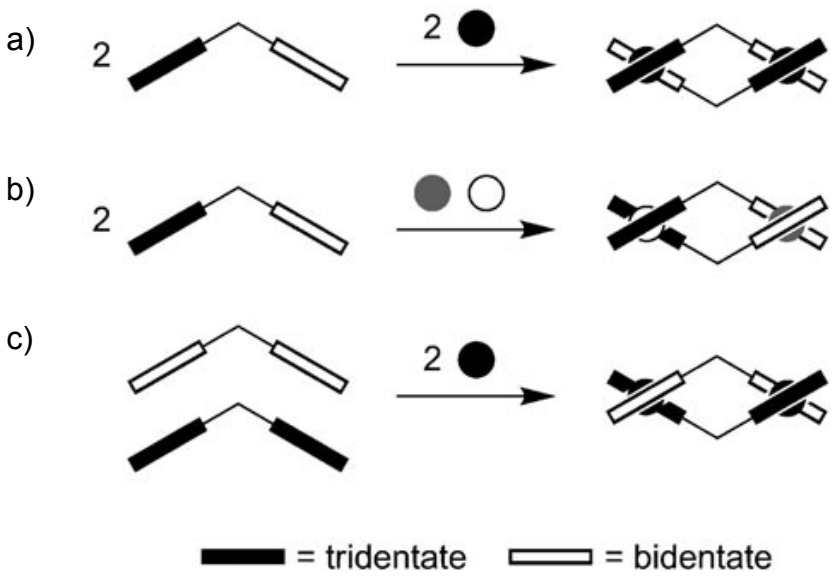

Fig. 19: a) HT homoleptic dinuclear double helicate, b) HH homoleptic dinuclear double helicate, c) heteroleptic dinuclear double helicate.[29]

1.6.2 Homoleptic Helicates

Homoleptic helicates are a result of two ligand strands with identical binding units. They comprise the same denticity, connectivity and donor atoms.[30,31] An example of this was produced by Lehn and co-workers in 1986.[33] The research showed that taking a poly(2,2'-bipyridine) ligand and coordinating it with a metal ion of specific (in this case tetrahedral) coordination geometry formed a complex with a double stranded helical motif (Fig. 20).[30,33]

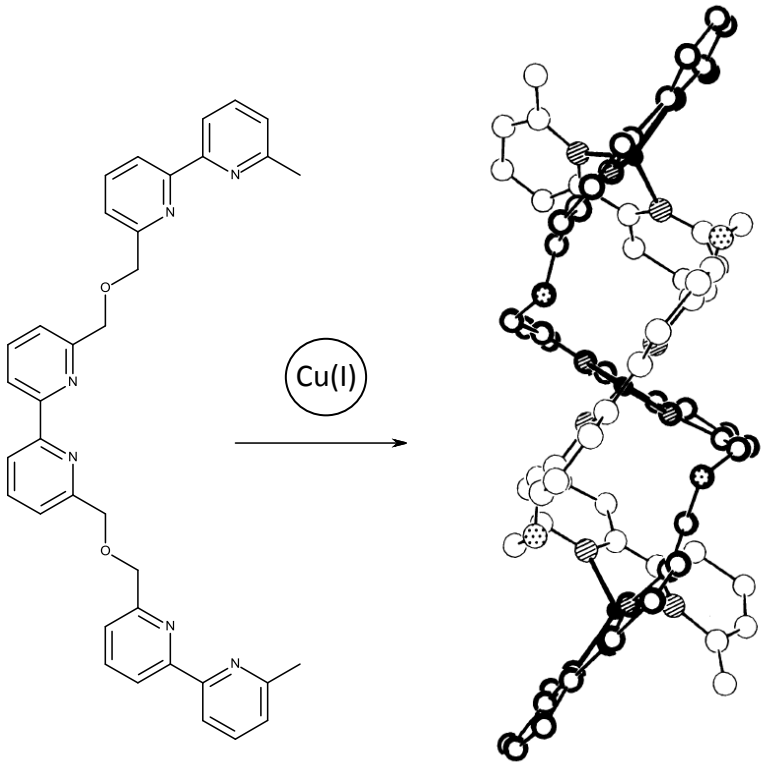

Fig. 20: Self-assembly of a trinuclear homotopic double-stranded helicate.[30,32]

Fig. 20 shows that using Cu(I), which has a preference for tetrahedral coordination geometry, produces a tri-nuclear homoleptic double-stranded helicate through coordination of the metal with two bipyridine units of each ligand.

1.6.3 Heteroleptic Helicates

When two different ligands coordinate the same metal ion(s) then the helicate is said to be heteroleptic.[90] The metal ion used in these helicates often induces the formation of one of the species in higher yield.[33,34] One such example of this was produced by Lehn *et al.*[40] who synthesised two tritopic linear ligands (Fig. 21a & b). These ligands had previously been shown to produce homoleptic helicates in the presence of a mononuclear cation e.g. Cu(I), which can adopt either a tetrahedral or octahedral coordination geometry. However, on coordination of the ligands with a divalent metal ion e.g. Cu(II) in a 1:1:3 ratio the metal ion's preference for a five-coordinate distorted octahedral geometry gave rise to a heteroleptic helicate. The Cu(II) ions coordinate a bidentate domain from one ligand and a tridentate domain from another (Fig. 21c).[34]

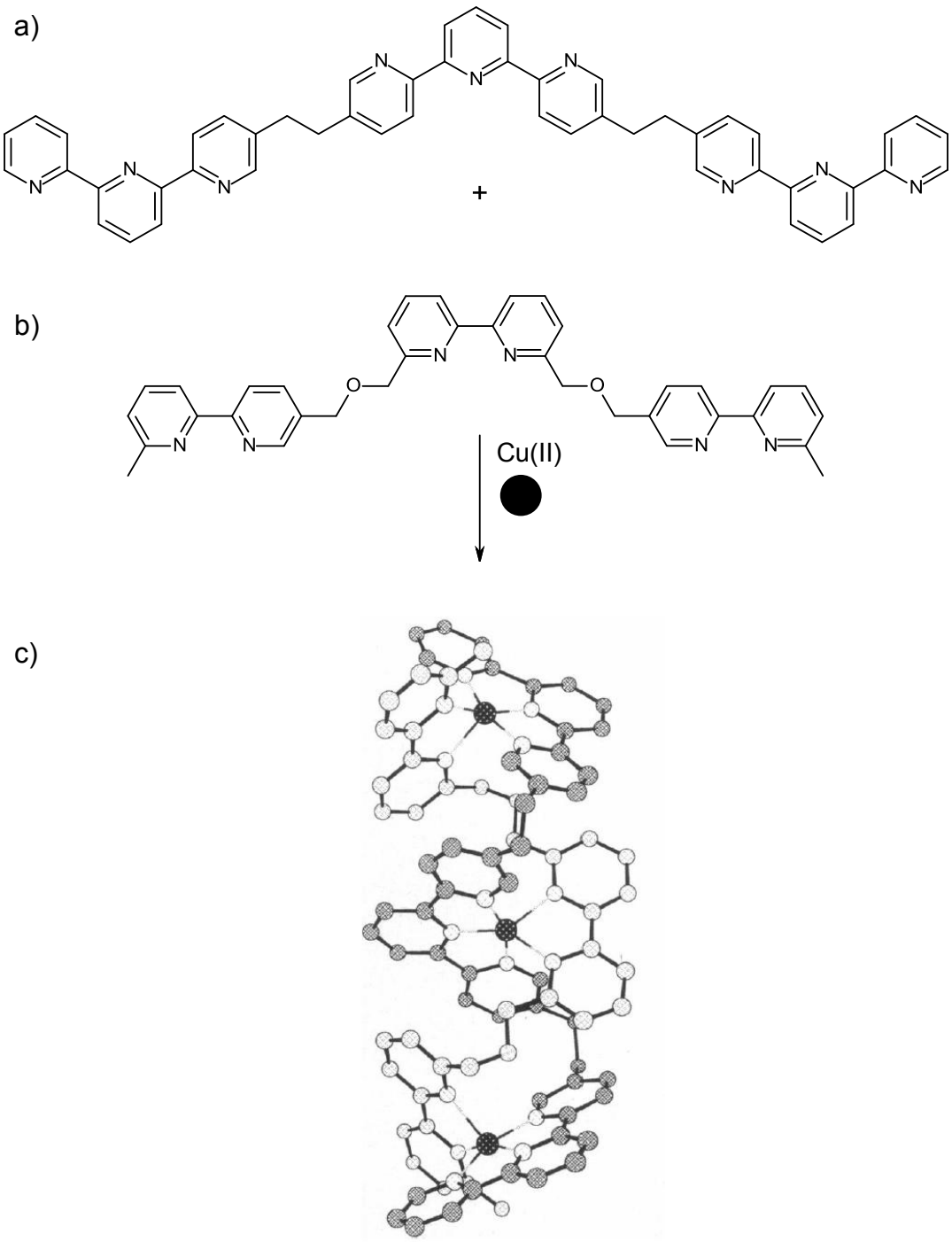

Fig. 21: Synthesis of a heteroleptic helicate, a) Ligand strand 1 b) Ligand strand 2 c) Heteroleptic helicate.[34]

It is possible for heteroleptic systems and asymmetric ligands to arrange themselves in more than one way depending on their preference for a metal ion; this can result in helicates with different isomeric forms, *i.e.* head-to-tail (HT) or head-to-head (HH) (Fig. 19a and b respectively).[1,28,29]

1.6.4 Head-to-tail helicates

A ligand can be partitioned into two separate binding domains via the addition of a linker or spacer. If these binding domains contain a different number of coordination sites *i.e*. bidentate and tridentate (different functionalities) then it is quite possible that a head-to-tail helicate will form whereby a different end of each ligand coordinates the same metal ion (Fig. 19a).

Constable *et al.* synthesised a series of HT and HH di-copper(I) double helicates from asymmetrical quaterpyridine ligands. It was shown that it takes several different modes of steric interactions to determine a preference for one isomer over another (HH or HT); simply increasing steric bulk at the 4-position to favour the formation of the HH species did not lead to an overriding preference.[35]

1.6.5 Head-to-head helicates

A head-to-head helicate is where the same ends of a heterotopic ligand strand coordinate the same metal ion *i.e.* bidentate/bidentate (Fig. 19b). The formation of a head-to-head complex is often favoured over its head-to-tail counterpart due to steric repulsion of the substituents; the ratio of formation between these two species is strongly dependant on the size of the connected R groups and the helical pitch (ratio of axially linear to angular properties).[28,30]

It's also often due to the coordination geometry of the metal, for example two bidentate domains will coordinate a tetrahedral metal whereas two tridentate domains will coordinate an octahedral metal.

Given this preference there have been many examples of head-to-head helicates in the literature; André *et al.* used a ligand's affinity for a particular metal ion to dictate the overall outcome of formation. They were able to complex a heterodimetallic triple-stranded helicate which forms in 90% favour of the HHH isomer (Fig. 22).[36, 37]

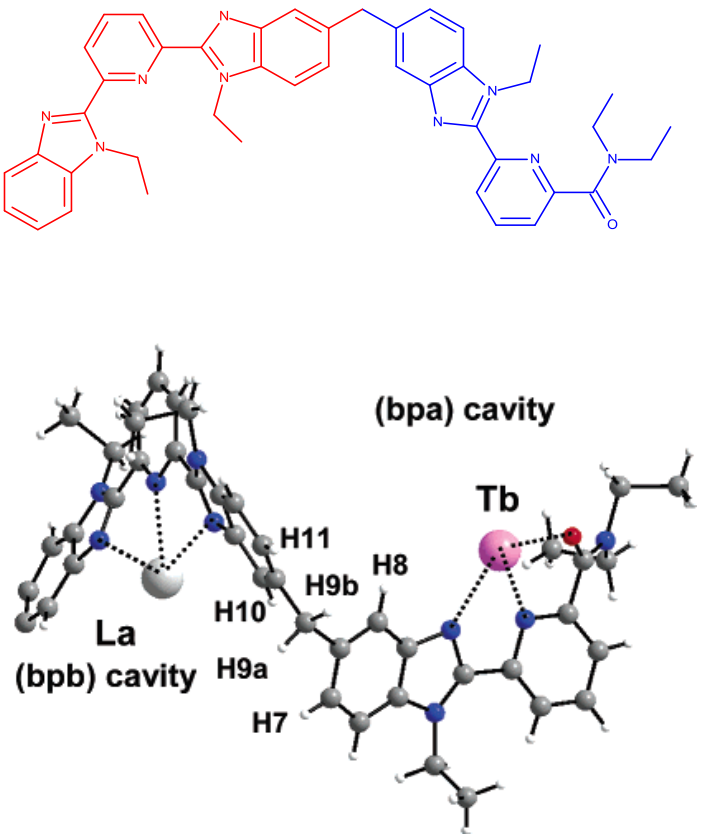

Fig. 22: A heterotopic ligand capable of forming a HHH triple-stranded helicate.[36]

1.6.6 Unsaturated Helicates

So far this discussion has focussed on saturated helicates; helicates that have both the metal and the ligand fully coordinated. Unsaturated helicates form as a product of a mismatch between the inbuilt information / pre-organisation of the components.[30] There are a number of ways in which this disparity can occur: a) incomplete use of all of the ligand strands' binding domains or b) an unfulfilled coordination geometry of the metal ion, the vacant binding sites are then free to be taken up by anions or solvent molecules.[30]

Examples of both hetero- and homotopic unsaturated helicates have been shown within the literature.[30,38,39] Goodgame and co-workers described the self-assembly of an unsaturated homoleptic triple-stranded helicate (Fig. 23a). The bis-monodentate ligand reacts with Nd(III) cations resulting in an unsaturated helicate (Fig. 23b), the coordination geometry of the neodymium centres (9-coordinate) are then satisfied by three nitrate anions (NO_3^-).[38]

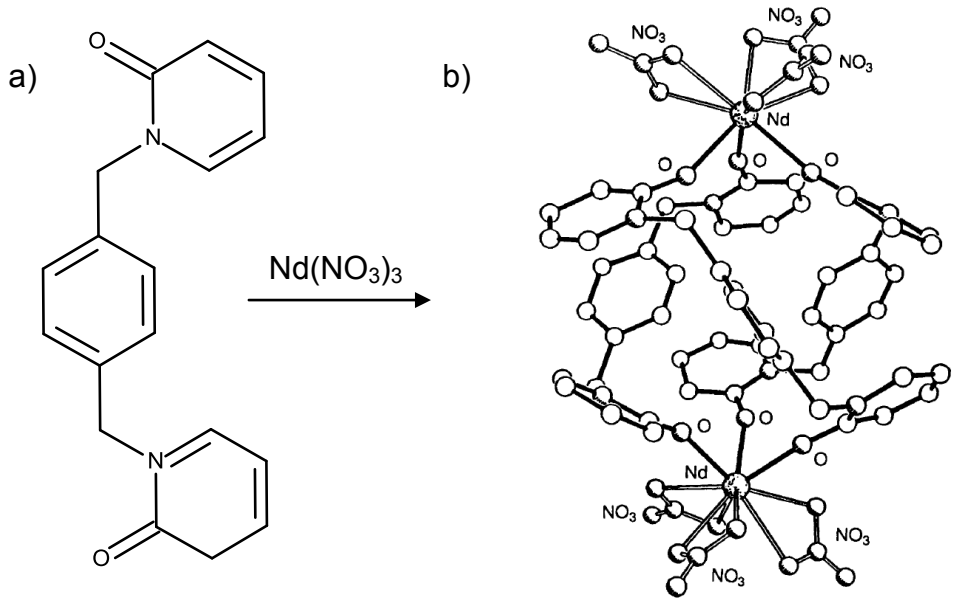

Fig. 23: a) Bis-monodentate ligand strand, b) Unsaturated triple-stranded helicate $[Nd_2(L)_3(NO_3)_6]$.[38]

Unsaturated hetero-species form when unsymmetrical ligand strands do not possess binding domains capable of fully coordinating the metal ion.[30] A very well-documented example of this is by Constable *et al.* who synthesised a quinquepyridine ligand (Fig. 24a) that in the presence of Cu(II) consequently formed a HH unsaturated heteroleptic double-stranded helicate (Fig. 24b). Due to the versatile coordination behaviour of Cu(II) each of the copper centres exhibits a different coordination geometry, one Cu(II) centre is coordinated by the two tridentate domains (terpyridine) in an octahedral coordination environment, while the second is bound by two bidentate bipyridine domains with one acetate anion in the less favoured five-coordinate site.[30,39]

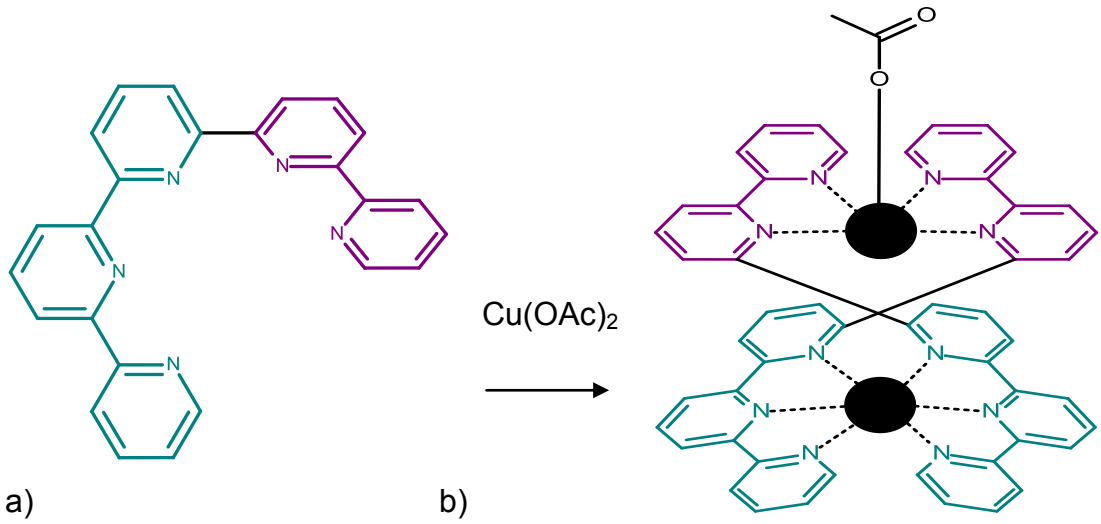

Fig. 24: a) Green tridentate domains, purple bidentate domains, b) Unsaturated double-stranded helicate (HH)-$[Cu_2(L)_2(OAc)]^{3+}$.

1.6.7 Hetero-metallic helicates

Up to now the only discussed examples of helicates have been 'homometallic/homonuclear' meaning the all the metal centres have been the same.[32-34,38,39] However, it is possible to form helical species where the structure contains different metal ions.[36,40,41] This is generally the case when the metal centres used vary in their preferred coordination geometry; one example of a heterometallic species was again introduced by Constable *et al.* who took the previously described quinquepyridine ligand (Fig. 24a) and coordinated it with two different metal ions (Ag(I) and Co(II)). Previously it formed an unsaturated double-stranded helicate when introduced to Cu(II), but in the presence of a mono- and divalent cation with their preferences for tetrahedral and octahedral geometries respectively, a fully saturated double-stranded helicate forms with the Ag(I) occupying the tetrahedral bipyridine sites and the octahedral Co(II) occupying the terpyridine sites (Fig.25).[41]

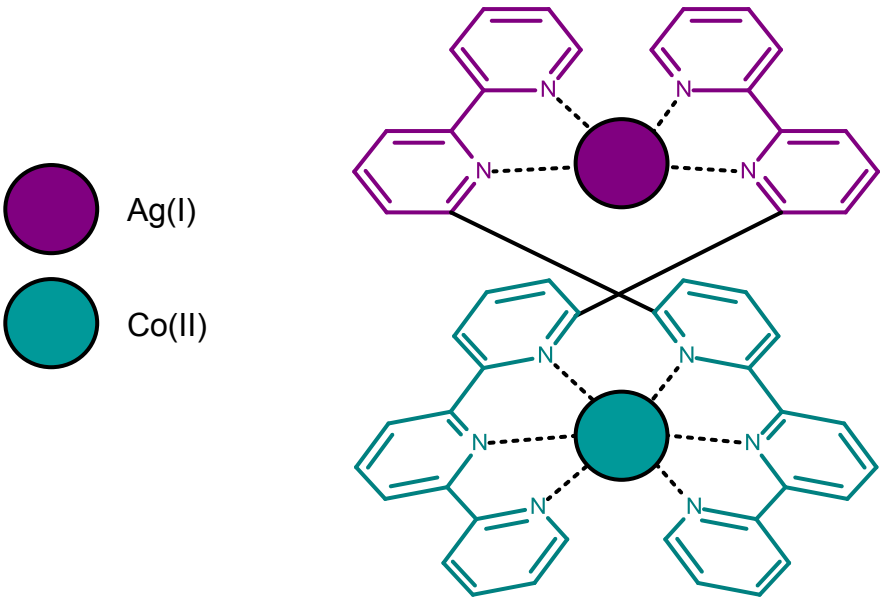

Fig. 25: Saturated double-stranded helicate (HH)-$[CoAg(L)_2]^{3+}$.

1.6.8 Chirality of helicates

The screw principle or helical chirality as it is better known has already been touched upon; however it is of more importance when discussing enantiospecific helicates. Chiral compounds exist in all forms of chemistry, but only its role in the formation of supramolecular structures will be discussed here.

Helicity is a special form of chirality and its best explained as a motif generated by the directional movement about a helical axis. Each helicate can be defined using the Cahn-Ingold-Prelog notation: M (left-handed) and P (right handed) (Fig. 26).[2,30,42]

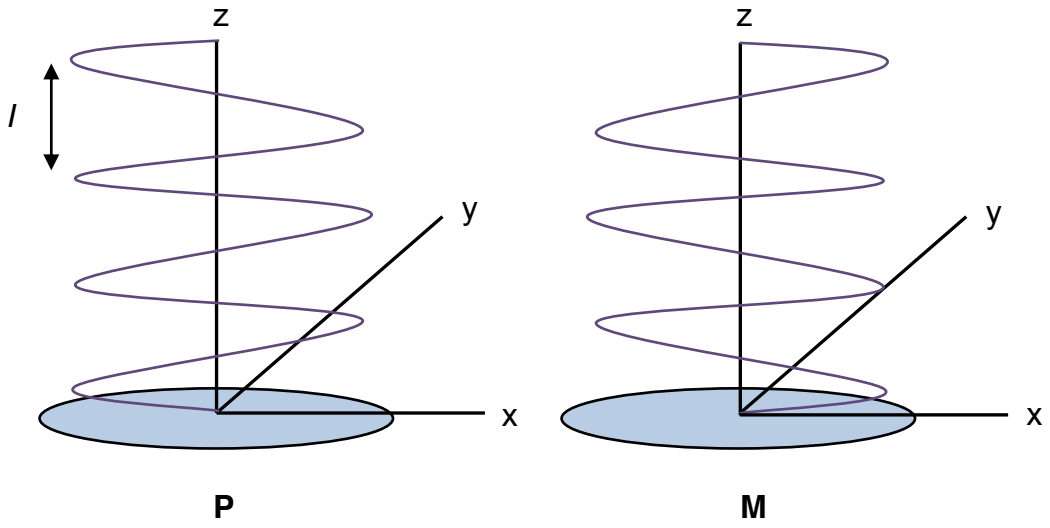

Fig. 26: Ilustration of the different forms of helical chirality; (x,y) directional plane, (l) pitch, (z) helical axis.

The axis is a straight line and the directional movement is both circular and linear whilst maintaining a constant distance from the axis thereby producing a constant pitch (*l*). This can lead to the clockwise (M) or anticlockwise (P) directions illustrated above.[42]

For a helicate complex the axis is defined by the line passing through the central metal ion(s) with the ligands acting as the helical array. This is quite straightforward for a double helicate but incorporating more ligands into the overall structure can change the helical properties as the different arrangements of atoms about the ligand chain such as cyclic molecules and bulky substituents can cause steric repulsion. This leads to a rapid expansion of the ligands and an alteration in the helicate's pitch.[30]

In order to selectively form the M or P isomers there has to be a large degree of stereochemical information. The chiral properties of the complex are largely dependent on the number of metal ions used (n). If the structure consists of two metal ions (2n) each with an opposing stereochemistry then a mesocate (side-by-side) structure is formed and the assembly is said to be achiral due to the fact that it possesses a plane of symmetry.[30] However, if both metal ions express the same stereochemistry then a chiral helicate results (Fig. 27a & b). Increasing the number of metal ions (n > 2) can in turn increase the complexity of both the chiral and achiral species.

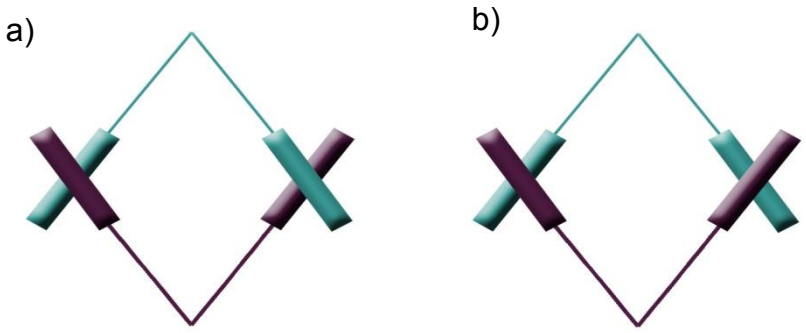

Fig.27: Example of the formation of a chiral helicate (M,M) (a) and an achiral mesocate (M,P) (b).

Some further examples of chirality within the literature have been produced by Mamula, Baum and Constable.[43-45] Mamula and co-workers produced a detailed publication on the formation of these species by creating a plethora of chiragen ligands (two bipyridine units connected by a chiral bridge [B]) (Fig. 28) capable of undergoing chiral self-recognition when coordinated with metal ions.[43]

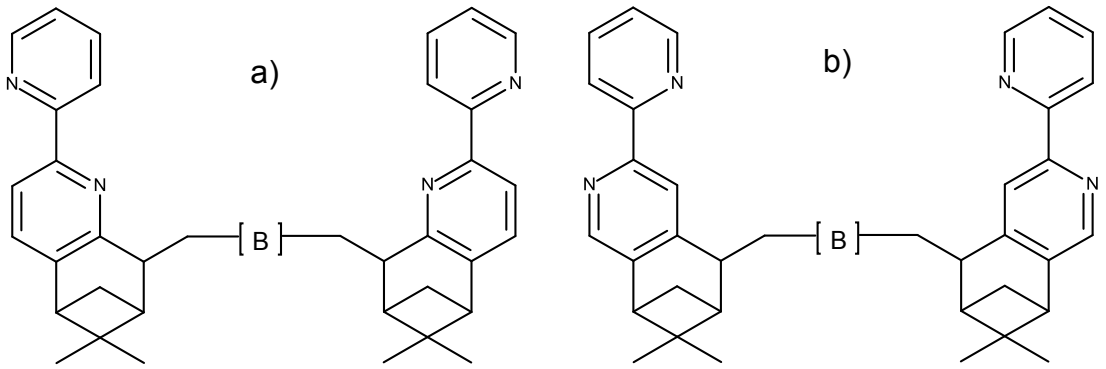

Fig. 28: a) 5,6-Chiragen ligand b) 4,5-Chiragen ligand.

Two ligands capable of selectively forming a number of different complexes upon coordination with metals of distinct coordination geometries are the; 4,5-chiragen, which forms a dinuclear triple helicate with octahedral metal ions, and the 5,6-chiragen which has a preference for tetrahedral metal centres due to its steric complexity. One example contains a bridging *para*- substituted phenyl ring (Fig. 29a & b).

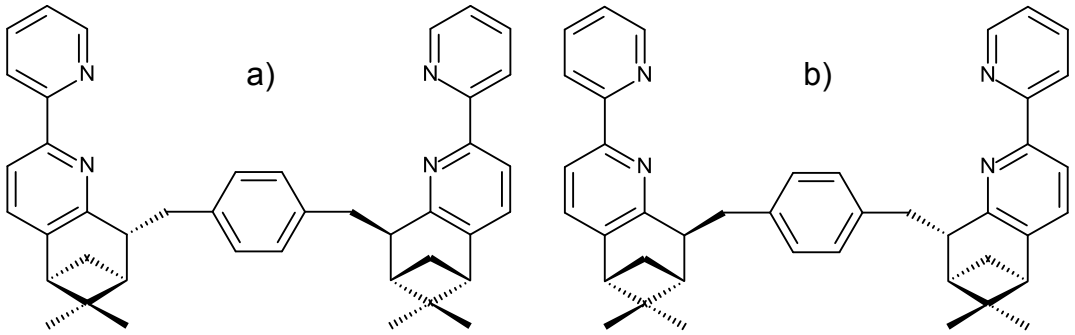

Fig. 29: a) (+)-isomer of the chiragen L, b) (-)-isomer of the chiragen L.

Mamula *et al.* discovered that when a racemic mixture of the two enantiomers was coordinated with Cu(I) they individually pre-organised into a left-handed and right-handed circular helicate, *i.e.* two separate chiral forms (M and P).[43]

Baum *et al.* discovered something similar when they synthesised a series of quaterpyridines (Fig. 30).[44] Again upon coordination with a monovalent cation e.g. Ag(I), these species undergo self-recognition forming different chiral dinuclear double helicates (M and P).

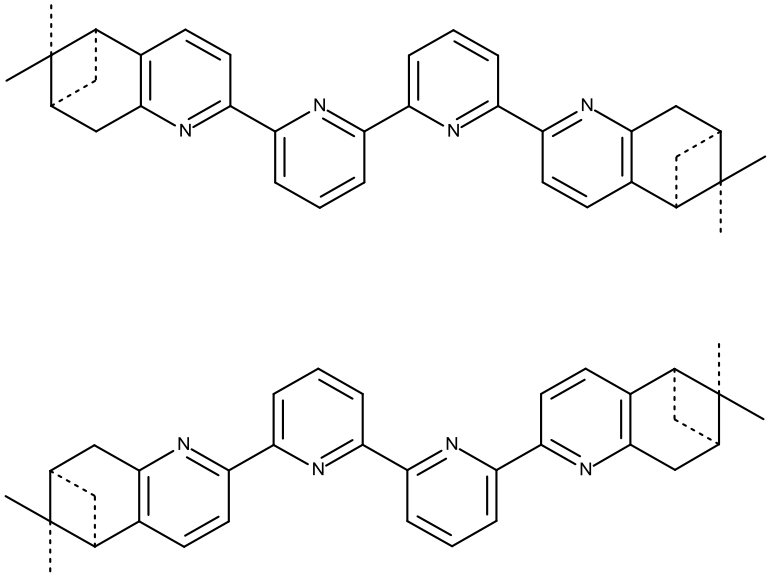

Fig. 30: Entaniomeric ligands capable of forming dinuclear double helicates with Ag(I).

1.6.9 Circular Helicates

The formation of double and triple helicates has been well explored over the years, [46] however the self-assembly of larger supramolecular species haven't been as well studied.

Circular helicates are one such example; these circular structures form *via* self-assembly, and comprise of three or more ligand strands helically wrapped around a central array of metal ions in an under and over fashion.[47,48]

Hopfgartner and co-workers reported a bis-tridentate ligand (Fig. 31) that on coordination with octahedral metal ions such as Fe(II), Co(II) and Ni(II) results in the formation of the circular helicate (Fig. 31b) over that of the expected dinuclear double helicate (Fig. 31a).[28,30,49]

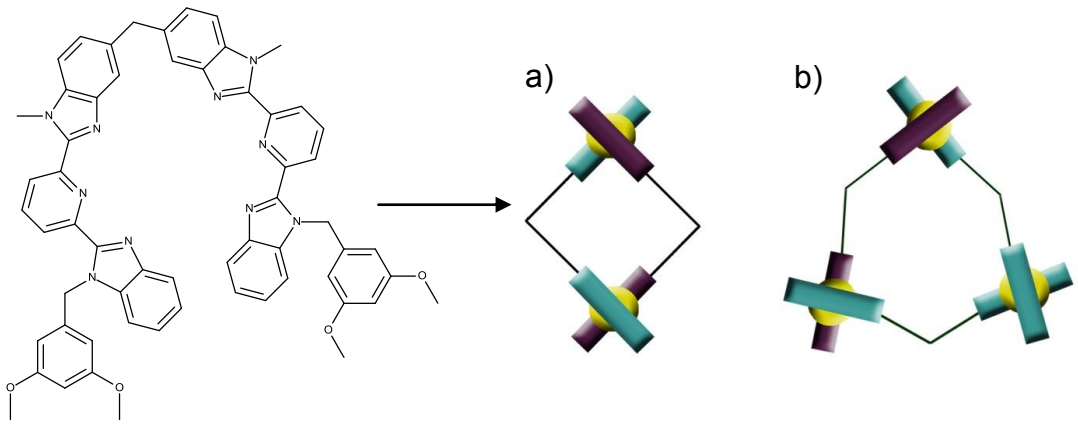

Fig. 31: Self-assembly of two different architectures (helicate (a), circular helicate (b)) from the same ligand strands.

Due to unfavourable steric constraints induced by the 5,5´-diphenylmethane spacer the reaction foregoes the formation of the dinuclear helicate in favour of the circular. In theory both outcomes are possible however the large inter-planar angles between the tridentate units required in the formation of the dinuclear helicate is sacrificed in favour of a more thermodynamically stable species.

The metal plays a key role in the formation of circular helicates; size, shape and overall coordination preference have to be considered. Other factors can also affect the preferential formation of one species over another; the chemical information contained within the system has to be considered carefully. In order for the larger and more complex circular helicate to form it has to overcome the formation of the more entropically favoured dimer. Preventing the thermodynamically favoured species can either be achieved *via* intermolecular destabilising interactions or intramolecular stabilising interactions, which in turn are governed by the metal ion used.[47]

A good example of destabilising intermolecular interactions can be found in a paper published by Rice *et al.* The author demonstrated how inter-ligand steric interactions dictated by the size of the metal ion lead to the overall formation of a circular helicate over the more entropically favoured double helicate.[47] The formation of one species over another can be attributed to the metal ion used (Zn(II) or Cd(II)) and its effects on the spatial arrangement of the ligands.

Previously the coordination preference of the metal ion has led to one structure being favoured over another; however, in this case it is the size of the metal ion which becomes the driving force. The larger Cd(II) ion (0.95 Å) provides ample space for the protons of opposing phenyl spacers to reside, once the resulting double helicate has formed (Fig. 32). Substituting the Cd(II) cation for one with a smaller radius such as Zn(II) (0.75 Å) drastically reduces the gap, thus bringing them into an unfavoured and sterically hindered environment. This in turn destabilises the formation of the double helicate allowing the formation of an alternative complex, a pentanuclear circular helicate (Fig. 32b).[47]

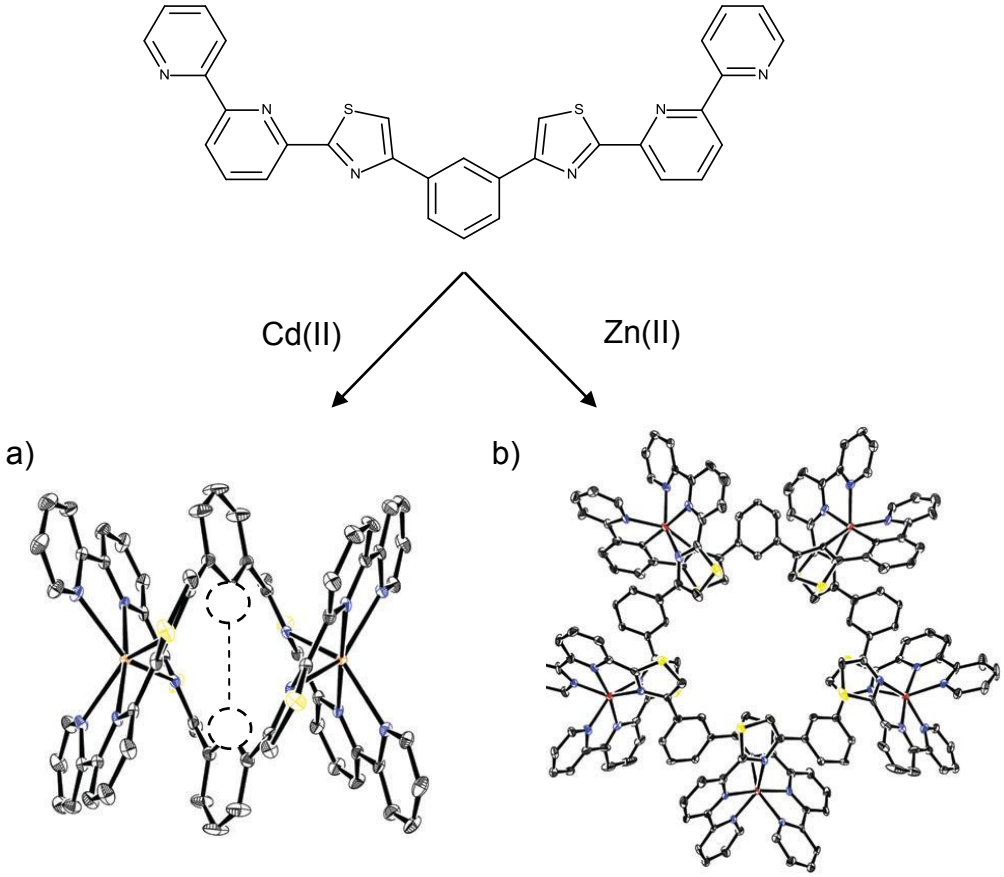

Fig. 32: a) Formation of a dinuclear double helicate with Cd(II), b) formation of a pentanuclear circular helicate with Zn(II).[47]

More recently Rice *et al.* have developed a series of ligands with a mixed number of coordination sites (Fig. 33a, b & c) which when coordinated with metal ions yield some interesting results. Ligand two (Fig. 33a) demonstrates the first head-to-tail pentanuclear circular helicate by combining both inter- and intramolecular forces.[48] The authors built upon their previous experience with unfavourable steric interactions, and used this knowledge to synthesise a series of ligands that, when coordinated with metal ions of a smaller radius, would forego their preference for a double helicate due to unfavourable interactions between the protons of the phenyl spacers (Fig.32a).[48]

Furthermore, utilising intramolecular interactions as stabilising effects can greatly increase the chances of circular helicate formation. This was achieved through coordination of the ligand with a versatile metal ion such as Cu(II) which allowed all 5-, all 6- and even mixed 5- and 6-coordinate sites to be achievable, thus leading to the formation of both the head-to-tail and heteroleptic pentanuclear circular helicates (Fig. 34a & b).

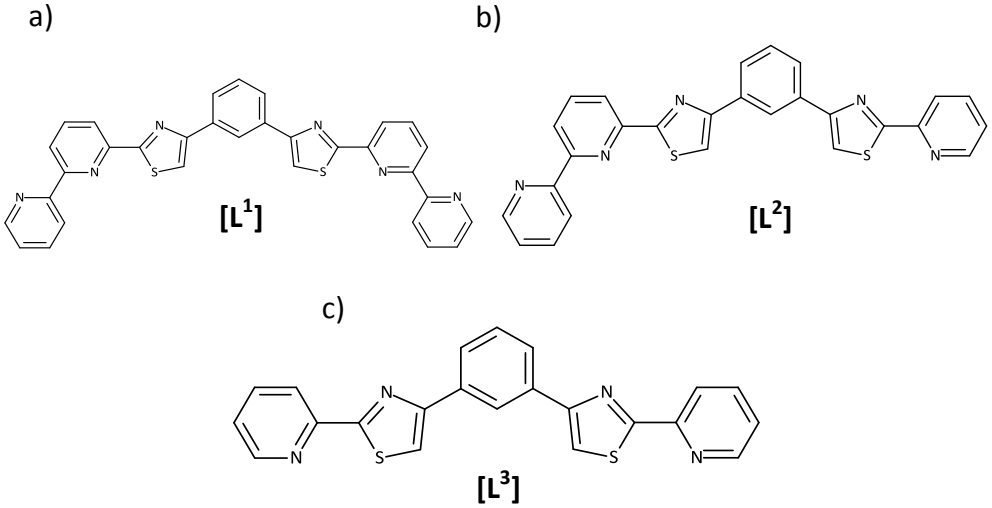

Fig. 33a, b & c: Ligands used in the formation of Rice and co-workers circular helicates.

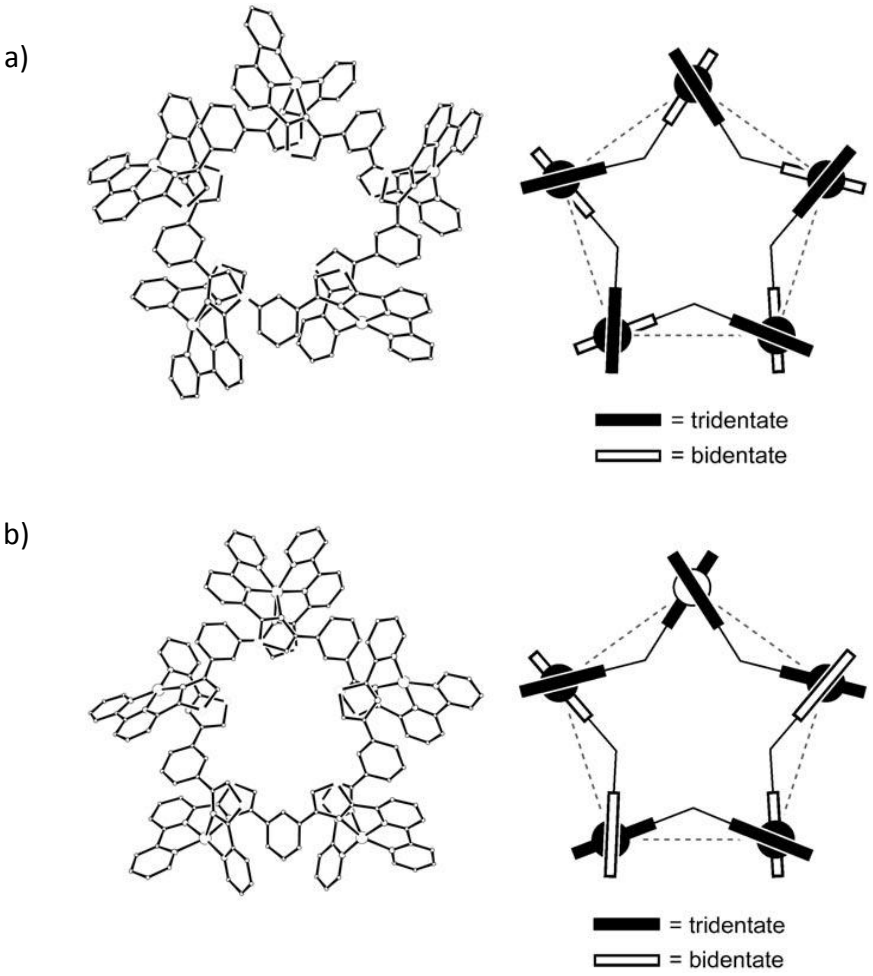

Fig. 34: a) HT-$[Cu_5(L^2)_5]^{10+}$ circular helicate, b) heteroleptic $[Cu_5(L^1)_3(L^3)_2]^{10+}$ circular helicate.[48]

1.7 Anion Coordination & Recognition

Research into anion chemistry, although limited, was first established in the 1960s; during this time Lehn and Pedersen worked on a number of crown ethers and cryptands, exploring their use in formation of metal complexes. Due to the overwhelming interest in the subject it has since developed the area of supramolecular chemistry into a mature branch of science.[50, 51, 52]

There are many reasons why anion binding has been a poorly-studied area in the past, possibly due to their poor binding affinity (poor charge to radius ratio). It is only recently that anion coordination and recognition has piqued the interest of the supramolecular chemist. Anions play a large role in everyday life whether it is aiding in the transportation of genetic information *via* anionic enzyme substrates and co-factors in DNA, or contributing towards the synthesis of new medicines and catalytic systems.[53, 55]

The chemistry of anions is wide-ranging but the main interest for supramolecular chemists is the coordination and binding of these molecules. This can be of particular interest in the cases of capturing pollutant anions which have been linked with the eutrophication of rivers (phosphate-containing fertilizers) or carcinogenesis (metabolites of nitrate).[56,57]

More recent areas of anion chemistry have been developed incorporating a wealth of chemistry knowledge for the binding, sensing and separation of these ions, most of which will be outlined in detail throughout this introductory chapter.

1.7.1 Anion receptors

Unlike the design of cation receptors, anion receptors can prove difficult to prepare. There are many reasons for this: charged anions are significantly larger than their cationic counterparts (Fig. 35) which leads to a lower overall charge to radius ratio. The consequence of this is that much weaker electrostatic interactions are observed.[52]

Cation	r [Å]	Anion	r [Å]
Na^+	1.16	F^-	1.19
K^+	1.52	Cl^-	1.67
Rb^+	1.66	Br^-	1.82
Cs^+	1.81	I^-	2.06

Fig. 35: A comparison of cation and anion radii (r).

Anions are sensitive to changes in the pH of their environment, becoming protonated at low pH therefore losing their negative charge. This poses a large problem for the chemist who has to synthesise a receptor that not only has to function at a varied pH, but must also be selective for the anion they wish to complex.

This can lead to further complications as ionic species vary in their geometries (Fig. 36); therefore, designing a receptor with sufficient information to act as a complimentary binding site for the guest as well as being thermodynamically stable is non-trivial.[52]

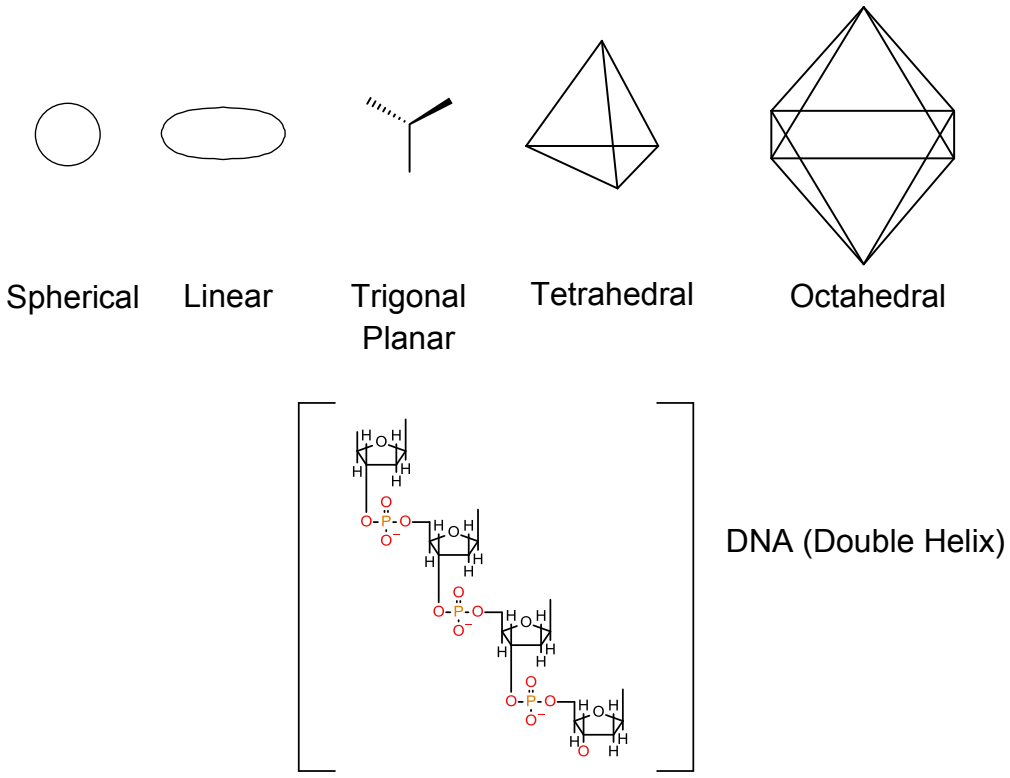

Fig. 36: Anion geometries.

To achieve some control over the formation of anion-receptor complexes it is important to consider solvation effects which may compete with the receptor for

selectivity and binding strength. Electrostatic interactions are the overriding force in anion solvation with hydroxylic solvents forming strong hydrogen bonds with anions.[52]

For example a neutral receptor that binds anions *via* ion–dipole interactions may only coordinate anions in atropic organic solvents, whereas a charged receptor has the capacity to bind highly solvated (hydrated) anions in protic solvents.

The Hofmeister series is an important tool in supramolecular anion coordination and one which plays a crucial role in the selectivity of a receptor. The Hofmeister series (Fig. 37) orders anions by their hydrophobicity and how likely they are to interact with aqueous media. It was first discovered by studying the effect of salts on the solubility of proteins with the generalized conclusion that hydrophobic anions are bound more strongly in hydrophobic binding sites.[52]

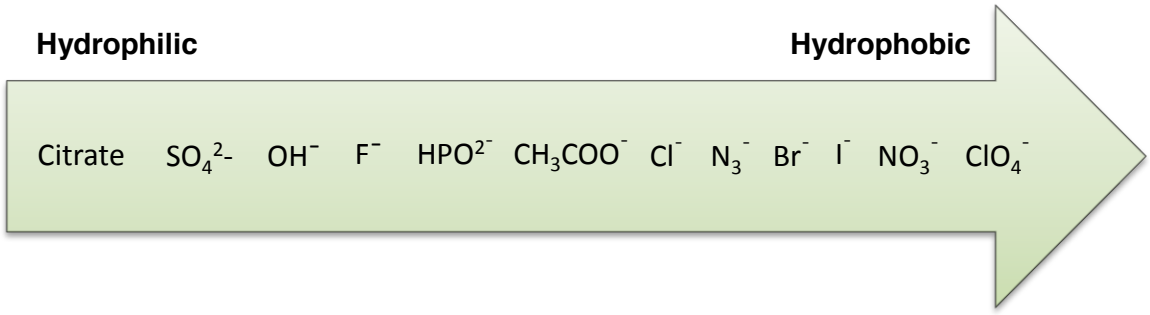

Fig. 37: The Hofmeister Series displaying anions in order of their hydrophobicity.

A number of non-covalent interactions have previously been outlined in this report however is it important to consider the interactions which take place between anions and their pre-designed receptors, these include:

I. Electrostatic interactions,

II. Hydrogen bonding,

III. Coordination to a metal ion,

IV. As well as combinations of these effects.

These interactions will be discussed further in terms of their contribution to stable anion complexes.

1.7.2 Electrostatic Interactions

Recognition of anions *via* electrostatic interactions is possibly the most obvious method, using a positively charged species to provide a strong electrostatic ion-ion interaction. Furthermore, using an array of positively charged species like those observed in ligand chemistry would increase the overall charge therefore becoming more effective and decrease the probability of any competing interactions from other positively charged species.

Increasing the number of positively charged moieties in a receptor can cause significant design problems due to the repulsion observed from the positive charges. To contest this, a number of rigid or cyclic groups are often introduced to the system to act as restraints.[1]

Schmidtchen and co-workers reported a macrotricyclic receptor comprising of four positively charged nitrogen corners which create a pocket for the negatively charged anion guests.[58,59] Fig. 38 shows the template for the macrotricyclic receptor which can be increased in size through the addition of extra $–CH_2$ linkers [X].

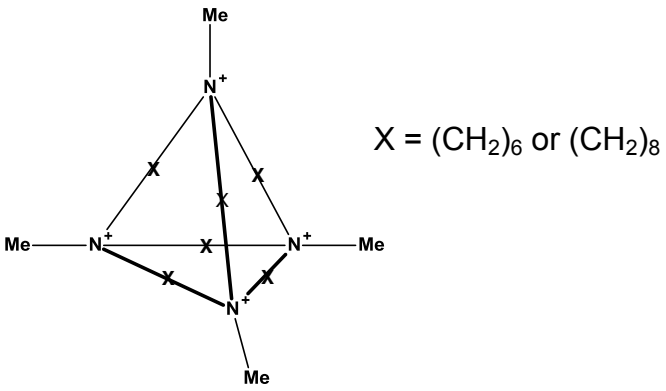

Fig. 38: Schmidtchen and co-workers macrotricyclic anion receptor.[58,59]

When introduced to a series of anions (I^-, Br^- and Cl^-) it was reported that the cyclic species encapsulated the anion within the central cavity, holding it equidistant from each of the nitrogen atoms. Additionally, the larger $(CH_2)_8$ chains were preferred for anions such as I^- and Br^- due to their larger diameter thus proving a better fit.

Schmidtchen and co-workers demonstrated how the design of the receptor can exhibit size selectivity as the larger of the two species ($(CH_2)_8$) not only binds larger anions with more success but it also shows a preference for larger anions such as nitrophenolate.[58, 69]

These receptors possess an overall positive charge which must be balanced by counter ions; this poses a problem as the anion can compete with the target species for a space within the cavity. To overcome this many groups including Schmidtchen's have developed complexes without a net charge (zwitterionic hosts) and therefore no competing counter ion.[60]

1.7.3 Hydrogen Bonding

The interaction between an electron pair acceptor and an electron pair donor has previously been outlined in this work, however if we consider an anion as an electron pair donor and a hydrogen atom as an electron pair acceptor then it is feasible for them to form hydrogen bonds.

Pascal was the first to demonstrate an anion host that functions entirely through hydrogen bonding (Fig. 39) Using NMR spectroscopy it was shown that each proton from the convergent amide groups bound fluoride anions in DMSO.[61]

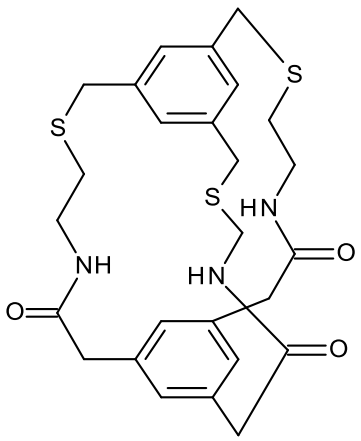

Fig. 39: Fluoride receptor.

Ureas and thioureas are often used as hydrogen bond donors and act as excellent receptors in anion chemistry. In 1992 Wilcox explored the functionality of a urea derivative (Fig. 40a & b) and its ability to interact with phosphonates, sulfates and carboxylates in dichloromethane.[62]

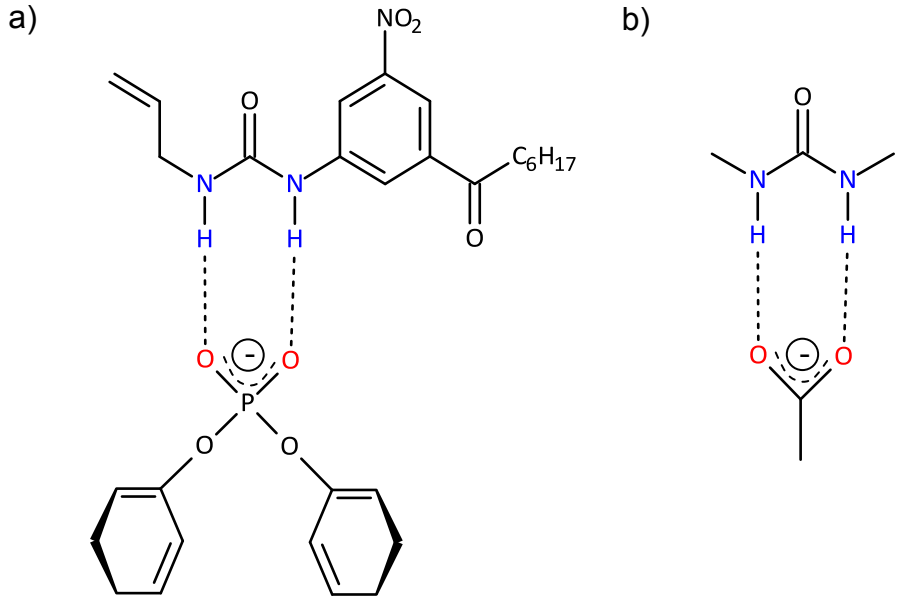

Fig. 40: a) Hydrogen bonding interactions between a urea and a phosphonate b) Hydrogen bonding interactions between a urea and a carboxylate.

The urea group donates two parallel hydrogen atoms which are geometrically complimentary to the oxygen atoms of an oxoanion thus, leading to the formation of a stable 1:1 complexes through N-H···O interactions.

Since Wilcox's early work many adaptations of the urea based receptor have arose. In a recent review by Amendola *et al.* the incorporation of nitrophenyl substituent's into the ligand chain gave increased functionality. The addition of a nitrophenyl group into the ligand chain further polarises the urea leading to enhanced H-bond donating tendancies.[62]

Furthermore intense absorption bands are observed which facilitates the monitoring of interactions with anions in solution, this is of particular interest in the formation of supramolecuar complexes.

1.7.4 Coordination to metal ions

Lewis acid centres are electron deficient and, as previously discussed, anions can donate an electron pair.[1] Therefore Lewis acids are capable of undergoing a binding interaction with anions *via* an orbital overlap. In 1967 Shriver and Biallas developed the first anion receptor of this kind (Fig. 41a).[63] Together they created a boron-based chelating ligand capable of accepting two electron pairs. It was discovered that the ligand formed strong bonds with methoxy anions over the proposed monodentate boron trifluoride.[52,63]

Katz furthered the research by incorporating a rigid framework between the two boron atoms (Fig. 41b). The naphthalene spacer led to the coordination of electron rich (hard) anions such as hydride and fluoride; it was found that these molecules could be selectively removed from other compounds using this simple ligand.[64, 76]

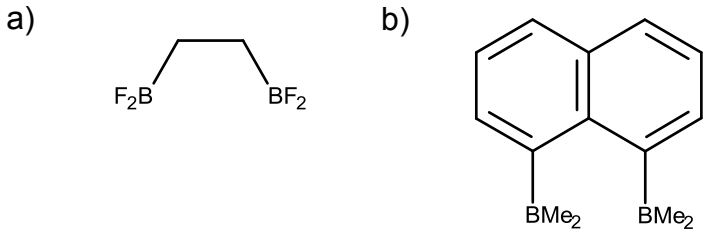

Fig. 41 a) Shriver & Biallas' boron-based anion receptor, b) Katz's boron based anion receptor.

1.7.5 Combinations of interactions

The most effective anion receptors originally used a combination of interactions such as electrostatic interactions and hydrogen bonding. A combination of these effects can be seen in Simmons and Park's early work.[65] Reported was a macrotricyclic receptor which hydrogen bonds a guest anion within the central cavity (Fig. 42). The two positively charged nitrogen atoms attract a negatively charged anion which undergoes hydrogen bonding, in turn creating a larger order of stability. This complimentary system both attracts and binds anions through a series of hydrogen bonding and electrostatic interactions giving rise to a strong complex.[65]

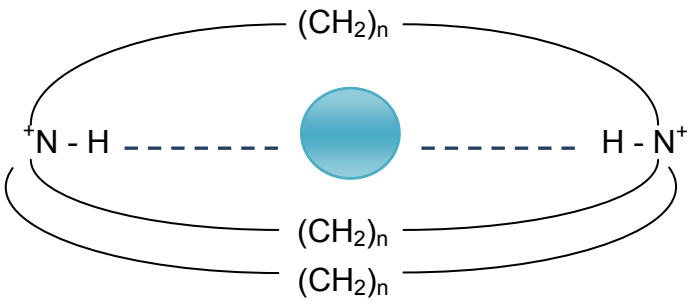

Fig. 42: Anion receptor exhibiting two forms of interactions; electrostatic and hydrogen bonding.

1.7.6 Optical and Electrochemical sensors

There has been substantial research in the area of anion recognition with the aim being to synthesise receptors capable of selectively sensing and binding anions whilst emitting an electrochemical or optical response.[66-68]

1.7.6.1 Optical sensors

Optical responses, in particular fluorescence, are often much more sensitive to the presence of their target ion or molecule. This has led to them becoming highly researched techniques in the field of anion sensing. Throughout the literature examples of luminescent anion-responsive systems have been shown, culminating a range of recognition sites including polyammonium, guanidinium ions and zinc(II) amine.[50,69,70] However, by far the most explored is the use of ruthenium(II) as a reporter group due to its chemical stability, redox properties, excited state reactivity and luminescent emission.[71]

1.7.6.2 Electrochemical sensors

Many design principles have been employed for the electrochemical recognition of anions which can be broken down into four sub-categories; however the main topic for this body of work is their use in the extraction of a charged guest into a membrane (ISEs).[52]

The use of both neutral lipophilic ureas and thiourea-containing receptors has become a popular basis for ion-selective electrodes (ISEs). Umezawa and co-workers' research

provides a perfect example of how urea-based systems can be used to form selective membranes for the detection of anions, specifically chloride.

These authors developed a urea-based ligand (Fig. 43) with a high degree of selectivity for Cl^- anions at pH 7; it was shown that in comparison to a freshly prepared anion-exchange electrode, the successful detection of chloride anions over other ions (SCN^-, Br^-, I^- and NO_3^-) in a biological solution (horse serum) was extremely efficient.[72]

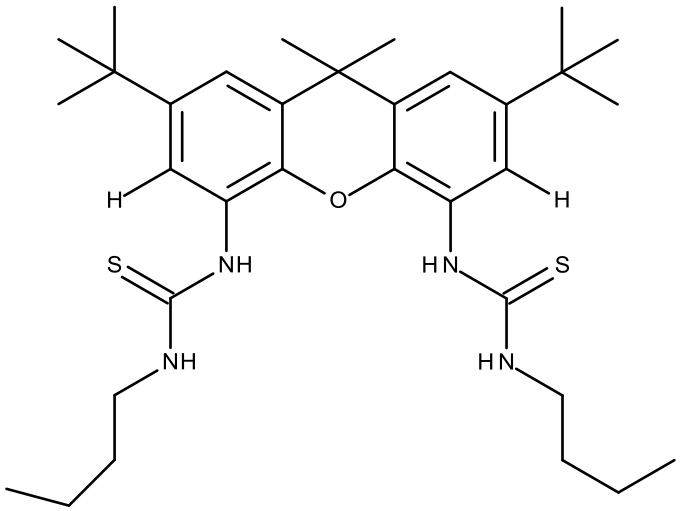

Fig. 43: An ionophore selective for Cl^- ions.

This is due to the exceptional binding capabilities of the urea groups; they are able to form strong bonds with good hydrogen bond acceptors like Cl^- and weak hydrogen bonds with very poor acceptors such as NO_3^-.

1.7.6.3 Combined sensors

The formation of complexes combining both optical and electrochemical properties have been examined and shown to be very effective. Beer and co-workers have produced a plethora of different receptors (Fig. 44a-e) including acyclic, macrocyclic and calix[4]arene-based species.[52]

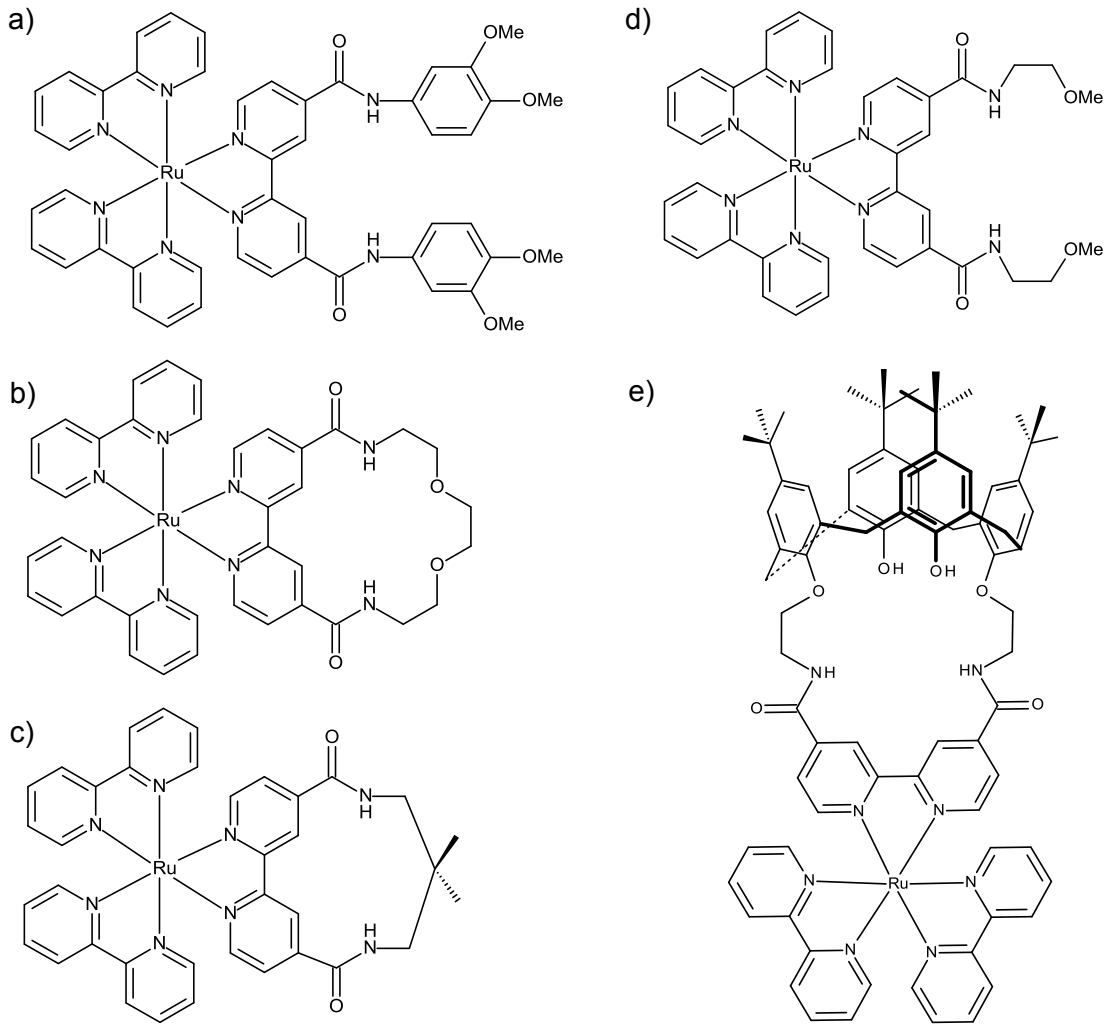

Fig. 44: *A series of ligands capable of optically and electrochemically sensing anions. All complexes have an overall charge of 2^+ and contain two hexafluorophosphate counter ions (not shown).*

Beer *et al.* were able to show that in the presence of anions, mainly Cl^- and $H_2PO_4^-$, a number of these ligands formed strong complexes through hydrogen bonding with the anion and the amide functional groups. Ligand (a) displayed very strong affinities for Cl^- whilst ligands (b), (c) and (d) formed strong complexes with the phosphate ion.[73,74]

Through electrochemical anion-recognition experiments with receptor (e) Beer and co-workers were able to show substantial anion-induced cathodic shifts of the redox couple associated with the reduction of the central amide-substituted bipyridine. The receptor's preference for $H_2PO_4^-$ over any other anion was demonstrated clearly when a tenfold excess of HSO_4^- was introduced without any significant effect.[73,74]

Furthermore, luminescence emission measurements were carried out in order to study the anion binding process. It was noted that all complexes exhibit a significant blue-shift in the metal to ligand charge transfer (MLCT) band when introduced to Cl^- and $H_2PO_4^-$. These shifts cannot be seen with the un-functionalized $[Ru(bpy)_3]^{2+}$.[73,74]

This response can be attributed to the bound anion displaying stabilization effects by acting as an anchor for the complex through bonding, thus rigidifying the receptor and inhibiting relaxation through vibration.

1.7.7 Directed assembly using anions

Up until the end of the millennium the use of anions in the formation of large self-assembled species was almost unheard of; however, recently many examples of anions and their roles within coordination chemistry can be found in the literature. Where once cation coordination was the focus of supramolecular chemists, anion coordination chemistry is now approaching the forefront, providing equally interesting and diverse supramolecular architectures.

1.7.7.1 Helicates

The role of transition metal ions in directing self-assembly of helicates has been researched exhaustively over the years; however, the use of anions as a central templating unit is less studied. The first ever example of a double helicate using anions as the templating species was discovered by Mendoza *et al.* in 1995.[75]

A tetraguanidinium ligand strand containing a CH_2SCH_2 bridging unit was designed that in the presence of sulfate ions, self-assembled into a double helix motif which was capable of self-assembling around sulfate anions in a double helix motif (Fig. 45). The bridging unit acts as linker between the two adjacent monoanions, thus is crucial in the formation of the double helix as it restricts the two guanidinium subunits from wrapping around a single sulfate anion. Therefore, two strands are forced to assemble around the sulfate ion which due to its chiral nature forces the formation of the helix.[75]

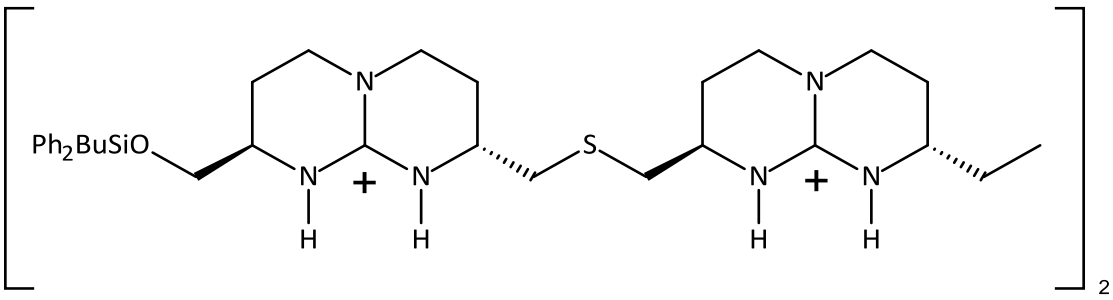

Fig.45: A tetraguanidinium ligand strand containing a CH_2SCH_2 bridging unit produced by Mendoza et al.

Similarly, Martin and co-workers synthesised a diamino-bis-pyridine ligand (Fig. 46a) that in the presence of chloride ions forms a double helicate with the Cl^- ion being bound by a pyridine ring from each ligand strand.[77]

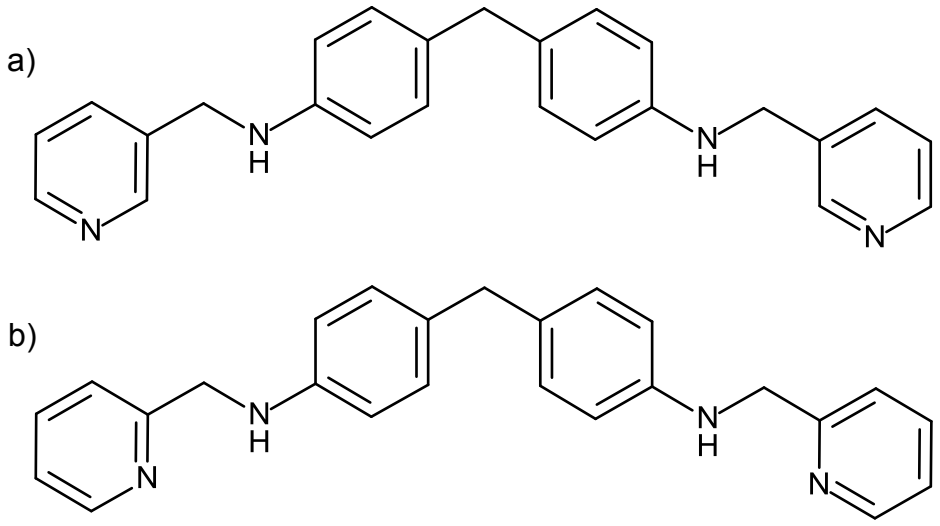

Fig. 46: a) Diamino-bis-pyridine ligands produced by Martin et al. b) di-amino-bis-pyridine ligands produced by Kureshy et al.

Kureshy *et al.* expanded on the research carried out by Martin and produced a very similar ligand consisting of the same diamino-bis-pyridine motif with the only difference being the position of the $–CH_2NH$ group being transferred from the *meta* position to the *ortho* position (Fig. 46b). On addition of Br_2 anions a similar double helicate structure was observed (Fig.47).[78]

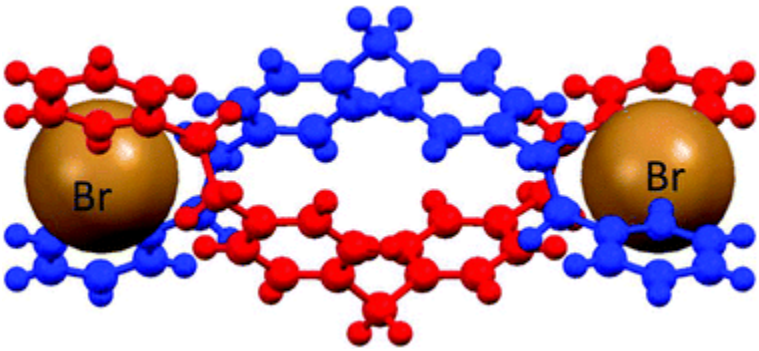

Fig .47: Bromide ion directed double stranded helicate.[78]

Qian-Shu Li *et al.* were able to mimic themes observed in metal coordination chemistry by tailoring ligands to accept anions instead of their positively-charged counterparts. They found that on coordination of phosphate anions by a bis(biurea) ligand (Fig. 48a) a triple anion-containing helicate was produced (Fig. 48b). The inherent information within the ligand strand was able to drive formation of a structure not dissimilar from that found in oligobipyridine-containing helicates with metal ions.[79]

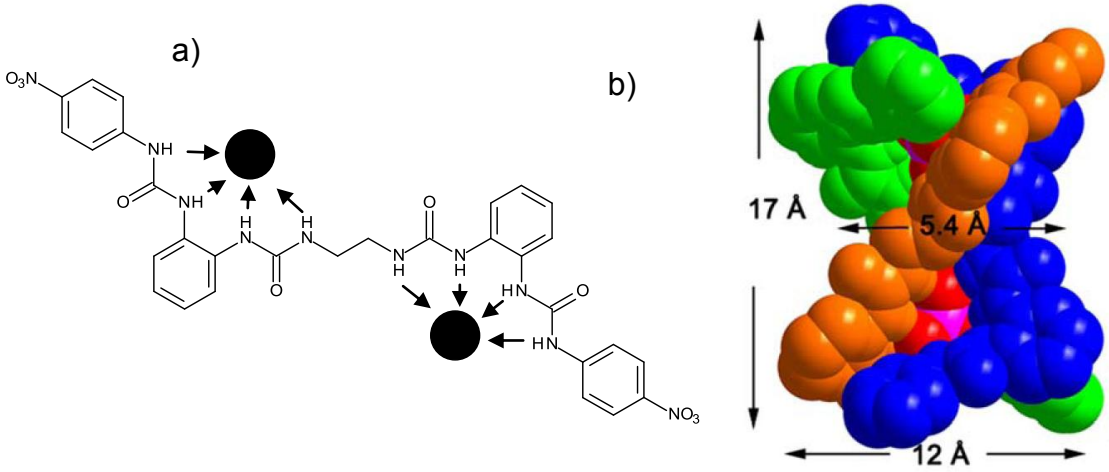

Fig. 48: a) Bis(biurea) ligand showing potential anion binding, b) triple anion helicate.[79]

1.7.7.2 Circular helicates

So far all of the architectures discussed have formed through anion interactions only; however, it is possible to form mixed anion/cation complexes whereby each ion plays a pivotal role. One outstanding example was the formation of a pentametallic circular helicate by Lehn *et al.*[9] Mixing the tris(bipyridine) ligand (Fig. 49) with an equimolar amount of $FeCl_2$ in ethylene glycol at 170°C gave rise to this large supramolecular species (Fig. 50).[1,52] Each bipyridine unit is interwoven with another ligand strand and

coordinates iron(II) in an octahedral geometry to give the helicate motif previously observed in many of these complexes; however, it is the chloride ion within the central cavity that templates the overall formation.[9]

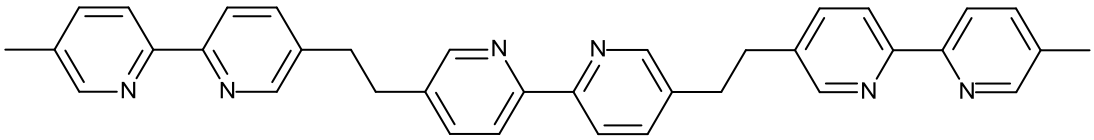

Fig. 49: Tris(bipyridine) ligand strand capable of forming a pentametallic circular helicate in the presence of $FeCl_2$ ions and a hexametallic circular helicate with $FeSO_4$.

The large chloride ion is held irreversibly within the pocket and cannot be exchanged for any other anions such as triflate ($CF_3SO_3^-$) or tetrafluroborate (BF_4^-). If the anion is substituted for another (*e.g.* sulfate) a different structure is observed in the form of a hexametallic complex (Fig. 51), thus showing that the anion is clearly the driving force behind the formation of these extraordinary complexes.

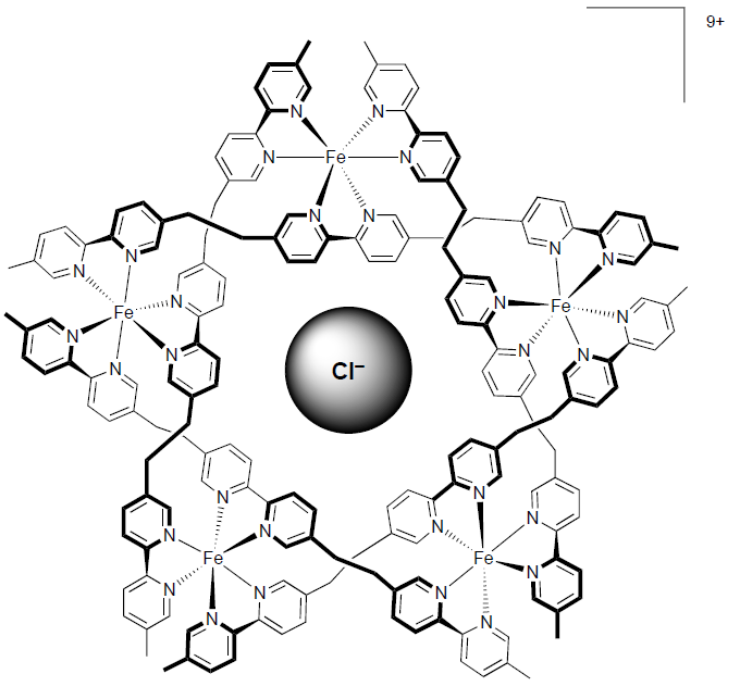

Fig. 50: Pentametallic circular helicate observed in the presence of Cl^-.[9]

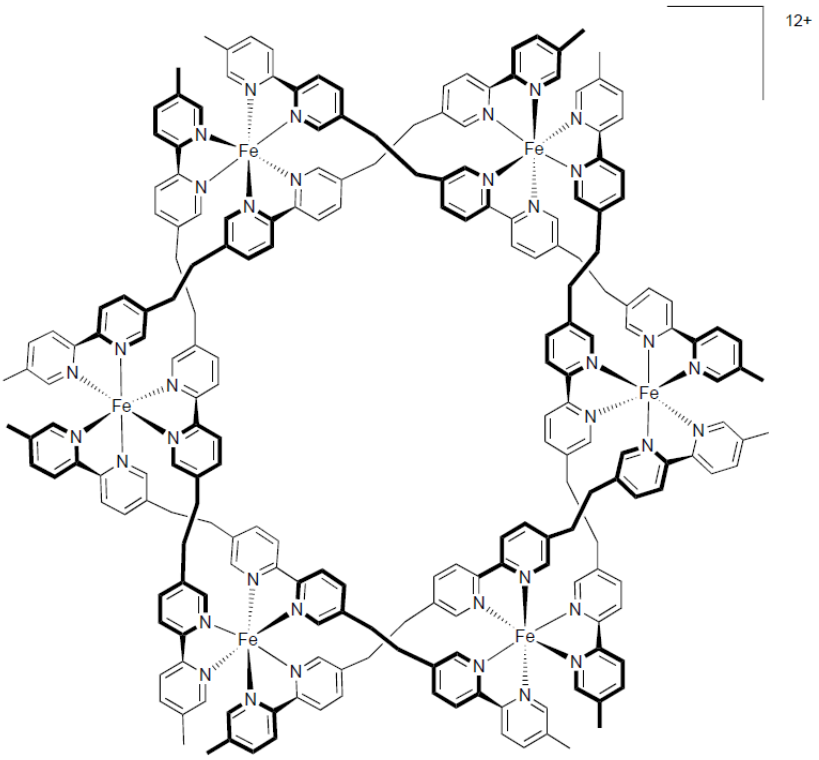

Fig. 51: Hexametallic circular helicate observed in the presence of SO_4^{2-}.[9]

1.7.7.3 Cages

This early work by Lehn *et al.* has led to the formation of some elaborate architectures using cations and anions to direct the course of assembly. In this section the formation of large supramolecular cages will be looked at along with the anions' contribution to the overall complex.

Cage complexes generally possess a central cavity with the potential to hold a guest, the nature of this guest is entirely dependent on the charge of the overall complex. For example, a neutral species would usually only bind solvent molecules within its cavity due to the lack of potential electrostatic interactions.[80,81] However, charged structures may readily bind anions which may exchange with others in solution.

Ward and co-workers synthesised two bis-bidentate bridging ligands (Fig. 52a & b) which upon coordination with cobalt(II) in the presence of either BF_4^- or ClO_4^- formed a tetrahedral cage complex (Fig. 53).[82]

a)

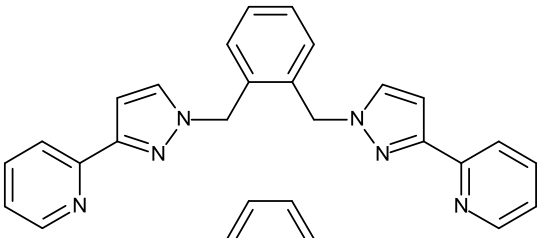

b)

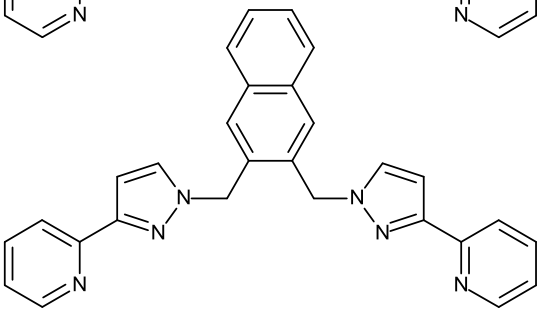

Fig. 52: Two bis-bidentate bridging ligands synthesised by Ward et al.

A large degree of pre-organisation is required to form the tetrahedral cage complex $[Co_4(\mu\text{-}L)_6X][X]_7$ (X = BF_4^- or ClO_4^-, L = ligands a or b).[82] The structure is aided by the anions complimentary charge, shape and size for the cavity, the BF_4^- tetrahedron is inverted with each fluoride positioned at the centre of a triangular face of the Co(4) tetrahedron. Ward *et al.* found that each of the Co···F bond lengths (5.61–5.98 Å) were similar indicating the anion is directly situated within the centre of the cavity. Thus leading to stabilising effects through hydrogen bonding interactions with the ligands CH_2 groups.

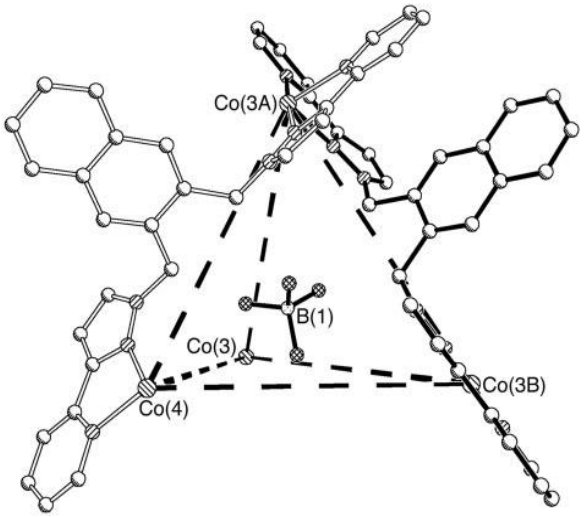

Fig. 53: Two L^b bridging ligands encapsulating a BF_4^- anion $[Co_4(L^b)_6(BF_4)][BF_4]_7$.[82]

Similarly Wu and co-workers developed a ligand containing a tris(bisurea) moiety centred around a symmetric triphenylamine group which formed a cage complex without the presence of a metal ion.[83] Using the urea group's exceptional ability to undergo strong hydrogen bonds with unsaturated anions, in this case PO_4^{3-}, they were able to form a strong and thermodynamically stable structure (Fig. 54). By incorporating themes from metal–ligand coordination Wu *et al.* showed the first anion-directed cage complex comprising 48 hydrogen bonds.

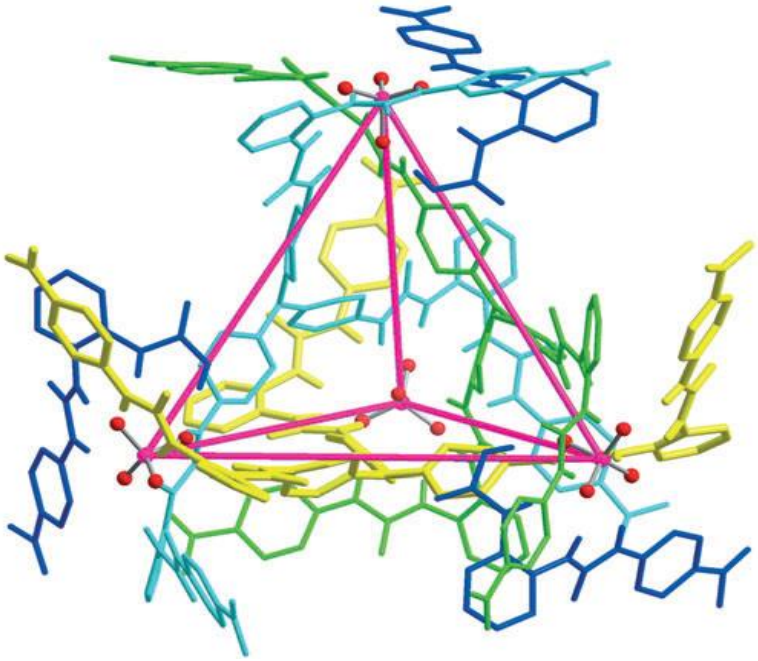

Fig. 54: A tetrahedral anion cage held together by PO_4^{3-} anions $[(PO_4)_4L_4]^{12-}$.[83]

1.7.7.4 Polymers

Wu *et al*. have since progressed their work to look at anion coordination polymers (ACPs) whereby a bis-bisurea ligand with a rigid naphthylene linker (Fig. 55) forms an ACP with a variety of different anions (sulfate, acetate and terephthalate).[84]

The ligand undergoes one-dimensional coordination with anions consequently forming ACPs. This has led to a number of different structures being observed on the addition of sulfate anions into the system. The bis-urea groups within the ligand hydrogen bond to the anion in a pincer-like fashion through a total of eight hydrogen bonds from four urea groups.

The rigid naphthalene linker holds the ligand in a linear direction with the sulfate ions acting as coordination nodes. Four urea group's hydrogen bond the anion whilst a further four from another ligand do the same in a chain like trend.[84]

Due to the long-range order exhibited by the information pre-programmed within the ligand, a continuous sharing of anion and binding sites is observed leading to the formation of an infinite polymer (Fig. 56 a & b).

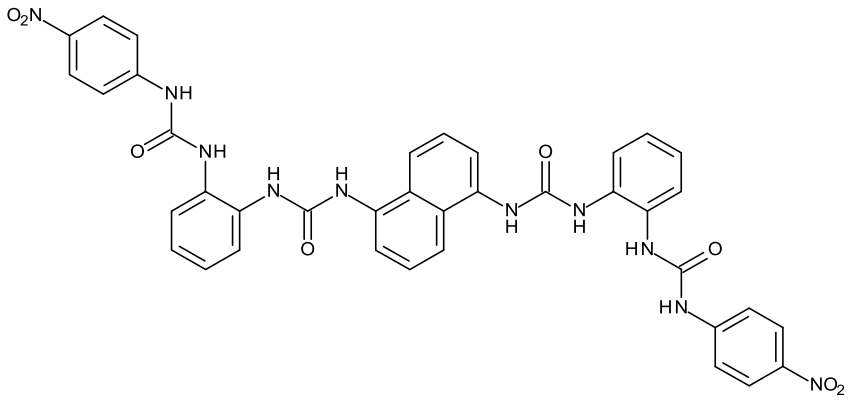

Fig. 55: Bis-bisurea ligand separated by a rigid naphthylene spacer.

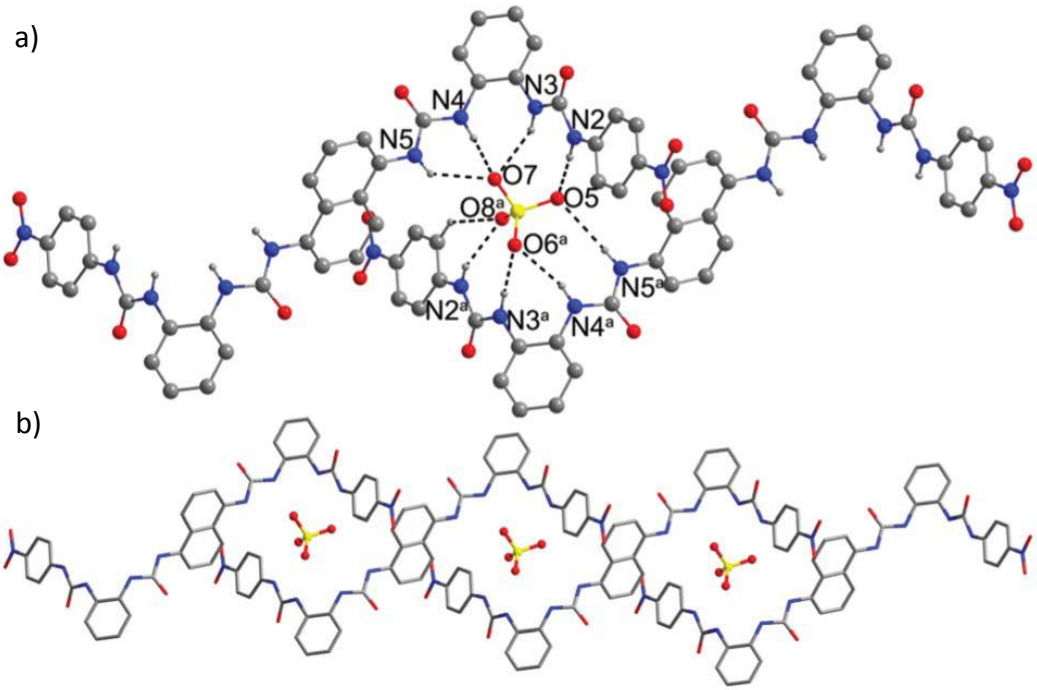

Fig. 56: a) Coordination sphere of the sulfate anion, b) A segment of the infinite 1-dimensional polymer.[84]

1.8 Ligand Design

The preparation and forethought that goes into the creation of a potential anion receptor is a lengthy process. The difficulties faced when trying to bind anions with any degree of selectivity or strength has been discussed at length throughout this report; however, despite the difficulties supramolecular chemists still persist to achieve new and unprecedented structures.

Before any complex can be created there are a number of design principles that must be considered:[85]

- The function of the target ligand
- Selectivity
- Conditions
- Binding interactions

1.8.1 Function

Before starting out it is important to consider the function of the ligand and the mechanism of detection of the anion; once the target species has been identified the chemist can work on the best way to achieve it, whether that be the correct binding domains, rigid spacers to act as scaffolding or lengthy side chains to aid solubility. All of this must be considered so that the chemist can design a ligand or receptor that is not only synthetically feasible but also selective for the target molecule.

1.8.2 Selectivity

Perhaps the most important factor is selectivity, as the receptors' success rests on its ability to bind the target molecule. Excellent binding strength and selectivity can be achieved by isolating the anion from its surrounding solvent via encapsulation within a rigid three dimensional host that is both complimentary in geometry and size. Such examples are outlined in a recent review by Gale and Caltagirone.[86] Gale and co-workers synthesised two cleft like anion receptors containing indole substituent's which selectively formed adducts with a smaller fluoride anion over its larger chloride counterpart. The ligands favourable interaction with fluoride anions over any other was due to the anions ability to fit within the cavity and undergo complimentary

hydrogen bonding interactions with the indole groups. Although simple in principle it can remain difficulty in reality, as even after the synthesis of a suitable complimentary host it is entirely possible that it will not prove rigid enough to prevent structural distortions therefore allowing the accommodation of competing guests.[52,86] It is therefore important to consider various outcomes; a structurally sound ligand must be created which is selective for the target species and can hold up to the demanding constraints of binding such as hydrophobicity and competing ions.[52]

1.8.3 Conditions

The conditions in which a receptor or ligand needs to work are of the upmost importance; there is no point creating a receptor for an anion if it cannot be detected within its environment. An example of this would be the requirement of an optimum pH for the target anion. It is also important that the host can survive the conditions of the environment with respect to solvation, chemical stability and solubility. It is important to consider that anions' charges are usually balanced in molecular systems by the presence of cations; this means that there may be a stoichiometric number of cations present which are natural competitors in the formation of supramolecular complexes. It is therefore important that the ligand used must undergo preferential binding to the target anion.[85]

1.8.4 Binding interactions

The way in which the target anion is bound by its receptor is a consideration for ligand design. There have been many different examples of binding species throughout this report including bipyridines, crown ethers, ureas and even boron based receptors, all of which use slightly different mechanisms for host-guest interactions. It is important to consider what functionality would best suit the capture of the target anion. For example, encapsulation is a well-known form of binding interaction and one which can be approached in many different ways. Encapsulation often focuses on the highest order of complementarity and pre-organisation, something which Ward *et al.* have explored in depth.[82]

Unlike the traditional receptor systems mentioned above, foldamers are one example of an encapsulating species that don't create a binding cavity brought about through a series of covalent bonds. Foldamers are made up of long monomeric chains which can be tailored to have a direct impact on the size of the cavity and therefore its ability to bind a target species. Furthermore the weak stabilizing interactions which are noncovalent in nature provide the foldamer with some degree of flexibility, a great advantage over their rigid counterparts.[87]

In a recent review, Jeong *et al* explored these species and their impact on anion binding. The information necessary for folding should be present in the design of the monomer; one example being the use of pyrrole groups as the designated hydrogen bond donor.[87,88] Pyrroles contain only hydrogen bond donors not acceptors, this fundamental design principle prevents the oligomeric strands from undergoing intra- or interstrand hydrogen bonding which could lead to a mass aggregation of the foldamers.[87,88] One example of a pyrrole containing foldamer for the use of encapsulation of anionic species was produced by Sessler *et al.*[89,90] Using a hexapyrrole ligand Sessler was able to successfully encapsulate two Cl^- anions with each hydrogen bonding three of the six pyrrole groups (Fig. 57). Analysis of the crystal structure revealed that the foldamer exists in a planar geometry with an extended S-shaped conformation comprising of two pockets each containing a chloride ion.[90]

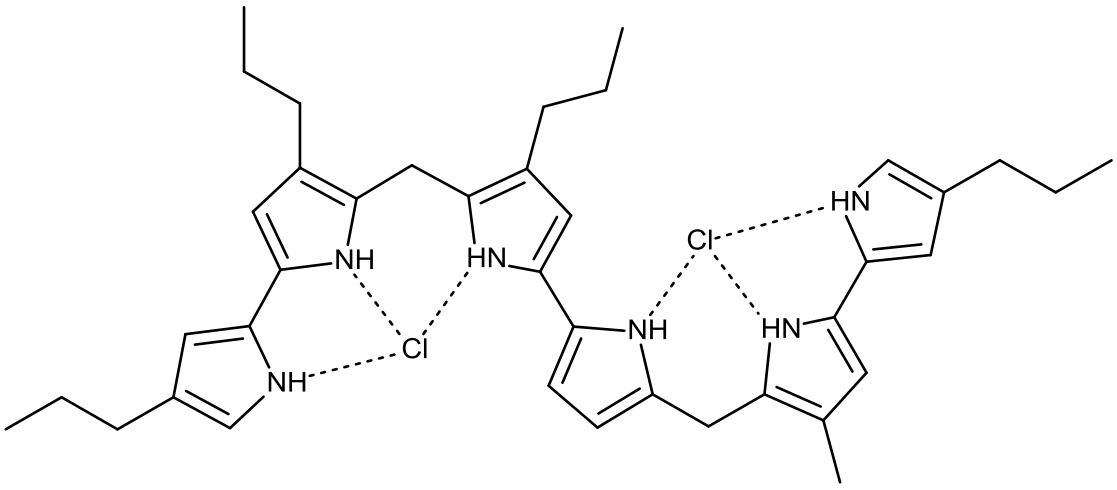

Fig. 57: Oligopyrrole ligand coordinating two chloride anions through hydrogen bonding.

1.9. Aims:

The overall aim of this research is to synthesise ditopic ligands that are capable of both coordination of transition metal cations and interaction with anions. It is hoped that either; the interaction of anions will affect the coordination chemistry of the ligand strand or vice versa, e.g. the coordination of metal ions will affect the way the anions are bound. This work is centred upon the synthesis of multi-dentate pyridyl-thiazole containing ligands which are good coordinators of transition metal ions and the inclusion of either amide or amine units which are well known to interact strongly with anions. The metal binding domains within the ligand strand will vary along with the exact position of the anion binding unit.

Chapter two focuses on the development of work carried out by Cox *et. al*. to expand upon the ligand **[L^1]** that not only acts as an cation coordinating unit through interaction of the metal ion and the ligands *N*-donor units (bipyridine and two thiazole units), but in addition displays preferential interactions with a series of anions. Its thought that coordination of the tetradentate *N*-donor domain with a *divalent* metal cation may leave the acetyl-amide arms free for further interaction with a variety of anions and single crystal X-ray diffraction could be used to analyse the complex in the solid state. Furthermore reaction of the ligand with *monovalent* cations could possibly result in the partitioning of the ligand into two bidentate binding domains resulting in the formation of a dinuclear double helicate. Additionally it is hoped that interaction of anions with the amide substituents on the ligand chain may induce a conformational change and therefore give different structures in the solid state.

In addition to the further development of **[L^1]**, the aim of chapter three is to grow this body of research to include a second ligand **[L^2]** that contains the same *N*-donor heterocycles for the coordination of cations but increased functionality of the ligand arms. In theory the inclusion of a second acetyl / amide functional group for the interaction with anions will increase the ligands ability to undergo hydrogen bonding interactions, thus creating a larger guest species for anion coordination.

The target of chapters four and five is to synthesise a pair of ligands (**[L^3]** and **[L^4]**) which are made up of the same bipyridine / thiazole *N*-donor architecture shown in

chapters two and three. However, the arrangement and functionality of the ligand arms will be decidedly different.

The aim of chapters four and five is to change the groups capable of hydrogen bonding interactions with anions. It is hoped that altering the ligand strand to include some large, bulky groups such as indoles and phenyls may lead to some novel structural changes when coordinated with both mono and divalent metal ions. Therefore incorporating a urea group **[L^3]** and indole group **[L^4]** onto the terminal position of the ligand arms is thought to have a dramatic effect on the ligands ability to form long range order complexes and therefore may lead to the a series of different structures in the solid-state.

The goal of chapter six is to focus on a ligand strand **[L^5]** which unlike ligands **[L^1]** – **[L^4]** will contain an amine unit, not on the periphery of the ligand strand but incorporated within the actual ligand chain. It is hoped that the central position of these anion binding units will result in a change in the coordination ability of the ligand unit when the self-assembled complexes are reacted with different anions.

The final chapter (seven) will expand on the work carried out in chapter six by taking the existing ligand **[L^5]** and altering its functionality through substituting the central phenyl group for a series of different spacers such as; pyridine, di-substituted naphthalene and phenanthrene. The idea being that including additional *N*-donors or larger spacers with conformational rigidity may lead to different coordination properties.

2. Chapter 2: Synthesis and coordination chemistry of a ligand containing both N-donor and hydrogen bond donor units separated by a central bi-pyridine ring:

The ligand **[L^1]** is a ditopic species which contains both a bipyridyl-dithiazole domain and two acetyl-amide groups in the 3-position of each central bipyridine units (Fig. 58). The central bipyridyl-dithiazole domain has the potential to act as chelating units for the coordination of metal ions, whilst each acetyl-amide arm has the functionality and arrangement to undergo interactions with anions.

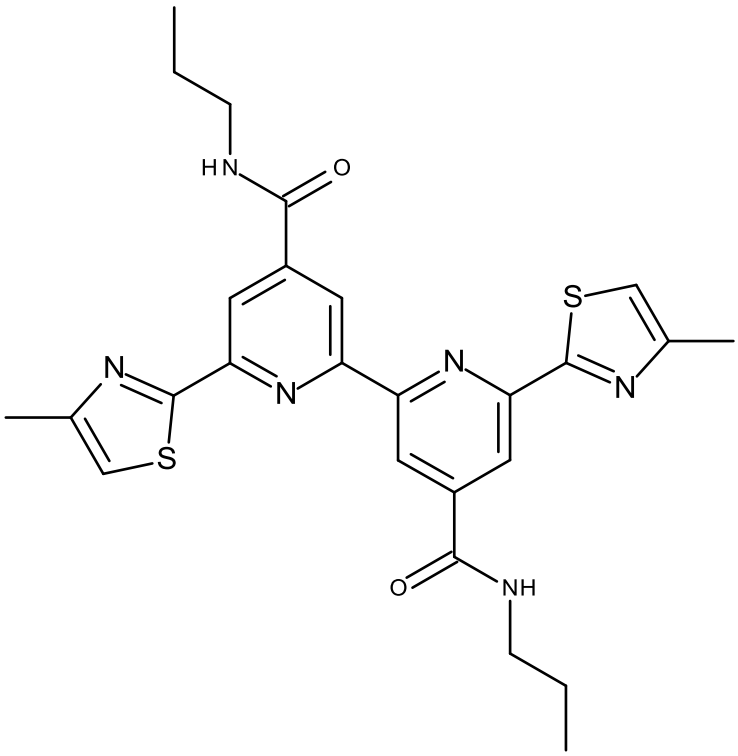

Fig. 58: Bis-bidentate amine-containing ligand **[L^1].**

2.0 Synthesis of [L^1]:

Synthesis of **[L^1]** was carried out in a multi-step process (Scheme 1). Firstly 4',4-dimethyl-2',2-bipyridyl **[1]** was reacted with an excess of chromium oxide in concentrated sulphuric acid at 0°C before heating at 75°C for four hours. Following the reaction 20 mL of H_2O was added and a series of acid and base extractions carried out, giving the diacid **[2]**. Confirmation of the successful formation of this species was obtained by ^{1}H NMR spectroscopy which showed a total of four signals; three aromatic signals (8.92, 8.85 and 7.92 ppm respectively) integrating to six protons corresponding to the aromatic pyridine rings, but importantly the spectrum shows a broad singlet at 13.85 ppm which is indicative of a carboxylic acid group.

The diacid was then reacted with thionyl chloride for 12 hours under N_2 to give the acid chloride **[3]**. The resulting product was then dissolved in anhydrous DCM and propylamine added at 0°C. After 12 hours at room temperature the reaction gave the diamine **[4]** which precipitated out of solution. Confirmation of the successful synthesis of the product was obtained by ^{1}H NMR spectroscopy which showed a total of seven proton environments; the signals of note are three aromatic protons at 8.87, 8.79 and 7.86 ppm corresponding to the pyridine ring and a triplet at 8.97 ppm which corresponds to the NH proton.

Activation of the bipyridine was carried out by a reaction of the diamide with a slight two-fold excess of *m*CPBA in DCM at 50°C. Column chromatography using a silica solid phase gave the bis-*N*-oxide as a pure solid **[5]**. Confirmation of the pure product was obtained via ^{1}H NMR spectroscopy which showed seven proton signals however there had been an increased shift in the ppm of the aromatic peaks due to the oxidized nitrogen atoms 8.50, 8.15 & 7.98 ppm respectively.

The bis-*N*-oxide was then dissolved in DCM and to this added benzoyl chloride and TMS-CN and the reaction warmed to 50°C for four hours. The reaction was then allowed to stand for 20 hours at room temperature during which time a precipitate formed which was filtered off to give the di-cyano as a solid **[6]**. Confirmation of successful formation of the product was obtained by ^{1}H NMR spectroscopy which showed a total of six signals with only two aromatic protons (8.91 and 8.47 ppm), this

is due to the loss of an aromatic proton (previously observed at 7 ppm) by incorporation of the cyano group. The di-cyano was then reacted with H_2S in ethanol giving the bipy-thioamide **[7]** as a precipitate. Confirmation of the product was carried out by ^{1}H NMR spectroscopy which showed a total of eight protons; signals of note are two aromatic singles at 9.19 and 8.94 ppm, an amine signal at 9.03 ppm and a further two singlets at 10.51 and 10.31 ppm corresponding to the thioamide group.

The thioamide was further reacted with chloroacetone in ethanol to yield the protonated ligand **[L^1]**. The solid was suspended overnight in concentrated ammonia to yield **[L^1]** as the free base. Confirmation of the successful synthesis of **[L^1]** was carried out by ^{1}H NMR spectroscopy which showed a total of eight proton environments; the most noteworthy being a noticeable singlet at 7.57 ppm corresponding to the formation of a thiazole ring. Furthermore the product was not soluble enough for ^{13}C NMR spectroscopy however an ESI-MS showed an ion at *m/z* 521 corresponding to $[\mathbf{L^1}+H]^+$.

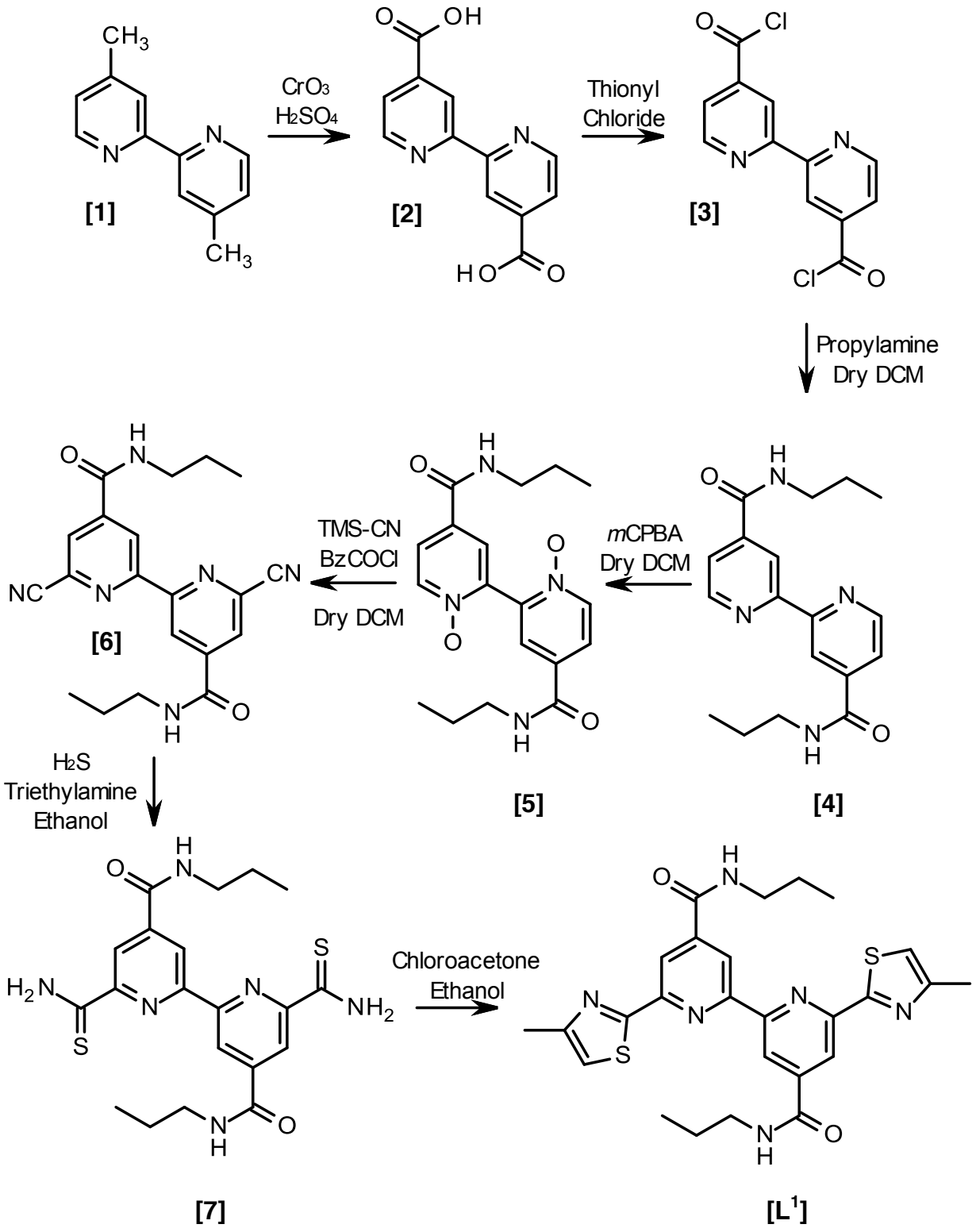

Scheme 1: Synthesis of ***[L^1]***.

3.0 Coordination Chemistry of [L^1]:

2.1.1 Coordination with $Co(BF_4)_2$:

Reaction of the ligand **[L^1]** with $Co(BF_4)_2$ in MeCN gave a clear pale orange solution from which orange crystals formed upon slow diffusion of diisopropyl ether. Analysis by single-crystal X-ray diffraction showed that in the solid state a mono-nuclear species ($[Co(\mathbf{L^1})](BF_4)_2$) is formed. The ligand acts as a planar tetradentate donor coordinating the equatorial coordination sites of the metal ion (Fig.59). The cobalt ion is further coordinated by two water molecules giving a vaguely octahedral geometry (ave. Co-N bond length 2.200 Å; ave. Co-O bond length 2.027 Å).

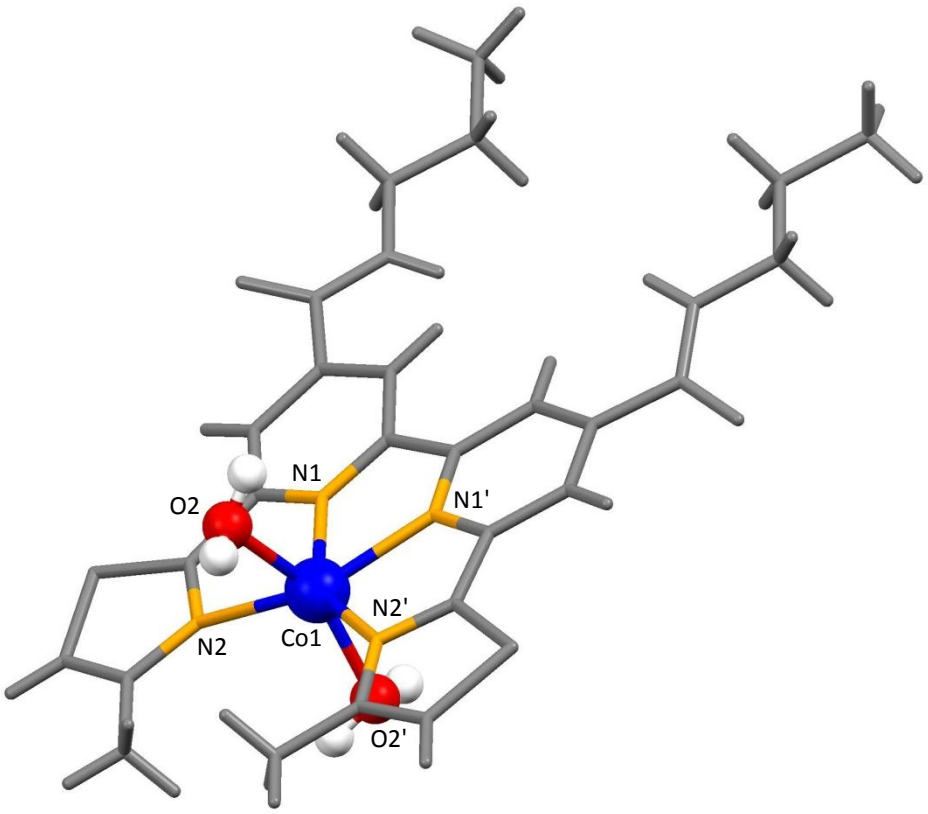

Fig. 59: Solid state structure of ($[Co(\mathbf{L^1})(H_2O)_2](BF_4)_2$) anions omitted for clarity.

On the opposite side of the complex the two amide groups lie co-planar with the central bipyridine units with both amides pointing towards each other (Fig. 60). Furthermore two tetrafluoroborate anions lie slightly above and below the plane of the complex (Fig. 61a, b & c). Each of these form short contacts to the amide hydrogen atoms and the aromatic hydrogen atoms in the 3,3'-position of the bipyridine units.

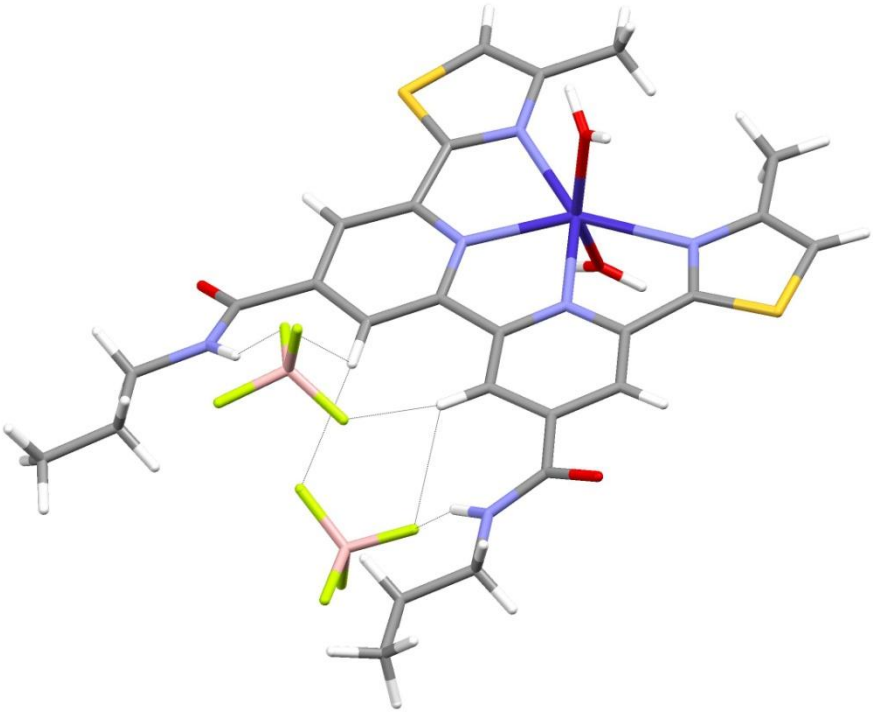

*Fig. 60: Capped stick view of complex ([Co(**L**^{1})(H_2O)$_2$](BF_4)$_2$), showing the arrangement of the amide groups.*

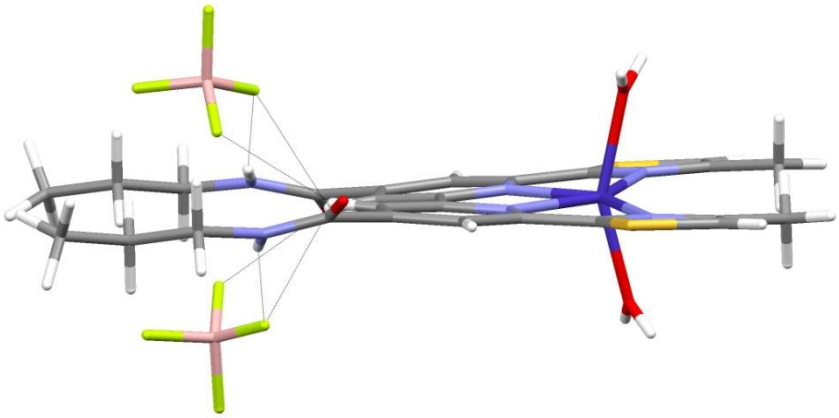

*Fig. 61a: Side view of ([Co(**L**^{1})(H_2O)$_2$](BF_4)$_2$) showing the position of the BF_4 anions in relation to the plane of the complex.*

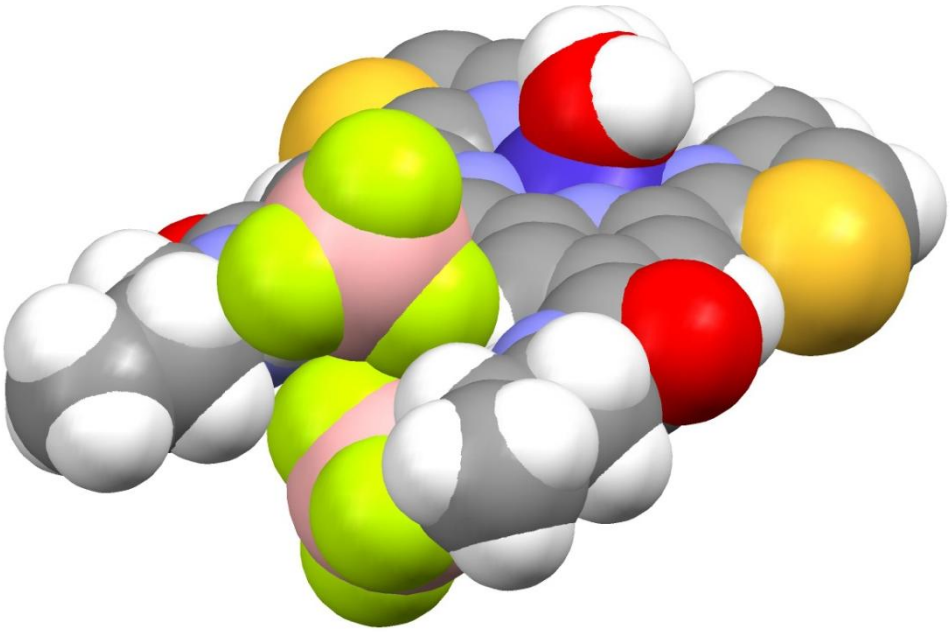

Fig. 61b: Space filling model of ([Co(L^1)(H_2O)$_2$](BF_4)$_2$).

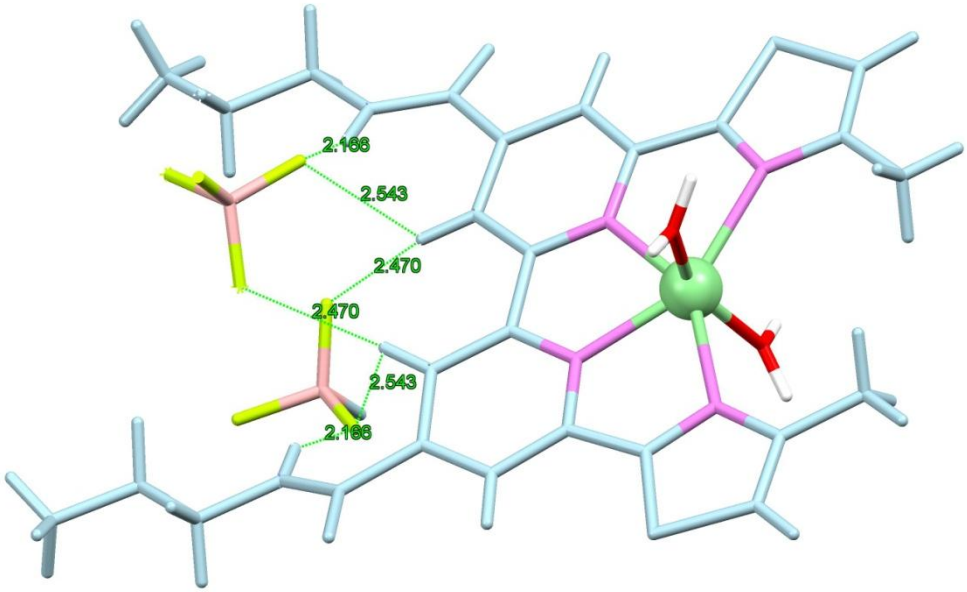

Fig. 61c: Anion interactions ([Co(L^1)(H_2O)$_2$](BF_4)$_2$).

Selected bond lengths and angles for the complex are shown in tables 1.1 and 1.2 below; relevant atom labels are shown in Fig. 59.

Atom 1	Atom 2	Bond Length (Å)
Co1	N1	2.1198 (2)
Co1	N2	2.2814 (2)
Co1	O2	2.0269 (2)

*Table 1.1: Selected bond lengths for complex ([Co(**L**^{1})(H_2O)$_2$](BF_4)$_2$).*

Atom 1	Atom 2	Atom 3	Bond Angle (°)
N1	Co1	N2	74.43 (12)
N1	Co1	O2	97.62 (12)
N2	Co1	O2	84.56 (13)
N1	Co1	N1´	73.91 (17)
N1	Co1	N2´	148.19 (13)
N1	Co1	O2´	102.61 (14)
N2	Co1	N1´	148.19 (13)
N2	Co1	N2´	137.34 (18)
N2	Co1	O2’	86.28 (12)
O2	Co1	O2´	154.60 (2)

*Table 1.2: Selected bond angles for complex ([Co(**L**^{1})(H_2O)$_2$](BF_4)$_2$).*

2.1.2 Coordination with $Hg(ClO_4)_2$:

Reaction of **[L^1]** with $Hg(ClO_4)_2$ in MeCN resulted in a colourless solution from which colourless crystals were produced upon slow diffusion of diisopropyl ether. Analysis by single X-ray diffraction showed that the ligand remained a planar mononuclear species ($[Hg(\mathbf{L^1})](ClO_4)_2$). The Hg metal ion retains its preference for an octahedral geometry with each pyridyl/thiazole domain acting as a planar tetradentate donor as seen in the previous crystal structure (Fig. 62). (ave. Hg-N 2.3105 Å).

However, unlike the Co^{2+} complex the two amide units are pointing away from each other and these form intermolecular interactions to the carbonyl oxygen atoms of a different complex (Fig. 63).

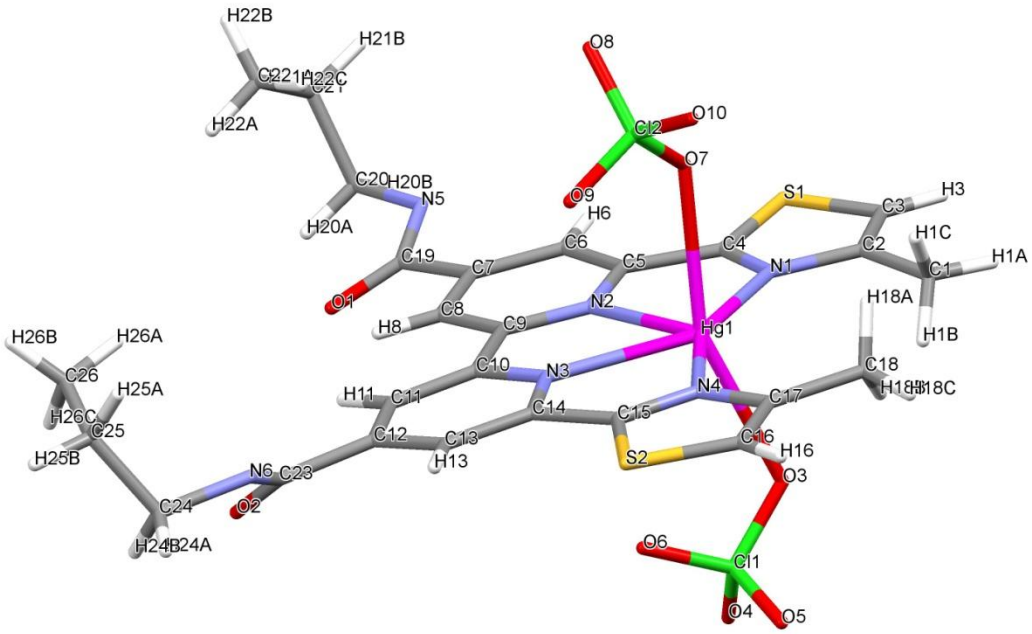

Fig. 62: Solid state structure of ($[Hg(\mathbf{L^1})](ClO_4)_2$).

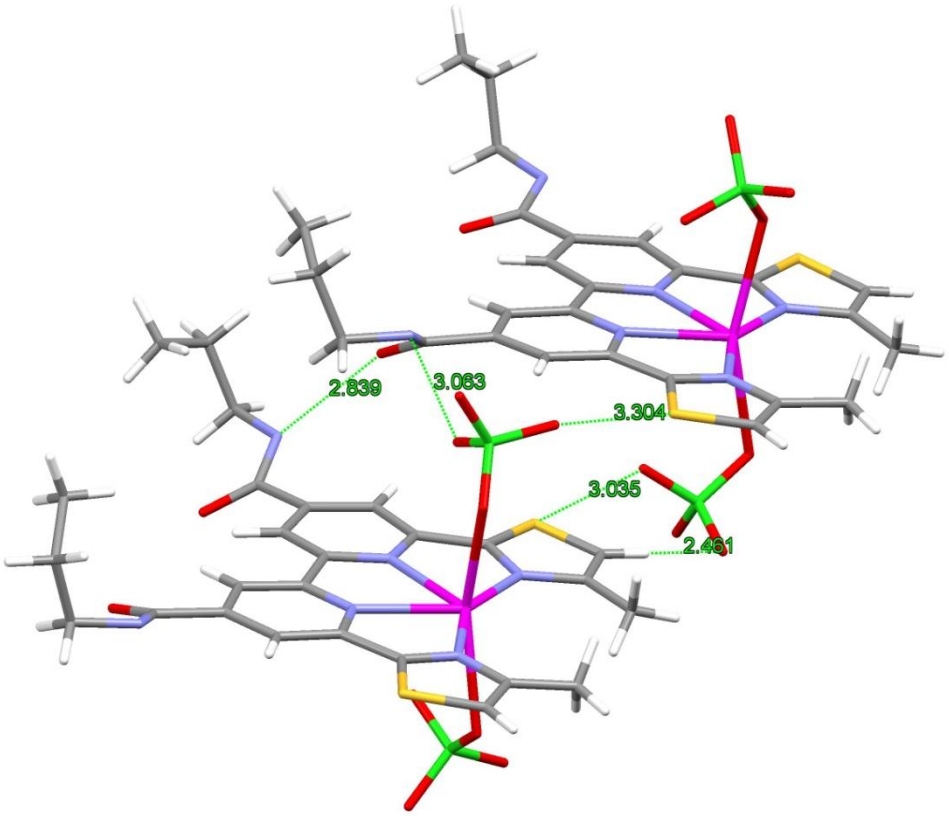

Fig. 63: Short interactions between neighbouring complexes.

Furthermore, unlike the cobalt structure the mercury ions coordination sphere isn't completed by water molecules but by the perchlorate counter ions. This difference is possibly due to both the coordinating ability of the perchlorate counter ion and the soft nature of the mercury ion.

The perchlorate anions which are coordinated to the metal ion undergo a series of interactions with the hydrogen atoms of the pyridine rings *and* the amide arm of a second structure resulting in a sequence of long range order interactions (Fig. 64a & b).

ESI-MS was carried out in order to confirm the solution-state behaviour and this analysis gave two distinct ions at *m/z* 821 and 1741. The smaller ion corresponds to the complex $\{[Hg(\mathbf{L^1})(ClO_4)]\}^+$ showing this persists in solution. However, the larger ion corresponds to the dinuclear double helicate $\{[Hg_2(\mathbf{L^1})_2(ClO_4)_3]\}^+$ which indicates that there is some aggregation during the ESI-MS process resulting in this dinuclear species.

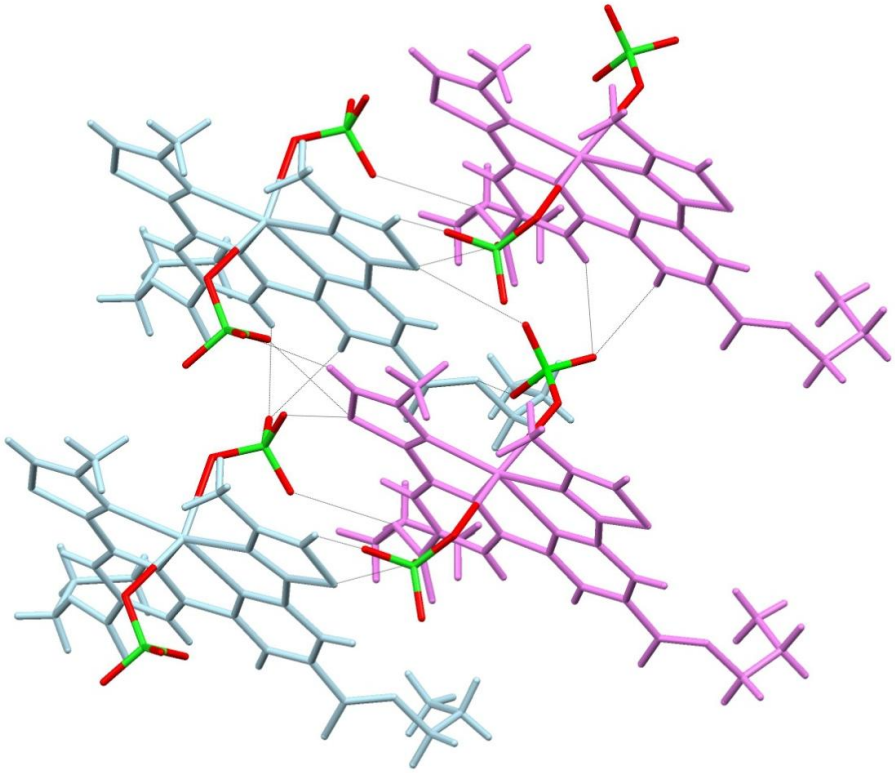

*Fig. 64a: Solid state structure of ([Hg(**L**^{1})](ClO$_4$)$_2$), showing the hydrogen bonding interactions between the axial perchlorate anion and neighbouring protons.*

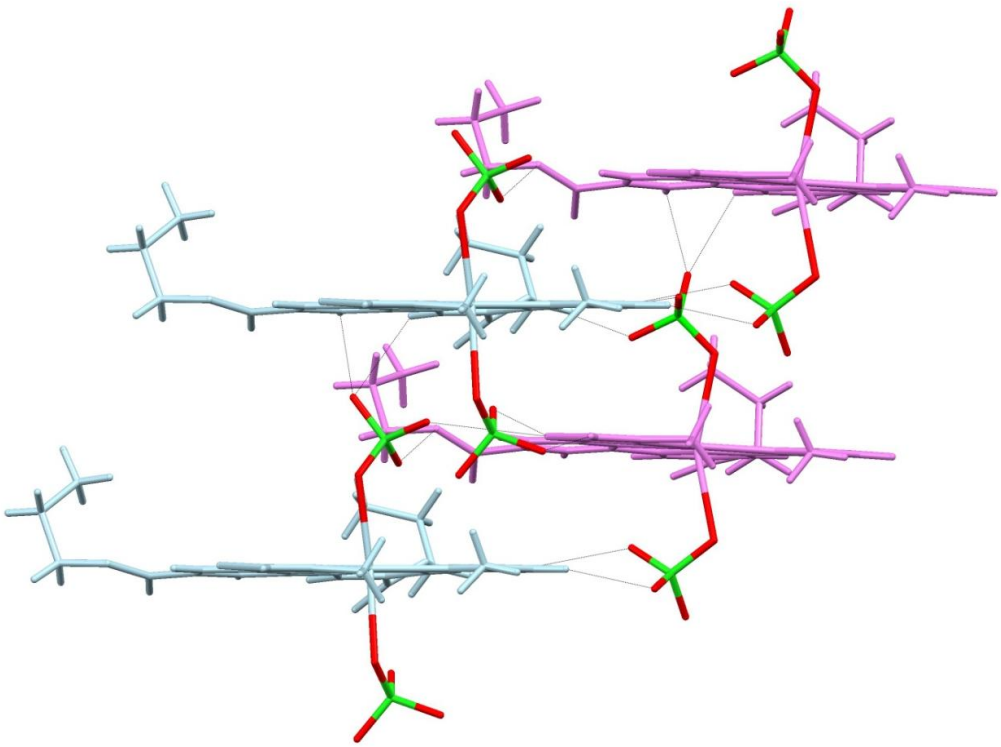

Fig. 64b: Long range stacking of the complex ([Hg(**L**^{1})](ClO$_4$)$_2$).

Selected bond lengths and angles for the complex are shown in tables 1.3 and 1.4 below; relevant atom labels are shown in Fig. 62.

Atom 1	Atom 2	Bond Length (Å)
Hg1	N4	2.2061 (1)
Hg1	N1	2.2251 (1)
Hg1	N2	2.4172 (1)
Hg1	N3	2.3938 (1)
Hg1	O3	2.6458 (1)
Hg1	O7	2.5420 (1)

*Table 1.3: Selected bond lengths for complex ([Hg(**L**^{1})](ClO$_4$)$_2$).*

Atom 1	Atom 2	Atom 3	Bond Angle (°)
N4	Hg1	N1	153.89
N4	Hg1	N2	136.20
N4	Hg1	N3	70.97
N4	Hg1	O3	92.21
N4	Hg1	O7	98.40
N1	Hg1	N2	69.90
N1	Hg1	N3	135.13
N1	Hg1	O3	80.45
N1	Hg1	O7	80.80
N2	Hg1	N3	65.24
N2	Hg1	O3	99.29
N2	Hg1	O7	87.56
N3	Hg1	O3	106.97
N3	Hg1	O7	96.43
O3	Hg1	O7	156.40

*Table 1.4: Selected bond angles for complex ([Hg(**L**^{1})](ClO$_4$)$_2$).*

2.1.3 Coordination of [L^1] with Cu(I) and anions; (PF_6^-), (ClO_4^-), (BF_4^-) and (NO_3^-):

Reaction of **[L^1]** with Cu(PF_6) in MeCN with 1 equivalent of tetra-*N*-butyl ammonium perchlorate resulted in a deep red solution from which dark red / brown crystals were formed upon slow diffusion of ethyl acetate. Single X-ray diffraction showed that in the solid state the ligand formed a dinuclear double helicate ($[Cu_2(\mathbf{L^1})_2](ClO_4)_2$) (Fig. 65a).

The ligand strand partitions into two distinct binding domains with a pyridyl / thiazole unit of each ligand coordinating a different metal ion (ave. N – Cu 2.0485 Å). Through formation of the double helicate the amide arms can no longer form the co-planer arrangement seen previously in the Co^{2+} and Hg^{2+} structures. Instead the amide hydrogen atoms point in opposite directions; this creates a pocket on either end of the structure capable of further interactions with anions (Fig.65b).

a)

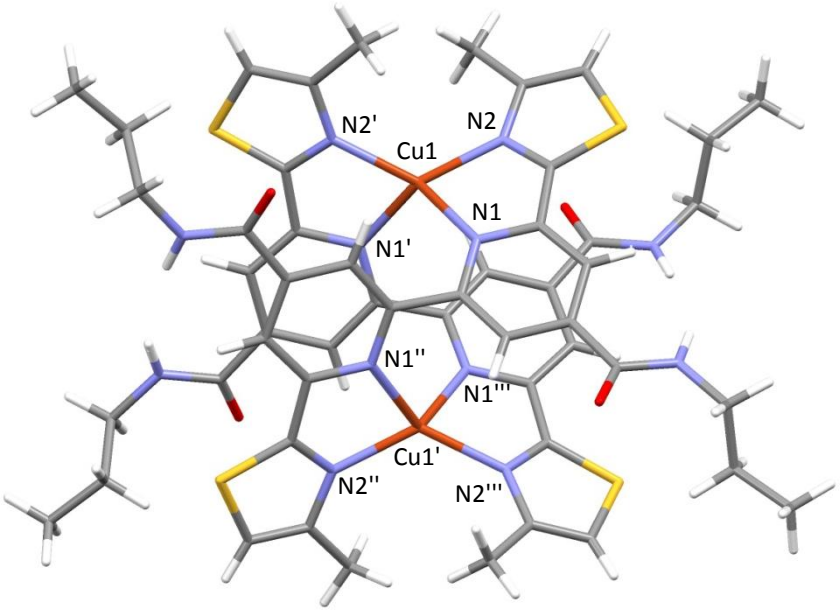

b)

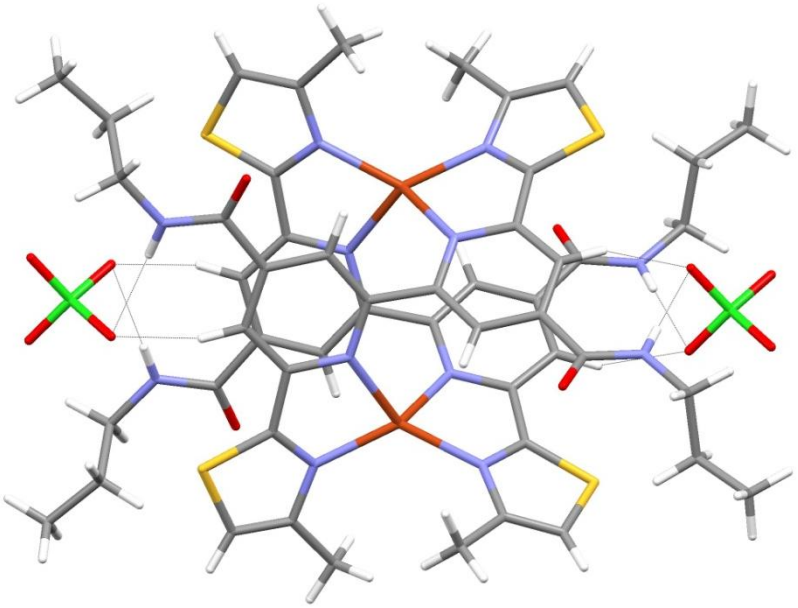

Fig. 65: a) Solid state structure of ([Cu_2($\mathbf{L^1}$)$_2$](ClO_4)$_2$) with anions omitted, b) Hydrogen bonding interactions of perchlorate anions with the amide functional groups.

As seen in Fig 65b the pocket that binds the anions arises from two different amide groups from different ligand strands. The binding is supplemented by interactions with the aromatic hydrogen atoms in the 5,5'-position of the central bipyridine ring (Fig.66).

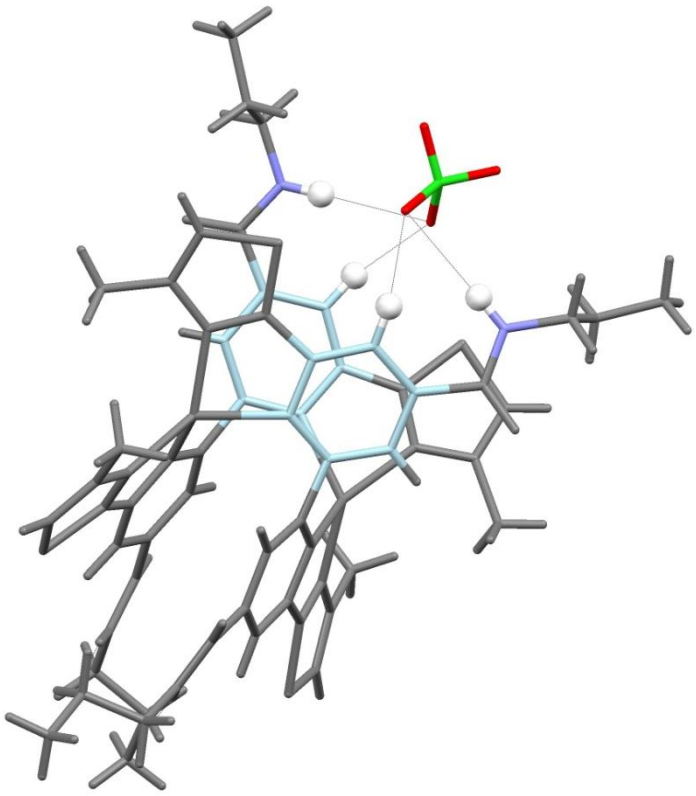

*Fig. 66: Solid state structure of ([Cu_2(**L**^{1})$_2$](ClO_4)$_2$) showing the interactions between the hydrogen atoms in the* 5,5'-position of the central bipyridine ring and the perchlorate anion (other anions omitted for clarity).

The preference for Cu(I) to adopt a tetrahedral coordination geometry foregoes the need for a planar species previously observed with octahedral cations (Co^{2+} & Hg^{2+}), instead a double helicate is brought about through the complete coordination of Cu(I) by the pyridine / thiazole units of each ligand strand. With the metal ions coordination sphere fulfilled by the ligand the perchlorate ion undergos hydrogen bonding interactions with the pyridine and amide arms (ave. NH···O 2.489 Å). This leaves the perchlorate anion with two free oxygen atoms which then undergo further hydrogen bonding interactions with the arms of a second structure in a polymeric motif (Fig. 67a, b & c).

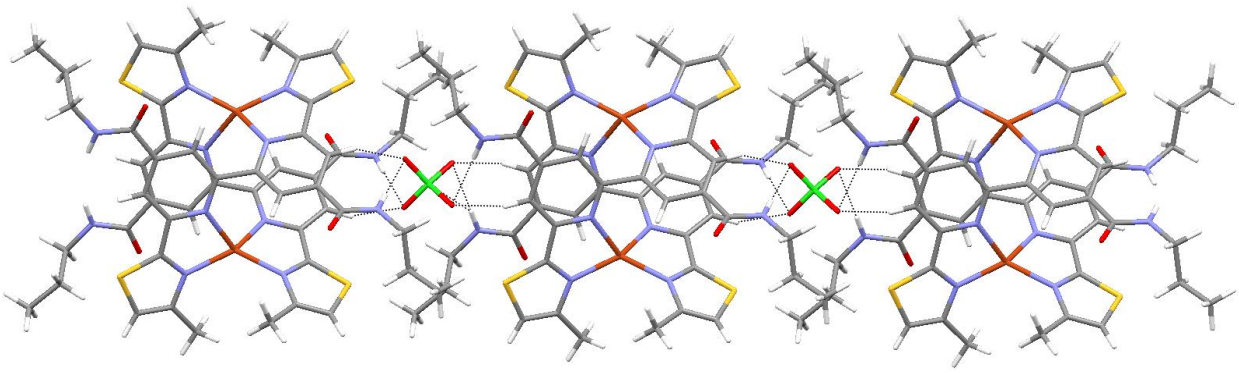

Fig. 67a: Long range order of the complex ($[Cu_2(\mathbf{L^1})_2](ClO_4)_2$).

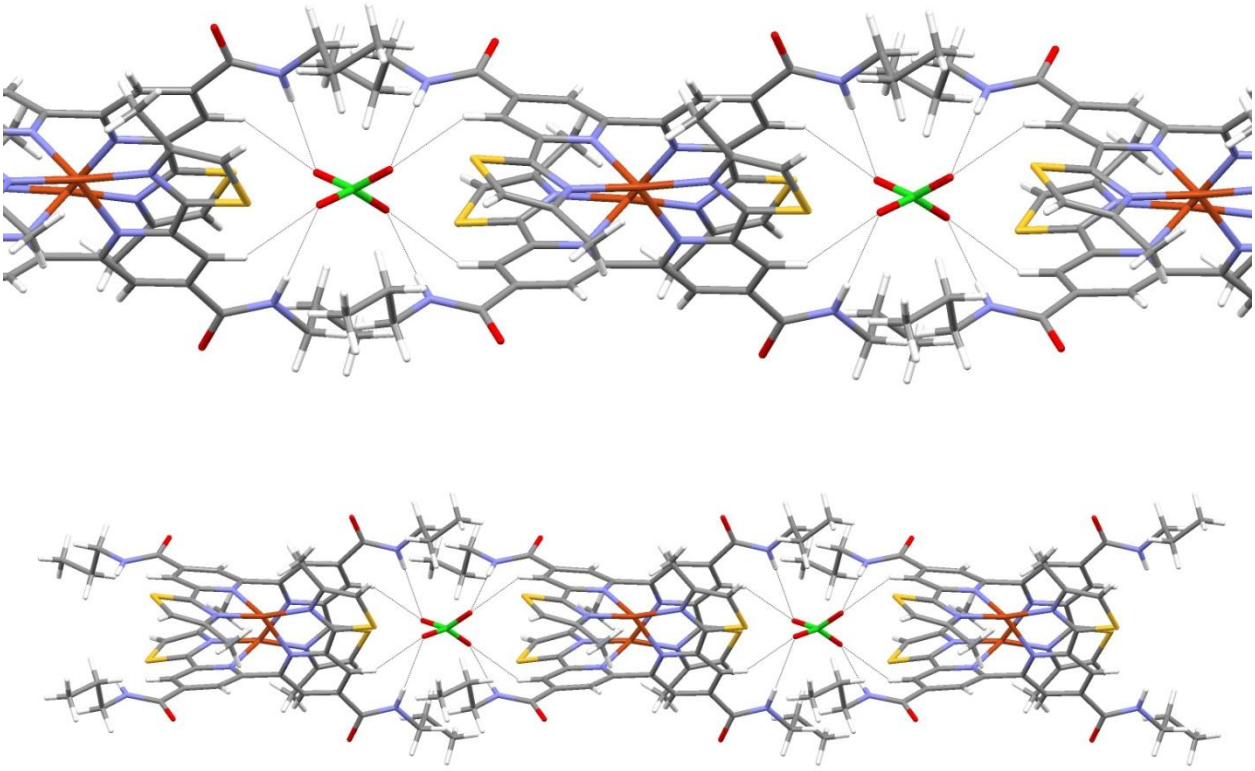

Fig. 67b & c: Contrasting views showing the long range order of ($[Cu_2(\mathbf{L^1})_2](ClO_4)_2$).

Selected bond lengths and angles for the complex are shown in tables 1.5 and 1.6 below; relevant atom labels are shown in Fig. 66a.

Atom 1	Atom 2	Bond Length (Å)
Cu1	N1	2.0899 (3)
Cu1	N2	2.0069 (3)

* The complex lies on a special position and only half of the molecule is crystallographically unique with the remaining molecule generated by symmetry.

Table 1.5: Selected bond lengths for complex ($[Cu_2(\mathbf{L^1})_2](ClO_4)_2$).

Atom 1	Atom 2	Atom 3	Bond Angle (°)
N1	Cu1	N2	80.15 (12)
N1	Cu1	N1'	106.36 (14)
N1	Cu1	N2'	134.75 (12)
N2	Cu1	N1'	134.75 (12)
N2	Cu1	N2'	127.19 (18)

* The complex lies on a special position and only half of the molecule is crystallographically unique with the remaining molecule generated by symmetry.

Table 1.6: Selected bond angles for complex ($[Cu_2(\mathbf{L^1})_2](ClO_4)_2$).

Reaction of $Cu(PF_6)$ with 1 equivalence of tetra-*N*-butyl-ammonium tetrafluroborate (in-place of ClO_4^-) resulted in an essentially iso-structural assembly ($[Cu_2(\mathbf{L^1})_2](BF_4)_2$). Reaction of the complex with BF_4^- in MeCN resulted in a dark red solution from which dark brown / red crystals were recovered upon slow diffusion of diisopropyl ether.

In a similar manner to the previous structure the ligand forms a dinuclear double helicate with monovalent cations, undergoing tetrahedral coordination. The amide containing arms undergo hydrogen bonding to the anions in the same manner previously seen in the complex ($[Cu_2(\mathbf{L^1})_2](ClO_4)_2$), suggesting that the formation of the double helicate is not anion dependant (Fig. 68a & b) nor is the formation of the anion-binding polymeric structure as two of the fluoride atoms form hydrogen bonds with

the amides of one complex and the remaining two fluoride atoms hydrogen bond a different set of amides leading to a polymeric array in the solid-state.

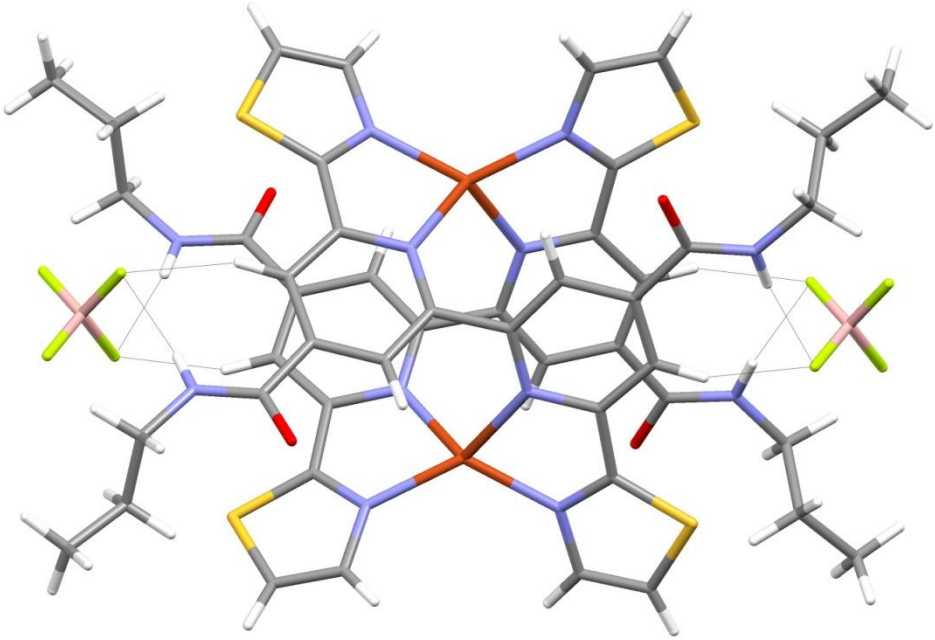

Fig. 68a: Solid state structure of ($[Cu_2(\mathbf{L^1})_2](BF_4)_2$).

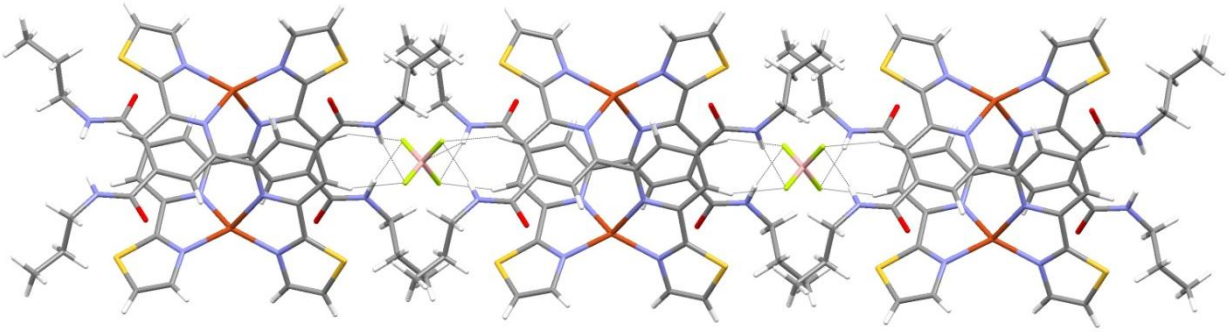

Fig. 68b: Solid state structure of ($[Cu_2(\mathbf{L^1})_2](BF_4)_2$) polymer.

Selected bond lengths and angles for the complex are shown in tables 1.7 and 1.8 below;

Atom 1	Atom 2	Bond Length (Å)
Cu1	N1	2.084 (3)
Cu1	N2	2.005 (3)

* The complex lies on a special position and only half of the molecule is crystallographically unique with the remaining molecule generated by symmetry.

Table 1.7: Selected bond lengths for complex ($[Cu_2(\mathbf{L^1})_2](BF_4)_2$).

Atom 1	Atom 2	Atom 3	Bond Angle (°)
N2	Cu1	N1	80.44 (14)
N2	Cu1	N2	126.80 (2)
N2	Cu1	N1	134.56 (15)
N1	Cu1	N2	134.56 (15)
N1	Cu1	N1	106.51 (17)
N2	Cu1	N1	80.44 (14)

* The complex lies on a special position and only half of the molecule is crystallographically unique with the remaining molecule generated by symmetry.

Table 1.8: Selected bond angles for complex ($[Cu_2(\mathbf{L^1})_2](BF_4)_2$).

Furthermore, when $Cu(PF_6)$ was reacted with a trigonal planar anion in the form of tetra-*N*-butyl ammonium nitrate (NO_3^-) (in-place of ClO_4^- & BF_4^-) it gave a dark red solution from which red crystal were recovered upon slow diffusion of diisopropyl ether. In the solid-state an analogous di-nuclear double helicate was observed ($[Cu_2(\mathbf{L^1})_2](NO_3)_2$) (Fig. 69).

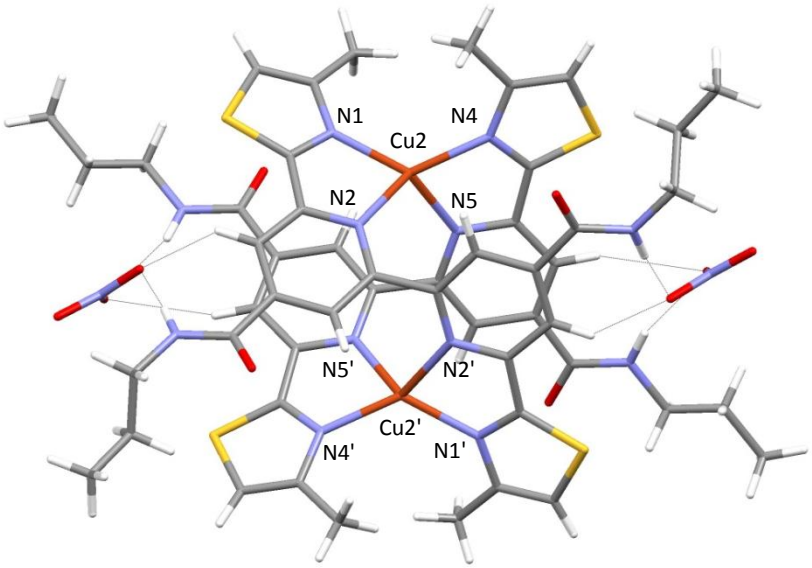

Fig. 69: Solid state structure of ($[Cu_2(\mathbf{L^1})_2](NO_3)_2$).

The arrangement of the structure is comparable with complexes that were reacted with tetrahedral anions, suggesting that the formation of the di-nuclear double helicate is entirely cation dependant. The metal ions preference for a tetrahedral coordination geometry is met by the pyridyl and thiazole groups of two separate ligands with the nitrate anion encapsulated by hydrogen bonding interactions to the amide arms and the pyridyl protons of not only two separate structures but also two separate ligand strands (Fig. 70a & b).

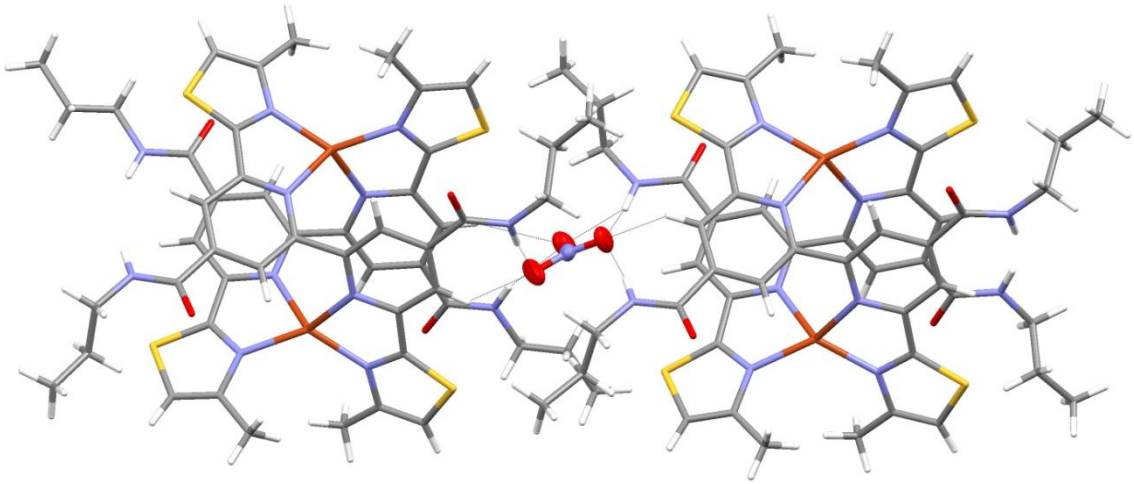

Fig. 70a: Solid state structure of ($[Cu_2(\mathbf{L^1})_2](NO_3)_2$) polymer (side view).

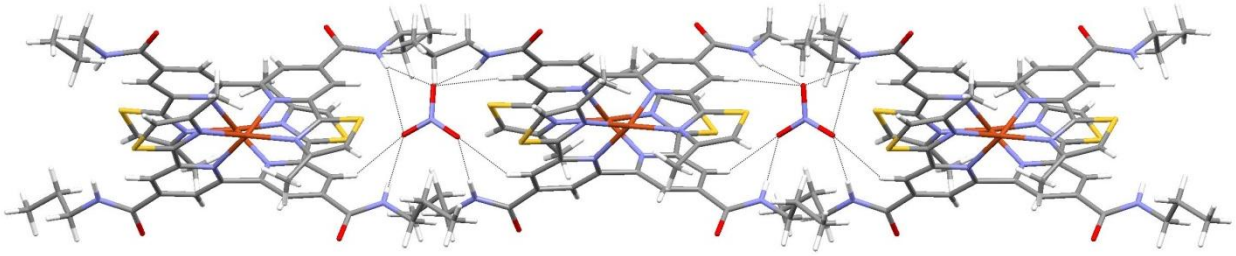

Fig. 70b: Solid state structure of ([Cu_2($\mathbf{L^1}$)$_2$](NO_3)$_2$) polymer (axial view).

Confirmation of the assemblies was achieved by ESI-MS which showed that in all cases that the PF_6 ion had been displaced and replaced by ClO_4^-, BF_4^- or NO_3^- anions.

An ESI-MS of the complex [($\mathbf{L^1}$)$_2$$Cu_2$($PF_6$)$_2$] with an addition of perchlorate showed a high intensity ion at *m/z* 1267 corresponding to {[Cu_2($\mathbf{L^1}$)$_2$(ClO_4)]}$^+$ (Fig.71a). In analogous fashion to the iso-structural complex containing perchlorate the ESI-MS on addition of tetrafluroborate showed a *m/z* ion at 1255 corresponding to {[Cu_2($\mathbf{L^1}$)$_2$(BF_4)]}$^+$ (Fig.71b). Furthermore an ESI-MS of the final complex with an addition of nitrate gave a *m/z* ion at 1230 showing the presence of {[Cu_2($\mathbf{L^1}$)$_2$(NO_3)]}$^+$ (Fig. 71c) in solution.

The observed and expected Isotope patterns for the above complexes are shown in figures 71a-c;

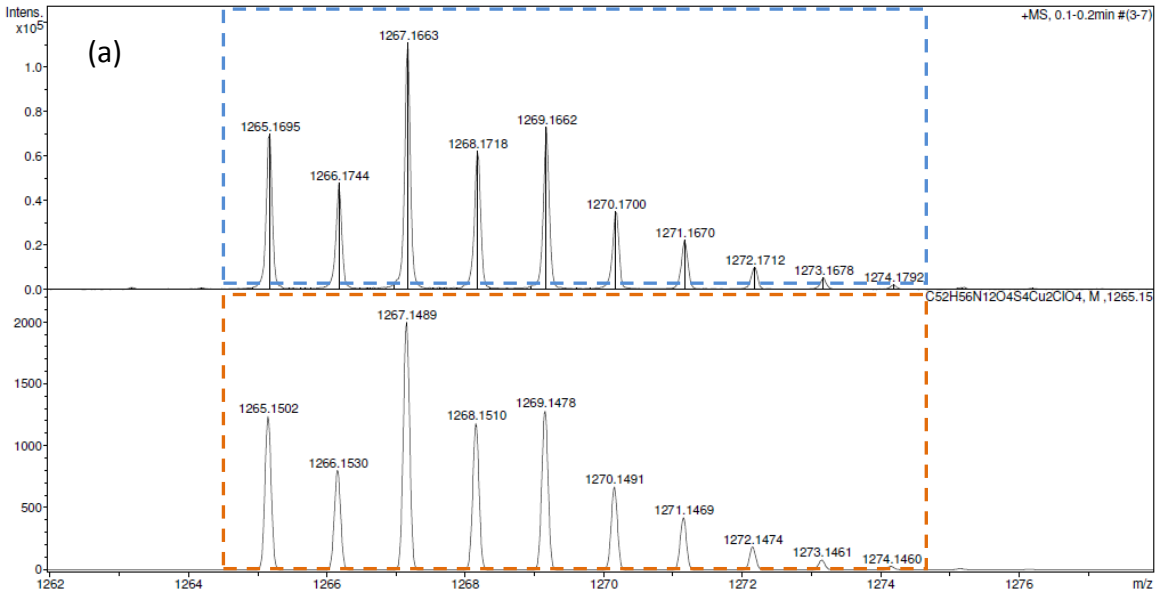

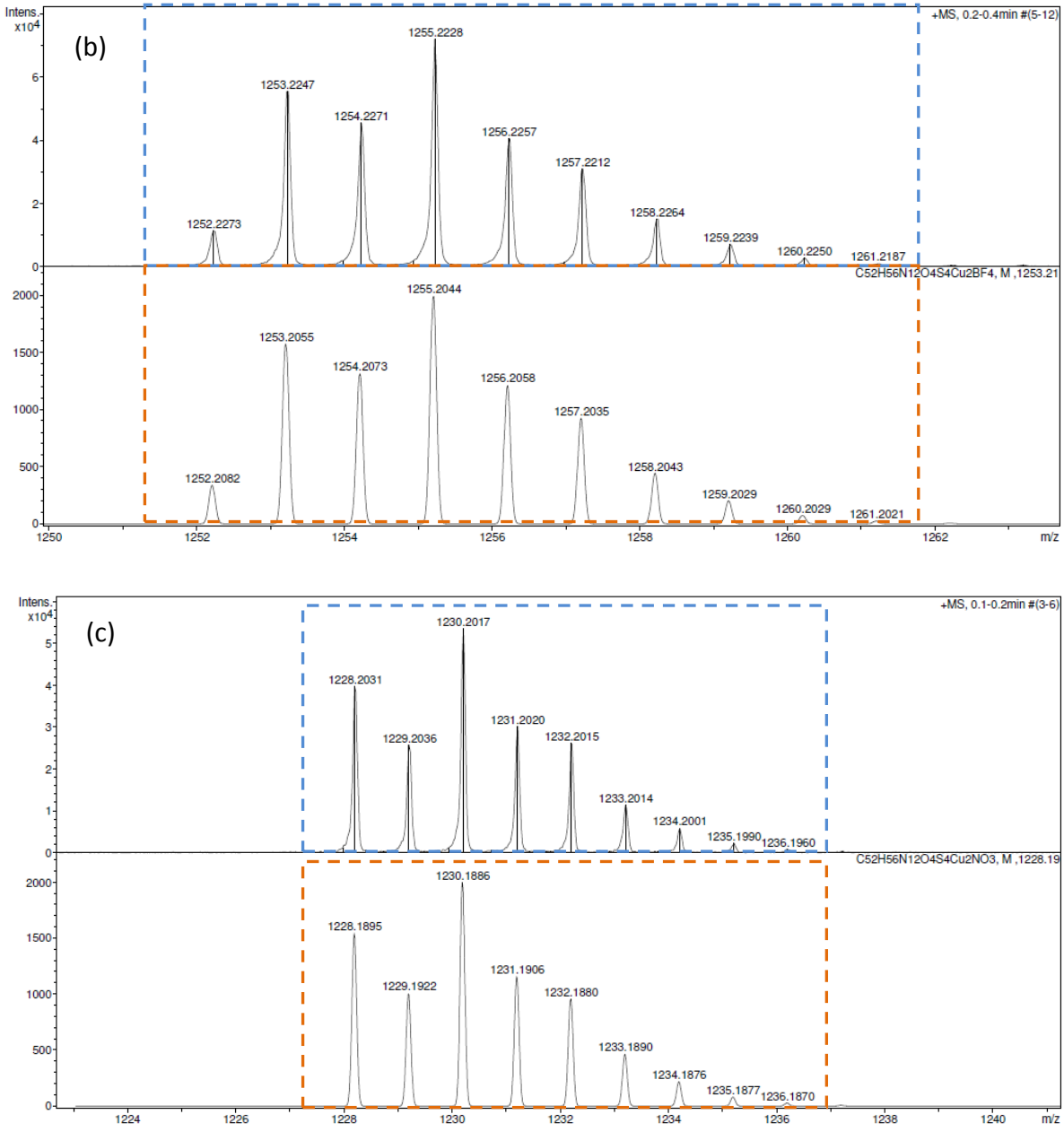

Fig.71a, b & c: Observed (Blue) and expected (orange) isotope patterns for complexes; a) $\{[Cu_2(\mathbf{L^1})_2(ClO_4)]\}^+$, b) $\{[Cu_2(\mathbf{L^1})_2(BF_4)]\}^+$ and c) $\{[Cu_2(\mathbf{L^1})_2(NO_3)]\}^+$.

Selected bond lengths and angles for the complex are shown in tables 1.9 and 2.0 below;

Atom 1	Atom 2	Bond Length (Å)
Cu1	N1	2.005 (3)
Cu1	N2	2.098 (4)
Cu1	N4	2.013 (3)
Cu1	N5	2.085 (3)

* The complex lies on a special position and only half of the molecule is crystallographically unique with the remaining molecule generated by symmetry.

Table 1.9 Selected bond lengths for complex ($[Cu_2(\boldsymbol{L^1})_2](NO_3)_2$).

Atom 1	Atom 2	Atom 3	Bond Angle (°)
N7	Cu1	N8	80.49 (14)
N7	Cu1	N10	133.91 (16)
N7	Cu1	N11	128.18 (12)
N8	Cu1	N10	106.16 (13)
N8	Cu1	N11	133.91 (16)
N10	Cu1	N11	80.49 (14)

* The complex lies on a special position and only half of the molecule is crystallographically unique with the remaining molecule generated by symmetry.

Table 2.0: Selected bond angles for complex ($[Cu_2(\boldsymbol{L^1})_2](NO_3)_2$).

2.2. Summary:

In summary the formation of a dinuclear double helicate over that of its mononuclear counterpart can be attributed to the metal ion used; when **[L^1]** is reacted with a monovalent cation (e.g. Cu^+) a dinuclear double helicate is observed however if **[L^1]** is reacted with a divalent metal ion capable of an octahedral geometry (e.g. Co^{2+}) the mononuclear species is observed.

However, even though both the Co^{2+} and Hg^{2+} metal ions adopt the same coordination geometry (and the ligand acts as a planar equatorial tetradentate species) the two structures adopt two different motifs of anion binding interactions. When a hard metal ion is used (e.g. Co^{2+}) the two amides point towards each other and interact with a BF_4^- counter anion. However, in the Hg^{2+} structure each of the amides point away from each other forming inter-molecular interactions with carbonyl oxygen atoms. This is due to the fact that the perchlorate anions are bound to the metal centre (water coordination is possibly avoided due to the soft nature of the metal ion) avoiding any hydrogen bonding to the amide hydrogen atoms.

In each of the Cu^+ containing dinuclear double helicates (ClO_4^-, BF_4^-, NO_3^-) a solid-state polymer is obtained. In all case the anion is bound to aromatic and amide hydrogen atoms from two different dinuclear double helicates giving rise to a polymeric structure and even with the trigonal planar anion (e.g. NO_3^-) the structure is remarkably similar to that of the tetrahedral anions.

3. Chapter 3: Synthesis and coordination chemistry of a ligand containing both *N*-donor and hydrogen bond donor units separated by a central bi-pyridine ring:

Reaction of **[L^1]** with a series of anions and cations resulted in some interesting structures. The ligand can act as either a tetradentate or bis-bidentate *N*-donor ligand depending on which transition metal ion it is coordinated to. In both cases the structures demonstrated interesting anion binding properties through interaction with the acetyl / amide arms of the ligand strand.

Increasing the ligands functionality has been shown to have profound effects upon its coordination properties, therefore natural progression would be to include further groups capable of interactions with anions, in the hope that their effects would result in a series of different complexes.

[L^2] includes a second acetyl and amide functional group on each of the ligand arms (Fig. 72). Each amide has the ability to undergo hydrogen bonding interactions with anions, thus creating a larger guest species for anion coordination.

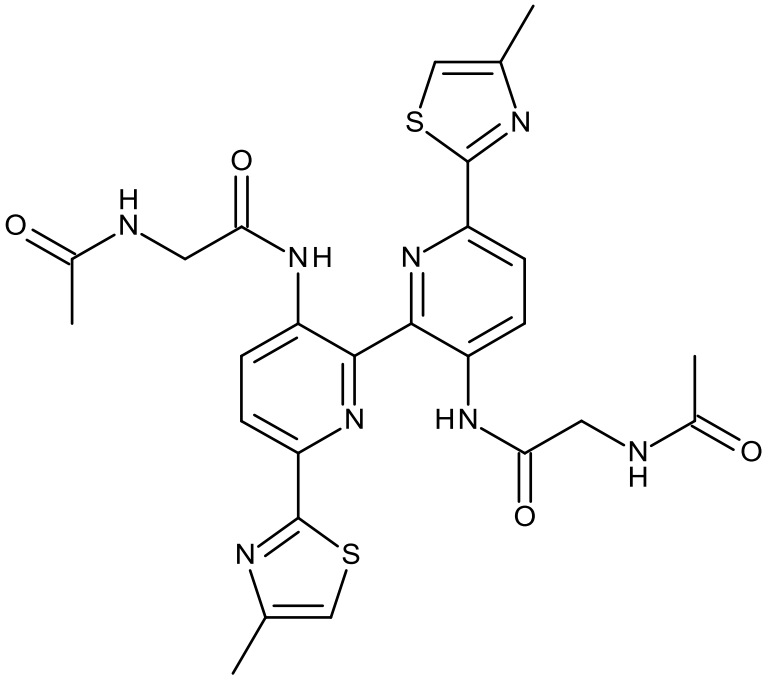

*Fig. 72: Bis-bidentate amine-containing ligand **[L^2]**.*

3.1 Synthesis of [L^2]:

Synthesis of **[L^2]** was carried out in a multi-step process (Scheme 2). Firstly 3-amino-2-chloropyridine **[1]** was reacted with acetic anhydride for 12 hours to form the acetylated product **[2]**. The product was then reacted with copper bronze in dimethylformamide at 80°C for 16 hours under an atmosphere of N_2. Following a filtration and subsequent wash with aqueous ammonia the product was extracted and given as a brown solid **[3]**. Confirmation of the successful synthesis was obtained by ^{1}H NMR spectroscopy which showed a total of four proton environments in the aromatic region. The spectrum shows a broad singlet at 9.60 ppm worth a total of two protons which is indicative of an amide; the three doublets of doublets at 9.12, 8.36 and 7.40 ppm respectively correspond to the three aromatic protons of the pyridine rings.

Activation of the bipyridine was carried out by a reaction of the diamide with a slight two-fold excess of *m*CPBA in DCM at room temperature, the reaction was allowed to stand for 8-10 days before being purified via column chromatography to give the bis-*N*-oxide as a solid **[4]**. Confirmation of the pure product was obtained via ^{1}H NMR spectroscopy which showed the four proton signals however there had been an increased shift in the ppm of the aromatic peaks due to the oxidized nitrogen atoms.

The bis-*N*-oxide was then dissolved in dimethylsulphate and heated at 60°C for 24 hours, after which an oil formed by addition of diethyl ether. After decanting the solvent and washing with diethyl ether the oil was suspended in water containing sodium cyanide which then gave the di-cyano as a cream solid **[5]**. The ^{1}H NMR spectrum gave confirmation of the di-cyano product with the signals of note being two aromatic protons at 8.59 and 8.13 ppm corresponding to the pyridine rings. The loss of an aromatic signal indicates the loss of an aromatic proton due to the incorporation of the cyano group. The di-cyano was then reacted with H_2S in ethanol giving the bipy-thioamide **[6]** as a precipitate. Confirmation of the product was carried out by ^{1}H NMR spectroscopy which showed a total of six protons; the most significant being two singlet's at 10.17 and 9.76 ppm respectively corresponding to the thioamide group.

The bis-thioamide was reacted in dimethylformamide with chloroacetone at 80°C for four hours giving the reacted thiazole ligand as a precipitate **[7]**. Confirmation of the

successful formation of the thiazole ring was carried out by ^{1}H NMR spectroscopy which showed a total of four signals in the aromatic region with a large singlet at 7.42 ppm indicative of the formation of a thiazole ring.

Compound **[7]** was then hydrolysed in concentrated HCl at 80°C for a total of eight hours. After which the reaction was suspended in H_2O giving an orange precipitate, which after neutralisation gave the diamine product **[8]** as a yellow solid. Characterization of the diamine was carried out via ^{1}H NMR spectroscopy which showed a total of five signals; signals of note are two doublets at 7.89 and 7.34 ppm which correspond to the hydrogen's of the pyridine ring, a signal at 7.31 ppm corresponding to the thiazole singlet and a broad singlet integrating to four protons at 7.82 ppm which is indicative of an amine proton.

The diamine precursor **[8]** was then added to a flask containing a prepared solution of *N*-acetylglycine and oxalylchloride in anhydrous pyridine at 0°C. The reaction was allowed to stir at room temperature for 72 hours, after which time a yellow precipitate formed. Isolation of the solid via vacuum filtration gave **[L^2]** as an orange solid. Confirmation of the successful synthesis of **[L^2]** was carried out by ^{1}H NMR spectroscopy which showed a total of five signals in the aromatic region; the most noteworthy of which being two singles at 8.78 and 8.21 ppm corresponding to the protons of the bipyridine ring, the thiazoyl singlet at 7.43 ppm and a singlet at 10.3 ppm related to the amide proton. Coincident with one of the bipyridine signals is the aliphatic amide proton which is a triplet due to coupling to the adjacent $-CH_2-$. Furthermore, ESI-MS showed an ion at *m/z* 579 corresponding to [**L^2**+H]$^+$.

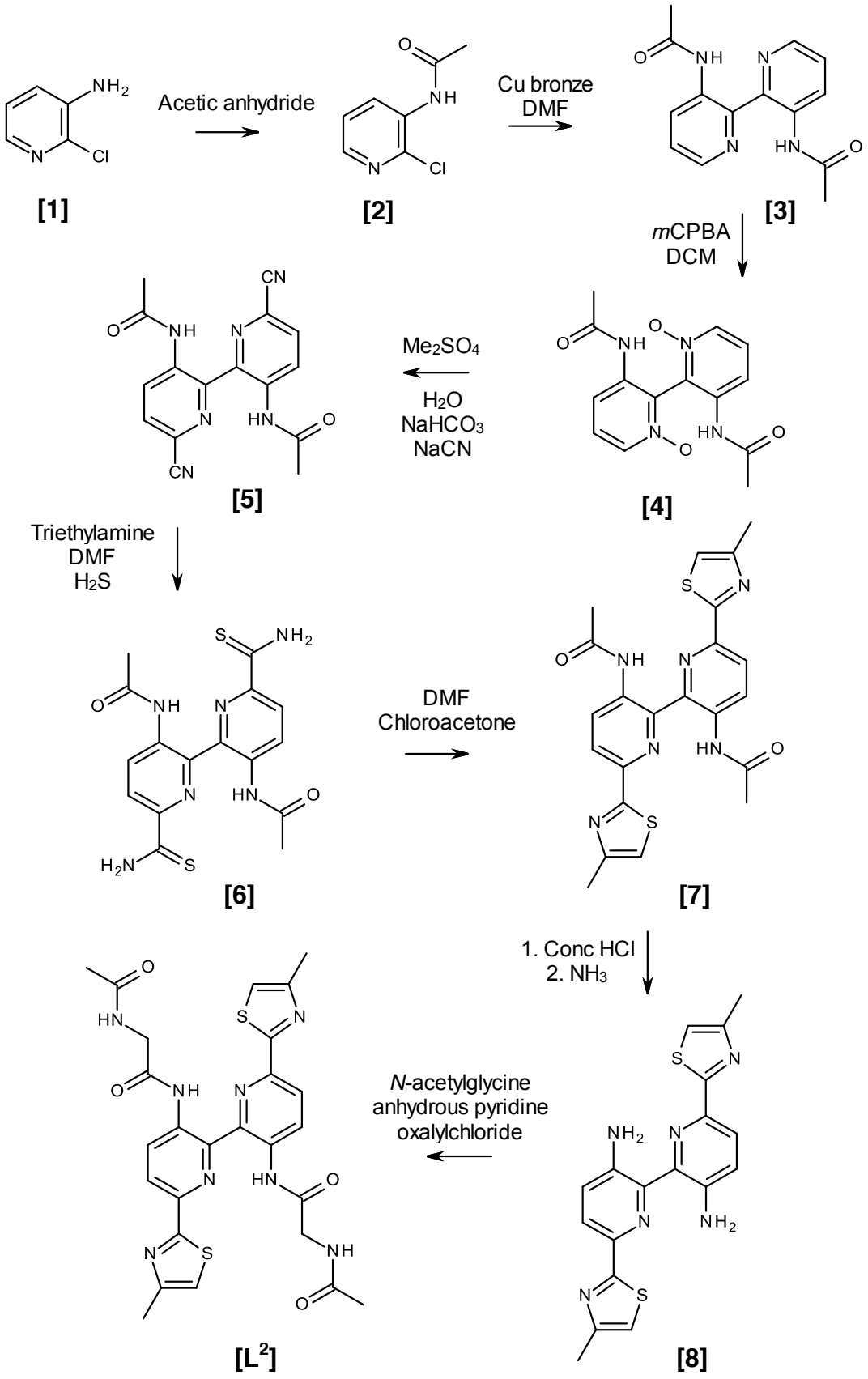

Scheme 2: Synthesis diagram of **[L^2]**.

3.2 Coordination Chemistry of [L^2]:

3.2.1 Coordination of [L^2] with $Cu(ClO_4)_2$:

Reaction of **[L^2]** with $Cu(ClO_4)_2$ in $MeNO_2$ gave a clear green solution from which green crystals were formed upon slow diffusion of ethyl acetate. Analysis by single-crystal X-ray diffraction showed that in the solid state a mono-nulcear species ([Cu(**L^2**)]$(ClO_4)_2$) is formed. The ligand acts as a non-planar tetradentate donor coordinating the equatorial coordination sites of the metal ion (Fig. 73).

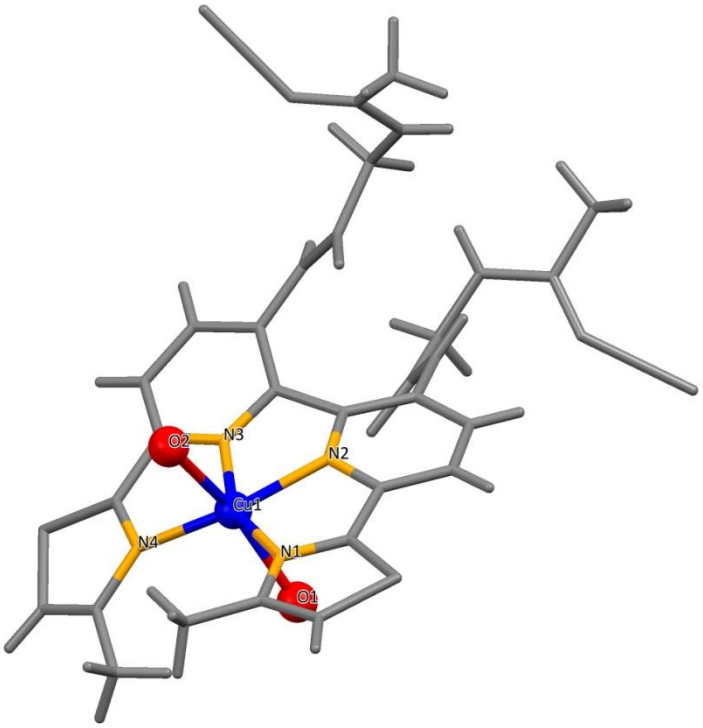

*Fig. 73: Solid state strucutre of [Cu(**L^2**)]$^{2+}$, anions omitted for clarity.*

The *N*-donor domain of the ligand can only occupy four of copper's six coordination sites and so in order to fill its coordination sphere the metal undergoes further coordination with the amide oxygen atoms of a ligand in a *different* complex (ave. Cu-O 2.301 Å) (Fig. 74a & b). In each structure the amide arms position themselves in opposite direcions with the amide groups pointing inwards and the acetyl groups facing away from the complex (Fig. 75).

a)

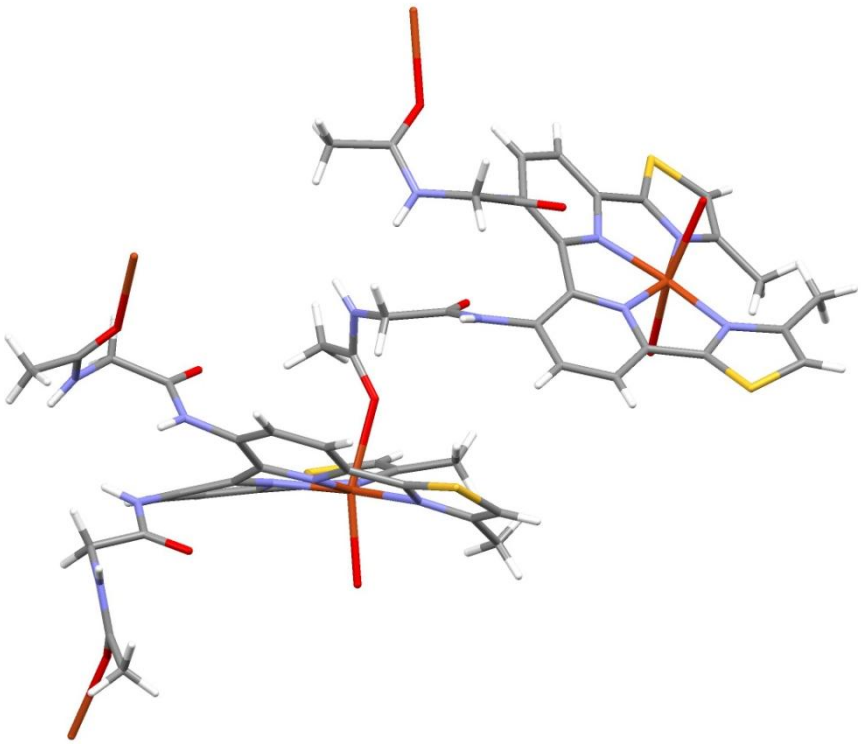

b)

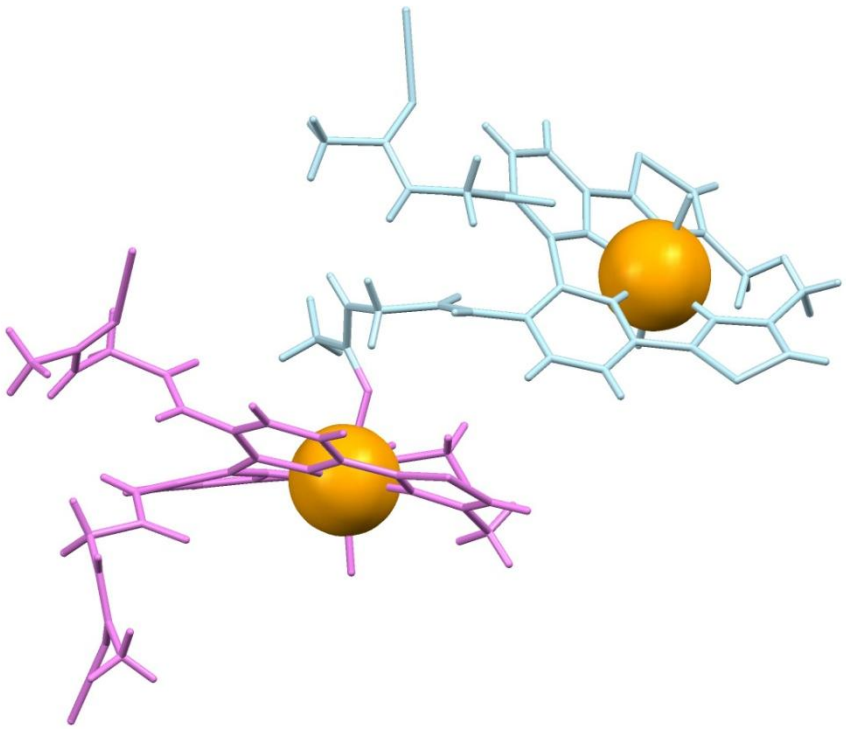

*Fig. 74a & b: Solid state state structure of ([Cu(**L**^{2})](ClO_4)$_2$) showing the interactions between the Cu^{2+}centres and the acetyl groups of another complex (anions omitted for clarity).*

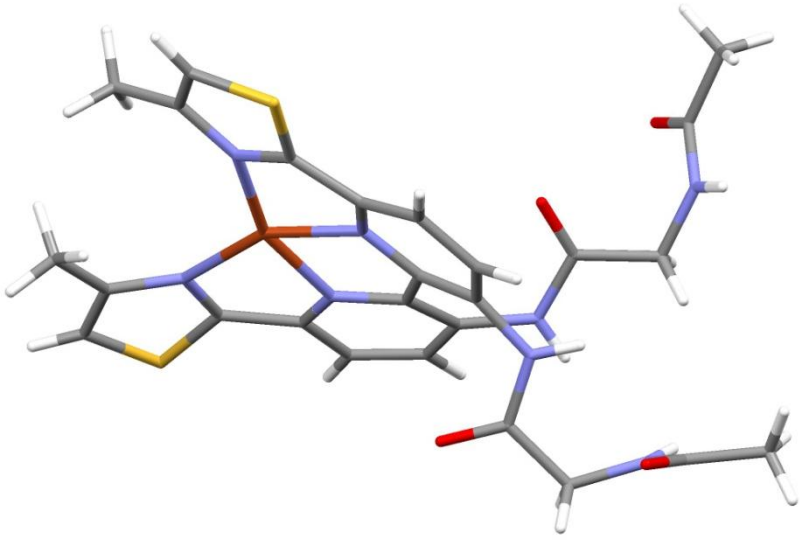

*Fig. 75: Solid state structure of ([Cu(**L**^{2})]$(ClO_4)_2$) showing the orientation of the ligand arms, anions omitted for clarity.*

The amides directly bound to the bipyridine unit do not coordinate the metal ions, instead they converge inwards forming a small pocket which is capable of hydrogen bonding interactions to perchlorate anions (ave NH-O 2.175 Å) (Fig. 76a & b). Each perchlorate anion hydrogen bonds to an amide from each ligand as well as the –CH_2– proton of one arm and the pyridyl proton of another.

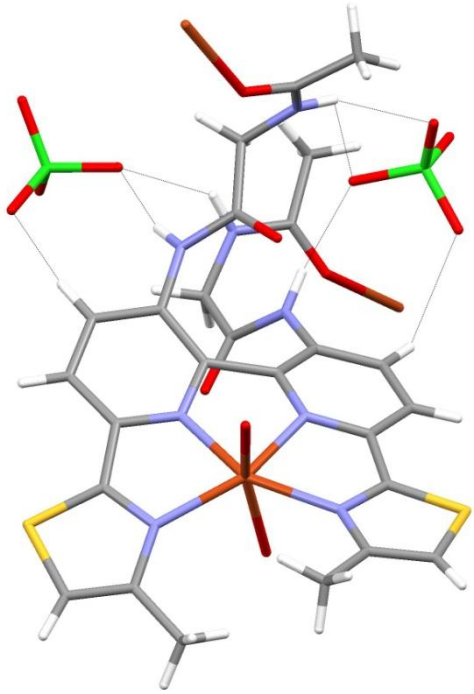

*Fig. 76a: Amide/ anion interactions in the solid state structure ([Cu(**L**^{2})]$(ClO_4)_2$).*

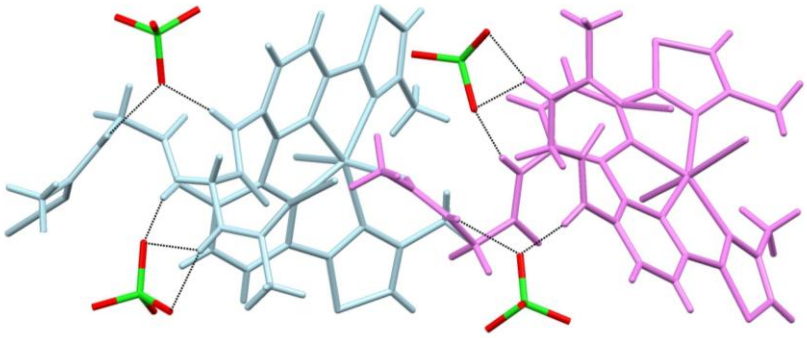

Fig. 76b: Amide/ anion interactions across two solid state structures, ([Cu($\mathbf{L^2}$)](ClO$_4$)$_2$).

This intermolecular coordination results in a polymeric motif whereby each metal ion is coordinated in the axial position by the acetyl oxygen atom of another complex (Fig. 77). Furthermore, the uncoordinated amide groups interact with anions.

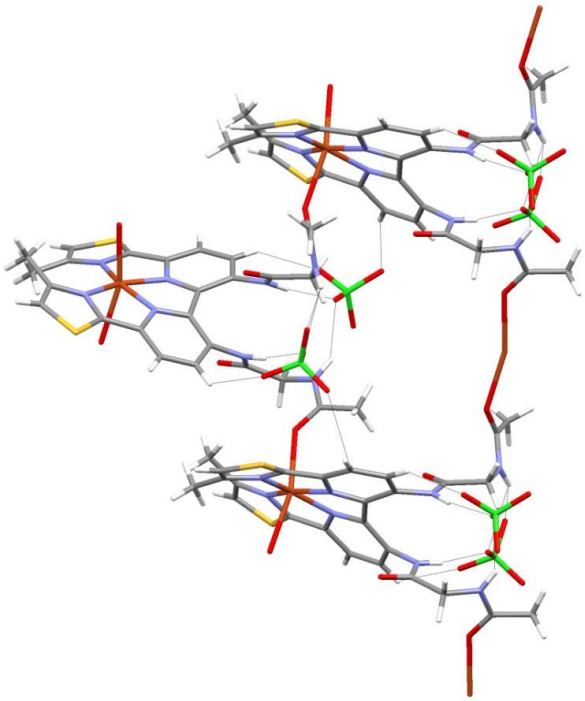

Fig. 77: Solid state structure of complex ([Cu($\mathbf{L^2}$)](ClO$_4$)$_2$).

ESI-MS analysis did not show the expected ion e.g. {[Cu($\mathbf{L^2}$)(ClO$_4$)]}$^+$ it did however show an ion at *m/z* 1383 corresponding to {[Cu$_2$($\mathbf{L^2}$)$_2$(ClO$_4$)]}$^+$. This is a consequence of the ESI-MS process which has reduced the Cu(II) to Cu(I) and as this mono-valent ion prefers a four-coordinate geometry a dinuclear double helicate results. Reduction of copper ions in the ESI-MS process is documented and not unusal with *N*-donor ligands.[91]

Selected bond lengths and angles for the complex are shown in tables 2.1 and 2.2 below;

Atom 1	Atom 2	Bond Length (Å)
Cu1	N1	2.1172 (1)
Cu1	N2	1.9859 (1)
Cu1	N3	1.9868 (1)
Cu1	N4	2.0870 (1)
Cu1	O1	**p*** 2.3038 (2)
Cu1	O2	**p*** 2.3008 (1)

***p**: Intramolecular bond lengths

Table 2.1: Selected bond lengths for complex ([Cu($\boldsymbol{L^2}$)]$(ClO_4)_2$).

Atom 1	Atom 2	Atom 3	Angle (°C)
N2	Cu1	N3	77.51
N2	Cu1	N1	79.64
N2	Cu1	N4	154.85
N2	Cu1	O1	84.61
N2	Cu1	O2	101.72
N3	Cu1	N1	156.59
N3	Cu1	N4	79.46
N3	Cu1	O1	100.54
N3	Cu1	O2	98.25
N1	Cu1	N4	123.92
N1	Cu1	O1	82.20
N1	Cu1	O2	81.46
N4	Cu1	O1	89.80
N4	Cu1	O2	91.43
O1	Cu1	O2	161.08

Table 2.2: Selected bond angles for complex ([Cu($\boldsymbol{L^2}$)]$(ClO_4)_2$).

Formation of complex ([Cu(**L²**)](ClO_4)$_2$) is similar to the mononuclear species observed between **[L¹]** and Co^{2+} / Hg^{2+}. Both ligands form mononuclear complexes with the ligand strand coordinating the metal ion in the equatorial position.

Reaction of **[L¹]** with an octahedral metal ion i.e. Co^{2+} or Hg^{2+} exclusively forms a planar mononuclear species with adjoining anions (H_2O/ClO_4^-) completing the metal ions coordination. Reaction of **[L²]** with an octahedral metal ion, in this case Cu^{2+} gives the mononuclear species however the metal ions coordiantion sphere is now fulfilled by coordination with another complex.

Much like the structures observed with **[L¹]** it is the metal ion that forces the formation of the mononuclear complexes however with **[L²]** the addition of a second amide and acetyl group increasing the length of the ligand arm inhibits the formation of a totally planar species.

3.2.2 Coordination of [L²] with $Zn(ClO_4)_2$:

Reaction of **[L²]** with $Zn(ClO_4)_2$ (as opposed to $Cu(ClO_4)_2$) resulted in an essentially iso-structural assembly. Reaction of **[L²]** with $Zn(ClO_4)_2$ in $MeNO_2$ gave a clear yellow solution from which yellow crystals formed upon slow diffusion of dichloromethane. Analysis by single-crystal X-ray diffraction showed that in the solid state the mononuclear species persists ([Zn(**L²**)](ClO_4)$_2$). Similarly the ligand partitions into two binding domains with the pyridyl/thiazoyl groups coordinating the metal ion (ave. Zn-N 2.1685 Å) and each amide arm pointing away from the complex in an axial fashion (Fig. 78).

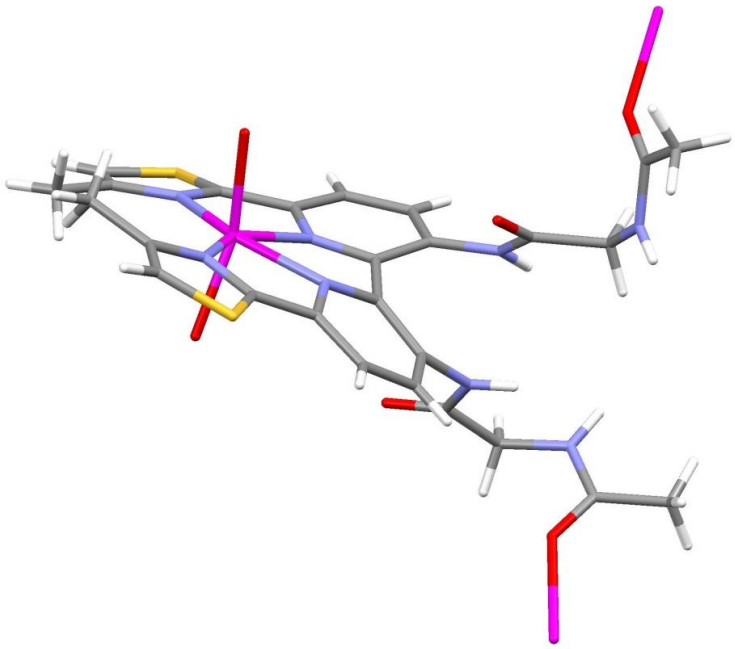

*Fig. 78: Solid state structure of ([Zn(**L**^{2})]$(ClO_4)_2$), anions omitted for clarity.*

An acetyl from each of the amide arms undergoes identical coordination with the metal ion of another complex, completing the metal ions preference for 6 coordinate. Furthermore the second acetyl of the ligand arm engages in hydrogen bonding interactions with terminal methyl group of another arm, providing stabilizing interactions (Fig. 79).

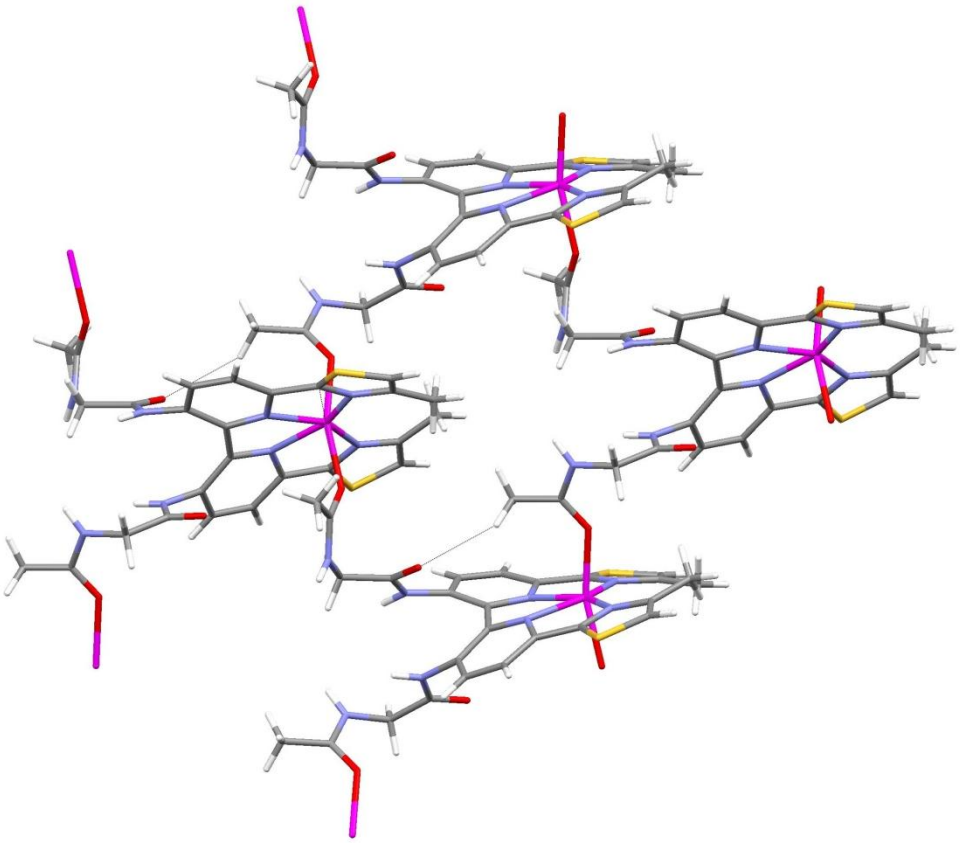

*Fig. 79: Stacking interactions of the solid state structure ([Zn(**L**^{2})](ClO$_4$)$_2$), anions omitted for clarity.*

As previously seen with the complex containing Cu^{2+} there is no distinct anion binding pocket however each perchlorate anion undergoes hydrogen bonding interactions with two amides, one from each arm (ave. NH···O 2.1725 Å) as well as the hydrogen on the 4-position of the pyridyl ring (Fig. 80). The same long range order is observed with each anion sitting within the polymeric lattice (Fig. 81).

Analysis by ESI-MS did show an ion at *m/z* 743 corresponding to the simple mono-nuclear species $\{[Zn(\mathbf{L}^2)(ClO_4)]\}^+$. However, there are other higher molecular weight ions at 906 and 1170 corresponding to $\{[Zn_2(\mathbf{L}^2)(ClO_4)_3]\}^+$ and $\{[Zn_3(\mathbf{L}^2)(ClO_4)_5]\}^+$ respectively and it is likely that this arises from the polymeric structure seen in the solid-state.

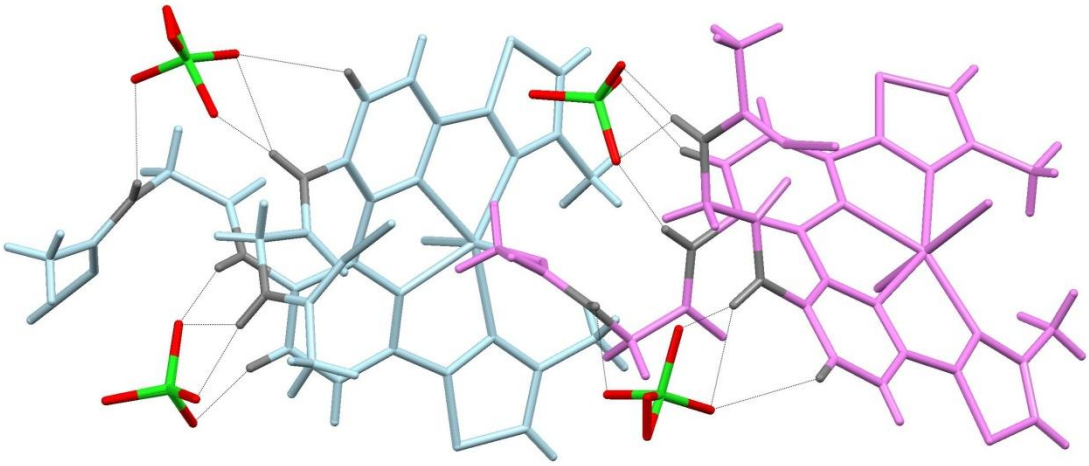

*Fig. 80: Solid state structure of ([Zn(**L**^{2})](ClO$_4$)$_2$), showing the interaction between the perchlorate anions and the NH protons.*

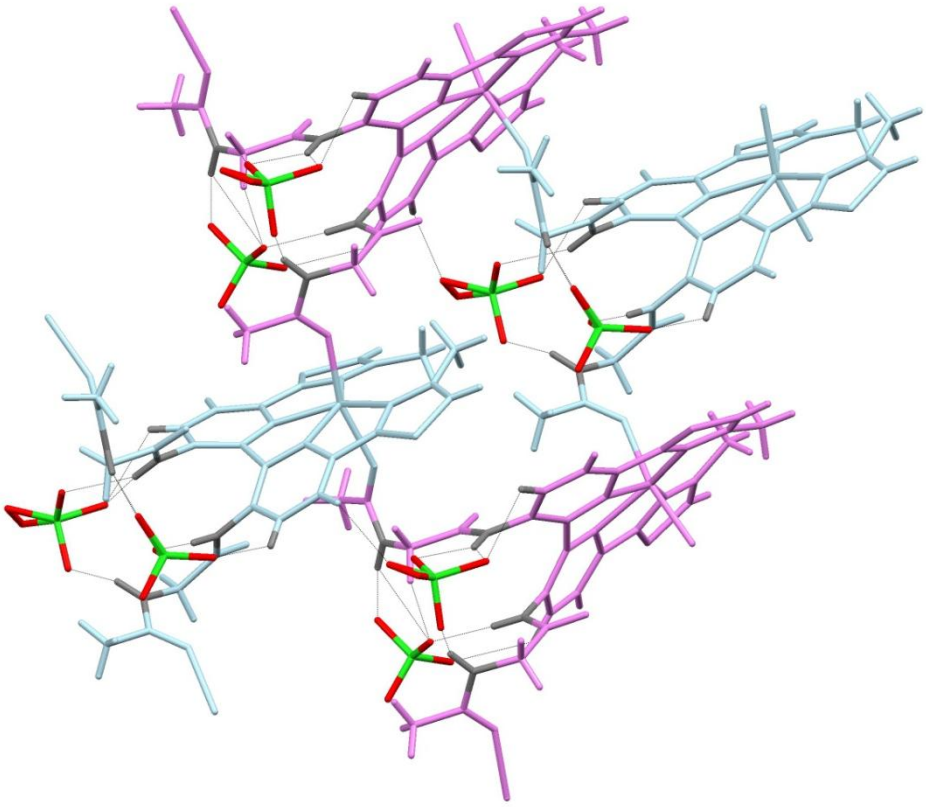

*Fig. 81: Stacking of solid state structure ([Zn(**L**^{2})](ClO$_4$)$_2$), showing the interaction between the perchlorate anions and the NH protons.*

Selected bond lengths and angles for the complex are shown in tables 2.3 and 2.4 below;

Atom 1	Atom 2	Bond Length (Å)
Zn1	N2	2.1575 (3)
Zn1	N3	2.1530 (3)
Zn1	N1	2.1998 (3)
Zn1	N4	2.1635 (3)
Zn1	O2	***p** 2.1058 (3)
Zn1	O1	***p** 2.1186 (3)

***p**: Intramolecular bond lengths

Table 2.3: Selected bond lengths for complex ($[Zn(\boldsymbol{L}^{2})](ClO_4)_2$).

Atom 1	Atom 2	Atom 3	Angle (°C)
N2	Zn1	N3	72.29 (11)
N2	Zn1	N1	76.17 (12)
N2	Zn1	N4	148.21 (12)
N2	Zn1	O2	87.05 (11)
N2	Zn1	O1	100.21 (11)
N3	Zn1	N1	148.45 (12)
N3	Zn1	N4	76.28 (11)
N3	Zn1	O2	95.46 (11)
N3	Zn1	O1	102.65 (10)
N1	Zn1	N4	135.17 (13)
N1	Zn1	O2	83.27 (11)
N1	Zn1	O1	82.32 (11)
N4	Zn1	O2	91.32 (11)
N4	Zn1	O1	91.08 (11)
O2	Zn1	O1	161.79 (11)

Table 2.4: Selected bond angles for complex ($[Zn(\boldsymbol{L}^{2})](ClO_4)_2$).

3.2.3 Coordination of [L^2] with Ag(NO_3):

Reaction of **[L^2]** with Ag(NO_3) in $MeNO_2$ gave a colourless solution from which colourless crystals formed upon slow diffusion of ethyl acetate. Analysis by single-crystal X-ray diffraction showed that in the solid state a dinuclear double helicate is formed ($[Ag_2(\mathbf{L^2})_2](NO_3)_2$). Each metal centre is coordinated by a pyridine ring and thiazoyl of each ligand (ave. 2.3985 Ag-N Å) which partitions into two distinct binding domains (Fig. 82a). Due to the formation of the double helicate the structure is no longer planar and each amide arm points away from the complex with the acetyl and amide groups alternating in direction (Fig. 82b).

The orrientation of the amide arms shows no visual binding pocket however each strand does undergo hydrogen bonding interactions to a nitrate anion through an amide hydrogen atom (ave NH···O 2.398 Å) (Fig. 83a & b). The other two amide arms positioned at the 'top' of the structure show no direct interactions with anions, instead these undergo further interactions with an acetyl group of a second and third structure respectively, creating a polymeric lattice (Fig. 84a & b).

Confirmation of the assembly by ESI-MS showed a high intensity ion peak at *m/z* 1471 which corresponds to $\{[Ag_2(\mathbf{L^2})_2(ClO_4)]\}^+$, showing the complex persists in solution.

a)

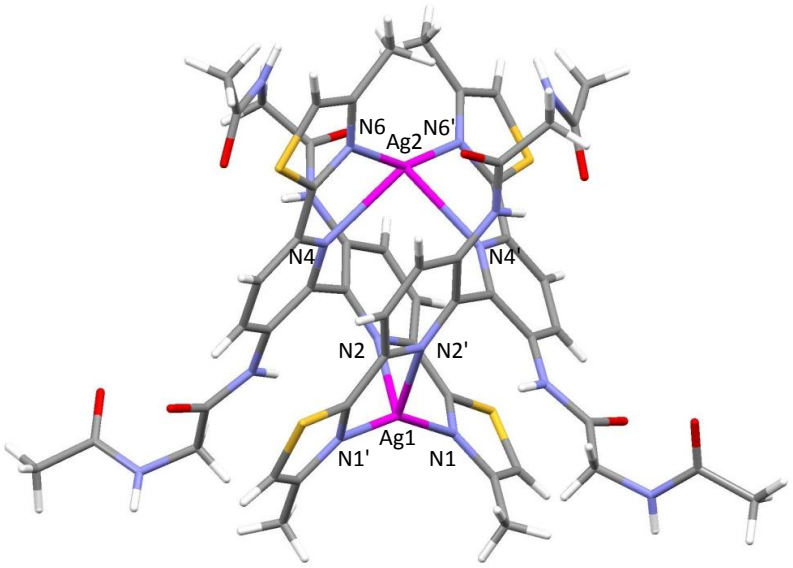

b)

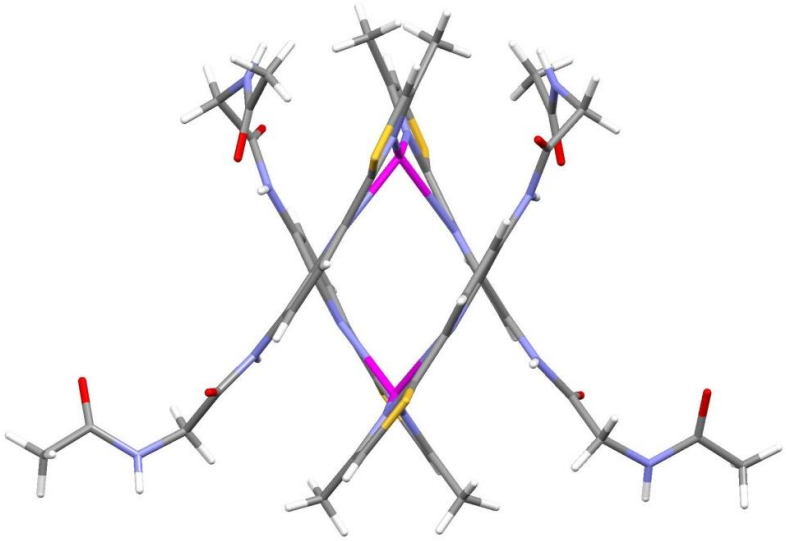

*Fig. 82: Solid state structures of ([Ag(**L**^{2})](NO$_3$)$_2$) a) 'front' view, b) 'side' view, anions omitted for clarity.*

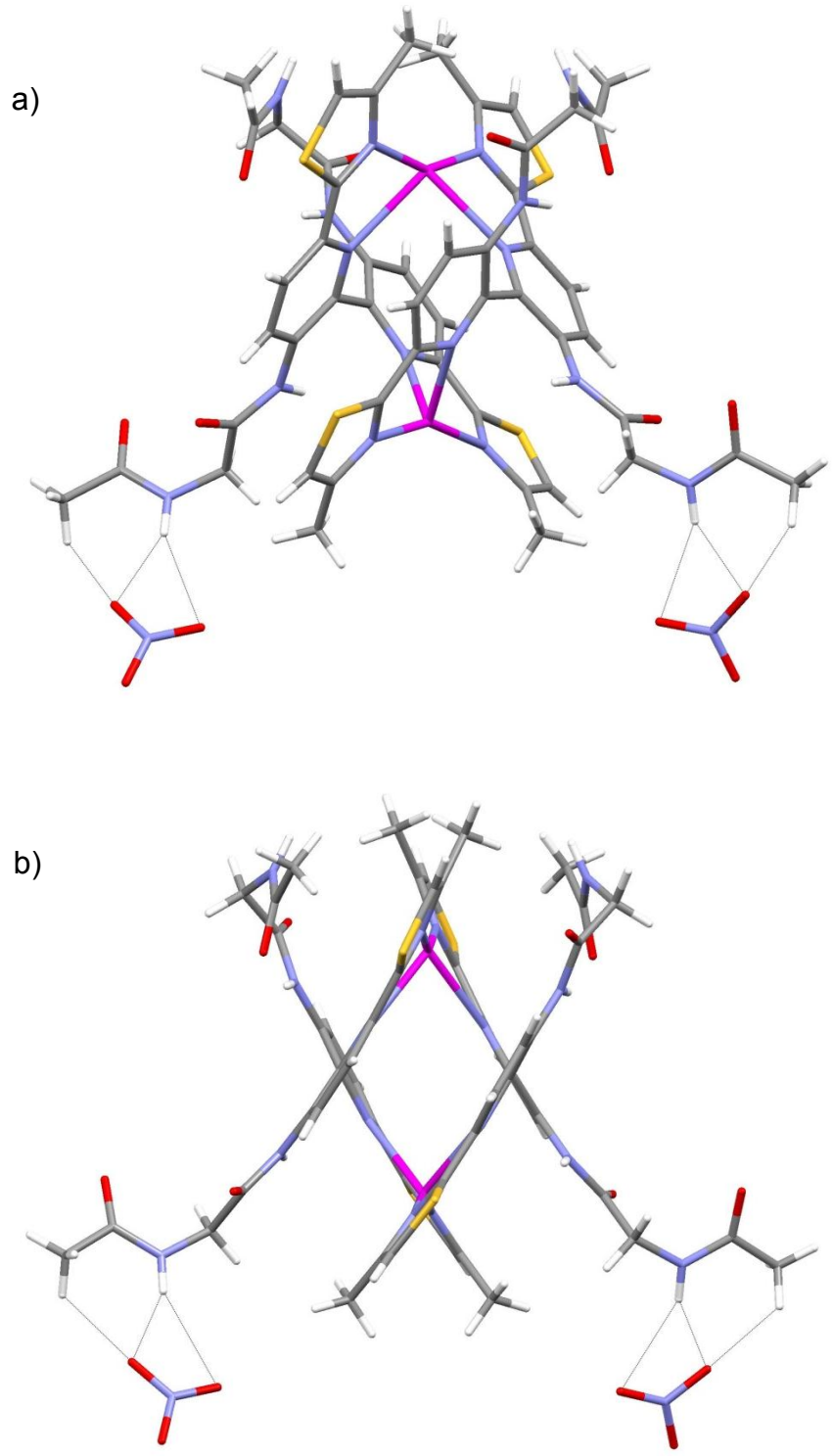

*Fig. 83: Solid state strucutres of ([Ag(**L**^{2})](NO$_3$)$_2$) a) 'front' view with NO$_3^-$ anion interactions, b) 'side' view with NO$_3^-$ anion interactions.*

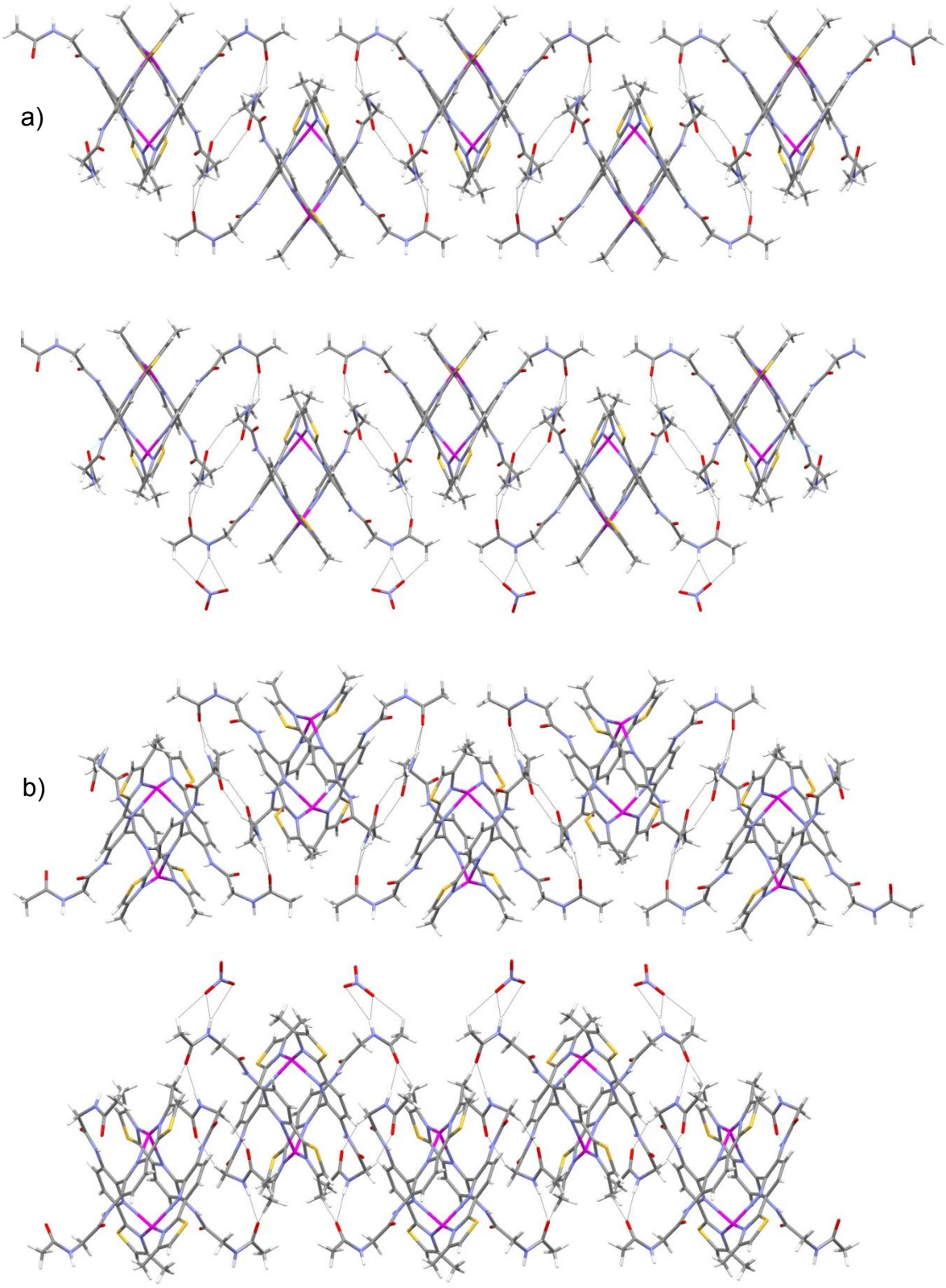

*Fig. 84a & b: Long range order of solid state structures of ([Ag(**L**^{2})]$(NO_3)_2$).*

Selected bond lengths and angles for the complex are shown in tables 2.5 and 2.6 below;

Atom 1	Atom 2	Length (Å)
Ag1	N1	2.285 (5)
Ag1	N2	2.484 (6)
Ag2	N4	2.566 (6)
Ag2	N6	2.231 (5)

*Table 2.3: Selected bond lengths for complex ([Ag(**L²**)](NO₃)₂).*

Atom 1	Atom 2	Atom 3	Angle (°C)
N1	Ag1	N2	71.83 (19)
N1	Ag1	N1	156.67 (3)
N1	Ag1	N2	125.75 (19)
N2	Ag1	N2	95.30 (2)
N4	Ag2	N6	70.61 (19)
N4	Ag2	N4	90.30 (2)
N6	Ag2	N4	130.60 (2)
N6	Ag2	N6	153.90 (3)

*Table 2.3: Selected bond angles for complex ([Ag(**L²**)](NO₃)₂).*

In comparison to the structures observed with **[L¹]** and monovalent cations the complex (**[L²]** + Ag^{+}) has some similar characteristics, both form dinuclear double helicates due to the cation's preference for tetrahedral coordination. Secondly each complex exhibits long range order forming a polymeric structure through intramolecular interactions; however each ligand forms a polymeric structure in different ways.

Complexes with **[L¹]** and monovalent cations form polymeric structures which arise as each of the dinuclear assemblies interact with anions giving alternate anion-helicate repeat units in the solid-state (Fig. 85a). However, with **[L²]** a polymeric structure is generated through interactions with the ligand strands of neighbouring complexes via amide oxygen and amide hydrogen interactions (Fig. 85b). The anions do hydrogen

bond with the arms of the helicate but on the outer regions of the polymeric lattice and not in a central pocket.

a)

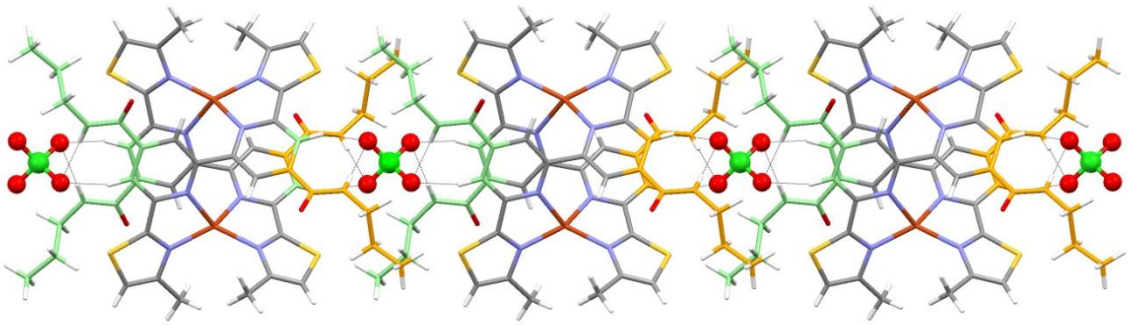

b)

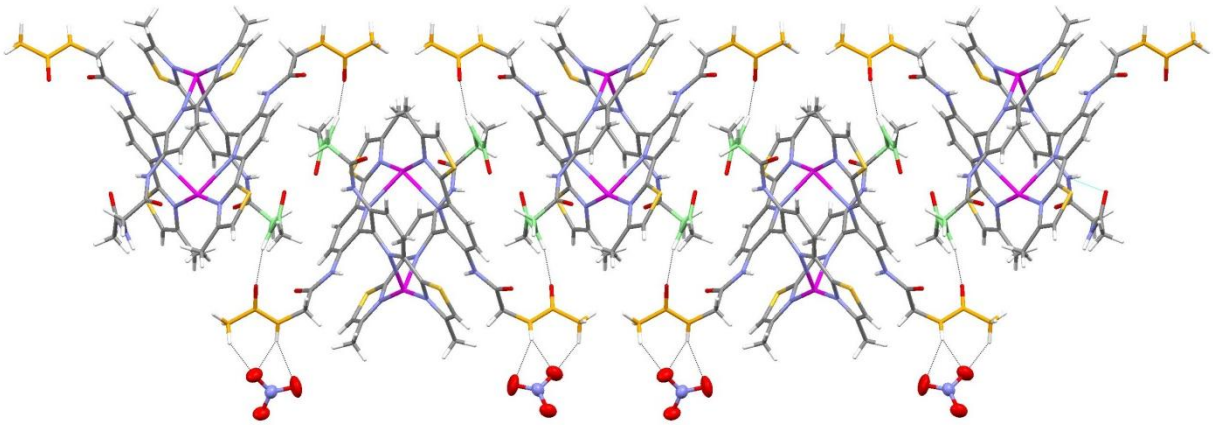

Fig. 85: Comparison between the long range order complexes a) ($[Cu_2(\mathbf{L^1})_2](ClO_4)_2$), b) ($[Ag(\mathbf{L^2})](NO_3)_2$).

3.3 Summary:

In summary formation of a dinuclear double helicate over that of the mononuclear species can, again, be attributed to the metal ion used. When **[L^2]** is reacted with a monovalent metal cation (e.g. Ag^+) a dinuclear double helicate is observed however when **[L^2]** is reacted with a divalent metal cation (e.g. Cu^{2+}) then the mononuclear species is observed. Although the coordination of different metal ions results in different structures, the change in the cation's coordination geometry has no impact on the ligands ability to interact with anions through the NH donors. When a mononuclear species is formed with divalent metal cations the ligand arms orientate outwards foregoing the planar conformation (due to the increase in steric bulk brought about by the addition of a second acetyl and amide functional group), each ligand arm undergoes internuclear interactions with a second and third structure through complimentary C-O-Cu interactions. Furthermore an amide from each ligand arm then experiences hydrogen bonding interactions with perchlorate counter ions.

The formation of a dinuclear double helicate with monovalent cation's leads to a similar long range order complex however, each ligand now polymerizes through favourable amide oxygen and amide hydrogen interactions. Additionally anion-amide hydrogen bonding interactions are observed indicating that the formation of the double helicate over the mononuclear species is entirely cation dependant.

Chapter 4.0: Synthesis and coordination chemistry of a ligand containing a tetradentate *N*-donor unit and two urea functional groups.

Comparisons made between structures observed with **[L^1]** and **[L^2]** have shown that changing the groups capable of hydrogen bonding interactions can lead to some novel structural changes when coordinated with both mono and divalent metal ions. Therefore incorporation of urea group onto the terminal position of the amide arms is thought to have a dramatic effect on the ligands ability to form long range order complexes. It is the hope that the incorporation of this unit into the architecture of **[L^3]** (Fig. 86) may lead to a series of different structures in the solid-state.

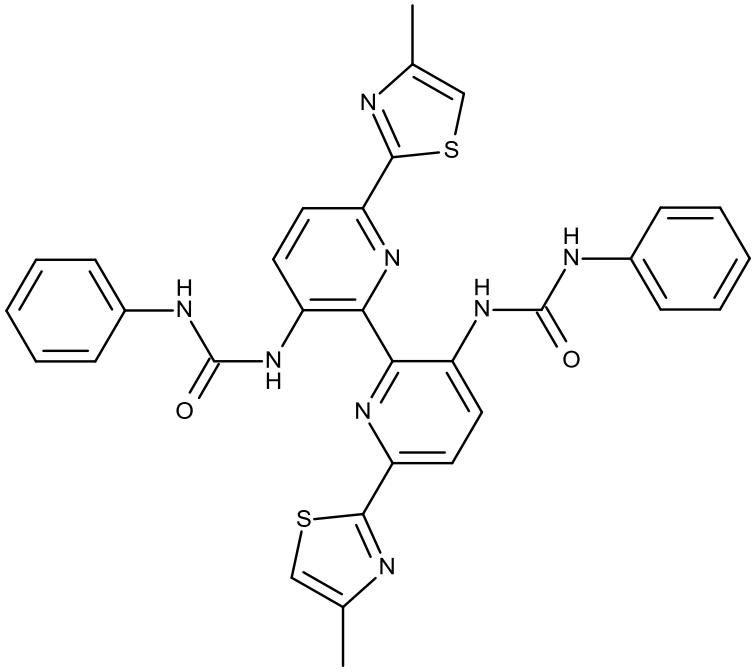

*Fig. 86: Urea containing ligand **[L^3]**.*

4.1 Synthesis of [L^3]:

Synthesis of **[L^3]** was carried out in a multi step process (Scheme 3) but is similar to the synthesis of **[L^2]**. For this ligand the diamino tetradentate ligand is reacted with phenyl ioscyanate to give the diurea ligand **[L^3]**. Thus the diamine precursor **[8]** was then reacted with phenyl isocyanate in anhydrous pyridine at room temperature for one hour. The resulting precipitate was isolated by filtration to give the ligand **[L^3]**. Confirmation of successful formation of **[L^3]** was carried out by ^{1}H NMR spectroscopy which showed a total of nine unique signals, the most noteworthy of which were two distinct singlet's at 9.29 and 8.49 ppm respectively corresponding to the NH protons of the urea group. Furthermore, ^{13}C NMR spectroscopy also showed 13 signals in the aromatic region. ESI-MS showed an ion at *m/z* 619 corresponding to [$\mathbf{L^3}$+H]$^+$.

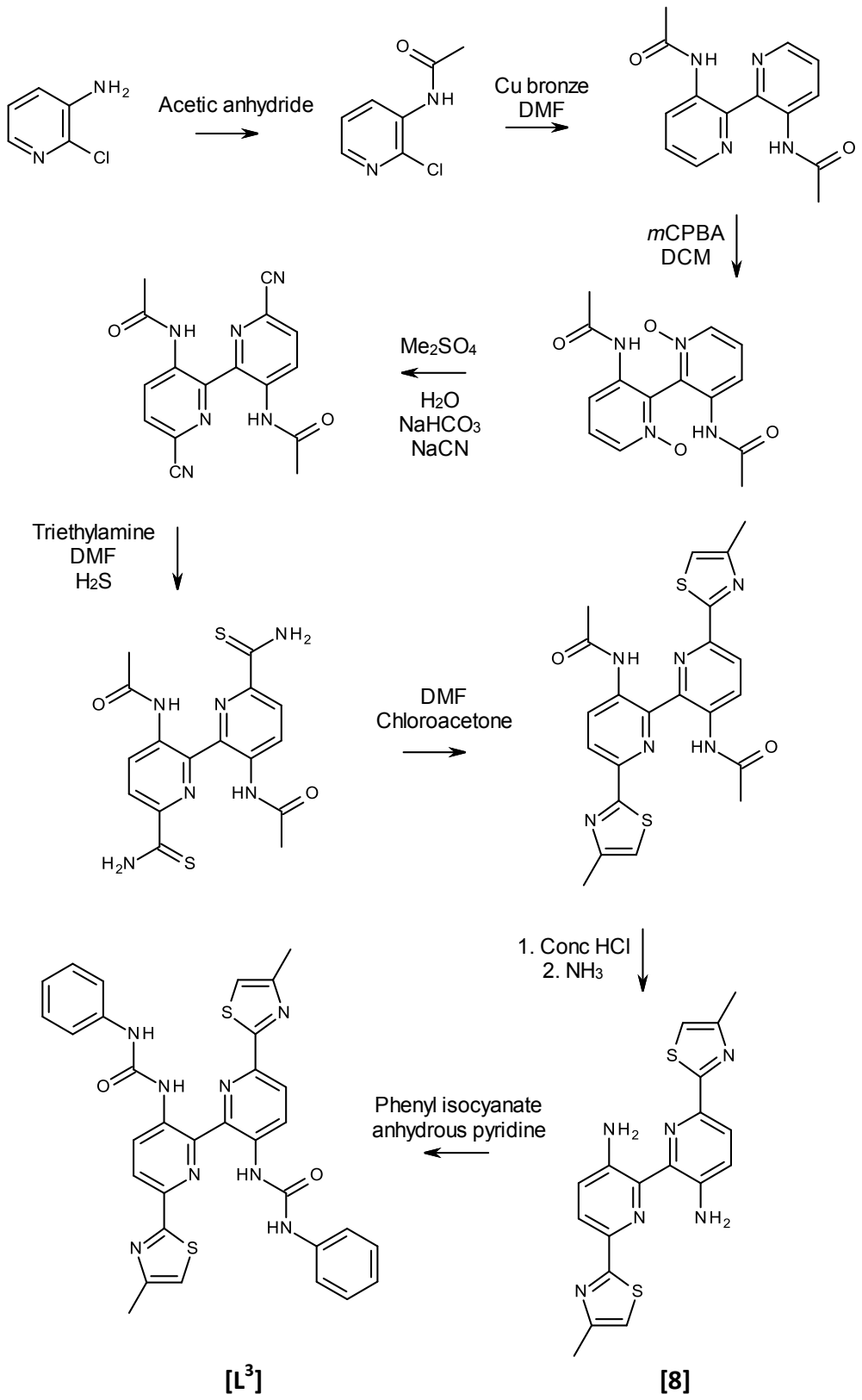

Scheme 3: Synthesis of **[L^3]**.

4.2: Coordination Chemistry of [L^3]

4.2.1 Coordination of [L^3] with $Cd(ClO_4)_2$:

Reaction of **[L^3]** with $Cd(ClO_4)_2$ in MeCN resulted in a clear yellow solution from which yellow crystals were formed upon slow diffusion of diisopropyl ether. Single-crystal X-ray diffraction showed that in the solid state a mono-nuclear species is formed ($[Cd(\mathbf{L^3})](ClO_4)_2$) (Fig. 87a). The ligand continues to act as a non-planar tetradentate donor coordinating the equatorial sites of the metal ion (Fig. 87b).

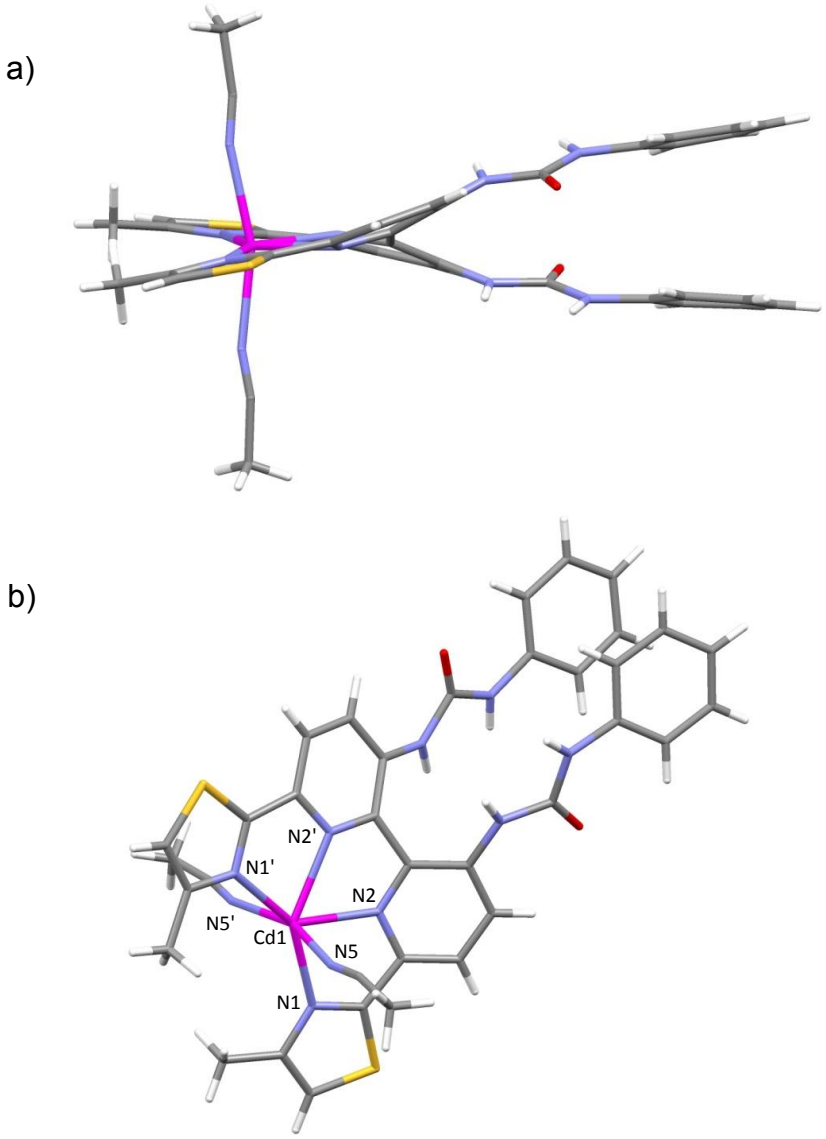

Fig. 87: Solid state structures of complex ($[Cd(\mathbf{L^3})](ClO_4)_2$). a) "side" view of the complex showing the orientation of the urea/phenyl arms, b) "top" view of the complex showing equatorial binding of the metral ion, anions omitted for clarity.

Each pyridyl/thiazole group of the ligand occupies four of the Cd^{2+} metal centres six coordination sites (ave. Cd-N 2.335 Å), as cadmium has a preference for an octahedral coordination geometry a further two acetonitrile molecules are coordinated in the axial position (ave. Cd-N 2.336 Å) (Fig. 87a). The urea arms of the ligand lie parallel to one another with both NH groups pointing to opposite sides of the structure. Furthermore two perchlorate anions lie to either side of the structure forming short contacts (ave. NH···O 2.288 Å) to the urea groups of the ligand arm (Fig. 88a & b).

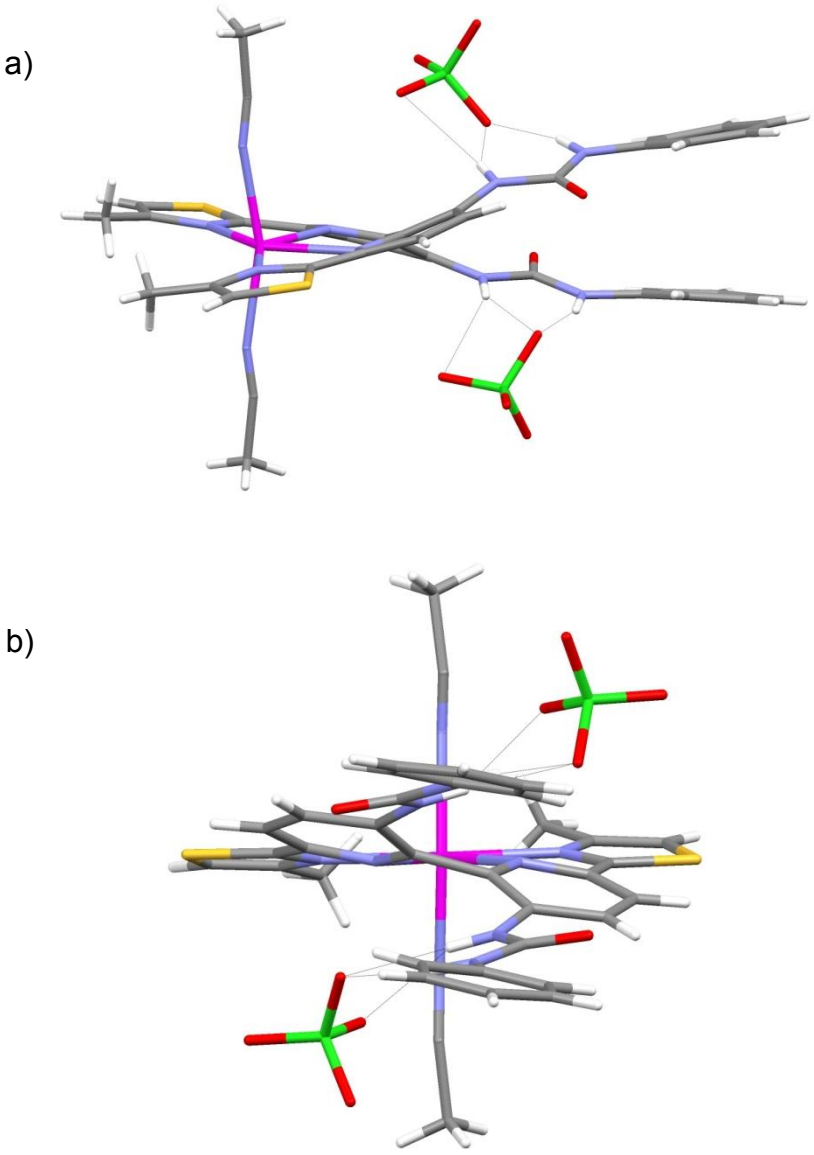

*Fig. 88: Solid state structures of complex ([Cd(**L**^{3})]$(ClO_4)_2$) showing anion interactions.*

On further examination a remaining oxygen atom of each perchlorate anion undergoes additional interactions with the aromatic hydrogen atoms in the 3-position of the bipyridine unit of another complex (Fig. 91a). These short contacts give rise to a series of long range interactions between neighbouring complexes leading to a polymeric motif of alternating structures (Fig. 89a & b).

a)

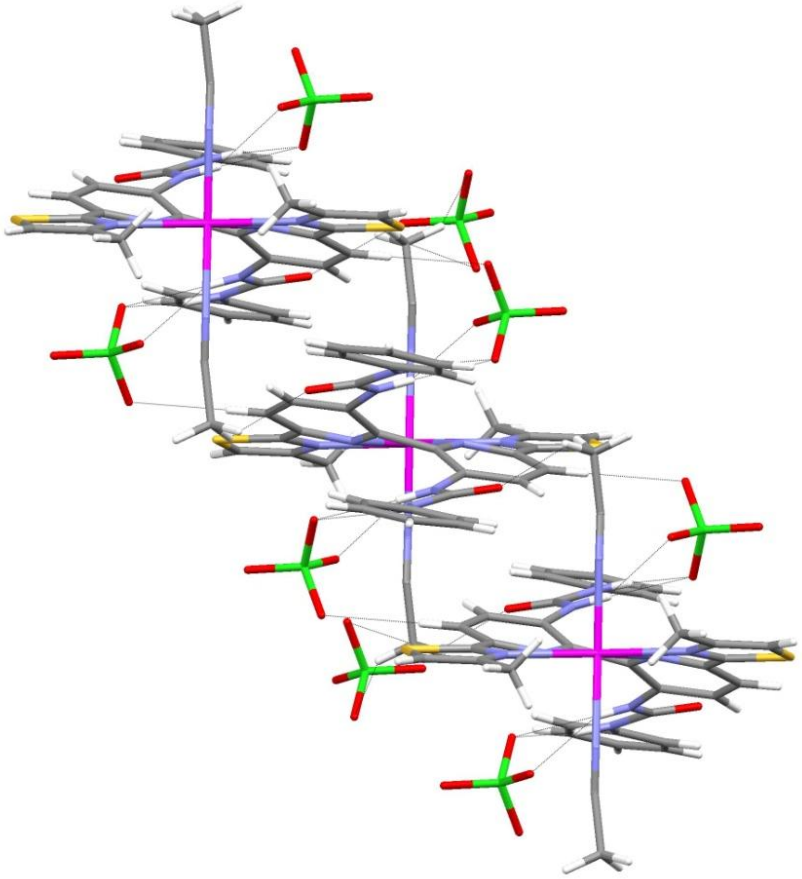

*Fig. 89a: Solid state structure of long range order complex: ([Cd(**L**^{3})](ClO_4)$_2$).*

b)

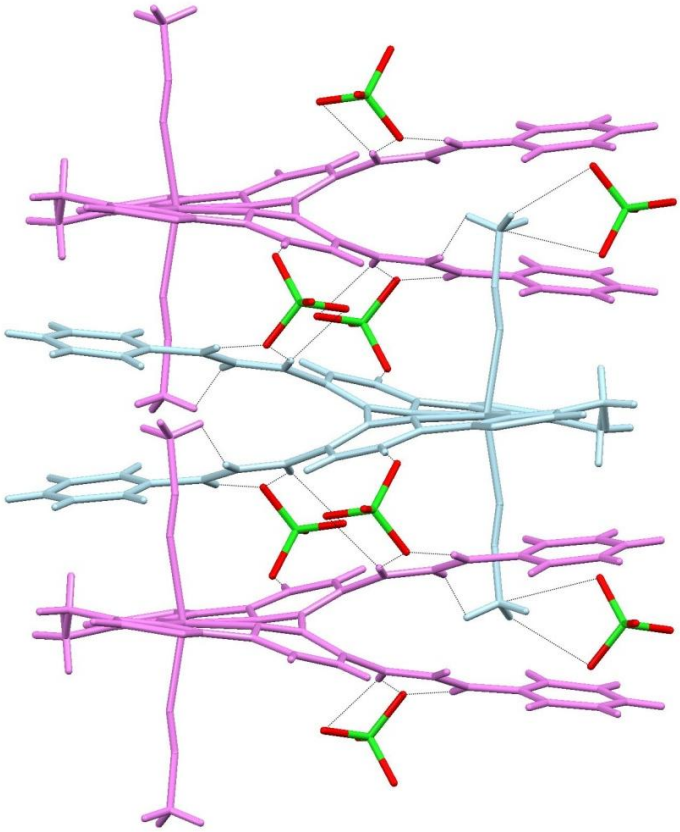

*Fig. 89b: Solid state structure of the long range order complex: ([Cd(**L**^{3})](ClO$_4$)$_2$).*

In previously observed structures with **[L^{1}]** and **[L^{2}]** which are coordinated to octahedral metal ions each resulting complex forms a vaguely polymeric species whereby the metal ions preference for an octahedral geometry necessitates the coordination of either anions or the ligand arm of neighbouring structures, thus leading to further intramolecular interactions with adjoining complexes. *All* form mono-nuclear species which divalent cations that undergo ancillary interactions with other species in the axial position; however in each case the species is different. This can be attributed to the functionality of the ligands arms, where previously the ligand arms have either been able to form a pocket for anion coordination **[L^{1}]** or long enough to undergo interactions with the metal ion themselves **[L^{2}]**, the incorporation of a urea group into the architecture of **[L^{3}]** has restricted its coordination properties (e.g. the urea oxygen atom is conformationally restricted and cannot coordinate with the metal ion).

Instead **[L^{3}]** forms a polymeric species in the solid state via interaction of the methyl group of the coordinated acetonitrile and the oxygen atom of the urea unit. In addition

the urea group exhibits excellent binding properties with anions leading to an interaction between it and the perchlorate anion.

Confirmation of the assembly was carried out by ESI-MS which showed ion peaks at *m/z* 831 and 1142 corresponding to $\{[Cd(\mathbf{L^3})(ClO_4)]\}^+$ and $\{[Cd_2(\mathbf{L^3})(ClO_4)_3]\}^+$ respectively. Higher *m/z* adducts (e.g. *m/z* 1760 $\{[Cd_2(\mathbf{L^3})_2(ClO_4)_3]\}^+$) were also observed which can be assigned as artifacts due to the ESI-MS process.

Selected bond lengths and angles for the complex are shown in tables 3.1 and 3.2 below;

Atom 1	Atom 2	Bond Length (Å)
Cd1	N1	2.319 (14)
Cd1	N2	2.350 (15)
Cd1	N5	2.336 (2)

Table 3.1: Selected bond lengths for complex ($[Cd(\mathbf{L^3})](ClO_4)_2$).

Atom 1	Atom 2	Atom 3	Bond Angle (°)
N1	Cd1	N2	70.84 (5)
N1	Cd1	N5	89.66 (6)
N1	Cd1	N2	139.41 (5)
N1	Cd1	N1	149.74 (8)
N1	Cd1	N5	85.79 (6)
N2	Cd1	N5	97.23 (7)
N2	Cd1	N2	68.63 (7)
N2	Cd1	N5	97.21 (7)
N5	Cd1	N5	162.51 (12)

Table 3.2: Selected bond angles for complex ($[Cd(\mathbf{L^3})](ClO_4)_2$).

4.3: Summary:

In summary, reaction of **[L^3]** with $Cd(ClO_4)_2$ resulted in a mononuclear species whereby the metal centre is coordinated by two thiazole and two pyridine *N*-donors of the same ligand strand. In a similar fashion to the previously observed structure of **[L^2]** with $Cu_2(ClO_4)_2$, the mononuclear complex is driven by the metal ions preference for an octahedral geometry which necessitates the coordination of either solvent molecules (in the case of **[L^3]**) or a ligand arm of neighbouring structures (in the case of **[L^2]**).

However, in each case the species is different. Where **[L^2]** forms a polymeric species with neighbouring complexes through interaction of its long acetyl /amide ligand arms with a central metal ion, **[L^3]** is conformationally restricted (e.g. the urea oxygen atom cannot coordinate with the metal ion due to the inclusion of a large phenyl group). Instead **[L^3]** forms a polymeric species via interaction of the methyl group of the coordinated acetonitrile and the oxygen atom of the urea unit while a NH of the urea unit exhibits hydrogen bonding interactions to a perchlorate anion.

Chapter 5.0: Synthesis and coordination of a ligand containing *N*-donor and hydrogen bond donor sites for the coordination of metal ions and anions:

The addition of different anion binding substituents into the ligand strand has been shown to great effect. The inclusion of a urea group into the ligand arms of **[L^3]** was shown to have preferential binding for anions, in turn giving rise to some interesting coordination complexes. Similarly the addition of an indole binding unit into the ligand arms of **[L^4]** (Fig. 90) should, *in theory*, have interesting effects on the ligands coordination properties leading to some novel metal complexes.

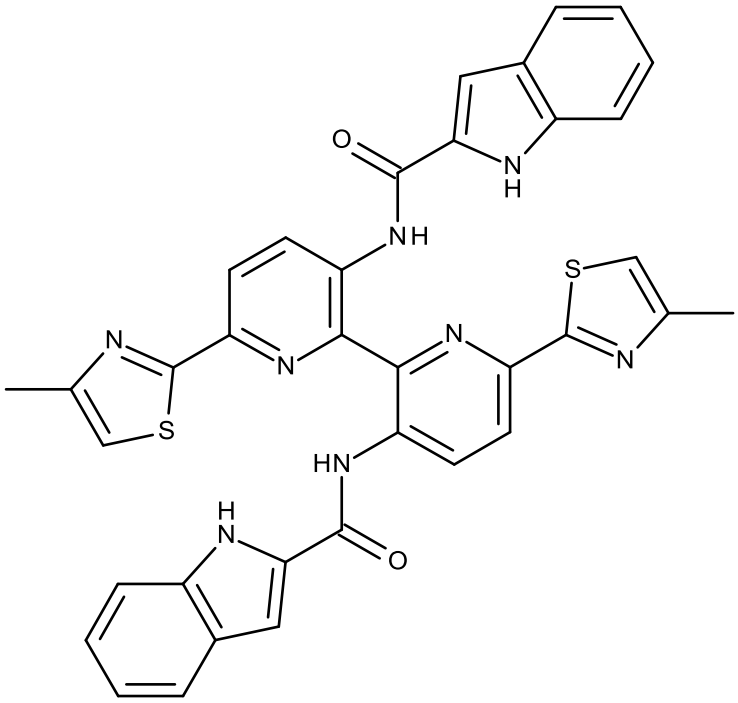

*Fig. 90: **[L^4]**.*

5.1: Synthesis of [L^4]:

Synthesis of **[L^4]** was carried out in a multi step process (Scheme 4) but again is similar to the synthesis of **[L^2]** / **[L^3]**. For this ligand the diamino tetradentate ligand **[8]** undergoes a reaction with indole-2-acid chloride **[9]**. Firstly indole-2-carboxylic acid was added to a 50 mL round bottom flask charged with anhydrous DCM, an equivalent of oxalyl chloride and a couple drops of DMF. The reaction was carried out under an atmosphere of N_2 at room temperature, after 10 minutes the reaction was added to a separate round bottom flask containing the diamine precursor **[8]**, anhydrous pyridine and DCM. The reaction was heated to 60°C for one hour, during which time a precipitate formed. The solid was isolated via vacuum filtration and washed with water, ethanol and ether. Confirmation of successful formation of **[L^4]** was carried out by ^{1}H NMR spectroscopy (Fig. 91) which showed a total of 11 environments with signals of note being two singlet's at 11.88 ppm and 10.96 ppm corresponding to the protons of the amide and indole respectively. Furthermore ESI-MS showed an ion at *m/z* 667 corresponding to [L^4+H]$^+$.

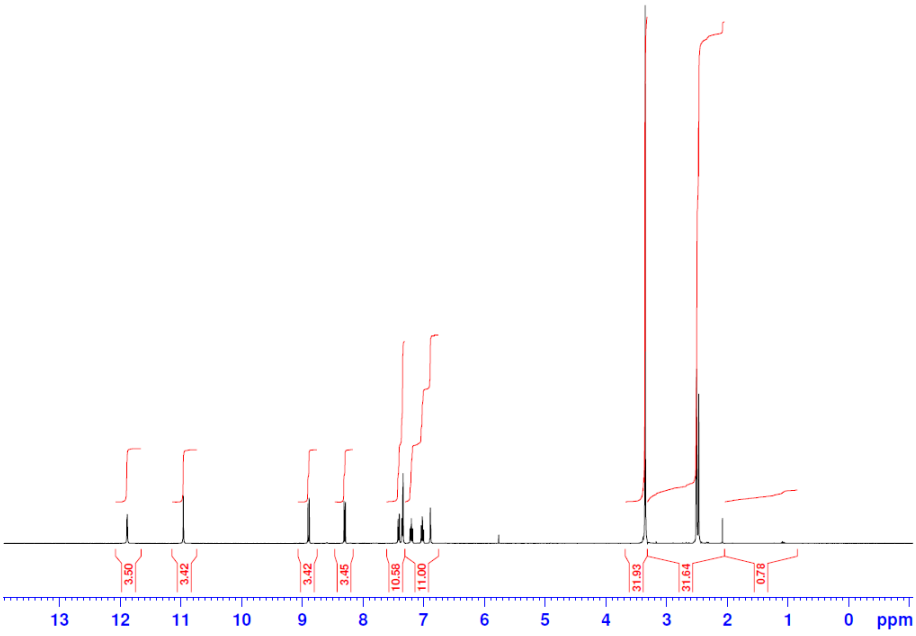

*Fig. 91: ^{1}H NMR spectrum of **[L^4]** (400MHz, d_6-DMSO).*

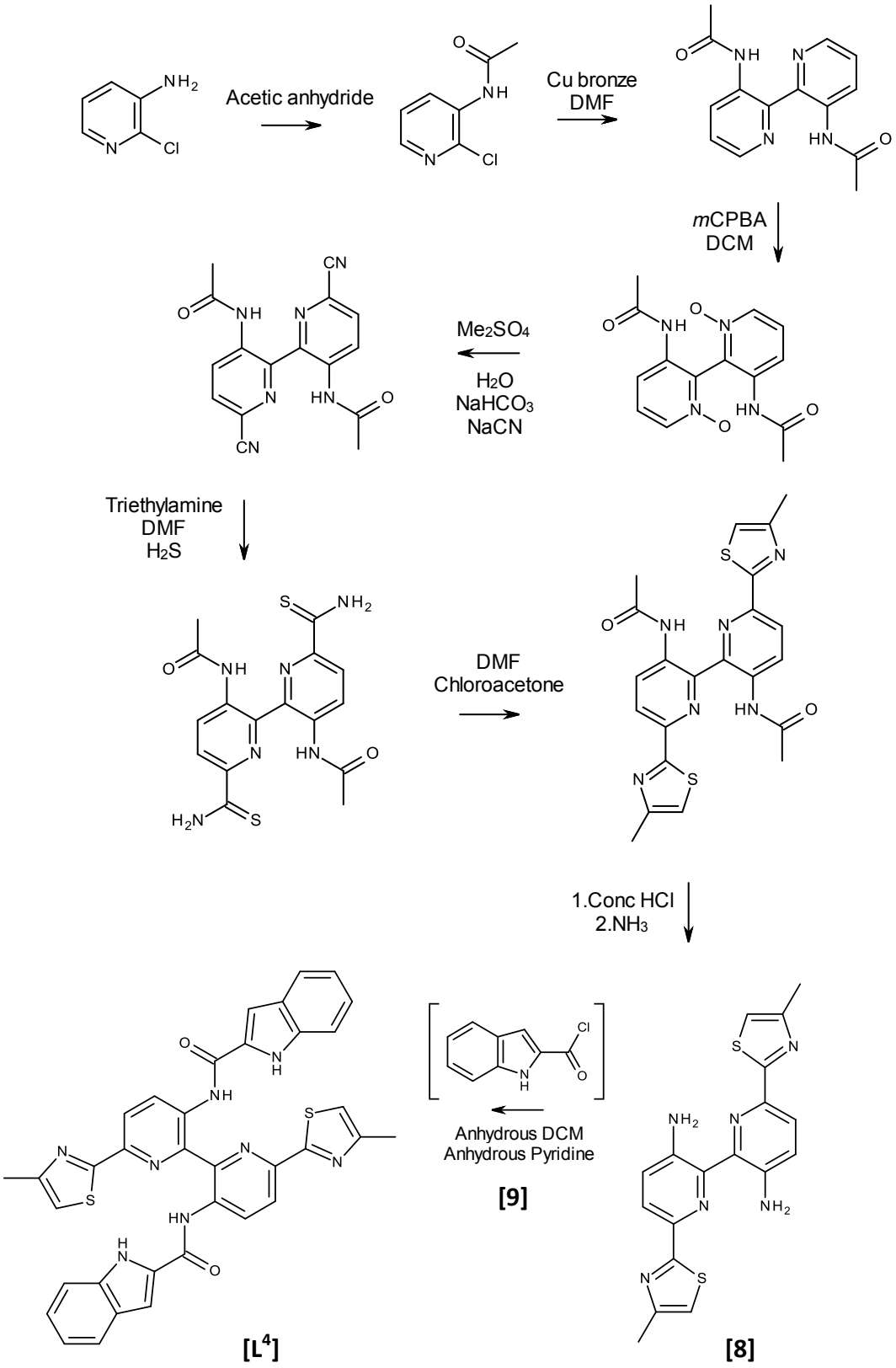

*Scheme 4: Synthesis of **[L^4]**.*

5.2: Coordination Chemistry of [L^4]:

5.2.1 Coordination of [L^4] with $Ag(ClO_4)$:

Reaction of the ligand **[L^4]** with $Ag(ClO_4)$ in $MeNO_2$ gave a clear and colourless solution from which colourless crystals formed upon slow diffusion of diisopropyl ether. Analysis by single-crystal X-ray diffraction showed that in the solid state a di-nuclear double stranded species is formed ($[Ag_2(\mathbf{L^4})_2](ClO_4)_2$) (Fig. 92).

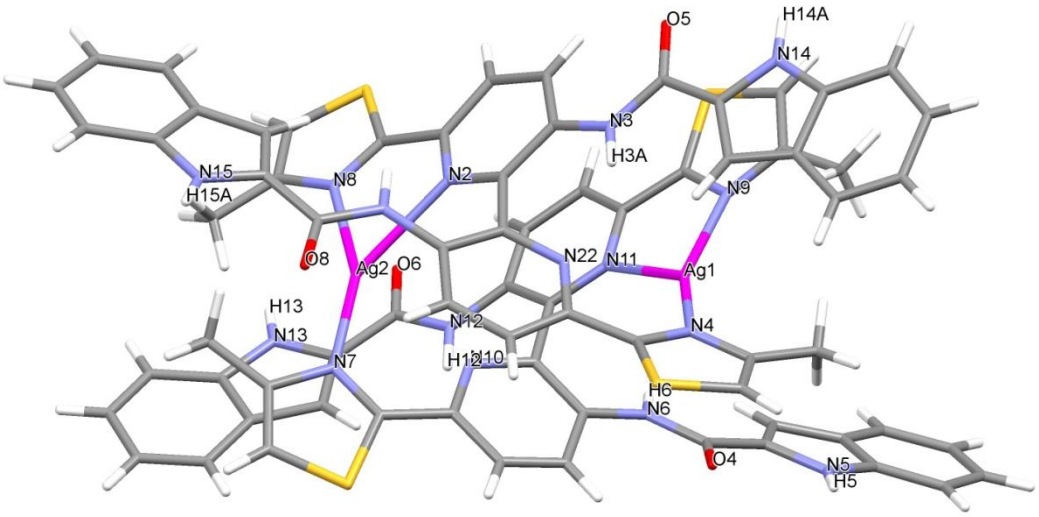

Fig. 92: Solid state structure of complex ($[Ag_2(\mathbf{L^4})_2](ClO_4)_2$), anions omitted for clarity.

Both ligands partition into separate mono and divalent binding domains whereby each metal centre exhibits a distorted trigonal planar geometry through coordinated with a pyridine and thiazole ring of one strand and a single thiazole ring of another (ave. N-Ag 2.318 Å). In previous structures the monovalent metal centres undergo coordination with the bipyridine nitrogen atoms, usually occupying two of the metals coordination sites. However in this particular species only one of the pyridine rings in each ligand undergoes coordination, leaving the second unbound. This is due to the larger distance between the second pyridine ring and the metal ion compared to that of the bound pyridine ring; 2.808 Å, 2.570 Å respectively (Fig. 93). Coordination of only one of the pyridine nitrogen atoms is possibly due to a large amount of steric bulk brought through addition of the indole group into the ligand strand.

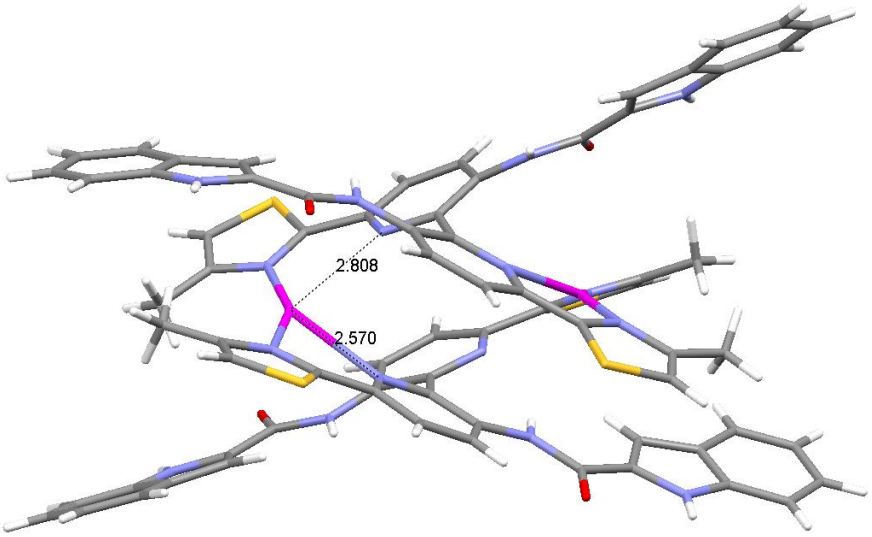

Fig. 93: Complex ($[Ag_2(\mathbf{L}^4)_2](ClO_4)_2$), showing the distances between the N-donor of each pyridine ring, anions omitted for clarity.

The ligand arms of each stand point to opposite ends of the complex with two of the four arms folding inwards towards the centre of the structure, in all cases the *NH*-donors of the indole point away from the structure with the amides pointing inwards (Fig. 94).

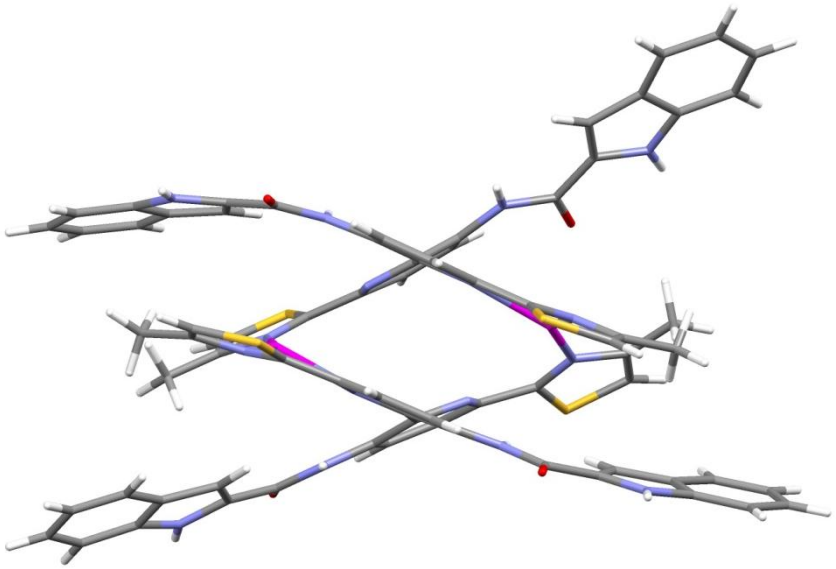

Fig. 94: 'Side' view of the complex ($[Ag_2(\mathbf{L}^4)_2](ClO_4)_2$), showing the orientation of the ligand arms, anions omitted for clarity.

Furthermore each indole of the ligand strands undergoes hydrogen bonding interactions with anions (N-H···O 2.162 Å) and solvent molecules (N-H···O 2.117 Å) through interaction with the N-H group (Fig. 39). Each ligand strand is made up of two indole groups, the first ligand strand hydrogen bonds a perchlorate anion with one indole and a diisopropyl ether solvent molecule by another. The second strand exhibits a different series of interactions; a diisopropyl ether solvent molecule remains hydrogen bonded to the N-H of an indole, however the perchlorate anion is bound to the amide of the ligand arm (N-H···O 2.349 Å) and the hydrogen atom in the 3-position of the same indole unit (C-H···O 2.463 Å) (Fig. 95).

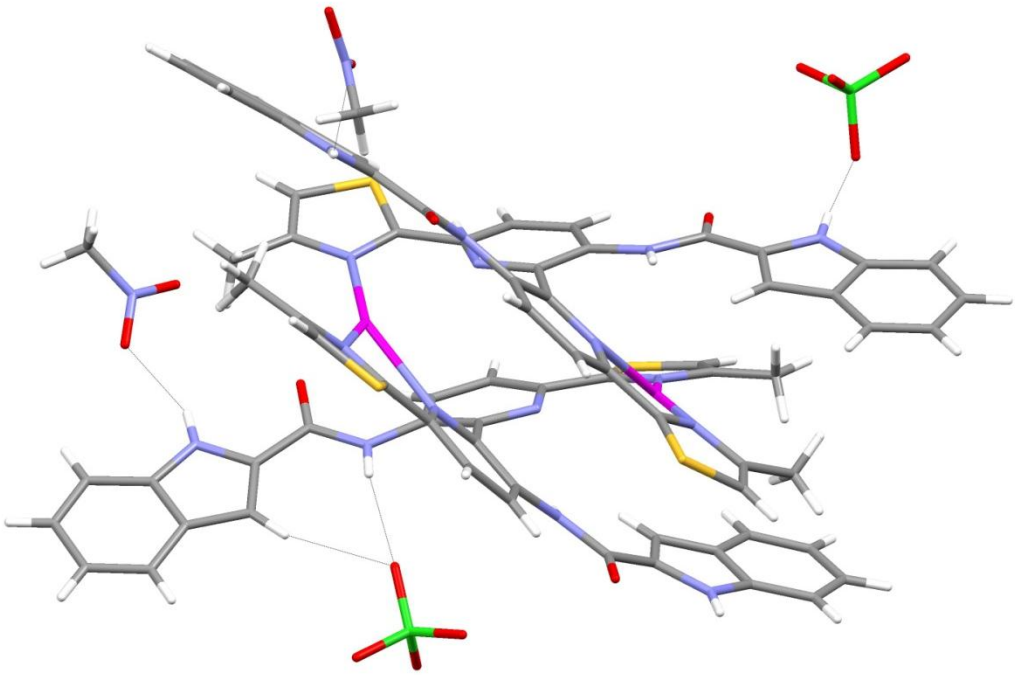

Fig. 95: Solid state structure of complex ($[Ag_2(\mathbf{L^4})_2](ClO_4)_2$), showing anion and solvent interactions.

The second indole unit shows no interactions with anions or solvent molecules; instead it exhibits a series of complimentary (Fig. 96c) intermolecular interactions between the indole (N-H···O-H 1.966 Å) and carbonyl (C-O··· H-N 1.966 Å) units of neighbouring complexes (Fig. 96a & b).

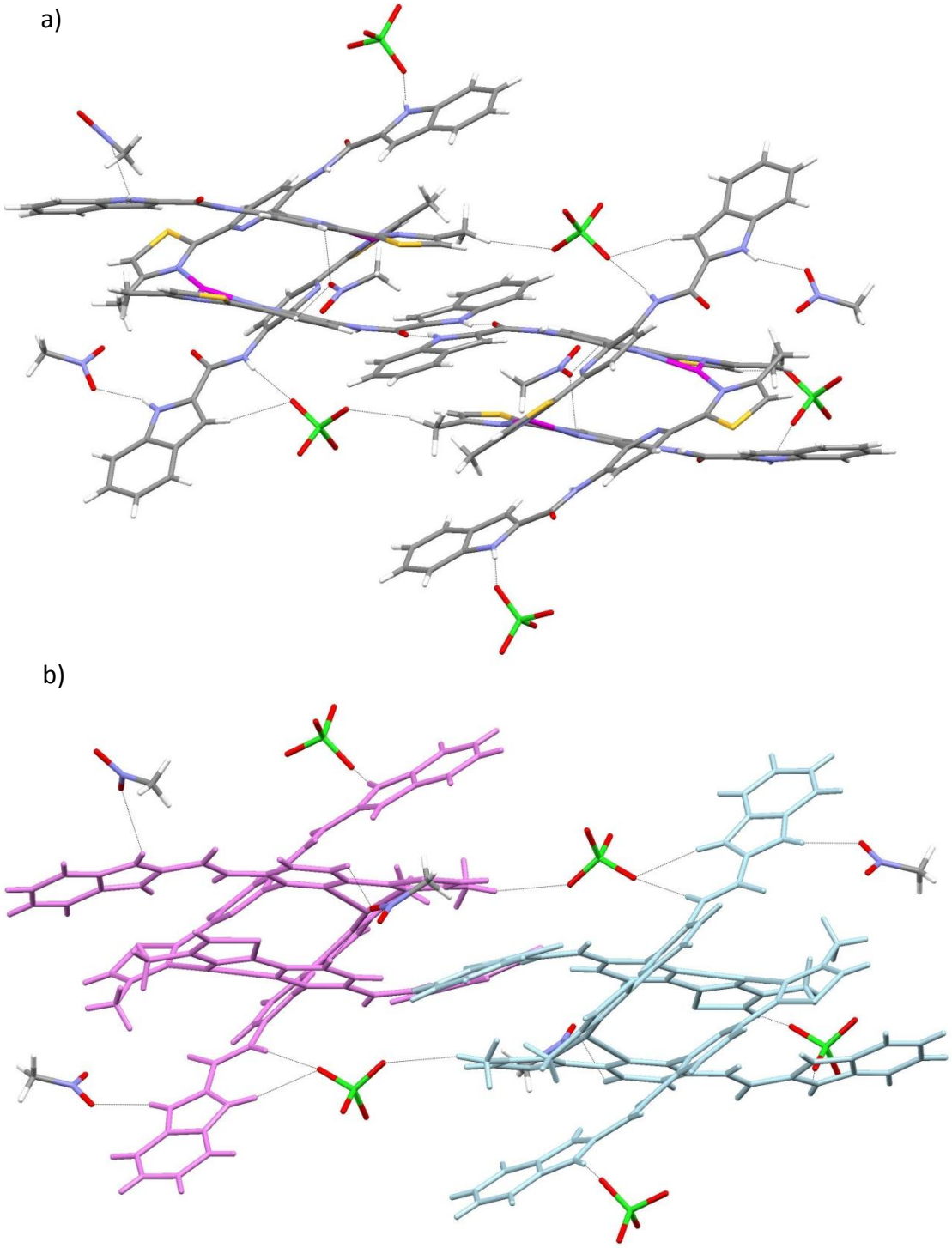

Fig. 96a & b: Long range order complexes showing the interactions between neighbouring indole / acetyl units.

Selected bond lengths and angles for the complex are shown in tables 4.1 and 4.2 below; relevant atom labels shown in Fig. 92.

Atom 1	Atom 2	Bond Length (Å)
Ag1	N11	2.435 (4)
Ag1	N4	2.174 (4)
Ag1	N9	2.232 (4)
Ag2	N2	2.570 (4)
Ag2	N7	2.173 (4)
Ag2	N8	2.209 (4)

Table 4.1: Selected bond lengths for complex ($[Ag_2(\mathbf{L^4})_2](ClO_4)_2$).

Atom 1	Atom 2	Atom 3	Bond Angle (°)
Ag1	N11	N4	139.24 (14)
Ag1	N11	N9	72.90 (13)
Ag1	N4	N9	147.60 (15)
Ag2	N2	N7	132.23 (14)
Ag2	N2	N8	69.99 (14)
Ag2	N7	N8	156.14 (16)

Table 4.2: Selected bond angles for complex ($[Ag_2(\mathbf{L^4})_2](ClO_4)_2$).

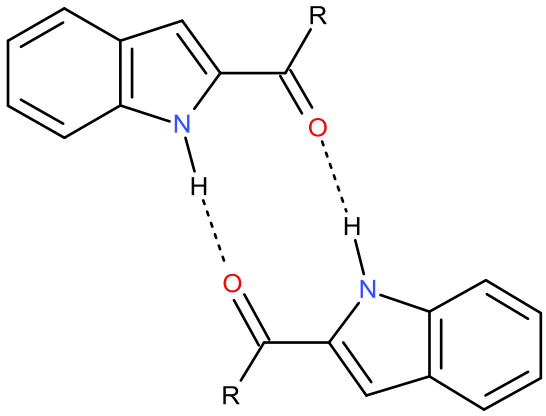

Fig. 96c: Complimentary interactions between the NH and O atoms of two indole units.

ESI-MS showed two high intensity mass ion peaks, one at *m/z* 775 which corresponds to $\{[Ag(\mathbf{L^4})]\}^+$ and a second at *m/z* 1649 which is consistent with $\{[Ag_2(\mathbf{L^4})_2(ClO_4)]\}^+$, therefore confirming that the species exists in solution.

5.3 Summary:

In summary reaction of **[L^4]** with Ag(ClO_4) resulted in a di-nuclear double stranded complex whereby each metal centre is coordinated by a thiazole of one ligand and a thiazole / pyridine of another, which is unlike any structure previously observed with **[L^1]**, **[L^2]** or **[L^3]**. Coordination of **[L^1]** and **[L^2]** with monovalent cations previously led to the formation of a series of di-nuclear double helicates, this can be attributed to the larger distance between the metal ion and the second pyridine ring (difference of 0.3 Å) making favourable coordination impossible.

Furthermore *all* ligands exhibit long range order with neighbouring complexes leading to structures with a polymeric motif; however **[L^4]** doesn't just rely on a series of hydrogen bonding anion-amide interactions which have previously been seen with **[L^1]**, **[L^2]** and monovalent cations (Fig. 97a & b). Instead **[L^4]** forms a larger aggregate species through interactions between complimentary indole / acetyl units of adjoining complexes as well as favourable anion-NH interactions (Fig. 41c).

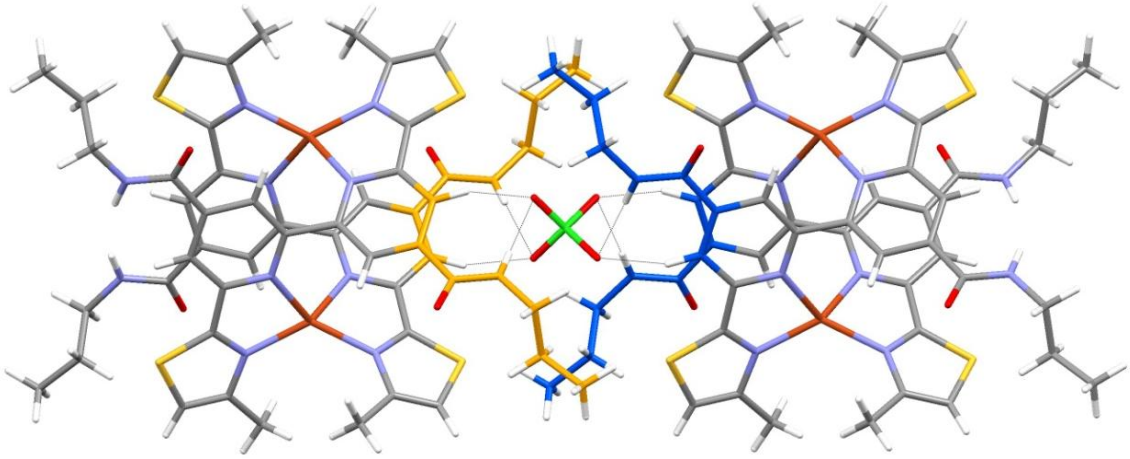

*Fig. 97: a) Long range order of the solid state structure, ([Cu_2(**L^1**)$_2$](ClO_4)$_2$).*

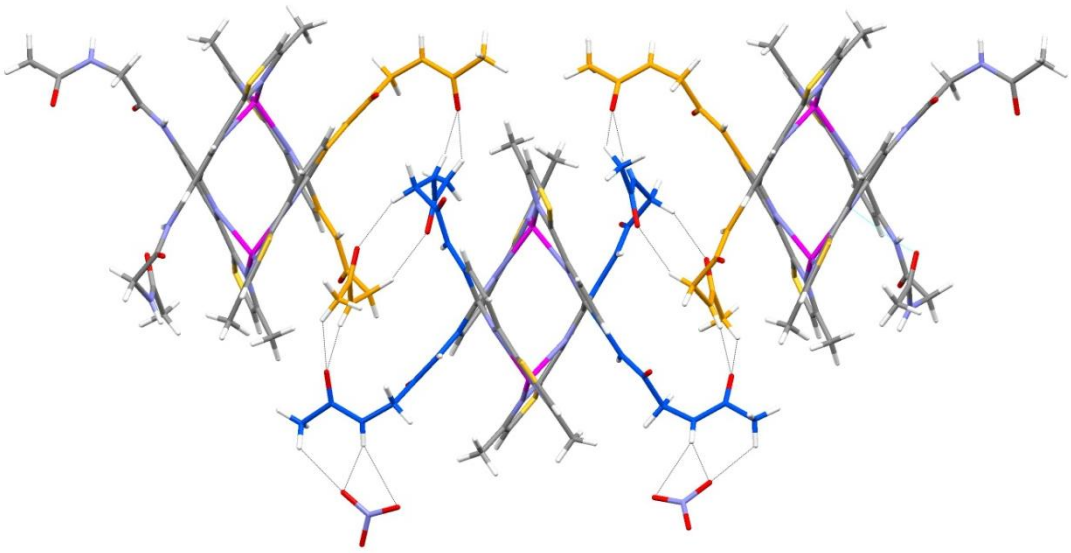

*Fig. 97: b) Long range order of the solid state structure, ([Ag(**L**^{2})](NO$_3$)$_2$).*

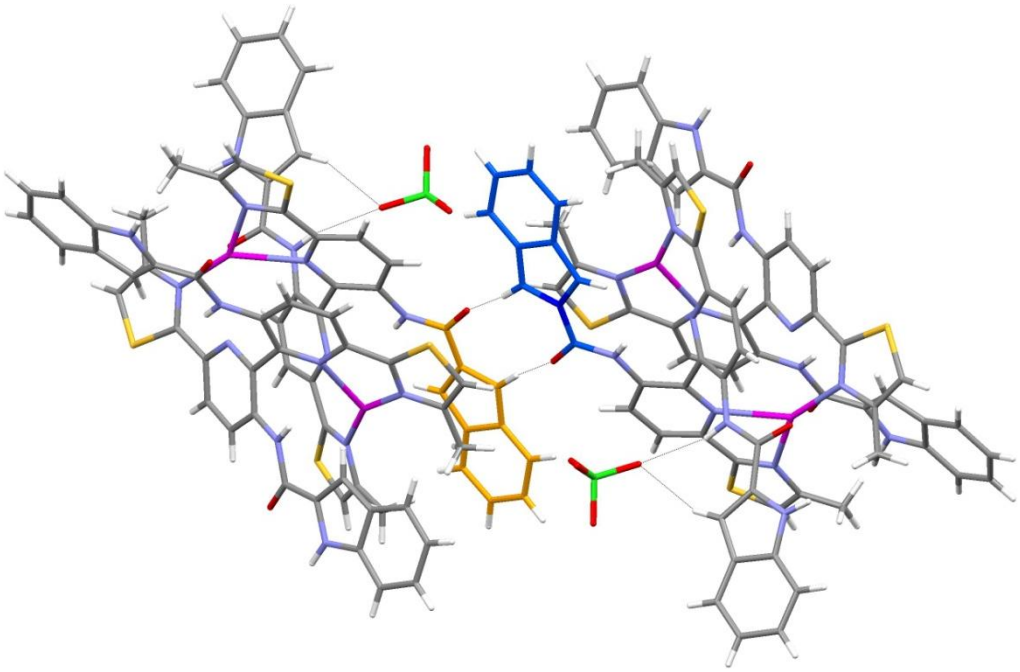

*Fig. 97: c) Long range order of the solid state structure, ([Ag$_2$(**L**^{4})$_2$](ClO$_4$)$_2$).*

Chapters 2-5 Experimental:

Synthesis of ligand [L^1]. To a 50 mL round bottom flask charged with 4,4`-dimethyl-2,2`-bipyridyl (1.00 g, 5.4 mmol) was added concentrated sulphuric acid (20 mL) and the reaction cooled to 0°C. To this was added aliquots of chromium (VI) oxide (3.26 g, 32.6 mmol) over 1 hour. The reaction was sonicated until all the reagents had dissolved and then heated at 75°C for 4 hours. The reaction was allowed to cool and then neutralized with water (10 mL) before being pored over ice (20 mL). During 30 minutes of stirring a pale yellow precipitate formed which was isolated via vacuum filtration and washed with water (2 x 10 mL), giving the di-acid. To a suspension containing the di-acid and water (100 mL) was added a solution of dilute potassium hydroxide until the reaction was basic (¬ 20 mL). During which time the reagents dissolved and a white precipitate formed, the green *solution* was isolated via vacuum filtration to give the deprotonated di-acid in solution.

To the basic solution was added concentrated hydrochloric acid (¬ 10 mL) drop wise over 10 minutes, during which time a precipitate formed which was isolated via vacuum filtration and washed sparingly with water (2 x 10 mL), giving the protonated di-acid (1.50 g) which was dried in a desiccator for 12 hours. The dried product was added to a 50 mL round bottom flask along with thionyl chloride (15 mL, 206 mmol) and refluxed with a condenser and guard tube for 24 hours. The solvent ($SOCl_2$) was removed via distillation with toluene (2 x 10 mL) and the reaction concentrated to dryness. To a 50 mL round bottom flask charged with bipy-dichloride and dichloromethane (20 mL) was added propylamine (5 mL, 60.82 mmol) drop wise at 0°C. The reaction was allowed to stir at room temperature during which time a pink precipitate formed. The solid was isolated via vacuum filtration and washed with dichloromethane (3 x 10 mL), giving the bipy-diamide as a pink solid (1.33 g).

A 50 mL reaction vessel was charged with bipy-diamide (0.10 g, 0.32 mmol) and a fourfold excess of *m*CPBA (77 %, 0.44 g, 2.52 mmol) in anhydrous DCM (25 mL), the reaction was allowed to stir at room temperature for 48 hours. After which time the reaction was concentrated and purified via column chromatography (10 % MeOH in DCM, Al_2O_3) giving the bis-*N*-oxide as a pure white solid (0.17 g). To a 50 mL round

bottom flask was added bis-*N*-oxide (0.17g, 0.50 mmol), benzoyl chloride (1 mL) and trimethylsilyl cyanide (1 mL) which was dissolved in anhydrous dichloromethane (25 mL). The reaction was stirred at 60°C for 12 hours, during which time an off white precipitate formed which was isolated via vacuum filtration and washed with dichloromethane (2 x 10 mL), giving the di-cyano as a solid (0.070 g). A solution of di-cyano (0.06 g, 0.15 mmol) and triethylamide (1 mL) in DMF (10 mL) was placed in a flask and H_2S was slowly bubbled through the solution for 15 minutes, during which time the solution turned yellow. The yellow solution was allowed to stand for 24 hours during which time a yellow solid precipitated out. The solid was isolated via vacuum filtration and washed with ethanol (2 x 5 mL) and ether (2 x 5 mL), giving the thioamide as a pale green solid (0.12 g).

To a 50 mL round bottom flask was added bipy-thioamide (0.12 g, 0.28 mmol) which was dissolved in ethanol (25 mL), to this was added chloroacetone (1 mL) and the reaction stirred and heated at 80°C for eight hours; after which time the reaction was allowed to cool to room temperature and stir for a further hour. During which time a thick white precipitate formed which was then isolated *via* vacuum filtration and washed with ethanol (2 x 5 mL) and ether (2 x 5 mL), giving the ligand as the hydrobromide salt. The salt was suspended in concentrated ammonia (10 mL) for 12 hours, re-filtered and washed with water (2 x 5 mL), ethanol (2 x 5 mL) and ether (2 x 5 mL), giving the free base ligand as a grey solid (0.08 g, 65 %, overall yield 12 %) (Fig. 98). ^{1}H NMR spectroscopy (400 MHz, d_6-DMSO) δ 9.19 (t, 2H, NH, *J* = 4.60 Hz), δ 8.84 (d, 2H, py, *J* = 1.19 Hz), δ 8.57 (d, 2H, *J* = 1.11 Hz), δ 7.57 (s, 2H, tz), δ 3.30 (dt, coincident with HOD peak), δ 1.60 (tq, overlap, 4H, *J* = 5.78 Hz), δ 1.09 (dt, 6H, *J* = 14.08, 5.58 Hz), δ 0.96 (t, 6H, *J* = 5.92 Hz). ESI-MS *m/z* 521 ($[M+H]^+$).

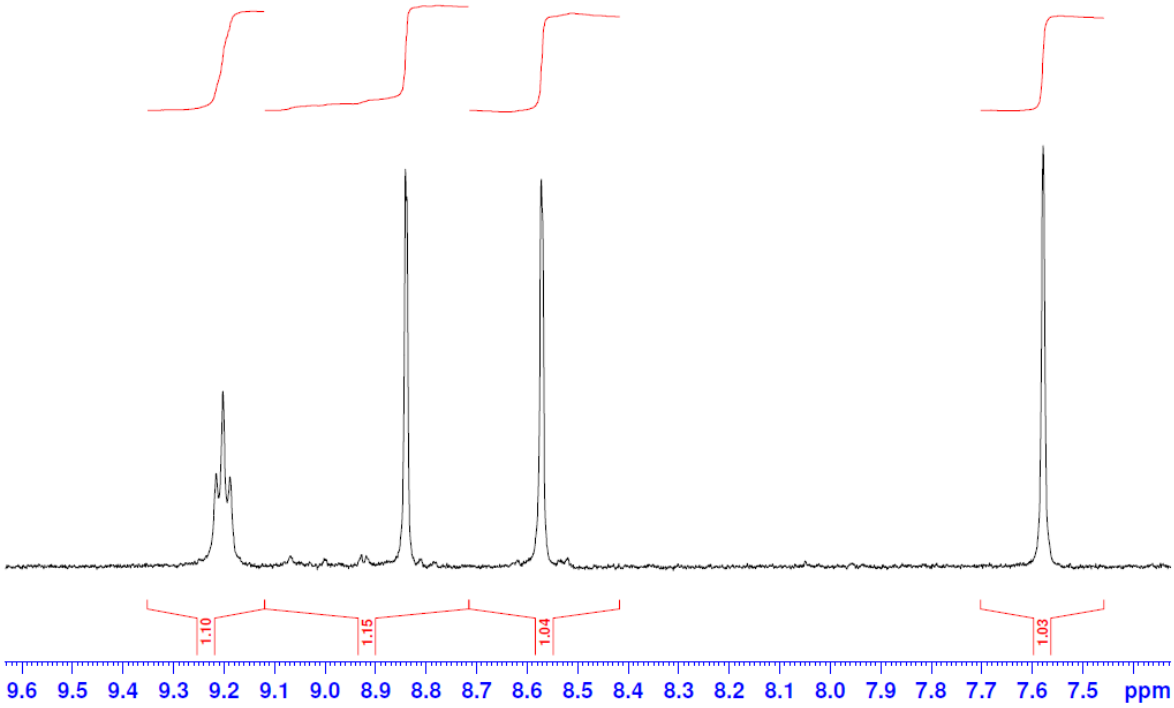

*Fig. 98: ^{1}H NMR spectrum of the aromatic region of **[L^{1}]**.*

Synthesis of [Co(L^{1})](BF$_4$)$_2$. To a suspension of $Co(BF_4)_2{\cdot}6H_2O$ (10 mg, 0.027 mmol) in MeCN (1 mL) was added a suspension of ligand **[L^{1}]** (11 mg, 0.021 mmol) in MeCN (1 mL) and the reaction warmed and sonicated until a clear orange solution had formed. Diisopropyl ether was slowly allowed to diffuse into the solution resulting in orange crystals.

Synthesis of [Hg(L^{1})](ClO$_4$)$_2$. To a suspension of $Hg(ClO_4)_2{\cdot}6H_2O$ (10 mg, 0.025 mmol) in MeCN (1 mL) was added a suspension of ligand **[L^{1}]** (11 mg, 0.021 mmol) in MeCN (1 mL) and the reaction warmed and sonicated until a clear and colourless solution had formed. Diisopropyl ether was slowly allowed to diffuse into the solution after several days colourless crystals formed. ESI-MS showed an ion at *m/z* 821 which corresponds to $\{[Hg(\mathbf{L^1})](ClO_4)]\}^+$.

Synthesis of [Cu$_2$(L^{1})$_2$](ClO$_4$)$_2$. To a suspension of $Cu(PF_6)$ (10 mg, 0.048 mmol) in MeCN (1 mL) was added a suspension of ligand **[L^{1}]** (11 mg, 0.021 mmol) in MeCN (1 mL) and the reaction warmed and sonicated until a clear deep red solution had formed. To this was then added $Bu_4N(ClO_4)$ (7.0 mg 0.021 mmol). Ethyl acetate was slowly allowed to

diffuse into the solution resulting in red / brown crystals. ESI-MS showed an ion at *m/z* 1267 which corresponds to $\{[Cu_2(\mathbf{L^1})_2](ClO_4)]\}^+$.

Synthesis of $[Cu_2(\mathbf{L^1})_2](BF_4)_2$. To a suspension of $Cu(PF_6)$ (10 mg, 0.048 mmol) in MeCN (1 mL) was added a suspension of ligand **$[\mathbf{L^1}]$** (11 mg, 0.021 mmol) in MeCN (1 mL) and the reaction warmed and sonicated until a clear deep red solution had formed. To this was then added $Bu_4N(BF_4)$ (7.0 mg 0.021 mmol). Ethyl acetate was slowly allowed to diffuse into the solution resulting in red / brown crystals. ESI-MS showed an ion at *m/z* 1255 which corresponds to $\{[Cu_2(\mathbf{L^1})_2](BF_4)]\}^+$.

Synthesis of $[Cu_2(\mathbf{L^1})_2](NO_3)_2$. To a suspension of $Cu(PF_6)$ (10 mg, 0.048 mmol) in MeCN (1 mL) was added a suspension of ligand **$[\mathbf{L^1}]$** (11 mg, 0.021 mmol) in MeCN (1 mL) and the reaction warmed and sonicated until a clear deep red solution had formed. To this was then added $Bu_4N(NO_3)$ (6.4 mg 0.021 mmol) and a couple of drops of MeOH to aid dissolution. Ethyl acetate was slowly allowed to diffuse into the solution resulting in red/ brown crystals. ESI-MS showed an ion at *m/z* 1230 which corresponds to $\{[Cu_2(\mathbf{L^1})_2](NO_3)]\}^+$.

Collection and analysis of all crystallographic data was carried out by Prof. C. Rice.

Crystal data for $[Co(\mathbf{L^1})](BF_4)_2$: $C_{28}H_{32}B_2Cl_6CoF_8N_6O_4S_2$, M = 513.99, *monoclinic,* α = 14.6413 (16), Å, b = 18.1675 (18) Å, c = 16.6563 Å, β = 107.451 (2) ˚, V = 4226.6 (8) Å^3, T = 150 K, space group *C2/c*, Z = 4, $\mu(MoK\alpha)$ = 0.961 mm^{-1}, 20905 reflections measured, 5263 independant reflections (R_{int} = 0.0617). The final R_1 values were 0.0761 ($I > 2\sigma(I)$). The final $wR(F^2)$ values were 0.2268 ($I > 2\sigma(I)$). The final R_1 values were 0.1075 (all data). The final $wR(F^2)$ = 0.2577 (all data). The goodness of fit on F^2 was 1.0604.

Crystal data for $[Hg(\mathbf{L^1})](ClO_4)_2$: $C_{27}H_{31}Cl_2HgN_7O_{12}S_2$, M = 981.22, *orthorhombic,* α = 8.7705 (4), Å, b = 15.6531 (8) Å, c = 24.9725 (12) Å, β = 90 ˚, V = 4226.6 (8) Å^3, T = 150 K, space group *C2/c*, Z = 4, $\mu(MoK\alpha)$ = 0.71073 mm^{-1}, 20096 reflections measured, 8836 independant reflections (R_{int} = 0.0406). The final R_1 values were 0.0395 ($I > 2\sigma(I)$). The final $wR(F^2)$ values were 0.0803 ($I > 2\sigma(I)$). The final R_1 values were 0.0607 (all data). The final $wR(F^2)$ = 0.0869 (all data). The goodness of fit on F^2 was 1.0067.

Crystal data for $[Cu_2(L^1)_2](ClO_4)_2$: $C_{52}H_{56}ClCu_2F_6N_{12}O_8PS_4$, *M* = 1412.83, *tetragonal*, *a* = 14.1454 (5) Å, *b* = 14.1454 (5) Å, *c* = 14.9372 (6) Å, *β* = 90 ˚, *V* = 2988.82 (19) Å^3, *T* = 150 K, space group *P42/c*, *Z* = 2, *μ(MoKα)* = 1.005 mm^{-1}, 22734 reflections measured, 5720 independant reflections (R_{int} = 0.0298). The final R_1 values were 0.0594 ($I > 2\sigma(I)$). The final $wR(F^2)$ values were 0.1659 ($I > 2\sigma(I)$). The final R_1 values were 0.0887 (all data). The final $wR(F^2)$ = 0.1932 (all data). The goodness of fit on F^2 was 1.029.

Crystal data for $[Cu_2(L^1)_2](BF_4)_2$: $C_{26}H_{28}BCuF_{10}N_4O_2PS_2$, *M* = 787.96, *tetragonal*, *a* = 14.1401 (4) Å, *b* = 14.1401 (4) Å, *c* = 15.0536 (5) Å, *β* = 90 ˚, *V* = 3009.85 (16) Å^3, *T* = 150 K, space group *P42/c*, *Z* = 4, *μ(MoKα)* = 1.015 mm^{-1}, 12141 reflections measured, 4601 independant reflections (R_{int} = 0.0271). The final R_1 values were 0.0672 ($I > 2\sigma(I)$). The final $wR(F^2)$ values were 0.1866 ($I > 2\sigma(I)$). The final R_1 values were 0.0877 (all data). The final $wR(F^2)$ = 0.2083 (all data). The goodness of fit on F^2 was 1.046.

Crystal data for $[Cu_2(L^1)_2](NO_3)_2$: $C_{52}H_{56}Cu_2F_6N_{13}O_7PS_4$, *M* = 1375.41, *tetragonal*, *a* = 28.0941 (7) Å, *b* = 28.0941 (7) Å, *c* = 14.8269 (5) Å, *β* = 90 ˚, *V* = 11702.6 (6) Å^3, *T* = 150 K, space group *P42/c*, *Z* = 8, *μ(MoKα)* = 0.71073 mm^{-1}, 57430 reflections measured, 13761 independant reflections (R_{int} = 0.0871). The final R_1 values were 0.0527 ($I > 2\sigma(I)$). The final $wR(F^2)$ values were 0.0969 ($I > 2\sigma(I)$). The final R_1 values were 0.1135 (all data). The final $wR(F^2)$ = 0.1179 (all data). The goodness of fit on F^2 was 1.0118.

Synthesis of ligand [L^2]. To a round bottom flask was added 3-amino-2-chloropyridine (2.00 g, 15.5 mmol) and acetic anhydride (15 mL) which was allowed to sit for 12 hours at room temperature. After which time the reagents had dissolved and the reaction was concentrated and re-crystalized from hot toluene (20 mL). During which time white crystals formed which were isolated via vacuum filtration and washed with hexane (2 x 5 mL), giving the product as a white solid (2.04 g).

Under an atmosphere of nitrogen, a 250 mL two neck round bottom flask was charged with pyridine amide (2.00 g, 10.9 mmol) and copper bronze (2.00 g) which was suspended in anhydrous DMF (30 mL). The reaction was heated at 80°C for 16 hours after which it was allowed to cool to room temperature before being poured over ice (100 mL). The reaction was allowed to stir for 10 minutes during which time a thick yellow precipitate formed. The yellow solid was filtered through a sintered funnel charged with celite then washed with concentrated ammonia (3 x 20 mL), giving a turquoise solid. The product was extracted into DCM (10 x 50 mL) and concentrated under vacuum to give bipy-acetyl-amide as a brown solid (0.90 g).

A 50 mL reaction vessel was charged with bipy-acetyl-amide (0.30 g, 1.1 mmol) and a threefold excess of *m*CPBA (77 %, 1.50 g, 8.7 mmol) in ahyderous DCM (25 mL), the reaction was allowed to stir at room temperature for 12 hours. After which time the reaction was concentrated and purified via column chromatography (10 % MeOH in DCM, Al_2O_3) giving the bis-*N*-oxide as a pure white solid (0.32 g). A solution of bis-*N*-oxide (0.90 g, 3.0 mmol) and dimethyl sulphate (25 mL) as stirred at 80°C for 24 hours, after which the product was precipitated *via* the addition of ether (20 mL) and allowed to stand for a further 24 hours. The ether was decanted off leaving the yellow oil. The solid was suspended in a solution of NaCN (0.50 g, 10.2 mmol) in H_2O (100 mL) and stirred for 10 minutes, after which time a cream precipitate formed. The solid was again isolated *via* vacuum filtration and washed with H_2O (3 x 10 mL), giving the bipy-di-cyano as a cream solid (0.63 g).

A solution of di-cyano (0.63 g, 1.97 mmol) and triethylamide (1 mL) in DMF (10 mL) was placed in a flask and H_2S was slowly bubbled through the solution for 15 minutes, during which time the solution turned yellow. The yellow solution was allowed to

stand for 24 hours during which time a yellow solid precipitated out. The solid was isolated via vacuum filtration and washed with ethanol (2 x 5 mL) and ether (2 x 5 mL), giving the thioamide as a pale yellow solid (0.33 g).

To a 50 mL round bottom flask was added bipy-thioamide (0.33 g, 0.85 mmol) which was suspended in DMF (25 mL), to this was added chloroacetone (0.5 mL) and the reaction stirred and heated at 80°C for eight hours; after which time the reaction was allowed to cool to room temperature and stir for a further hour. During which time a thick yellow precipitate formed which was then isolated *via* vacuum filtration and washed with ethanol (2 x 5 mL) and ether (2 x 5 mL), giving bipy-thiazole (0.25 g).

To a 50 mL round bottom flask was added bipy-thiazole (0.25 g, 0.54 mmol) which was suspended in dilute HCl (50 mL) and refluxed for three hours. After which time the reaction was cooled to 0°C and added to cold concentrated ammonia (50 mL). During addition a thick yellow precipitate formed which was isolated *via* vacuum filtration and washed with H_2O (2 x 10 mL), giving the diamine as a yellow solid (150 g).

Under an atmosphere of nitrogen, a 2 neck 50 mL round bottom flask was charged with *N*-acetylglycin (0.19 g, 1.71 mmol) and anhydrous pyridine (25 mL). The reaction was cooled to 0°C and to this added oxalyl chloride (0.7 mL, 1.28 mmol). The reaction was allowed to warm to room temperature and to this added bipy-diamine (0.03 g, 0.08 mmol). The reaction was then heated to 80°C for 12 hours until the reaction went from yellow to brown. During which time a precipitate formed which was isolated *via* vacuum filtration and washed with water (2 x 5 mL), ethanol (2 x 5 mL) and ether (2 x 5 mL), giving **[L^2]** as an off white solid (0.02 g, 66%). ^{1}H NMR spectroscopy (400 MHz, d_6-DMSO) δ 10.3 (s, 2H, NH), δ 8.78 (d, 2H, py, *J* = 8.75 Hz), δ 8.21 (d, 2H, py, J = 8.75), δ 8.20 (t, 2H, NH, *J* = 5.5 Hz), δ 7.43 (s, 2H, tz), δ 3.84 (d, 4H, CH_2, *J* = 5.5 Hz), δ 2.47 (s, 6H, -$COCH_3$), δ 1.67 (s, 6H, tz-CH_3). ESI-MS *m/z* 579 ($[M+H]^+$).

Synthesis of $[Zn(L^2)](ClO_4)_2$. To a suspension of $Zn(ClO_4)_2 \cdot 6H_2O$ (10 mg, 0.027 mmol) in $MeNO_2$ (1 mL) was added a suspension of ligand **$[L^2]$** (11 mg, 0.019 mmol) in $MeNO_2$ (1 mL) and the reaction warmed and sonicated until a clear yellow solution had formed. Ethyl acetate was slowly allowed to diffuse into the solution resulting in yellow crystals. ESI-MS showed an ion at *m/z* 743 which corresponds to $\{[Zn(\mathbf{L^2})](ClO_4)]\}^+$.

Synthesis of $[Cu(L^2)](ClO_4)_2$. To a suspension of $Cu(ClO_4)_2 \cdot 6H_2O$ (10 mg, 0.027 mmol) in $MeNO_2$ (1 mL) was added a suspension of ligand **$[L^2]$** (11 mg, 0.019 mmol) in $MeNO_2$ (1 mL) and the reaction warmed and sonicated until a clear green solution had formed. Ethyl acetate was slowly allowed to diffuse into the solution resulting in green crystals. ESI-MS showed an ion at *m/z* 1383 which corresponds to $\{[Cu_2(\mathbf{L^2})_2](ClO_4)]\}^+$.

Synthesis of $[Ag_2(L^2)_2](NO_3)_2$. To a suspension of $Ag(NO_3)$ (10 mg, 0.059 mmol) in $MeNO_2$ (1 mL) was added a suspension of ligand **$[L^2]$** (11 mg, 0.019 mmol) in $MeNO_2$ (1 mL) and the reaction warmed and sonicated until a clear and colourless solution had formed. Ethyl acetate was slowly allowed to diffuse into the solution resulting in colourless crystals. ESI-MS showed an ion at *m/z* 1471 which corresponds to $\{[Ag_2(\mathbf{L^2})_2](NO_3)]\}^+$.

Collection and analysis of all crystallographic data was carried out by Prof. C. Rice.

Crystal data for $[Zn(L^2)](ClO_4)_2$: $C_{27}H_{26}Cl_4N_8O_{12}S_2Zn$, *M* = 927.04*, monoclinic*, *a* = 12.258 (2) Å, *b* = 21.980 (4) Å, *c* = 14.932 (3) Å, *β* = 94.177 (4)˚, *V* = 3931.9 (12) Å^3, *T* = 150 K, space group *P21/n*, *Z* = 4, *μ(MoKα)* = 1.070 mm^{-1}, 46847 reflections measured, 11514 independant reflections (R_{int} = 0.0633). The final R_1 values were 0.0599 ($I > 2\sigma(I)$). The final $wR(F^2)$ values were 0.1714 ($I > 2\sigma(I)$). The final R_1 values were 0.1078 (all data). The final $wR(F^2)$ = 0.1992 (all data). The goodness of fit on F^2 was 1.035.

Crystal data for $[Cu(L^2)](ClO_4)_2$: $C_{28}H_{32}Cl_2CuN_{10}O_{16}S_2$, *M* = 963.20*, monoclinic*, *a* = 12.4851 (9) Å, *b* = 21.6790 (16) Å, *c* = 14.1739 (10) Å, *β* = 93.641 (2)°, *V* = 3828.6 (5) Å^3, *T* = 150 K, space group *P21/n*, *Z* = 4, *μ(MoKα)* = 0.905 mm^{-1}, 45253 reflections measured, 11202 independant reflections (R_{int} = 0.0492). The final R_1 values were 0.0437 ($I > 2\sigma(I)$). The final $wR(F^2)$ values were 0.1087 ($I > 2\sigma(I)$). The final R_1 values were 0.0680 (all data). The final $wR(F^2)$ = 0.1204 (all data). The goodness of fit on F^2 was 1.029.

Crystal data for $[Ag_2(L^2)_2](NO_3)_2$: $C_{52}H_{55}Ag_2N_{18}O_{15}S_4$, *M* = 1516.12*, orthorhombic*, *a* = 11.500 (2) Å, *b* = 17.453 (4) Å, *c* = 30.427 (6) Å, *β* = 90°, *V* = 6107 (2) Å^3, *T* = 150 K, space group *Pccn*, *Z* = 4, *μ(MoKα)* = 0.859 mm^{-1}, 39117 reflections measured, 9399 independant reflections (R_{int} = 0.1720). The final R_1 values were 0.0751 ($I > 2\sigma(I)$). The final $wR(F^2)$ values were 0.1537 ($I > 2\sigma(I)$). The final R_1 values were 0.2330 (all data). The final $wR(F^2)$ = 0.2200 (all data). The goodness of fit on F^2 was 0.980.

Synthesis of ligand [L^3]. The steps used for the synthesis of **[L^3]** are identical to the ones carried out in the synthesis of **[L^2]**. The procedure only differs from step six onwards.

To a 50 mL vial charged with bipy-diamine (0.030 g, 0.08 mmol) and anhydrous pyridine (10 mL) was added a fourfold excess of phenyl-isocyanate (0.34 mL, 3.1 mmol). The reaction was allowed to stir at room temperature for 30 minutes, during which time a yellow precipitate formed. The yellow solid was isolated *via* vacuum filtration and washed with ethanol (2 x 5 mL) and ether (2 x 5 mL), giving the ligand as a yellow solid (0.025 g, 83 %) (Fig. 99). ^{1}H NMR spectroscopy (400 MHz, d_6-DMSO) δ 9.29 (s, 2H, NH), δ 9.20 (d, 2H, py, *J* = 7.04 Hz), δ 8.94 (s, 2H, NH), δ 8.23 (d, 2H, py, *J* = 7.08 Hz), δ 7.39 (d, 4H, ph, *J* = 6.68 Hz), δ 7.32 (s, 2H, tz), δ 7.28 (t, 4H, ph, *J* = 6.48, 12.6 Hz), δ 6.99 (t, 2H, ph, *J* = 5.92, 11.8 Hz). ^{13}C NMR spectroscopy (100 MHz d_6-DMSO) δ 167.0, δ 153.2, δ 152.1, δ 143.4, δ 141.8, δ 139.1, δ 136.1, δ 128.9, δ 128.7, δ 122.3, δ 119.8, δ 118.6 and δ 116.3. ESI-MS *m/z* 619 ($[M+H]^+$).

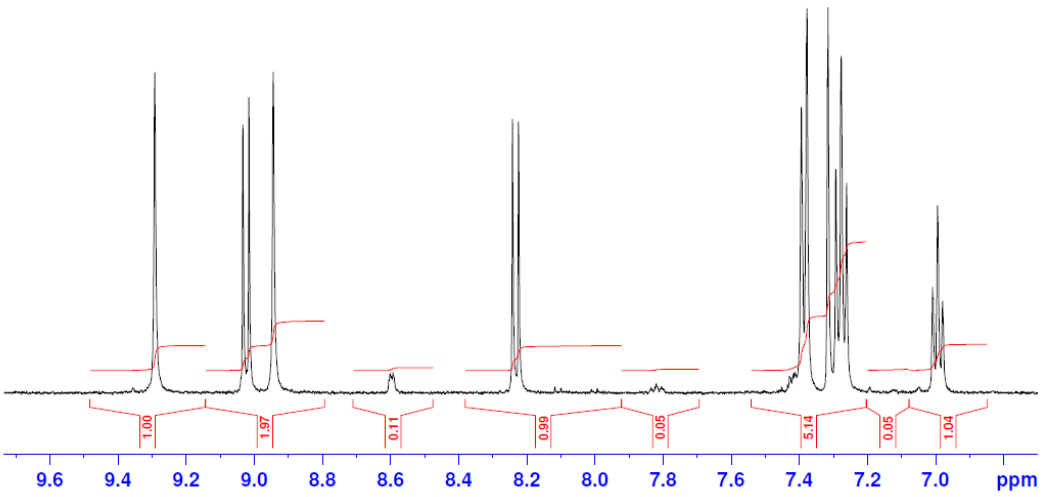

*Fig. 99: ^{1}H NMR spectrum of the aromatic region of **[L^3]**.*

Synthesis of $[Cd(L^3)](ClO_4)_2$. To a suspension of $Cd(ClO_4)_2 \cdot 6H_2O$ (10 mg, 0.032 mmol) in MeCN (1 mL) was added a suspension of ligand **$[L^3]$** (11 mg, 0.018 mmol) in MeCN (1 mL) and the reaction warmed and sonicated until a clear yellow solution had formed. Diisopropyl ether was slowly allowed to diffuse into the solution resulting in yellow crystals. ESI-MS showed an ion at *m/z* 831 which is consistent with $\{[Cd(\mathbf{L^3})(ClO_4)]\}^+$.

Collection and analysis of all crystallographic data was carried out by Prof. C. Rice.

Crystal data for $[Cd(L^3)](ClO_4)_2$: $C_{36}H_{32}CdCl_{12}N_{10}O_{10}S_2$, M = 1012.14*, monoclinic*, a = 18.6963 (9) Å, b = 17.2132 (9) Å, c = 14.2184 (7) Å, β = 115.02 (10) °, V = 4146.3 (4) Å^3, T = 150 K, space group *C2/c*, Z = 4, $\mu(MoK\alpha)$ = 0.825 mm^{-1}, 29956 reflections measured, 7219 independant reflections (R_{int} = 0.0471). The final R_1 values were 0.0352 ($I > 2\sigma(I)$). The final $wR(F^2)$ values were 0.0741 ($I > 2\sigma(I)$). The final R_1 values were 0.0559 (all data). The final $wR(F^2)$ = 0.0821 (all data). The goodness of fit on F^2 was 1.012.

Synthesis of ligand [L^4]. The steps used for the synthesis of **[L^4]** are identical to the ones carried out in the synthesis of **[L^2]**. The procedure only differs from step six onwards.

Under an atmosphere of nitrogen, a two neck 50 mL round bottom flask was charged with a fivefold excess of indole-2-carboxylic acid (0.085g, 0.53 mmol), anhydrous DCM (20 mL), and anhydrous DMF (0.2 mL). To the reaction was added an equivilant of oxalyl chloride (0.26 mL, 0.52 mmol) slowly over 10 minutes. After which time the reaction was transferred to a separate 50 mL two neck round bottom flask charged with; bipy-diamine (0.040 g, 0.1 mmol), anhydrous pyridine (1 mL) and anhydrous DCM (10 mL). The reaction was heated to 60°C for one hour during which time the reagents dissolved and a white precipitate formed. The solid was isolated *via* vacuum filtration and washed with water (2 x 5 mL), ethanol (2 x 5 mL) and ether (2 x 5 mL), giving the ligand as a pale yellow solid (0.033 g, 82.5 %) (Fig. 100). ^{1}H NMR spectroscopy (400 MHz, d_6-DMSO) δ 11.88 (s, 2H, NH), δ 10.96 (s, 2H, ind), δ 8.90 (d, 2H, py, *J* = 8.68 Hz), δ 8.30 (d, 2H, py, *J* = 8.68), δ 7.41 (d, 2H, ph, *J* = 8.40 Hz), δ 7.35 (d, 2H, ph, *J* = 6.16 Hz), δ 7.34 (s, 2H, tz) δ 7.21 (td, 2H, ph, *J* = 0.72, 7.92 Hz), δ 7.02 (td, 2H, ph, *J* = 7.72, 14.96 Hz), δ 6.89 (s, 2H, ind). ESI-MS *m/z* 667 ($[M+H]^+$).

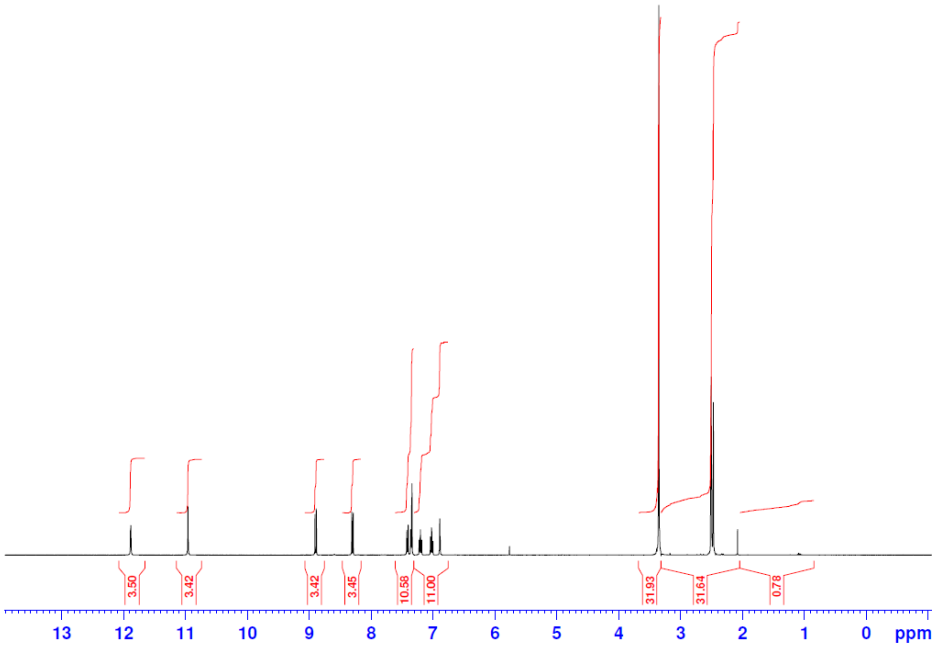

*Fig. 100: ^{1}H NMR spectrum of **[L^4]** (400MHz, d_6-DMSO).*

Synthesis of $[Ag_2(L^4)_2](ClO_4)_2$. To a suspension of $Ag(ClO_4)$ (10 mg, 0.048 mmol) in $MeNO_2$ (1 mL) was added a suspension of ligand **$[L^4]$** (11 mg, 0.017 mmol) in $MeNO_2$ (1 mL) and the reaction warmed and sonicated until a clear and colourless solution had formed. Diisopropyl ether was slowly allowed to diffuse into the solution resulting in colourless crystals. ESI-MS showed a distinct ion peak at *m/z* 1649 corresponding to $\{[Ag_2(\mathbf{L^4})_2(ClO_4)]\}^+$.

Collection and analysis of all crystallographic data was carried out by Prof. C. Rice.

Crystal data for $[Ag_2(L^4)_2](ClO_4)_2$: $C_{38}H_{33}AgClN_{10}O_{10}S_2$, M = 1011.44, *monoclinic*, a = 18.1782 (12) Å, b = 20.9455 (11) Å, c = 23.5818 (16) Å, β = 110.609 (2)°, V = 8404.2 (9) $Å^3$, T = 150 K, space group *P21/c*, Z = 8, $\mu(MoK\alpha)$ = 0.714 mm^{-1}, 82460 reflections measured, 21238 independant reflections (R_{int} = 0.0780). The final R_1 values were 0.0596 ($I > 2\sigma(I)$). The final $wR(F^2)$ values were 0.1522 ($I > 2\sigma(I)$). The final R_1 values were 0.1289 (all data). The final $wR(F^2)$ = 0.1856 (all data). The goodness of fit on F^2 was 1.025.

6. Chapter 6: Synthesis and coordination chemistry of a ligand containing both *N*-donor and hydrogen bond donor units:

The ligand **[L^5]** contains two pyridyl-thiazole units connected to a 1,3-diaminobenzene unit (Fig. 101). The *N*-donor heterocycles can act as bidentate chelates to transition metal ions and the amine can act as either a hydrogen-bond donors or, at least in theory, *N*-donor ligands. In this work we demonstrate that the arrangement of these groups on the ligand strand is optimized for favourable interactions with both anions and cations.

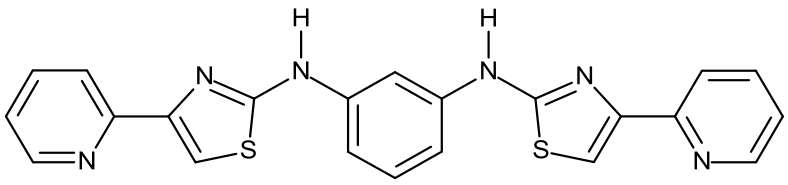

*Fig. 101: Bis-bidentate amine-containing ligand **[L^5].***

6.1 Synthesis of [L^5]:

Synthesis of **[L^5]** was carried out in a two-step process (Scheme. 5). Firstly 1,3-diaminobenzene **[1]** was reacted with ammonium thiocyanate in dilute hydrochloric acid at 90°C which gave phenyl-1,3-dithioamide as a precipitate after 12 hrs. Confirmation of the successful formation of this species was obtained by ^{1}H NMR spectroscopy which showed a total of five signals integrating to 10 protons. Importantly as well as the three signals corresponding to the three aromatic protons broad peaks at 7.8 and 9.8 ppm (integrating to two and four hydrogen environments respectively) corresponding to the thio-urea protons were also observed.

Formation of **[L^5]** was achieved by reaction of the dithioamine **[2]** with an excess of 2-(α-bromoacetyl)pyridine at 80°C for 12 hours. The precipitate was then isolated by filtration and suspended in concentrated ammonia overnight to give the free-base ligand. Examination of the ^{1}H NMR spectrum in d_6-DMSO indicated the successful formation of **[L^5]**. The spectrum showed 16 protons (although some of the environments are coincident) but importantly the spectrum shows a signal at 10.38 ppm which corresponds to the amine proton and a singlet at 7.57 ppm corresponding

to the thiazole unit (Fig. 102). Furthermore, ESI-MS showed an ion at *m/z* 429 corresponding to $[L^5+H]^+$ and ^{13}C NMR spectroscopy also showed 12 signals in the aromatic region.

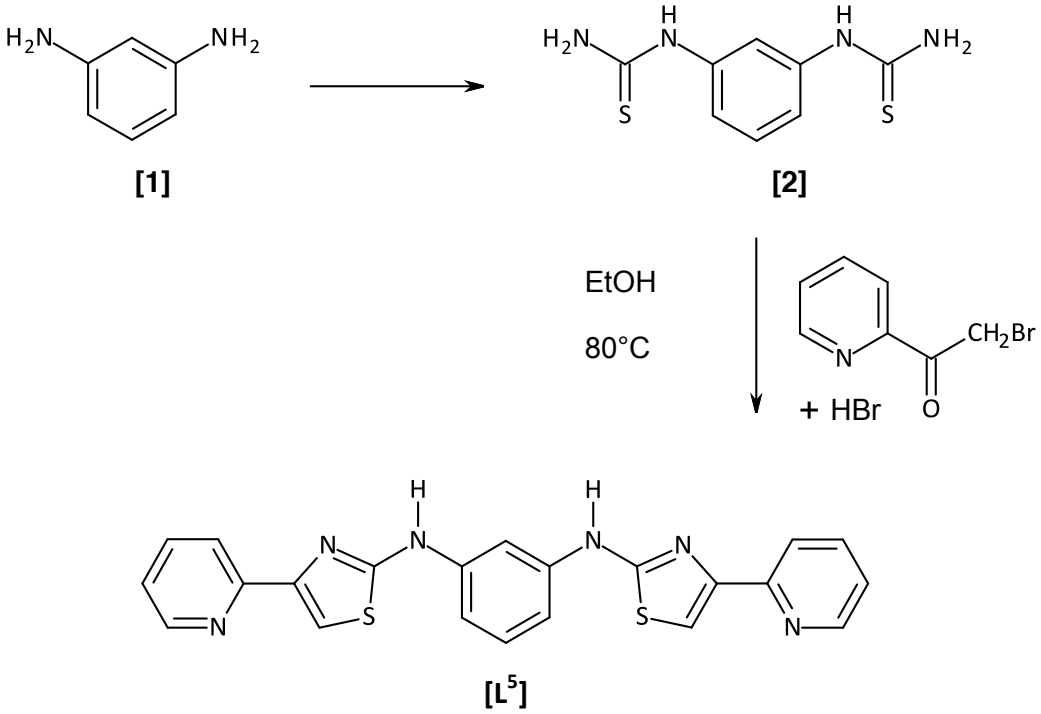

Scheme 5: Synthesis of **[L^5]**.

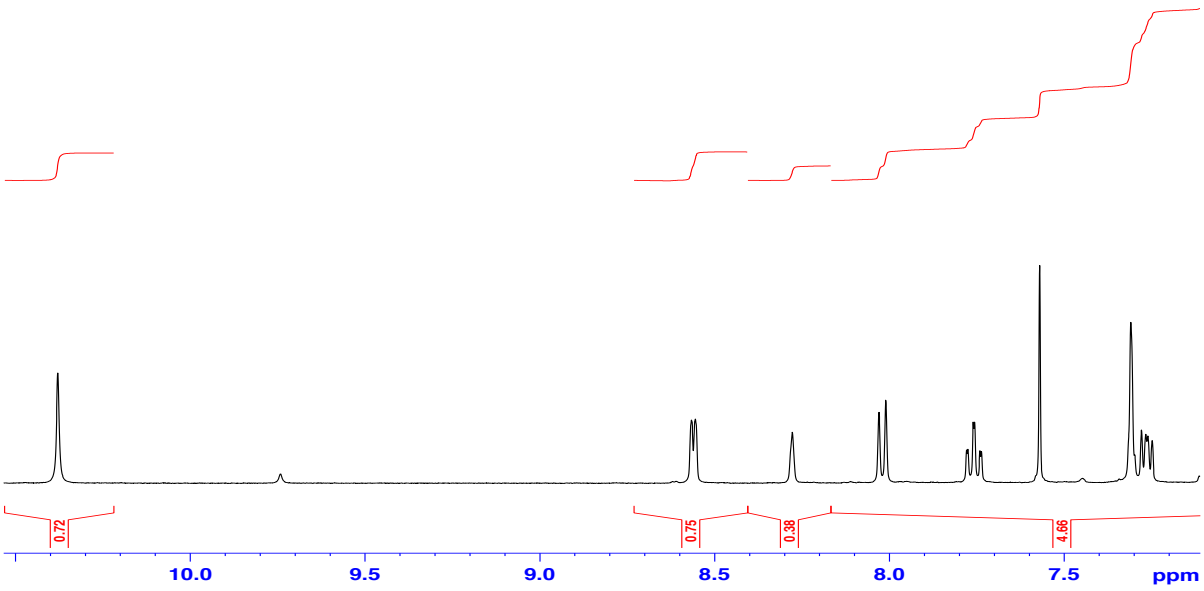

Fig. 102: ^1H NMR spectrum of the aromatic region of ***[L^5]****. (400MHz, d_6-DMSO) signals of note include the amine and thiazole proton (δ 10.38 and 7.57 respectively).*

6.2 Coordination Chemistry of [L^5]:

6.2.1 Coordination of [L^5] with $Cu(BF_4)_2$:

Reaction of the ligand with $Cu(BF_4)_2$ in $MeNO_2$ gave a dark blue solution from which dark blue crystals formed upon slow diffusion of diisopropyl ether. Analysis by single-crystal X-ray diffraction showed that in the solid state a dinuclear double helicate ($[Cu_2(\mathbf{L^5})_2]^{4+}$) is formed (Fig. 103).

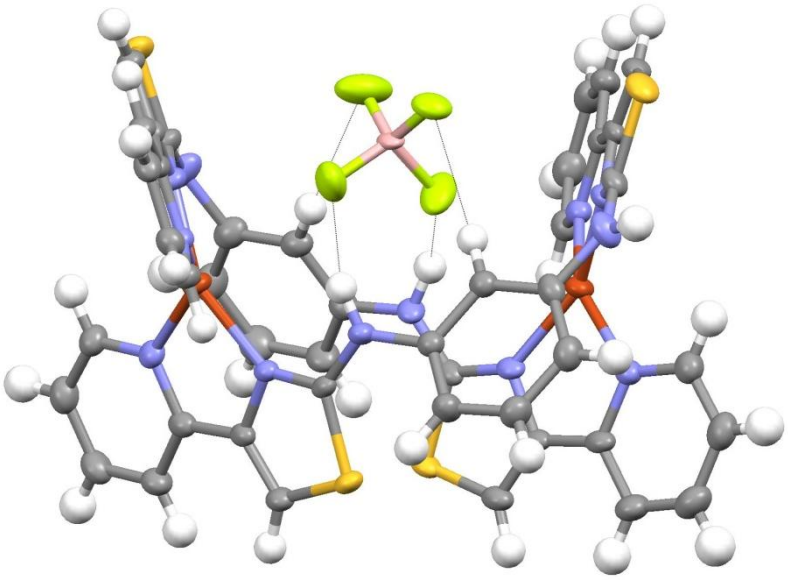

Fig. 103: Solid state structure of ($[Cu_2(\mathbf{L^5})_2](BF_4)$)$^{3+}$. Thermal ellipsoids are shown at the 50% probability level, remaining anions are omitted for clarity.

The geometry of each metal ion can possibly be considered distorted tetrahedral (Fig. 104). The plains formed by the two pyridyl – thiazole units are 46˚; roughly half way between the ideal angle for tetrahedral (90˚) and square planar (0˚).

The aforementioned distorted tetrahedral geometry is brought about by the coordination of the copper ions with the thiazole groups from each ligand (Cu-N bond lengths 1.991 (4) – 1.973 (4) Å). The ligands wrap around each other resulting in a twist which is typical of a linear helicate, in doing so it creates a cavity large enough to encapsulate a BF_4^- anion through hydrogen bonding between the fluorine atoms, two of the amines (ave. N-H···F 2.083 Å) and two protons from the phenyl rings (ave. C-H···F 2.599 Å).

Due to steric constraints brought about by the formation of the helicate the two remaining amines point outwards from the complex preventing them from any interaction with the central anion; instead they hydrogen bond with other tetrafluoroborate anions.

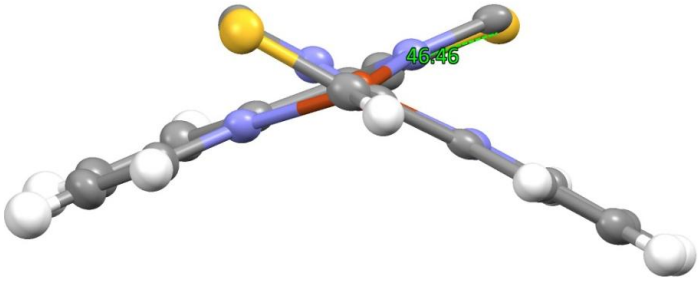

Fig. 104: A cross section of the complex ($[Cu_2(\mathbf{L^5})_2](BF_4)$),[3] showing the angle along the plane of symmetry.

Viewing the complex vertically shows the size of the central cavity in relation to the anion (Fig. 105). Examination of the structure shows that the cavity, brought about during formation, readily acts as a host to the anion due to its complimentary size and geometry. It seems highly likely that this may not be the case for anions with larger radii as their size may restrict their entry to the pocket and in turn the strong hydrogen bonding interactions.

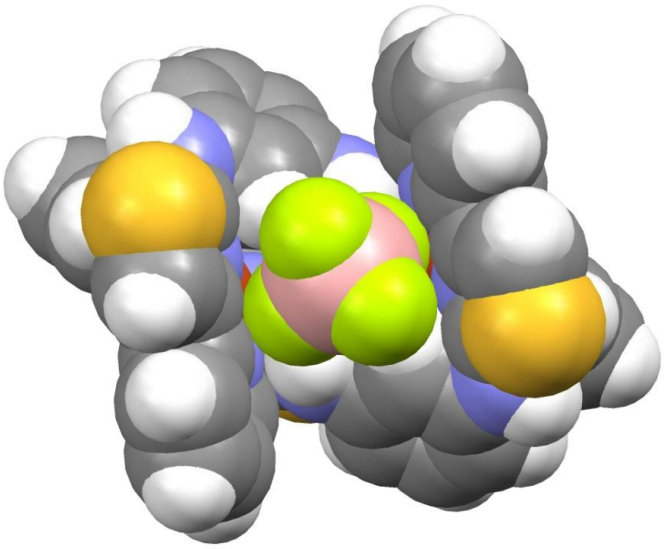

Fig. 105: Solid state structure of $([Cu_2(\mathbf{L^5})_2](BF_4))^{3+}$. Space filling model showing the encapsulation of the BF_4^- anion.

Selected bond lengths and angles for the complex are shown in Tables 5.1 and 5.2 below; relevant atom labels are shown in Fig. 106.

Atom 1	Atom 2	Bond Length (Å)
Cu1	N1	1.973 (4)
Cu1	N2	1.985 (4)
Cu1	N7	1.988 (4)
Cu1	N8	1.987 (3)
Cu2	N5	1.977 (4)
Cu2	N6	1.974 (4)
Cu2	N11	1.998 (4)
Cu2	N12	1.991 (4)

Table 5.1: Selected copper/nitrogen bond lengths for $[Cu_2(\mathbf{L^5})_2](BF_4)^{3+}$.

Atom 1	Atom 2	Atom 3	Bond Angle (°)
Cu1	N1	N2	83.35 (15)
Cu1	N1	N7	143.81 (15)
Cu1	N1	N8	102.78 (15)
Cu1	N2	N7	106.00 (16)
Cu1	N2	N8	154.40 (15)
Cu1	N7	N8	83.86 (15)
Cu2	N5	N6	83.20 (15)
Cu2	N5	N11	152.98 (15)
Cu2	N5	N12	103.58 (16)
Cu2	N6	N11	104.10 (16)
Cu2	N6	N12	149.86 (15)
Cu2	N11	N12	83.28 (16)

Table 5.2: Selected copper/nitrogen bond angles for $([Cu_2(\mathbf{L^5})_2](BF_4))^{3+}$.

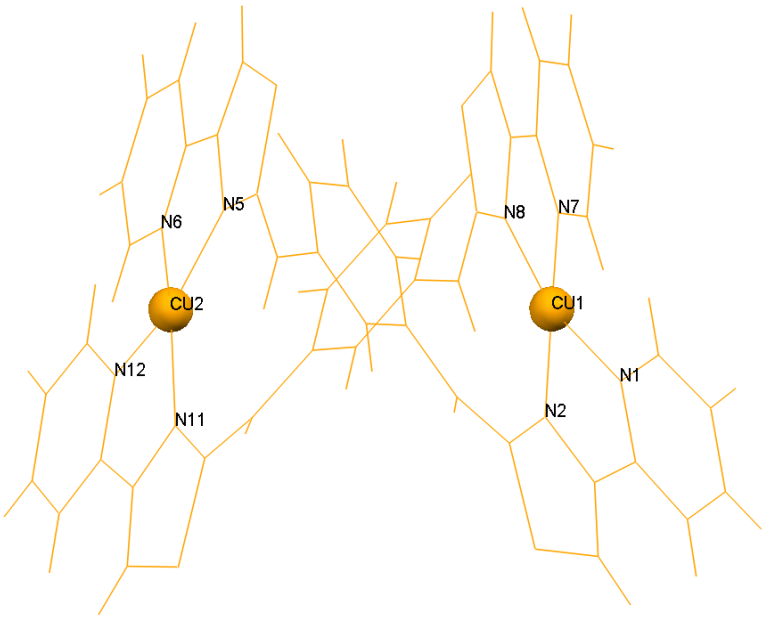

Fig.106: Selected atom labels for $([Cu_2(\mathbf{L^5})_2](BF_4))^{3+}$.

6.2.2 Coordination of $[L^5]$ with $Cu(ClO_4)_2$:

Reaction of **$[L^5]$** with $Cu(ClO_4)_2$ (in-place of $Cu(BF_4)_2$) resulted in an essentially iso-structural assembly. Reaction of the ligand with $Cu(ClO_4)_2$ in $MeNO_2$ resulted in similarly-coloured crystals upon slow diffusion of diisopropyl ether. Single-crystal X-ray diffraction showed that the ligand, again, partitions into two bidentate units each of which coordinates a different copper ion (Fig. 107) (ave. N – Cu bond length: 1.981 Å). The dinuclear double helicate structure persists with each metal centre remaining in a distorted tetrahedral geometry (Fig. 108a & b).

Similarly the anion remains in the pocket created by the helicate, binding to the amines (ave. N-H···O 2.335 Å) and phenyl rings (Cu-N bond lengths 1.987 (4) – 1.974 (4) Å) respectively. The formation of an equivalent structure demonstrates that the complex is not anion-dependant and that it is consistently formed, or at least in the presence of mono-ionic tetrahedral anions. The species exists in solution as an ion in the ESI-MS is observed at *m/z* 1281 which corresponds to $\{[Cu_2(\mathbf{L^5})_2](ClO_4)_3\}^+$. A similar fragment would be expected for the iso-structural complex $\{[Cu_2(\mathbf{L^5})_2](BF_4)\}^{3+}$.

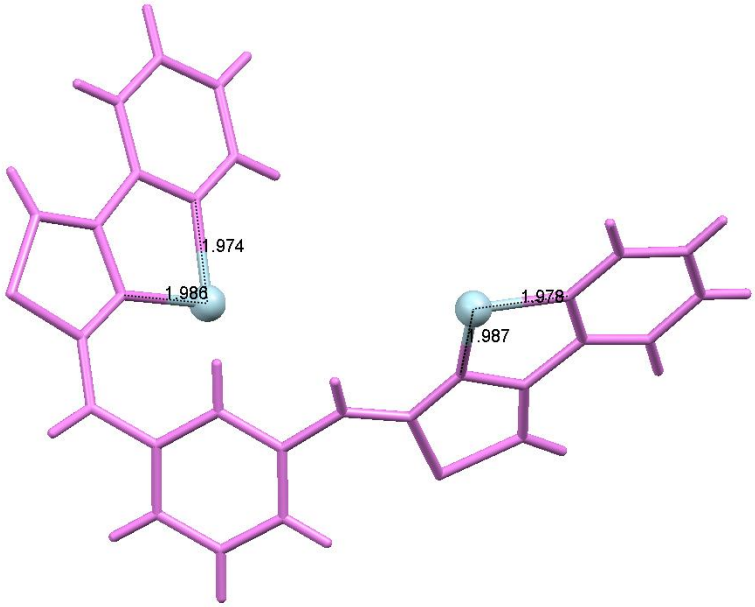

*Fig. 107: Coordination of **[L^5]** to two Cu^{2+} metal ions.*

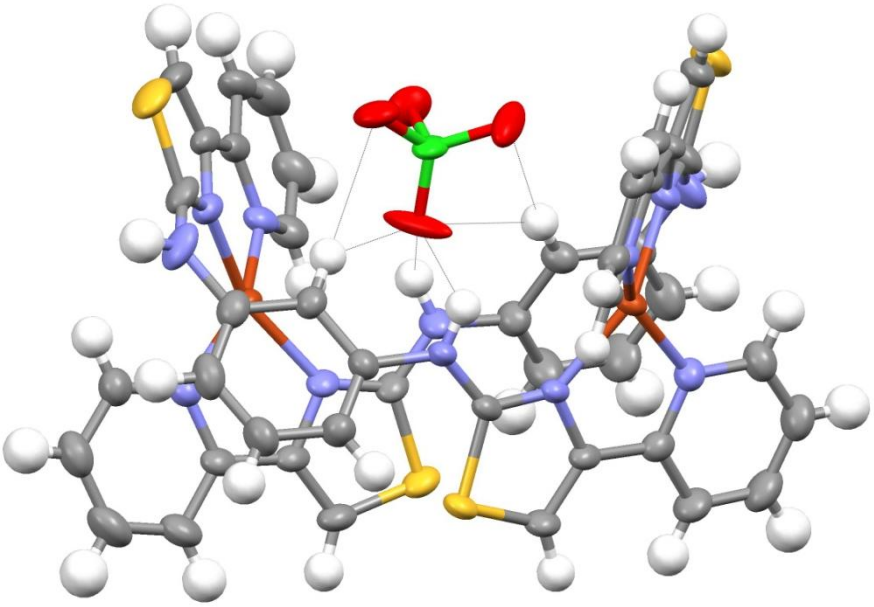

Fig. 108a: Solid state structure of $([Cu_2(\mathbf{L}^5)_2](ClO_4)_2)^{2+}$. Thermal ellipsoids are shown at the 50% probability level; remaining anions are omitted for clarity.

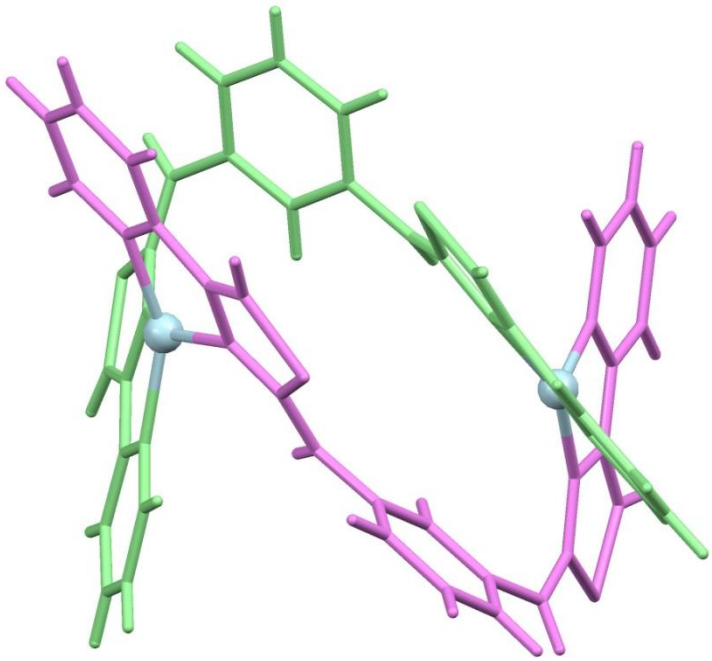

Fig. 108b: Capped stick view for the solid state structure of $([Cu_2(\mathbf{L^5})_2](ClO_4)_2)^{2+}$ (Anion omitted for clarity).

Selected bond lengths and angles for $([Cu_2(\mathbf{L^5})_2](ClO_4)_2)^{2+}$ complex are shown in Tables 5.3 and 5.4 below.

Atom 1	Atom 2	Bond Length (Å)
Cu1	N5	1.985 (4)
Cu1	N6	1.983 (4)
Cu1	N11	1.986 (4)
Cu1	N12	1.974 (4)
Cu2	N1	1.986 (4)
Cu2	N2	2.002 (4)
Cu2	N7	1.978 (4)
Cu2	N8	1.987 (4)

Table 5.3: Selected copper/nitrogen bond lengths for $[Cu_2(\mathbf{L^5})_2](ClO_4)_2$.

Atom 1	Atom 2	Atom 3	Bond Angle (°)
Cu1	N5	N6	83.75 (17)
Cu1	N5	N11	154.29 (16)
Cu1	N5	N12	103.23 (16)
Cu1	N6	N11	105.31 (18)
Cu1	N6	N12	144.79 (17)
Cu1	N11	N12	83.38 (17)
Cu2	N1	N2	83.19 (19)
Cu2	N1	N7	150.55 (17)
Cu2	N1	N8	103.50 (18)
Cu2	N2	N7	104.05 (19)
Cu2	N2	N8	152.87 (16)
Cu2	N7	N8	83.15 (17)

Table 5.4: Selected copper/nitrogen bond angles for $[Cu_2(\mathbf{L^5})_2](ClO_4)_2$.

6.2.3 Reaction of $[Cu_2(L^5)_2](CF_3SO_3)_4$ with $Bu_4N(HSO_4)$:

Reaction of $[Cu_2(\mathbf{L^5})_2](CF_3SO_3)_4$ with half an equivalent of $Bu_4N(HSO_4)$ in $MeNO_2$ results in a colour change of the solution from dark blue to yellow. Slow diffusion of diisopropyl ether resulted in yellow crystals which were analysed *via* single-crystal diffraction. Examination of the solid state shows the double helicate is preserved however there is a marked change in the overall arrangement (Fig. 109).

The structure retains its dinuclear assembly with each copper ion coordinating a bidentate domain of each ligand, formed by a pyridine ring (ave. Cu-N bond length 2.029 Å) and a thiazole ring (ave. Cu-N bond length 2.208 Å). However, the coordination geometry of each copper ion is supplemented by a sulphate anion (O2-Cu2 1.957 Å, O3-Cu1 1.970 Å). This changes the coordination geometry of the metal ion with it now adopting a 5-coordinate arrangement comprising of the bidentate *N*-donor ligand *and* a bridging sulphate anion. This leads to a reduction of 0.6 Å in the metal-metal bond distance within the structure (6.152 Å) when compared to the ClO_4 (6.734 Å) and BF_4 (6.731 Å) complexes respectively. As there are two triflate counter

ions present within the crystal structure it is assumed that the sulphate is dianionic (e.g. SO_4^{2-}). Furthermore as the formation of the dinuclear complex relies on other ligands to complete the coordination geometry of the metal ion (and not just the ligand strand), this species can be said to be an *unsaturated* helicate. This species persists in solution as an ion in the ESI-MS is observed at *m/z* 1229 which corresponds to $\{[Cu_2(\mathbf{L^5})_2](SO_4)(CF_3SO_3)\}^+$. Interestingly, little change in the ESI-MS is observed upon addition of an excess of sulphate anions showing that the dinuclear helicate is still present with excess anions (see later).

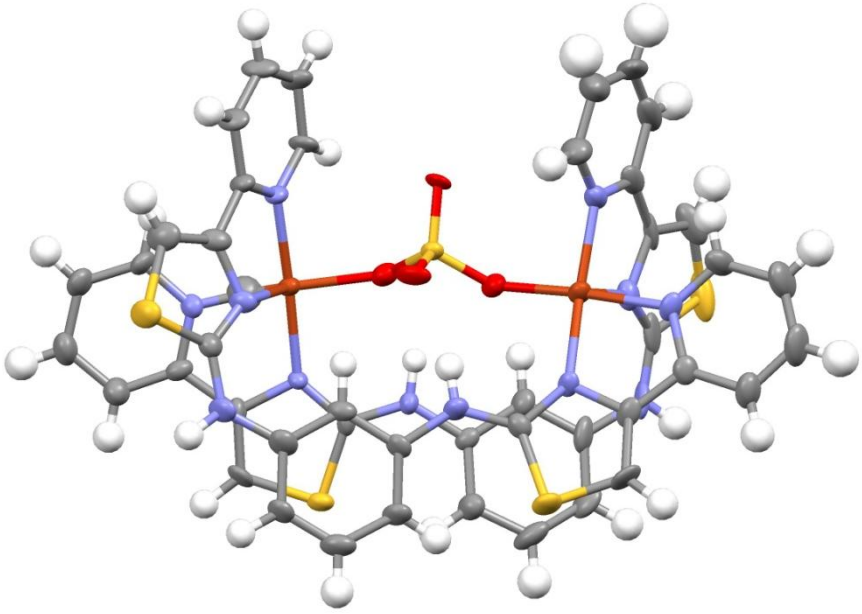

Fig. 109: Solid state structure of $[Cu_2(\mathbf{L^5})_2](SO_4)^{2+}$. Thermal ellipsoids are shown at the 50% probability level, remaining anions are omitted for clarity.

The sulphate anion which has taken up a more central position within the complex and forms hydrogen bonds to the hydrogen atoms of the amines (NH···O bond length 2.032 Å) (Fig. 110a & b).

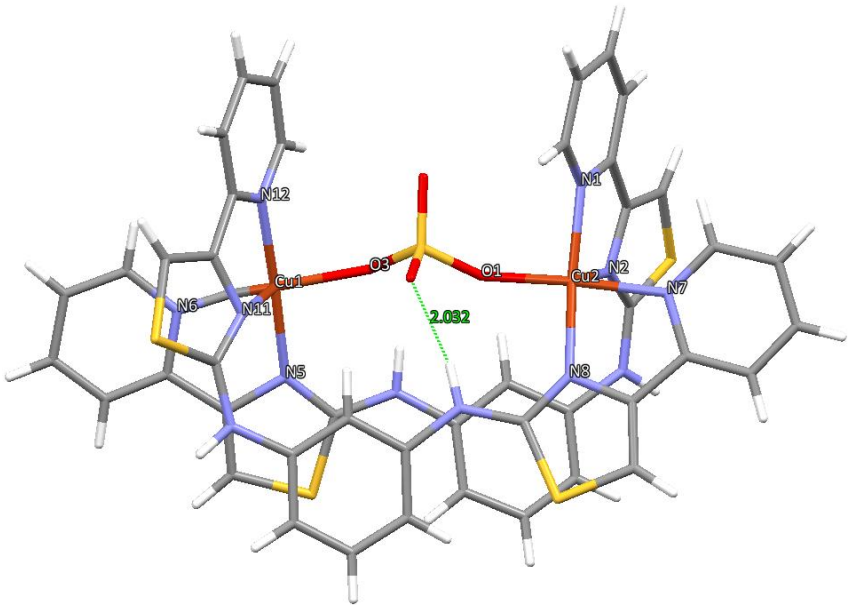

Fig. 110a: Interactions of the central SO_4^{2-} ion with the amine and Cu^{2+} centres. (Remaining anions omitted for clarity).

The coordination of the sulphate anion forces a contraction in the Cu···Cu distance which results in two terminal pyridines adopting a parallel arrangement. This can clearly be seen in figures 111a & b where the BF_4^- structure adopts a cup-like arrangement in comparison to the sulphate's dock motif.

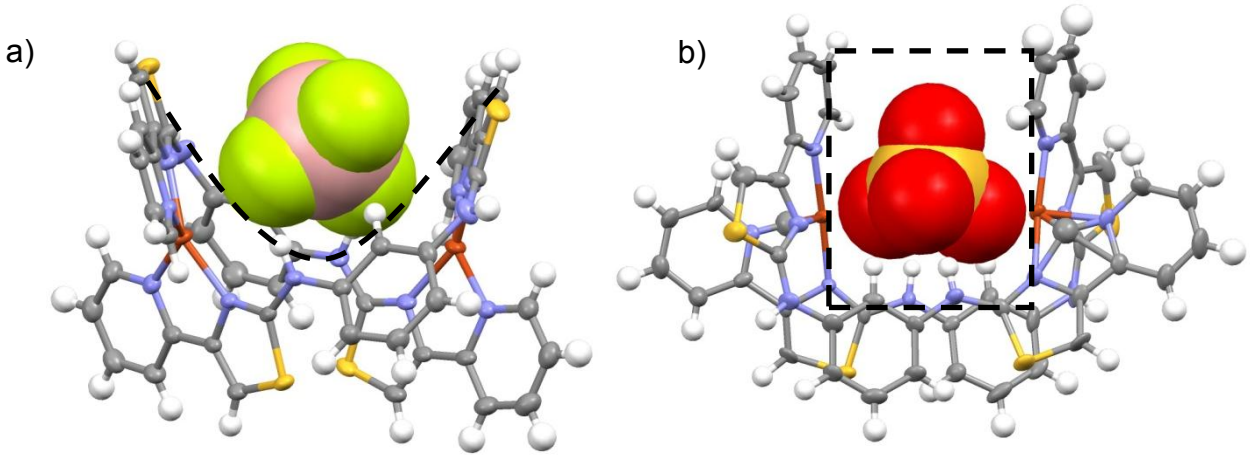

*Fig. 111: Comparison between **(a)** $[Cu_2(\mathbf{L^5})_2](BF_4)^{3+}$ & **(b)** $[Cu_2(\mathbf{L^5})_2](SO_4)^{2+}$ (remaining anions omitted for clarity).*

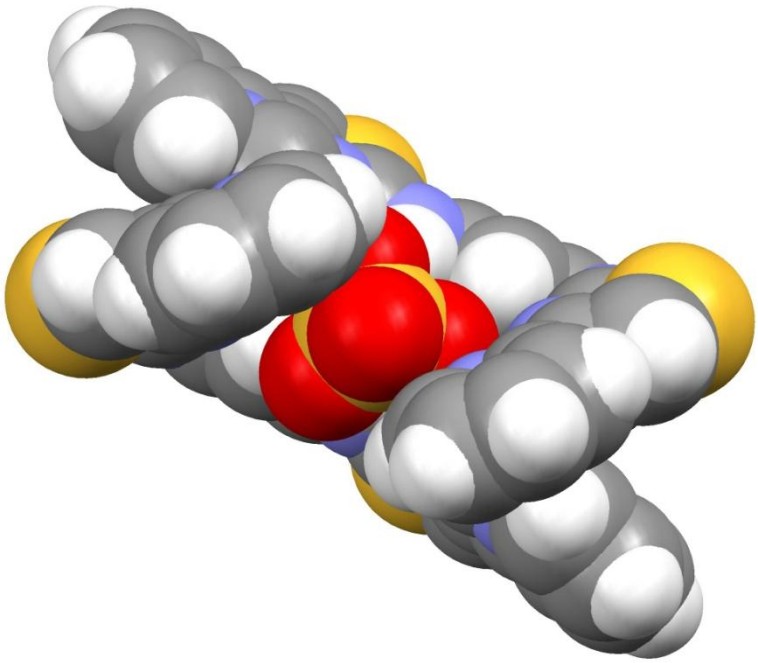

Fig. 110b: Space filling view of $[Cu_2(\mathbf{L^5})_2](SO_4)^{2+}$ showing the sulphate ion embedded within the complex .

Selected bond lengths and angles for the $[Cu_2(\mathbf{L^5})_2](SO_4)^{2+}$ complex are shown in Tables 5.5 and 5.6 below.

Atom 1	Atom 2	Bond Length (Å)
Cu1	N5	1.996 (6)
Cu1	N11	2.483 (6)
Cu1	N12	2.007 (6)
Cu1	N6	2.069 (7)
Cu1	O3	1.981 (6)
Cu2	O1	1.958 (6)
Cu2	N1	1.998 (7)
Cu2	N2	2.332 (7)
Cu2	N7	2.042 (7)
Cu2	N8	2.021 (6)

Table 5.5: Selected copper bond lengths for $[Cu_2(\mathbf{L^5})_2](SO_4)^{2+}$.

Atom 1	Atom 2	Atom 3	Bond Angle (°)
Cu1	N5	N11	99.4 (2)
Cu1	N5	N12	175.7 (3)
Cu1	N5	O3	92.5 (2)
Cu1	N11	N12	76.5 (2)
Cu1	N11	O3	110.5 (2)
Cu1	N12	O3	89.8 (3)
Cu2	N1	N2	79.5 (3)
Cu2	N1	N7	92.5 (3)
Cu2	N1	N8	167.5 (3)
Cu2	N1	O1	90.8 (3)
Cu2	N2	N7	87.1 (3)
Cu2	N2	N8	110.3 (3)
Cu2	N7	O1	89.4 (2)
Cu2	N7	N8	80.6 (3)
Cu2	N7	O1	174.7 (3)
Cu2	N8	O1	96.9 (3)

Table 5.6: Selected copper bond angles for $[Cu_2(\mathbf{L}^5)_2](SO_4)^{2+}$.

6.2.4 Reaction of $[Cu_2(L^5)_2](ClO_4)_4$ with 0.5 eq. $H_2PO_4^-$:

Reaction of $[Cu_2(\mathbf{L^5})_2](ClO_4)_4$ with half an equivalent of $Bu_4N(OPO_3H_2)$ in nitromethane results in a colour change of the solution from dark blue to light brown. Slow diffusion of ethyl acetate gave olive crystals which were analysed by single-crystal diffraction. Examination of the solid-state data showed a similar structure to that observed when the complex is reacted with sulphate (Fig. 112).

In the solid-state each ligand again partitions into two separate binding domains whereby each pyridyl-thiazole domain coordinates a different metal ion (Cu-N bond lengths 1.996 (3) – 2.357 (3) Å). In a similar fashion to the sulphate analogue the dihydrogen phosphate coordinates via two oxygen atoms and bridges the two metal ions (ave. Cu-OP 1.979 Å). In the crystal structure there are three perchlorate counter ions present it is assumed that, unlike the sulphate, the phosphate is only singly deprotonated (e.g. $OPO_3H_2^-$).

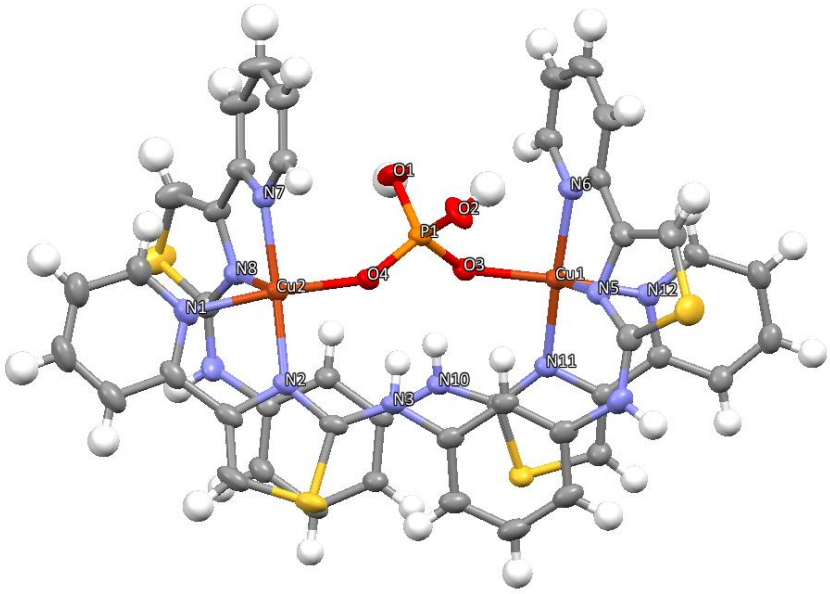

Fig. 112: Solid state structure of $[Cu_2(\mathbf{L^5})_2](PO_4)]^{3+}$. Thermal ellipsoids are shown at the 50% probability level, remaining anions are omitted for clarity.

Furthermore, the metal ions coordination sphere is completed by weak interactions from oxygen atoms of the perchlorate anions (ave. Cu-OCl 2.763 Å), resulting in a pseudo-octahedral geometry (Fig. 113).

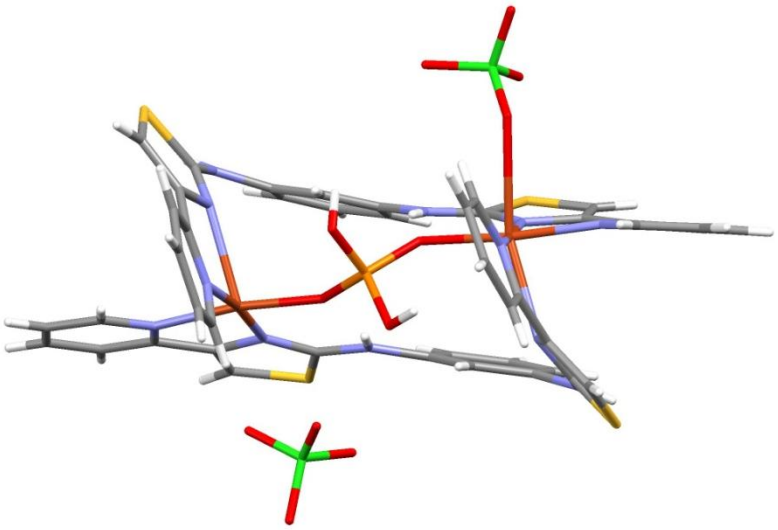

Fig. 113: Solid state structure of $[Cu_2(\mathbf{L^5})_2](PO_4)]^{3+}$ showing the weak interactions between the perchlorate anions and the metal centres.

The dihydrogen phosphate anion forms hydrogen bonds to two of the amines on the ligand strand (ave. NH···O bond length 1.390 Å) (Fig. 114) and in an analogous fashion to all of the previous dinuclear complexes, the two remaining amines point away from the complex. In a similar manner to the dinuclear structure observed with a sulphate anion, the formation of the complex relies on other ligands to complete the coordination geometry of the metal ion (again not just the ligand strand), this species can be said to be an *unsaturated* helicate.

The data was not of sufficient quality to locate the hydrogen atoms on the phosphate anion in the difference Fourier map and it was assumed that the non-coordinating oxygen atoms would bear the hydrogen atoms. Two of the bond distances are larger (ave. P-OH 1.557 Å *c.f.* ave. P-O 1.512 Å) and so where assumed to be the O-H bonds as it consummates with their single bond character.

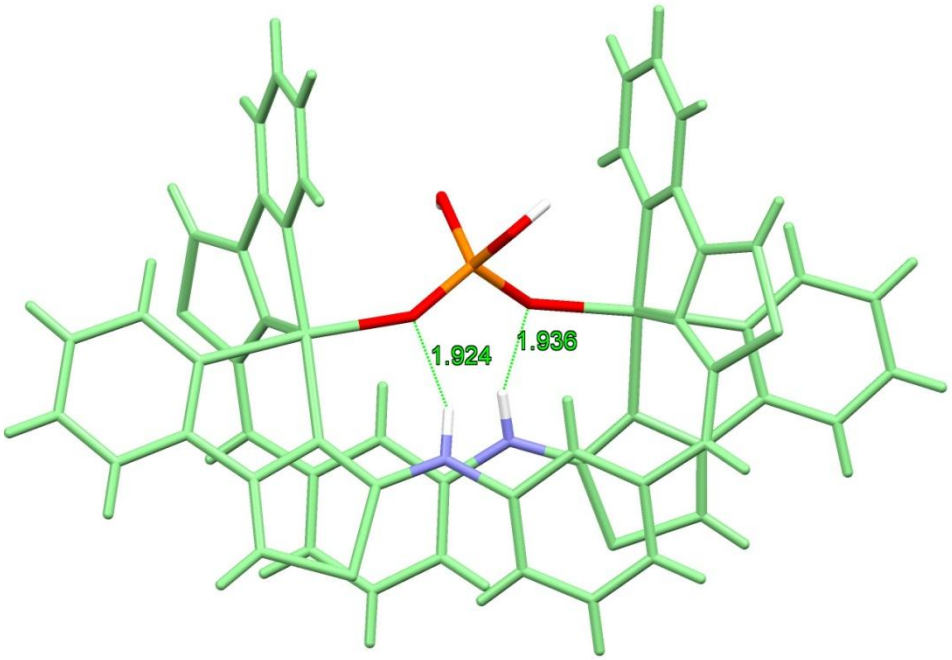

Fig. 114: Solid state structure of $[Cu_2(\mathbf{L^5})_2](PO_4)]^{3+}$. Hydrogen bonding interactions between the amines (violet) and phosphate ion (red).

ESI-MS was carried out in order to confirm the structure; ESI-MS gave an ion at m/z 1279 which corresponds to $\{[Cu_2(\mathbf{L^5})_2(OPO_3H_2)(ClO_4)_2]^+$ and although the masses for $OPO_3H_2^-$ and ClO_4^- are similar, they are sufficiently different for both $\{[Cu_2(\mathbf{L^5})_2(OPO_3H_2)(ClO_4)_2]+$ and $\{[Cu_2(\mathbf{L^5})_2(ClO_4)_3]^+$ to be differentiated.

Furthermore the formation of dianionic sulfate (e.g. SO_4^{2-}) and dihydrogen phosphate (e.g. $H_2PO_4^-$) structures can be explained by considering the pKa of the two anions. The triprotic phosphate can be deptotonated three times, with the sucessive pKa of:

- pKa1 = 2.12 (H_3PO_4)
- pKa2 = 7.21 ($H_2PO_4^-$)
- pKa3 = 12.67 (HPO_4^{2-})

The pKa values for each stage increase by approximately 5 and the phosphate becomes substantially less acidic after each deprotonation. In comparsion, sulfate is the more acidic of the two species with a sucessive pKa of -3 (H_2SO_4) and a pKa of 2 (HSO_4^-). As a result HSO_4^- is substantially more acidic than $H_2PO_4^-$ and the sulphate in the dinuclear complex undergoes double deprotonation whereas the phosphate is only singly deprotonated.

Selected bond lengths and angles for the $[Cu_2(\mathbf{L^5})_2](PO_4)]^{3+}$ complex are shown in Tables 5.7 and 5.8 below.

Atom 1	Atom 2	Bond Length (Å)
Cu1	N12	2.036 (3)
Cu1	N5	2.357 (3)
Cu1	N11	1.996 (3)
Cu1	N6	2.011 (3)
Cu1	O3	1.979 (3)
Cu2	N8	2.332 (3)
Cu2	N7	2.011 (3)
Cu2	N1	2.031 (3)
Cu2	N2	1.998 (3)
Cu2	O4	1.979 (3)

Table 5.7: Selected copper bond lengths for $[Cu_2(\mathbf{L^5})_2](PO_4)]^{3+}$.

Atom 1	Atom 2	Atom 3	Bond Angle (°)
Cu1	N12	N5	81.82 (12)
Cu1	N12	N11	81.43 (13)
Cu1	N12	N6	95.02 (13)
Cu1	N12	O3	173.01 (12)
Cu1	N5	N11	105.07 (12)
Cu1	N5	N6	77.78 (12)
Cu1	N5	O3	103.86 (11)
Cu1	N11	N6	174.99 (13)
Cu1	N11	O3	93.04 (12)
Cu1	N6	O3	90.23 (12)
Cu2	N8	N7	77.85 (12)
Cu2	N8	N1	85.49 (12)
Cu2	N8	N2	108.05 (12)
Cu2	N8	O4	101.89 (11)
Cu2	N7	N1	94.98 (14)
Cu2	N7	N2	172.53 (13)
Cu2	N7	O4	90.07 (12)
Cu2	N1	N2	81.14 (14)
Cu2	N1	O4	171.82 (12)
Cu2	N2	O4	93.10 (12)

Table 5.8: Selected copper bond angles for $[Cu_2(\mathbf{L^5})_2](PO_4)]^{3+}$.

6.2.5 Reaction of $[Cu_2(L^5)_2](BF_4)_4$ with 1 eq. $H_2PO_4^-$:

Reaction of $[Cu_2(\mathbf{L}^5)_2](BF_4)_4$ with one equivalent of $Bu_4N(OPO_3H_2)$ produced light brown crystals upon slow diffusion of diisopropyl ether. Analysis by X-ray diffraction showed that in the solid state an *unsaturated* trinuclear triple helicate had formed. In the solid state each metal centre coordinates two bis-bidentate N-donor units from different ligands (Cu-N bond lengths 1.947(5) – 2.149(5) Å) and a mono-dentate dihydrogen phosphate anion (Cu-OP 1.988(5) – 2.008(4) Å), leading to an overall 5-coordinate species. On inspection of the solid state data three tetrafluoroborate anions can be seen within the crystal structure, again indicating that the phosphates remains mono-ionic e.g. $([Cu(\mathbf{L}^5)(OPO_3H_2)]_3(BF_4)_3)$.

The 1,3-diaminophenylene spacers bridge each of the bidentate domains allowing all of the amine groups to point inwards, each hydrogen bonding to a dihydrogen phosphate anion. The organization of the molecules in an “over-and-under” conformation gives rise to the helical cyclic oligomer with a large central cavity which houses three dihydrogen phosphate anions (Fig. 115). The transformation of a linear helicate to a circular helicate either by anion templation or metal ion coordination has been widely reported in the literature; however the novel aspect of formation is the inclusion of three anions into the central cavity rather than the more prevalent single anion displays.

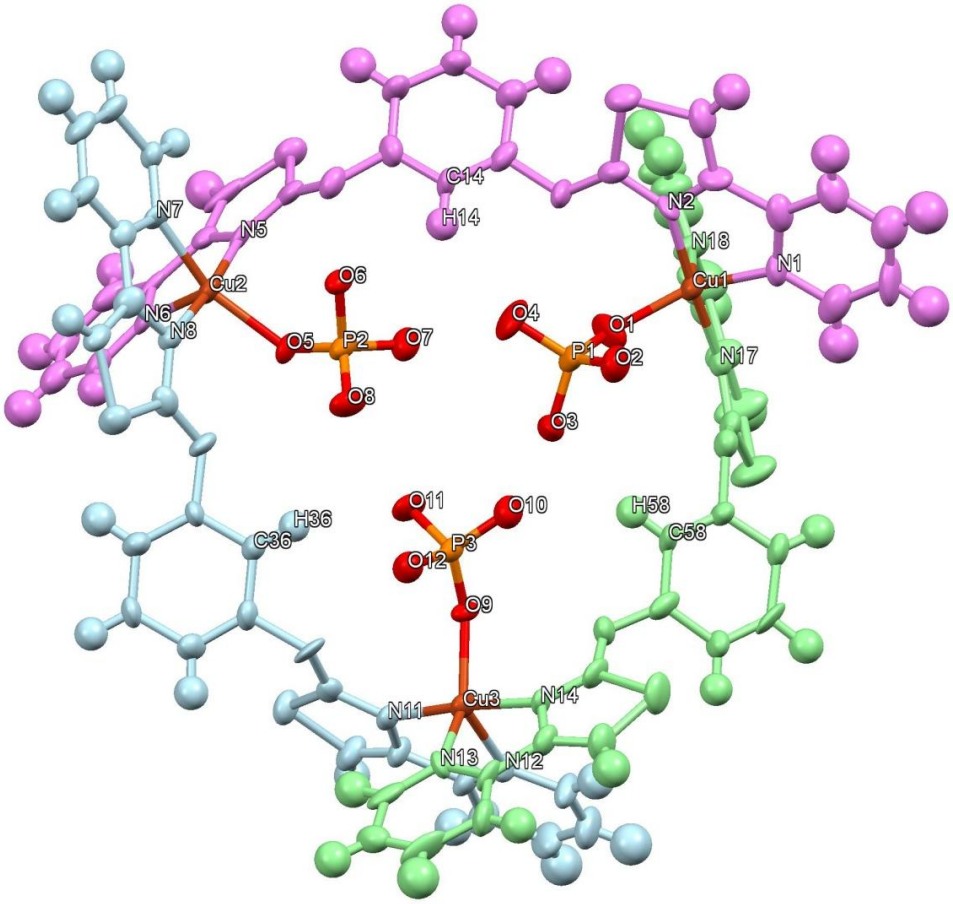

Fig. 115: Trinuclear circular helicate showing the inclusion of three dihydrogen phosphate anions, $[Cu_3(\mathbf{L^5})_3(OPO_3H_2)_3]^{3+}$. Thermal ellipsoids are shown at the 50% probability level.

It is clear from the study of the previous phosphate double helicate $[Cu_2(\mathbf{L^5})_2(OPO_3H_2)]^{3+}$ that there is adequate conformational flexibility to allow the additional phosphates in the structure to occupy the coordination sites previously occupied by the perchlorate anions i.e. for the two dihydrogen phosphate anions to be able to coordinate both the metal ions doesn't necessitate the formation of the trinuclear oligomer. This arrangement is presumably a consequence of hydrogen bonding between the amine N-H and phenyl C–H of the ligand and the phosphate oxygen atoms (N–H···O distances 2.137 – 2.861 Å; C–H···O distances 2.460 – 2.602 Å) (Fig. 116a), these interactions are then stabilized by a further set of cyclic interactions between the three central phosphates (P=O···HO–P (1.846 – 1.969 Å) (Fig. 116b). It can therefore be stated that the assembly of the overall structure is governed by a series of 'phosphate-ligand' and 'phosphate-phosphate' interactions.

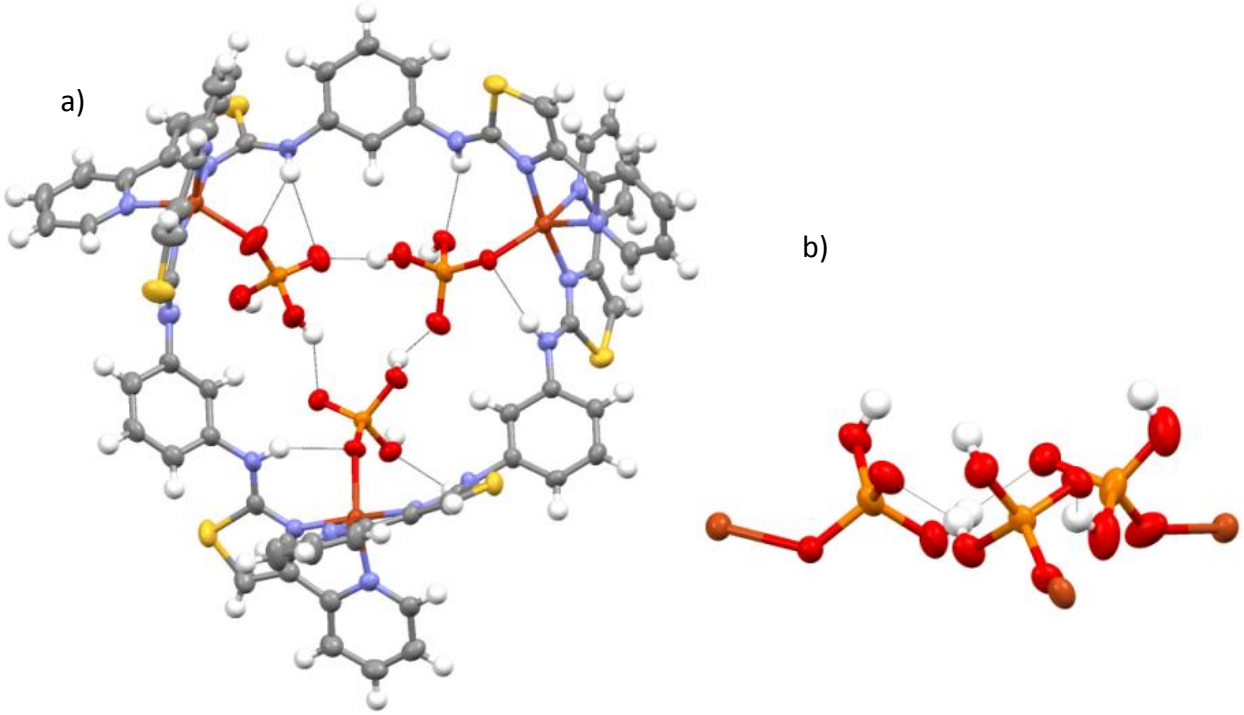

Fig. 116: (a) Trinuclear circular helicate showing the intra-molecular hydrogen bonding, (b) interaction between the three dihydrogen phosphate anions, $[Cu_3(\mathbf{L^5})_3(OPO_3H_2)_3]^{3+}$.

Selected bond lengths and angles for the $[Cu_3(\mathbf{L^5})_3(OPO_3H_2)_3]^{3+}$ complex are shown in Tables 5.9 and 5.10 below.

Atom 1	Atom 2	Bond Length (Å)
Cu1	N17	2.145 (5)
Cu1	N2	1.952 (4)
Cu1	N18	1.967 (4)
Cu1	N1	2.053 (5)
Cu1	O1	2.004 (4)
Cu2	N6	2.102 (5)
Cu2	N5	1.971 (5)
Cu2	N7	2.100 (5)
Cu2	N8	1.947 (5)
Cu2	O5	1.988 (5)
Cu3	N11	1.989 (5)
Cu3	N13	1.967 (5)

Cu3	N14	2.149 (5)
Cu3	N12	2.074 (5)
Cu3	O9	2.008 (4)

Table 5.9: Selected copper bond lengths for $[Cu_3(\boldsymbol{L^5})_3(OPO_3H_2)_3]^{3+}$.

Atom 1	Atom 2	Atom 3	Bond Angle (°)
Cu1	N17	N2	93.70 (2)
Cu1	N17	N18	80.35 (19)
Cu1	N17	N1	105.70 (2)
Cu1	N17	O1	113.40 (2)
Cu1	N2	N18	173.90 (2)
Cu1	N2	N1	80.70 (2)
Cu1	N2	O1	92.74 (18)
Cu1	N18	N1	99.72 (19)
Cu1	N18	O1	90.71 (18)
Cu1	N1	O1	140.69 (19)
Cu2	N6	N5	80.10 (2)
Cu2	N6	N7	112.47 (19)
Cu2	N6	N8	96.30 (2)
Cu2	N6	O5	110.80 (2)
Cu2	N5	N7	97.60 (2)
Cu2	N5	N8	174.90 (2)
Cu2	N5	O5	90.10 (2)
Cu2	N7	N8	80.40 (2)
Cu2	N7	O5	136.70 (2)
Cu2	N8	O5	94.60 (2)
Cu3	N11	N13	172.20 (2)
Cu3	N11	N14	79.97 (19)
Cu3	N11	N12	93.70 (2)
Cu3	N11	O9	93.84 (18)
Cu3	N13	N14	96.84 (19)

Cu3	N13	N12	100.25 (18)
Cu3	N13	O9	93.34 (18)
Cu3	N14	N12	80.40 (2)
Cu3	N14	O9	107.53 (17)
Cu3	N12	O9	152.08 (17)

Table 5.10: Selected copper bond angles for $[Cu_3(\mathbf{L^3})_3(OPO_3H_2)_3]^{3+}$.

Each of the three central dihydrogen phosphate anions has a remaining P-OH bond capable of further interactions. All three of the hydrogen atoms related to the phosphates point outwards from the core in such a way that they undergo further hydrogen bonding to another three oxygen acceptors encapsulated within a separate trinuclear oligomer giving a cyclic array of six (··HO-P=O··) donor/acceptor units (Fig. 117).

As with $[Cu_2(\mathbf{L^5})_2(OPO_3H_2)]^{3+}$ the data was not of sufficient quality to locate the hydrogen atoms on the phosphate anion in the difference Fourier map and in order to establish *inter*- and *intra*-molecular interactions within the structure a correct assignment of which phosphorous oxygen atoms bear the protons. Assignment of the singly bonded dihydrogen phosphate anions (HO-P) as opposed to the doubly bonded atoms (P=O) was confirmed by investigation of the bond lengths. Due to the shorter nature of the double bond the two larger bond values were assigned protons and the smallest value was regarded as being the double bond (ave. HO-P bond length: 1.55 Å, P=O bond length: 1.49 Å) (Fig. 118). It is also important to point out that the inter-molecular POH····OP distances are in the range 1.711 – 1.880 Å which is shorter than the intra-molecular distances of the same type.

Due to the *inter*-molecular hydrogen bonding interactions dimerization of the trinuclear circular helicates occurs giving $([Cu_3(\mathbf{L^5})_3(OPO_3H_2)_3]^{3+})_2$ (Fig. 119a-c). Thus the resultant supramolecular species is a result of a two-fold self-assembly process utilizing two separate classes of supramolecular interactions; firstly the ligand, metal ions and a phosphate anion undergo metallo-supramolecular assembly to form the trinuclear circular helicate. This then dimerises solely via the hydrogen bond donor/acceptor

phosphates to form the dimer $([Cu_3(\mathbf{L^3})_3(OPO_3H_2)_3]^{3+})_2$ resulting in a supramolecular architecture assembled from two separate classes of self-assembly.

Confirmation of the assembly by ESI-MS showed an ion at *m/z* 1966 which corresponds to $\{[Cu_3(\mathbf{L^5})_3(OPO_3H_2)_3](ClO)_2\}^+$ and an ion at *m/z* 4036 which corresponds to the dimer $\{[Cu_3(\mathbf{L^5})_3(OPO_3H_2)_3]_2(ClO)_5\}^+$ as well as an ion at *m/z* 1279 which corresponds to $\{[Cu_2(\mathbf{L^5})_2(OPO_3H_2)(ClO_4)_2]\}^+$.

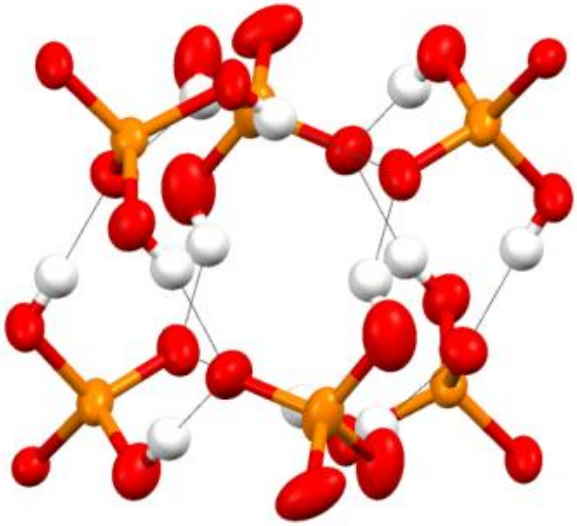

Fig. 117: Central dihydrogen phosphates from two separate trinuclear helicates involved in both intra and inter-molecular hydrogen bonding.

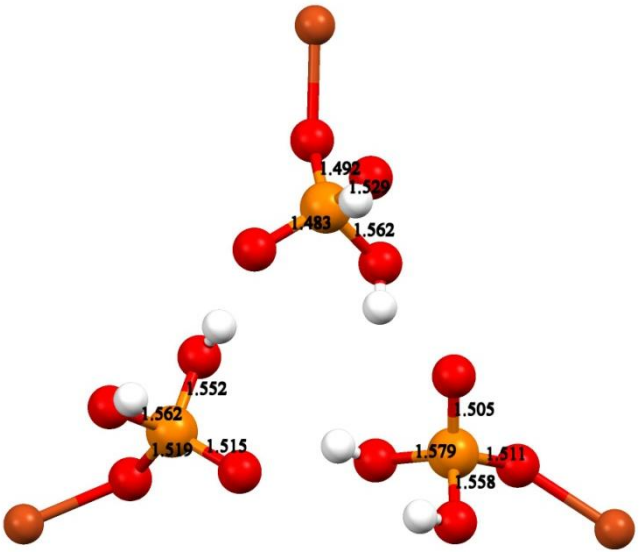

Fig.118: P-OH / P=O bond lengths.

a)

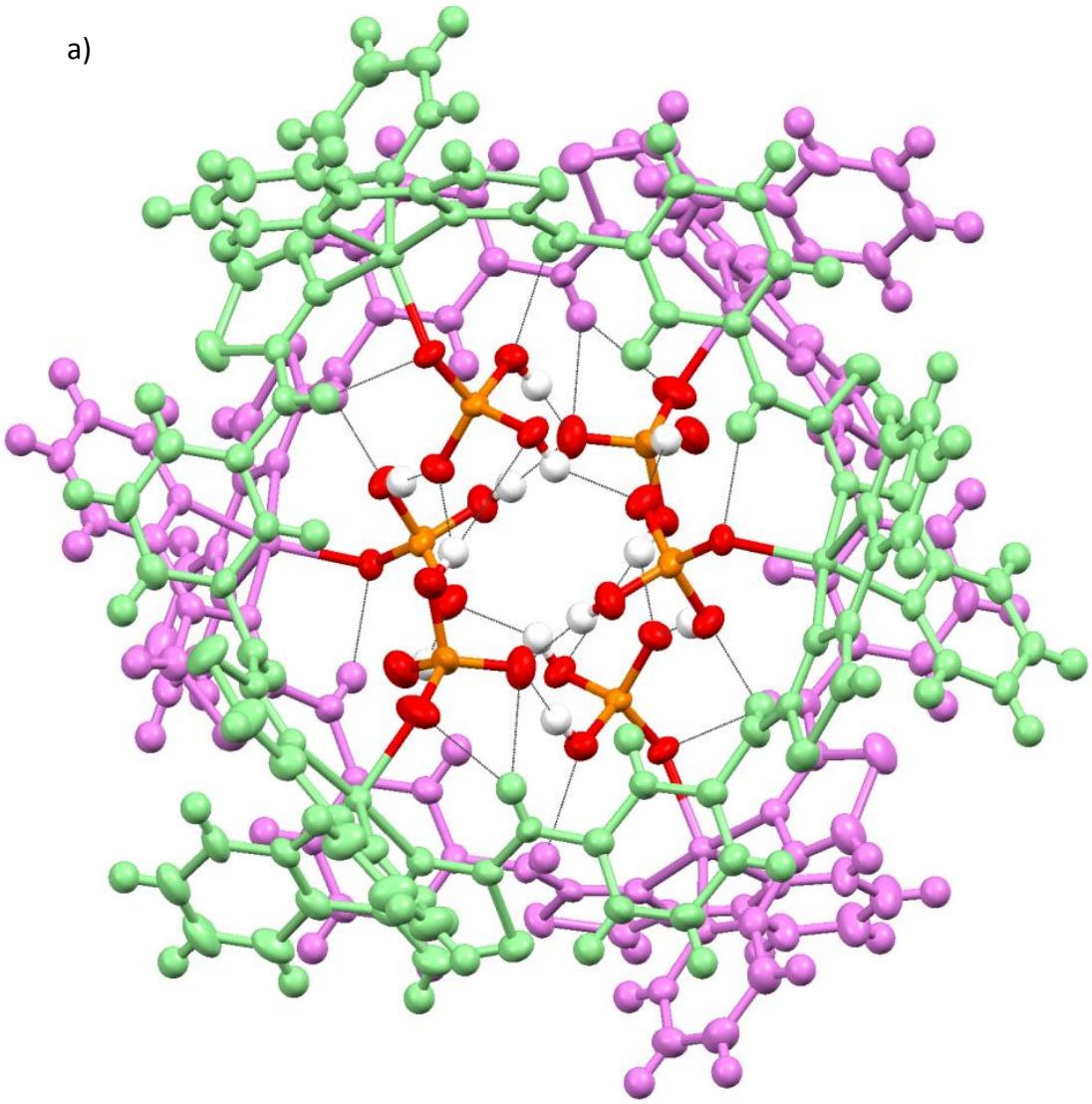

Fig. 119a: Axial view of the $([Cu_3(\mathbf{L}^5)_3(OPO_3H_2)_3]^{3+})_2$ *trimer.*

b)

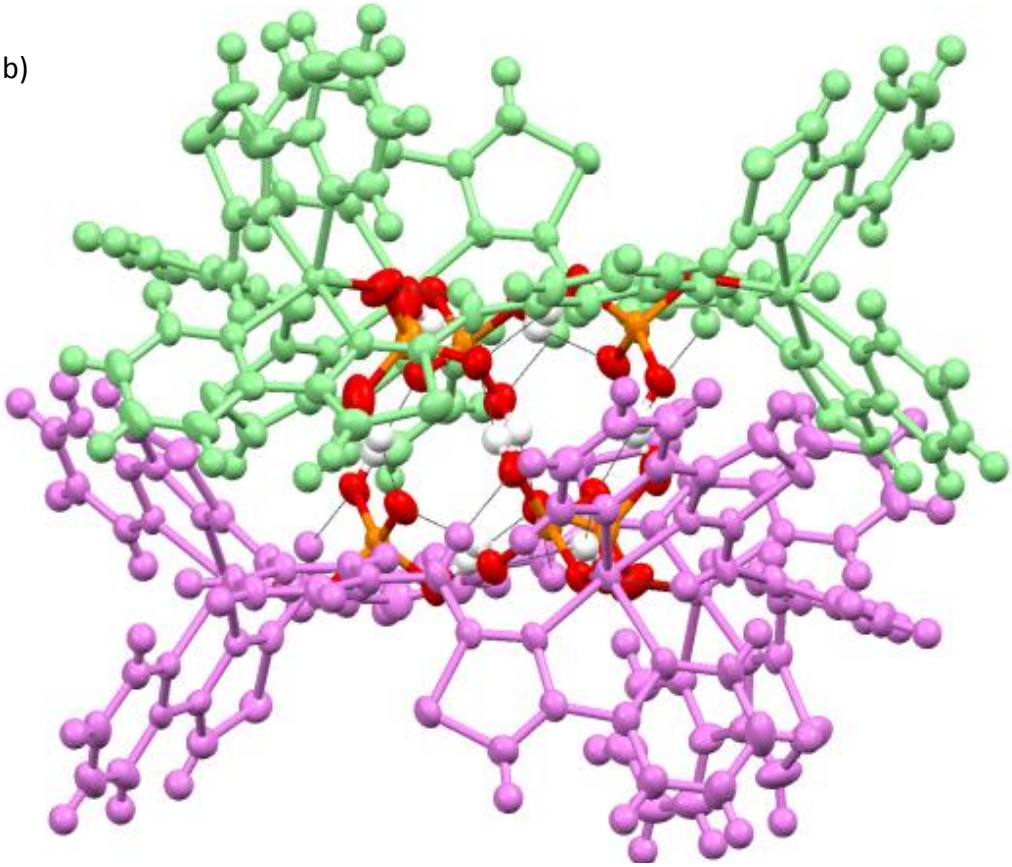

c)

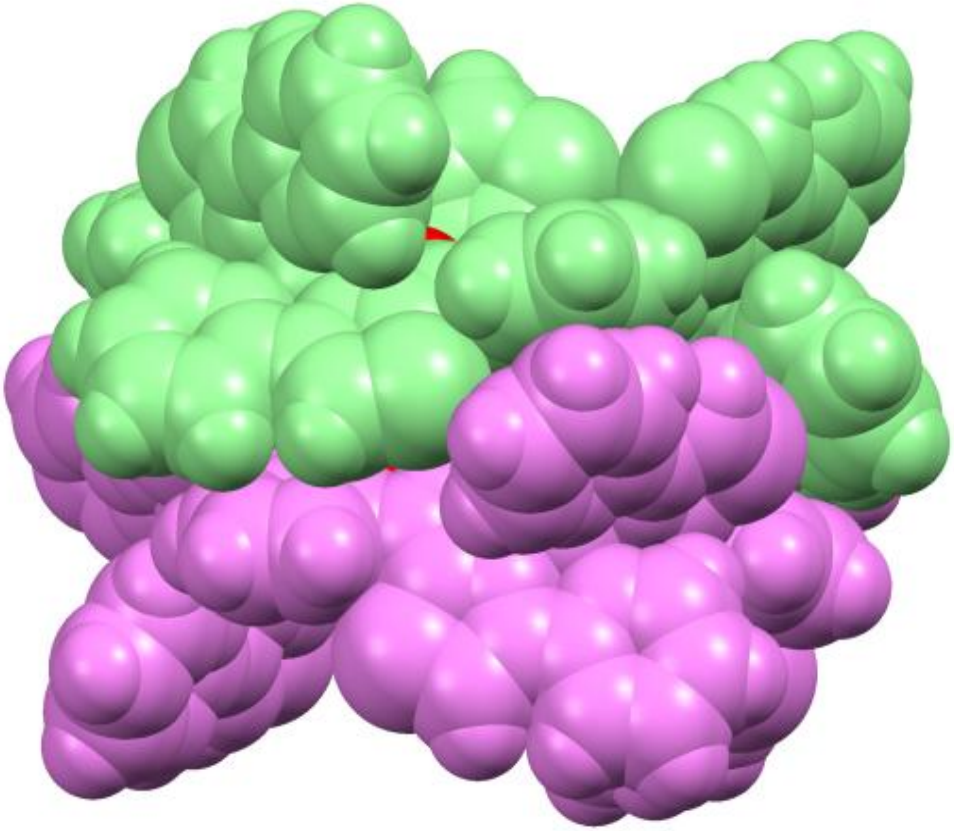

Fig. 119a &b: Side on view (b) and space filling view (c) of $([Cu_3(\mathbf{L^5})_3(OPO_3H_2)_3]^{3+})_2$.

6.2.6 Reaction of $[Cu_2(L^5)_2]^{4+}$ with $(Bu_4N)NO_3$:

As we have already established reaction of the diamine-containing ligand **$[L^5]$** with Cu^{2+} (with either; triflate, perchlorate or tetrafluroborate counter anions) gives the dinuclear double helicate $[Cu_2(\mathbf{L^5})_2]^{4+}$. However, reaction of this dinuclear species with one equivalent of $(Bu_4N)NO_3$ in $MeNO_2$ gave a clear green solution from which green crystals formed upon slow diffusion of chloroform. Analysis by single-crystal X-ray diffraction showed that in the solid state a hexanuclear circular *meso*-helicate (or mesocate) is formed (Fig. 120a, b & c).

In this structure the ligand separates into two bis-bidentate binding domains with each *N*-donor domain of a thiazole and pyridine ring coordinating two different Cu^{2+} metal centres (ave. 2.024 Å). Each metal centre exhibits a distorted octahedral arrangement with two ligand strands completing 4 of its 6 coordination sites, the remaining sites are occupied by two *O*-donors of a nitrate anion (ave. 2.048 Å) (Fig. 121).

Furthermore an amine of each ligand strand points into on the centre of the complex creating a cavity capable of hosting two nitrate anions. Each nitrate lies planar (Fig. 122), between the hexanuclear complex and hydrogen bonds an individual set of three ligand N-Hs (ave. 2.277 Å).

The formation of the circular species over that of the double helicate is directed by both the coordination of nitrate anions *and* their use in templating the self-assembly; firstly the nitrate anion coordinates the metal centre resulting in a distorted octahedral geometry. Secondly, the nitrate templates the self-assembly with the anion sitting in the core of the circular mesocate and undergoes hydrogen bonding interactions to the amine protons of the ligand strands. Unlike the previous double helicate complexes observed with **$[L^5]$** only one of the ligands –NH domains undergoes hydrogen bonding to the anion. The second amine of each ligand is forced outwards, away from the centre of the complex and forms a hydrogen bond to the coordinate nitrate anion.

a)

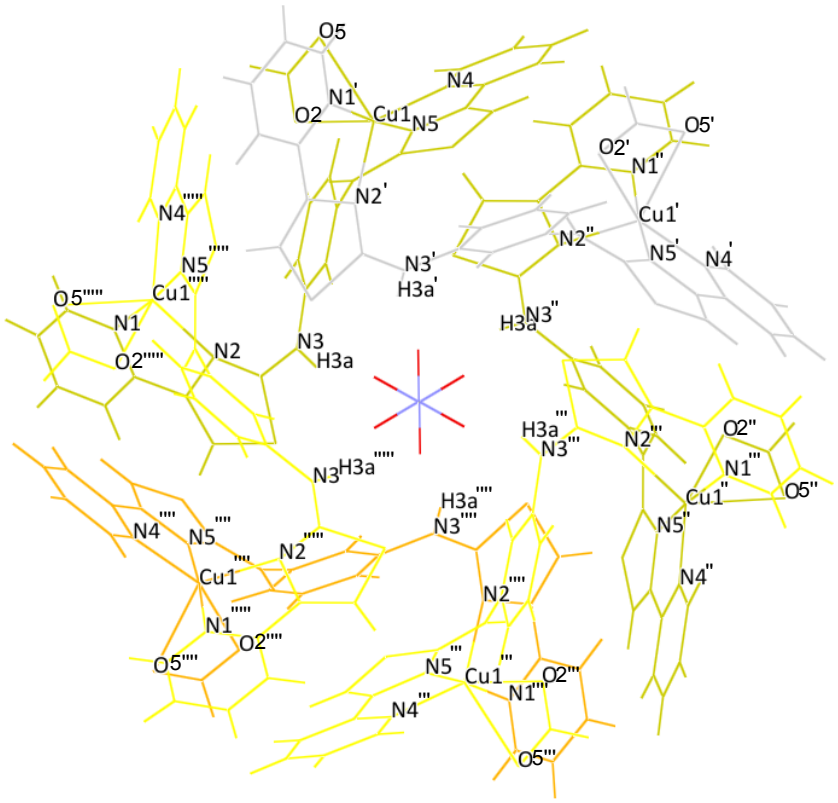

*Fig. 120a: Atom labels for the complex [(Cu(NO$_3$)**(L^5)**)$_6$(NO$_3$)$_2$]$^{4+}$. In the unit cell only one independent [Cu(L^1)(NO$_3$)]$^+$ fragment was present yielding a hexanuclear mesocate via the symmetry operations of the space group R-3.*

b)

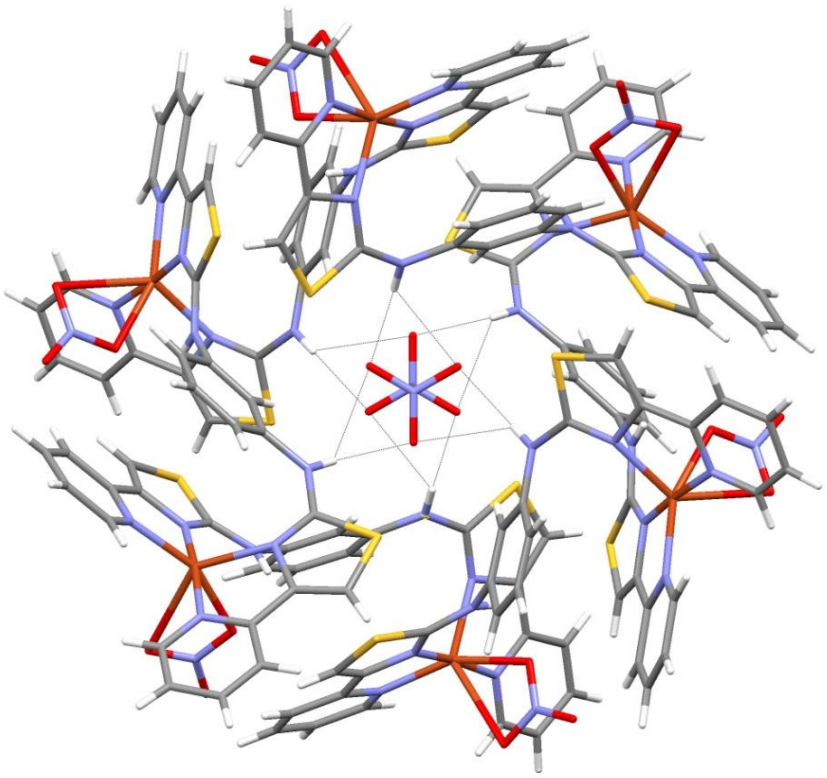

c)

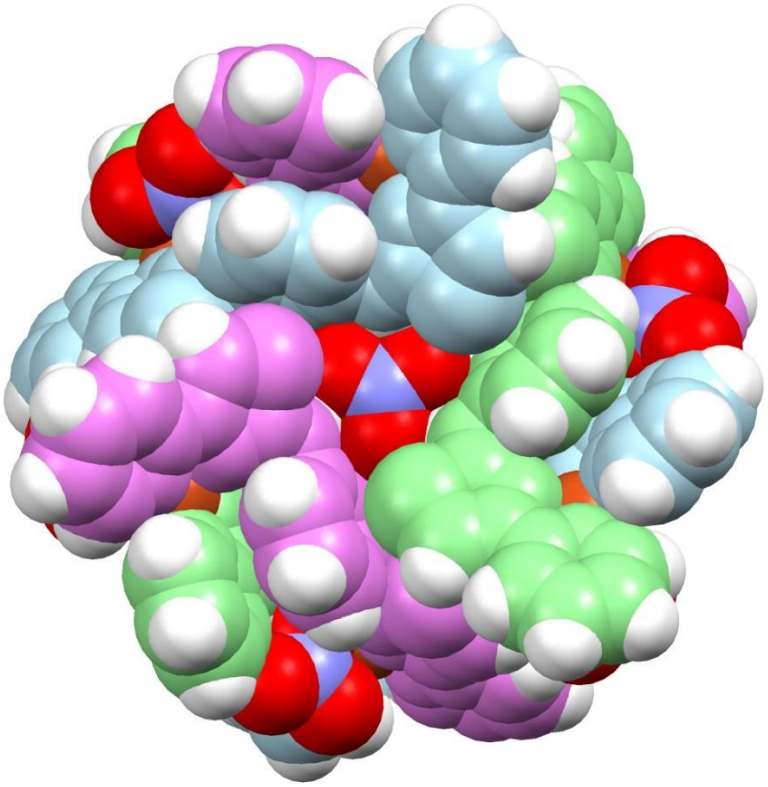

Fig. 120 b & c: Solid state structure of the hexanuclear circular meso-helicate (mesocate), $[(Cu(NO_3)(\mathbf{L^5}))_6(NO_3)_2]^{4+}$

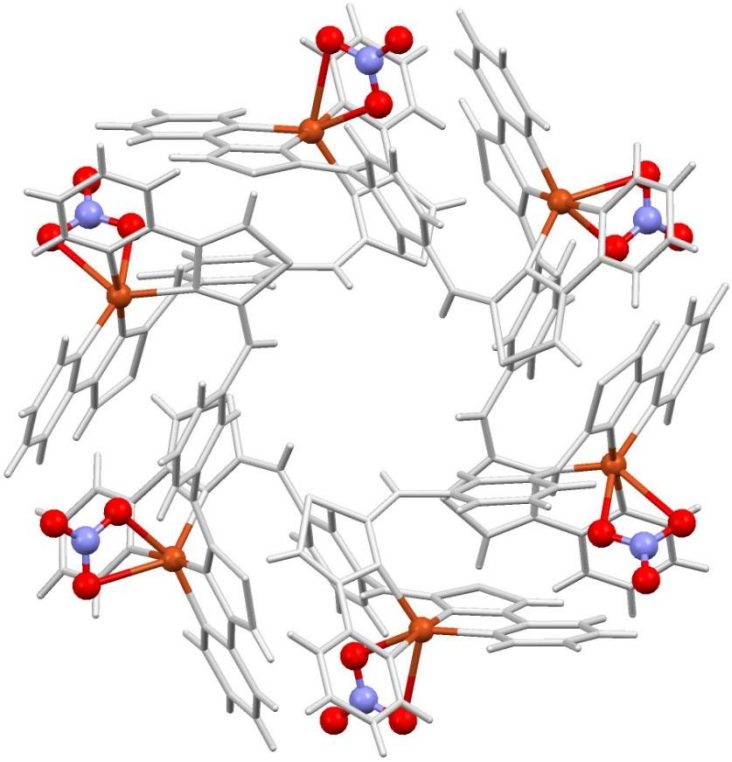

Fig. 121: Solid state structure of $[(Cu(NO_3)(\mathbf{L^5}))_6(NO_3)_2]^{4+}$ showing the interactions of the nitrate anions with the copper centres, remaining anions omitted for clarity.

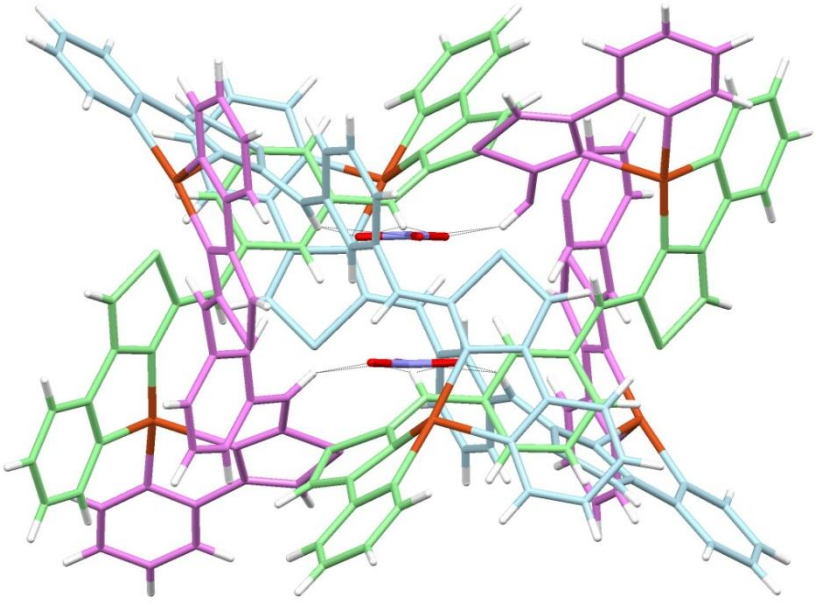

Fig. 122: Solid state structure of $[(Cu(NO_3)(\mathbf{L^5}))_6(NO_3)_2]^{4+}$ showing the arrangement of the encapsulated nitrate anions, coordinating anions omitted for clarity.

Selected bond lengths and angles for complex are shown in tables; 5.11 and 5.12 below.

Atom 1	Atom 2	Bond Length (Å)
Cu1	N5	1.957 (6)
Cu1	N4	2.021 (6)
Cu1	O5	2.157 (6)
Cu1	O2	2.684 (6)
Cu1	N2	2.133 (6)
Cu1	N1	1.984 (6)

Table 5.11: Selected bond lengths for complex $[(Cu(NO_3)(\mathbf{L^5})_6(NO_3)_2]^{4+}$.

Atom 1	Atom 2	Atom 3	Bond Angle (°)
N5	Cu1	N4	82.40 (3)
N5	Cu1	N2	104.70 (2)
N5	Cu1	N1	172.50 (3)
N4	Cu1	O5	153.93 (2)
N4	Cu1	N2	119.12 (3)
N4	Cu1	N1	99.54 (3)
O1	Cu1	N2	86.90 (2)
O1	Cu1	N1	85.30 (2)
N2	Cu1	N1	80.85 (3)

Table 5.12: Selected bond angles for complex $[(Cu(NO_3)(\mathbf{L^5})_6(NO_3)_2]^{4+}$.

The ESI-MS data for this complex upon addition of nitrate anions is non-trival for two reasons; firstly as both nitrate and triflate are present there are a large number of possible anions combinations (e.g. $\{[Cu_6(\mathbf{L^5})_6](trif)_{11}\}^+$, $\{[Cu_6(\mathbf{L^5})_6](NO_3)(trif)_{10}\}^+$, $\{[Cu_6(\mathbf{L^5})_6](NO_3)_2(trif)_9\}^+ \cdots \{[Cu_6(\mathbf{L^5})_6](NO_3)_{11}\}^+$). Secondly, reduction to Cu(I) is also observed (which can occur due to the ESI-MS process, see reference 91) and ions at *m/z* 1131 ($\{[Cu_2(\mathbf{L^5})_2](trif)\}^+$), 1281 ($\{[Cu_2(\mathbf{L^5})_2](trif)_2\}^+$) as well as higher nuclearity ions at *m/z* 1770 ($\{[Cu_2(\mathbf{L^5})_3](NO_3)(trif)_2\}^+$) and 2537 ($\{[Cu_4(\mathbf{L^5})_4](NO_3)_2(trif)_3\}^+$). For these reasons an ion corresponding to the hexanuclear assembly is *not* observed in the ESI-

MS. However, there is no reason to assume that the assembly doesn't persist in solution but it is possible this is solely a solid-state artefact.

6.3 Summary:

In summary the amine containing ligand **[L^5]**, composed of two bidentate pyridyl-thiazole moieties linked by a 1,3-diamino-phenylene unit, reacts with Cu^{2+} ions to form a dinuclear double helicate which exhibits favourable amine hydrogen bonding interactions with a series of anions within a central cavity (e.g. $([Cu_2(L^5)_2](ClO_4)_2)^{2+}$). Addition of half an equivalent of either $Bu_4N(OPO_3H_2)$ or $Bu_4N(HSO_4)$ results in an unsaturated dinuclear double helicate whereby each anion bridges the two Cu^{2+} centres (e.g. $([Cu_2(\mathbf{L^5})_2](SO_4))^{2+}$).

Furthermore addition of one equivalent of $Bu_4N(HSO_4)$ results in no change in the ESI-MS. However, addition of one equivalent of dihydrogen phosphate results in a trinuclear circular helicate which then self-assembles into a hexameric cluster due to a series of phosphate-ligand and phosphate-phosphate interactions.

Further reaction of the **[L^5]** dinuclear double helicate $[Cu_2(\mathbf{L^5})_2]^{4+}$ with one equivalent of $Bu_4N(NO_3)$ results in a hexanuclear circular meso-helicate whereby each metal ions preference for six coordinate is completed by the *N*-donors of two separate ligand strands with the remaining sites occupied by two *O*-donors of a nitrate anion. The formation of the circular species over that of the double helicate is directed by both the coordination of the nitrate anions and their use in templating the self-assembly; firstly the nitrate anion coordinates the metal centre. Secondly, the nitrate templates the self-assembly with the anion sitting in the core of the circular mesocate and undergoes hydrogen bonding interactions to the amine protons of the ligand strand.

7. Chapter 7: Synthesis and coordination chemistry of a ligand containing both *N*-donor and hydrogen bond donor units separated by a central pyridine ring:

Due to successful formation of coordination complexes using **[L^5]**, a development of the ligands architecture to include a central pyridine unit was carried out, since the inclusion of a central pyridine and therefore a further *N-donor* unit may lead to different coordination properties. **[L^6]** maintains the same pyridyl-thiazole moiety, however each group is separated by a 1,3-diaminopyridine unit (Fig. 123). In the work that follows we show how the alteration of a single atom can dramatically affect the resultant self-assembly processes.

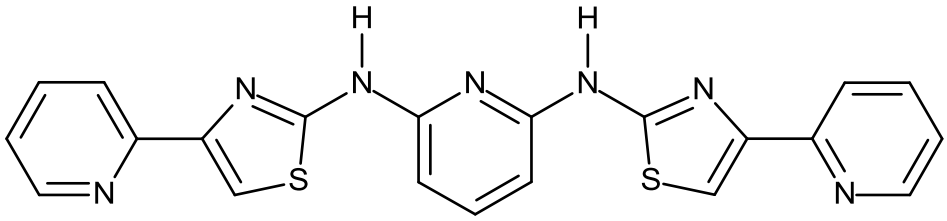

*Fig. 123: Bis-bidentate amine-containing ligand **[L^6]**.*

7.1 Synthesis of [L^6]:

Initial synthesis of **[L^6]** was thought to be possible *via* reaction of 2,6-diaminopyridine with ammonium thiocyanate in dilute hydrochloric acid at 90°C, in an analogous fashion to **[L^5]**. However, unlike the previous reaction no precipitate, corresponding to the desired product had formed; it was noted that the acidic environment of the reaction may have lessened due to HCl protonating the pyridine ring thus increasing the solubility of the product and inhibiting the precipitation. Further addition of acid and concentration of the reaction mixture gave little to no change resulting in an alternative synthesis route.

Instead, **[L^6]** was prepared *via* a different route which required more synthetic steps. The first product was prepared from an adapted method to a literature procedure. A solvent-free preparation of bis-1-(aroyl)-3-(aryl)thiourea by reaction of 1,3-diaminopyridine with ammonium thiocyanate and aryl chloride as described by

Mohebat *et al*.[92] was attempted, but in our hands the yields and purity were highly variable. However, the same reaction was carried out by reacting benzoyl chloride with ammonium thiocyanate in an acetonitrile and pyridine solution at room temperature for 30 minutes to give intermediate **[1]** (Scheme 6). After 30 minutes, 2,6-diaminopyridine was added to the reaction and it was allowed to stir at room temperature for a further four hours, after which time a precipitate formed which was isolated *via* vacuum filtration to yield pyridine aroyl-thiourea **[2]**.

Conversion to the thiourea **[3]** was carried *via* the literature procedure for the hydrolysis of amides using NaOH in diH_2O.

Formation of the final ligand **[L^6]** was achieved by reaction of the thiourea with an excess of 2-(α-bromoacetyl)pyridine in ethanol at 80°C for 12 hours. The resulting precipitate was isolated by filtration and suspended in concentrated ammonia overnight to give the free-base ligand. Examination of the ^{1}H NMR spectrum in d_6-DMSO indicated the successful formation of **[L^6]**. The spectrum shows a total of 15 signals with a signal at 11.07 ppm which corresponds to the amine protons and a singlet at 7.68 ppm corresponding to the thiazole unit (Fig. 124a &b). Furthermore, ^{13}C NMR spectroscopy also showed 11 signals in the aromatic region. ESI-MS showed an ion at *m/z* 430 corresponding to [L^6+H]$^+$.

a)

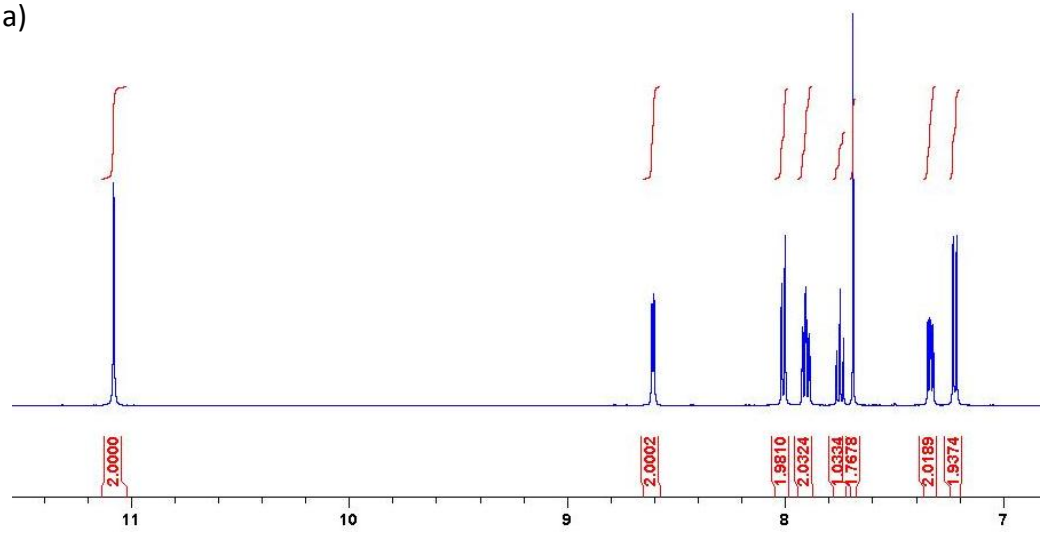

b)

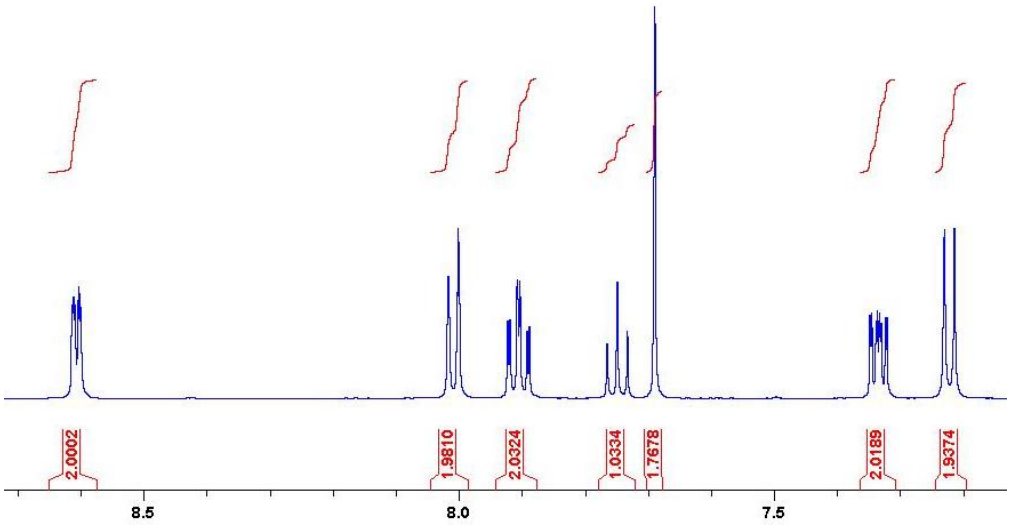

Fig. 124a & b: ^{1}H NMR spectrum of the aromatic region of ***[L^{6}]****.* (400MHz, d_6-DMSO) signals of note include the amine and thiazole proton (δ 11.07 and 7.68 respectively).

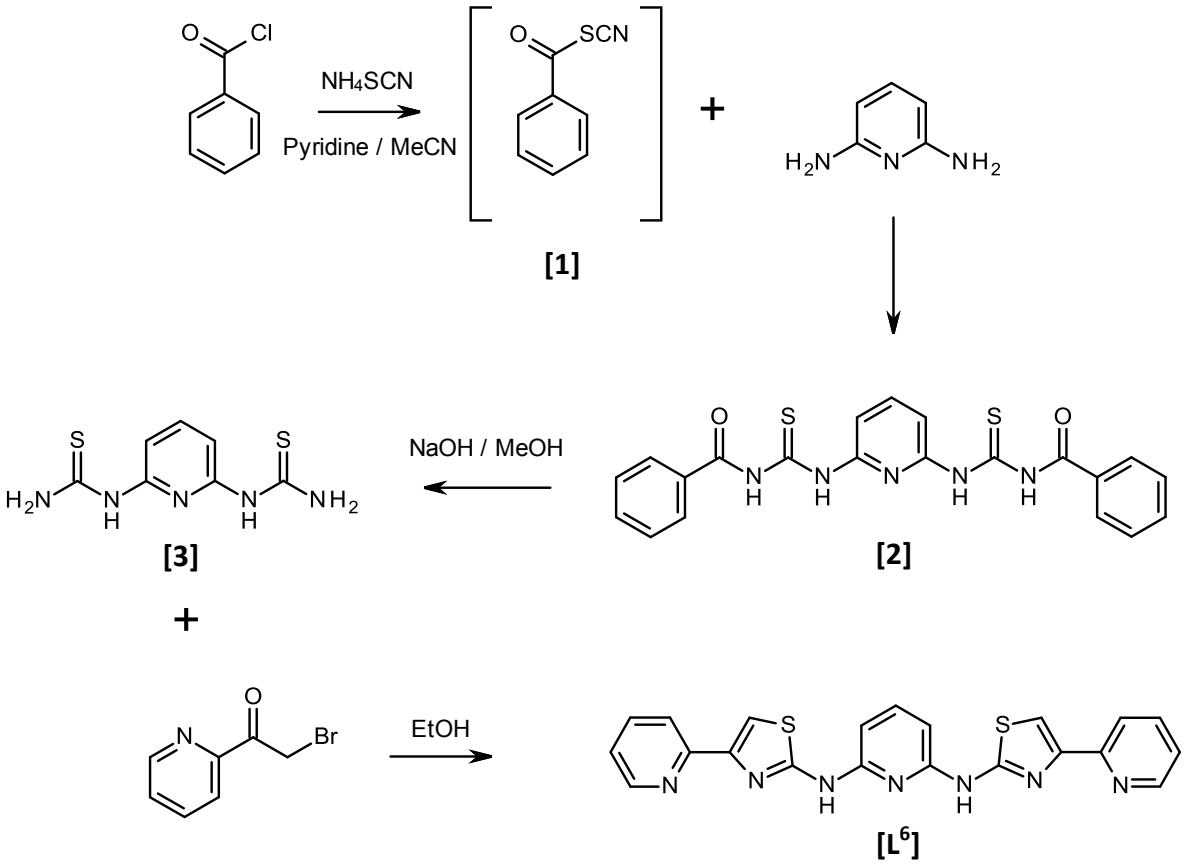

*Scheme 6: Synthesis of **[L^6]**.*

7.2 Coordination Chemistry of [L^6]:

7.2.1 Coordination of [L^6] with $Cu(ClO_4)_2$:

Equimolar amounts of **[L^6]** and $Cu(ClO_4)_2 \cdot 6H_2O$ were combined in $MeNO_2$ to produce an intense green solution which upon slow diffusion of diisopropyl ether gave green crystals. Structural characterization by X-ray diffraction showed that in the solid state a single mononuclear species comprising of one ligand and one metal ion (e.g. $[Cu(\mathbf{L^6})]^{2+}$) is formed (Fig. 125).

In the solid state the copper ion adopts an octahedral coordination geometry with each of the ligand's *N*-donor atoms fulfilling 5 of the copper's 6 coordination sites (Cu-N bond lengths 1.8996 (1) – 2.7096 (1) Å). The copper's preference for a 6-coordinate geometry is then completed by a single perchlorate anion, pointing outwards from the central atom, in an axial position (Cu-O···Cl 2.646 Å) (Fig. 126). Research into the coordination of solvents in the axial position of Cu(II) complexes has been a source of study for a number of research groups.[93-95] Comba *et. al.* developed a series of

mononuclear, five-coordinate, copper(II) complexes with perchlorate anions coordinated to the copper ion in the axial position. In similar fashion to the structure observed between **[L^6]** and $Cu(ClO_4)_2{\cdot}6H_2O$, Comba and co-workers also noted a large Cu-O bond length (2.76 Å) between the copper(II) and the oxygen atom of the perchlorate; indicating that this is a commonly observed bond length for the interaction of Cu-O···Cl in these species.

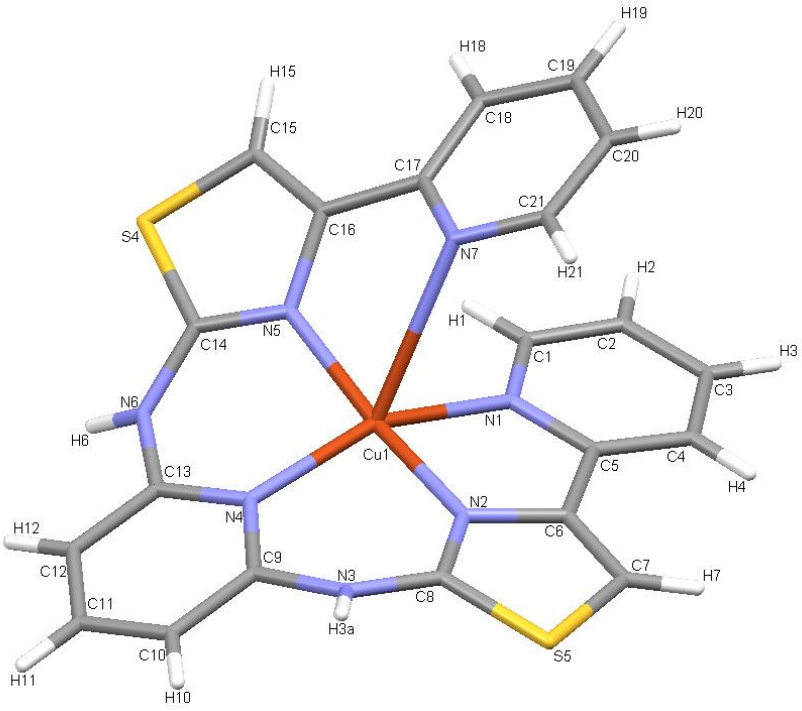

*Fig. 125: Solid state structure of [Cu(**L^6**)](ClO$_4$)$^+$; the remaining perchlorate anion is omitted for clarity.*

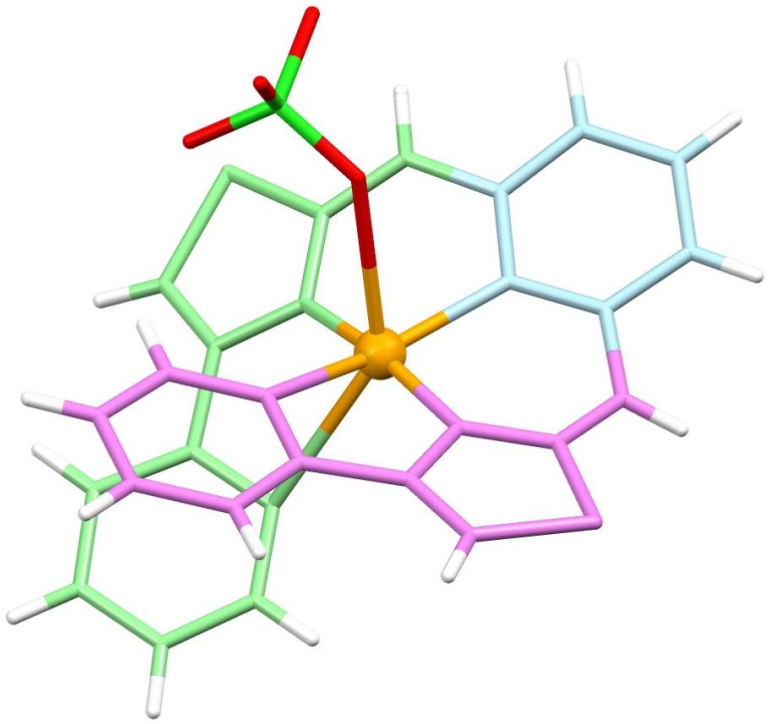

*Fig. 126: Solid state structure of [Cu(**L**^{6})](ClO$_4$)]$^+$, showing the axial interaction between the perchlorate anion and the copper centre.*

Formation of a mononuclear species over the dinuclear double helicates previously observed is a result of coordination of the Cu^{2+} ion with the nitrogen atom of the central pyridyl unit (Fig. 127).

Due to the difference in shape of the complex the two amine groups do not form a cavity as is observed with **[L^{5}]** and Cu^{2+}, instead each amine unit points outwards from the complex to allow each connecting thiazole / pyridine bidentate unit to complete the coordination. Neither amine is then involved in any interactions of note.

ESI-MS analysis did not show the expected ion e.g. {[Cu(**L**^{6})](ClO$_4$)]}$^+$ it did however show two mass ions at *m/z* 1082 and 1284 corresponding to {[Cu$_2$(**L**^{6})$_2$(ClO$_4$)]}$^+$ and {[Cu$_2$(**L**^{6})$_2$(ClO$_4$)$_3$]}$^+$ respectively. The smaller ion at *m/z* 1082 is a consequence of the ESI-MS process which has reduced the Cu(II) to Cu(I), an affect previously observed in this thesis.

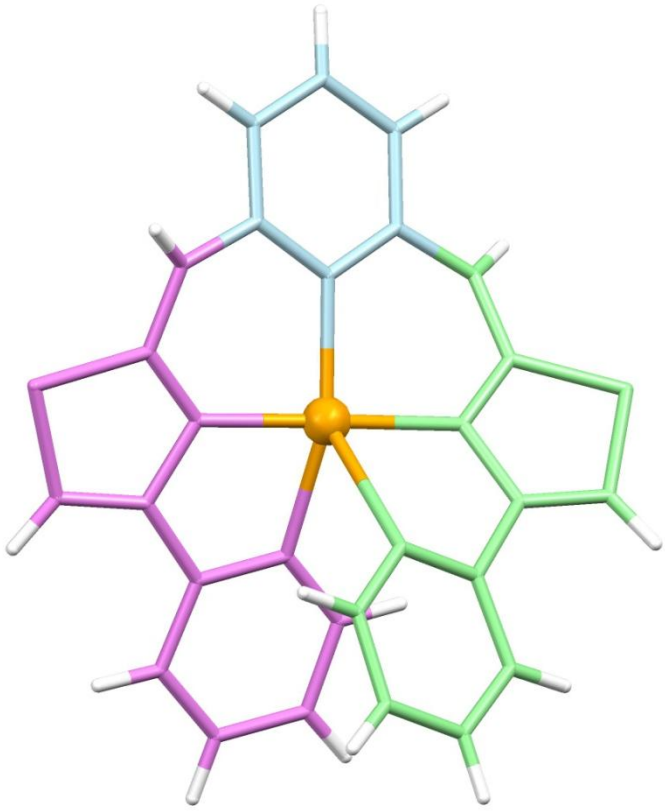

*Fig. 127: Solid state structure of [Cu(**L**^{6})](ClO$_4$)$^+$ showing the coordinating nature of the central pyridyl ring; the perchlorate anion is omitted for clarity.*

Selected bond lengths and angles for the complex are shown in Tables 6.1 and 6.2 below; relevant atoms labels are shown in Fig. 128.

Atom 1	Atom 2	Bond Length (Å)
Cu1	N2	1.899 (17)
Cu1	N5	1.920 (17)
Cu1	N4	2.055 (17)
Cu1	N1	2.088 (18)
Cu1	O1	2.646 (18)
Cu1	N7	2.710 (18)

*Table 6.1: Selected bond lengths for [Cu(**L**^{6})](ClO$_4$)$^+$.*

Atom 1	Atom 2	Atom 3	Bond Angle (°)
Cu1	N2	N5	167.68 (8)
Cu1	N2	N4	89.72 (7)
Cu1	N2	N1	80.03 (7)
Cu1	N2	O1	101.14 (8)
Cu1	N2	N7	101.38 (7)
Cu1	N5	N4	90.91 (7)
Cu1	N5	N1	103.41 (7)
Cu1	N5	O1	91.10 (8)
Cu1	N5	N7	68.92 (7)
Cu1	N4	N1	157.29 (7)
Cu1	N4	O1	80.55 (8)
Cu1	N4	N7	129.23 (7)
Cu1	N1	O1	81.63 (8)
Cu1	N1	N7	73.03 (7)
Cu1	O1	N7	142.31 (8)

Table 6.2: Selected bond angles for $[Cu(\boldsymbol{L^6})](ClO_4)^+$.

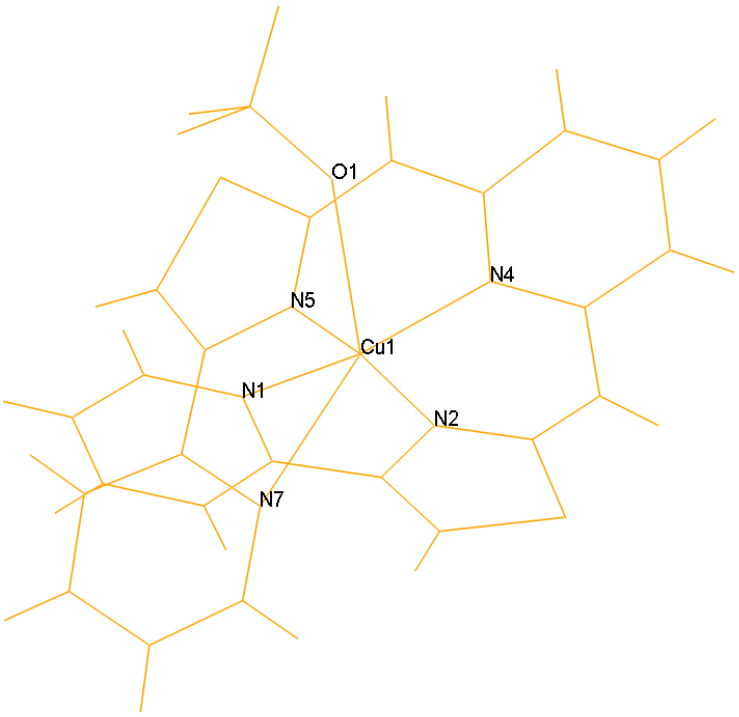

Fig. 128: Selected atom labels for $[Cu(\boldsymbol{L^6})](ClO_4)^+$.

An analogous structure was observed with BF_4^- showing that the formation of the mono-nuclear structure isn't dependent upon the anion.

7.2.2 Coordination of $[L^6]$ with $Cu(BF_4)_2$:

Reaction of **$[L^6]$** with $Cu(BF_4)_2$ (in-place of $Cu(ClO_4)_2$) in $MeNO_2$ resulted in similarly-coloured crystals upon slow diffusion of diisopropyl ether. Single X-ray diffraction showed the ligand remains partitioned into two bidentate binding domains with each thiazole-pyridyl linkage coordinating to the same central copper ion (Fig. 129 & 130) (ave. N – Cu bond length: 2.130 Å). The copper remains octahedral with the pyridine spacer and BF_4^- anion taking up the two remaining coordination sites.

The mononuclear structure persists with the BF_4^- anion sitting in an axial position to the Cu^{2+} centre (Fig. 131). As such no binding cavity is created with each -NH of the ligand pointing outwards from the centre of the structure foregoing any interactions.

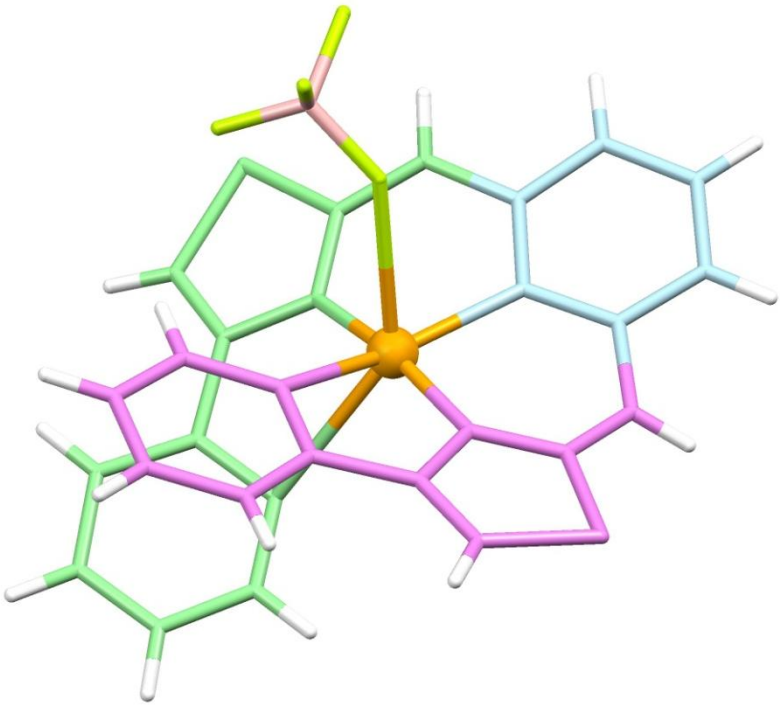

Fig. 129: Solid state structure of $[Cu(\boldsymbol{L^6})](BF_4)^+$, showing the axial interaction between the tetrafluroborate anion and the copper centre.

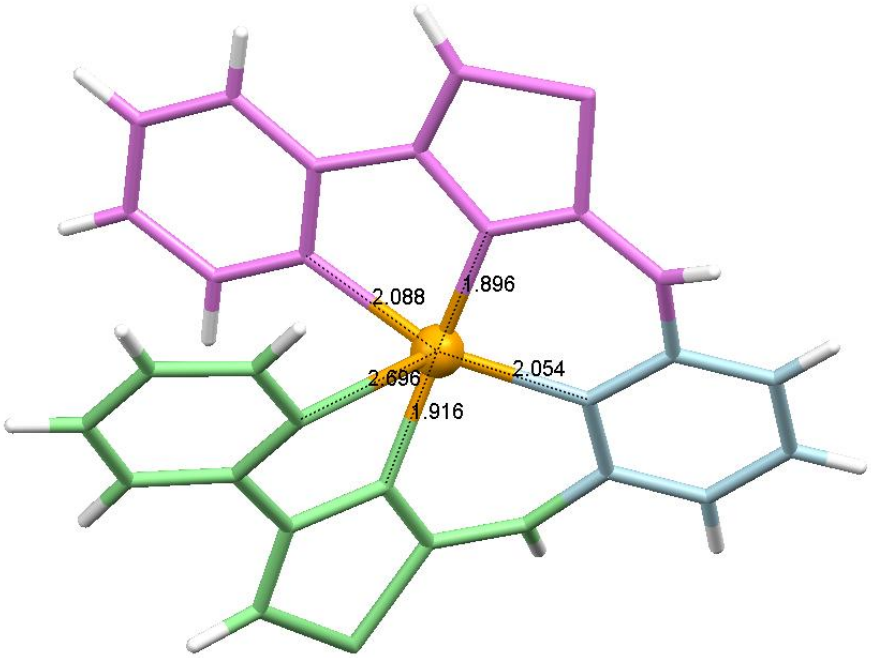

Fig. 130: Solid state structure [Cu($\mathbf{L^6}$)](BF$_4$)$^+$, N – Cu bond lengths.

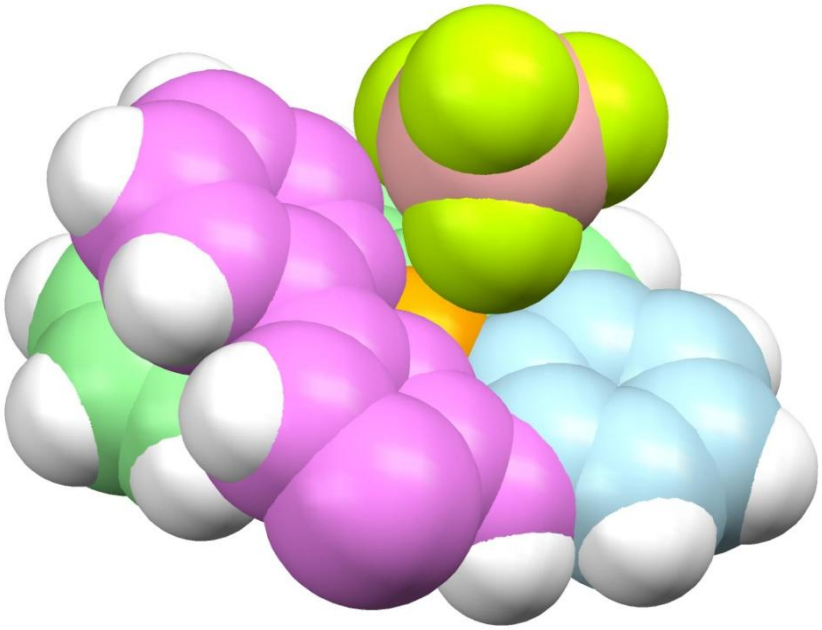

Fig. 131: Space filling diagram of the solid state structure [Cu($\mathbf{L^6}$)](BF$_4$)$^+$.

ESI-MS was carried out on the complex [Cu($\mathbf{L^6}$)](BF$_4$)$^+$ which gave a distinct ion at *m/z* 1071. The ion corresponds to {[Cu$_2$($\mathbf{L^6}$)$_2$(BF$_4$)]}$^+$ which showed a similar reduction of the Cu(II) to Cu(I).

Selected bond lengths and angles for the complex are shown in Tables 6.3 and 6.4 below; relevant atoms labels are shown in Fig. 128.

Atom 1	Atom 2	Bond Length (Å)
Cu1	N2	1.916 (2)
Cu1	N6	1.896 (2)
Cu1	N4	2.054 (2)
Cu1	N1	2.088 (2)
Cu1	F6	2.584 (3)
Cu1	N7	2.088 (2)

*Table 6.3: Selected bond lengths for [Cu(**L**^{6})](BF$_4$)$^{+}$.*

Atom 1	Atom 2	Atom 3	Bond Angle (°)
N2	Cu1	N6	167.40 (10)
N2	Cu1	N4	91.00 (10)
N2	Cu1	N1	69.12 (10)
N2	Cu1	F6	89.41 (10)
N2	Cu1	N7	103.19 (10)
N6	Cu1	N4	90.97 (10)
N6	Cu1	N1	100.07 (10)
N6	Cu1	F6	103.42 (10)
N6	Cu1	N7	80.03 (10)
N4	Cu1	N1	128.82 (10)
N4	Cu1	F6	81.40 (10)
N4	Cu1	N7	157.31 (9)
N1	Cu1	F6	141.08 (10)
N1	Cu1	N7	73.41 (10)
F6	Cu1	N7	81.22 (10)

*Table 6.4: Selected bond angles for [Cu(**L**^{6})](BF$_4$)$^{+}$.*

Although this result (i.e. the formation of a mono-nuclear complex with **[L^{6}]** and Cu^{2+}) may be expected, it is interesting to note that even a simple change in the ligand strand can have dramatic effects on the self-assembly process. Thus when a central 1,3-phenylene spacer is employed (i.e. **[L^{5}]**) a dinuclear double helicate is formed.

However, when a 1,3-pyridine unit is contained within the ligand strand (i.e. **[L^6]**) a simple mono-nuclear species is produced.

Given the exceptional binding properties of urea groups with anions the possibility of an anion only assembly with the **[L^6]** intermediate **[L^7]** was explored (Fig. 132). Formation of **[L^7]** was achieved via the same route of synthesis as **[L^6]** (Scheme 6), however the hydrolysis of step **[2]** was not carried out. Confirmation of successful synthesis of **[L^7]** was carried out by ^{1}H NMR spectroscopy which showed a total of nine signals integrating to 17 protons, signals of note being two singlet's at 13.23 ppm and 11.86 ppm corresponding to each NH of the thiourea. Furthermore ESI-MS of showed an ion at 436 m/z corresponding to $[L^7+H]^+$.

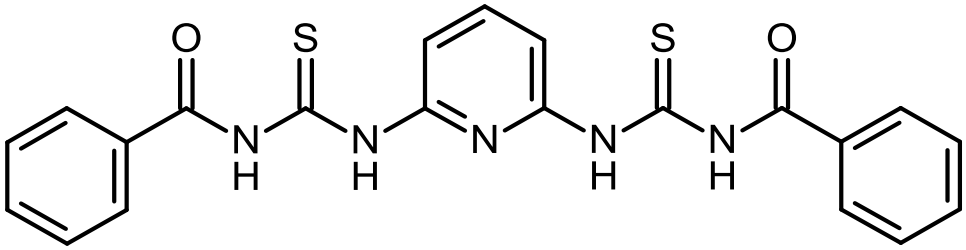

*Fig. 132: **[L^7]** (thiourea).*

7.2.3 Coordination with [L^7] with $(Bu)_4N(ClO_4)$:

Reaction of **[L^7]** with $(Bu)_4N(ClO_4)$ in DMF resulted in the formation of yellow crystals upon slow evaporation of DMF. Single X-ray diffraction shows a di-ionic double stranded structure whereby an amide from each of the thiourea binding domains undergoes favourable hydrogen bonding interactions with two perchlorate anions (ave. NH interaction length: 2.226 Å) (Fig. 133).

The ligand becomes almost perfectly linear with only a slight conformational twist around each of the Py-NH axis to allow for more thermodynamically favourable interactions (Fig. 134). One thiourea group deflects outwards coordinating a single perchlorate anion via hydrogen bonding interactions whilst the second thiourea repeats this in the opposite direction.

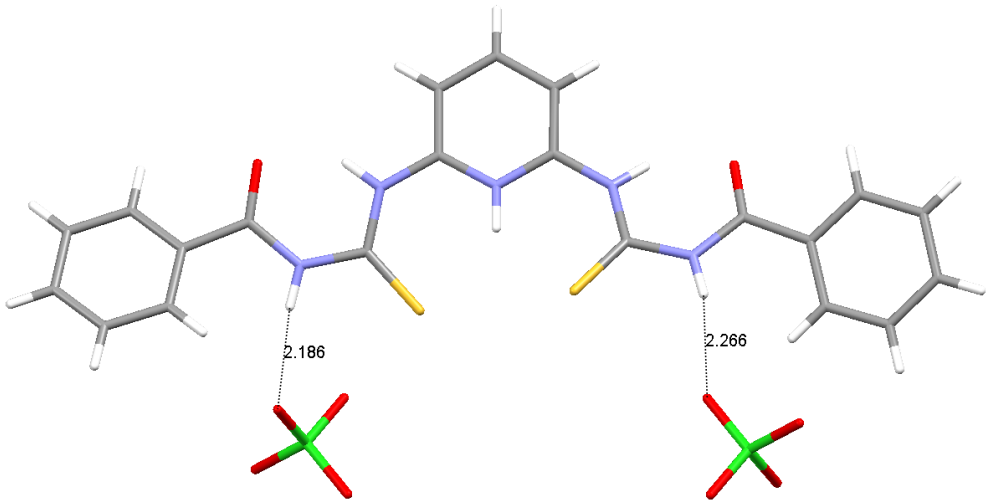

Fig. 133: Hydrogen bonding interactions of ***[L^{7}]*** *with perchlorate anions, [**L**^{7}(ClO$_4$)$_2$]$^{2-}$.*

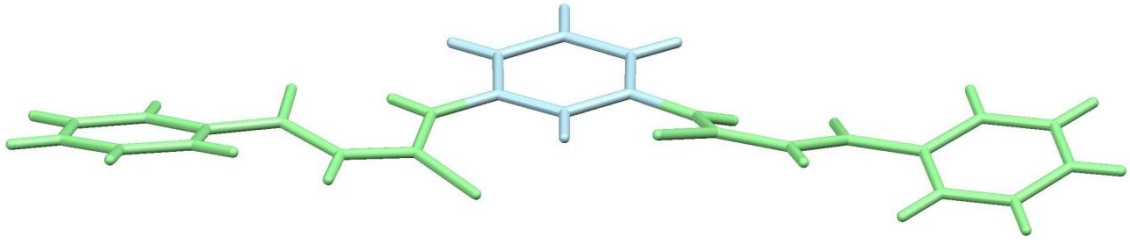

Fig. 134: Conformational twist of ***[L^{7}]*** *upon hydrogen bonding of ClO$_4^-$ anions (anions omitted for clarity).*

Each of the two urea amides hydrogen bonds to one oxygen atom of the perchlorate anion allowing for further hydrogen bonding interactions by a second ligand (Fig. 135a & b). This self-assembled species is clearly dependant on the stabilising hydrogen bonding interactions between the tetrahedral *O*-donor ClO_4^- anion and the δ^+ proton from the urea amide groups of each ligand (N4-O2, N1-O1) (Fig. 135a). As well as favourable interactions between each sulphur atom and the protonated pyridyl space group (S1, N3 and S2) (Fig. 136).

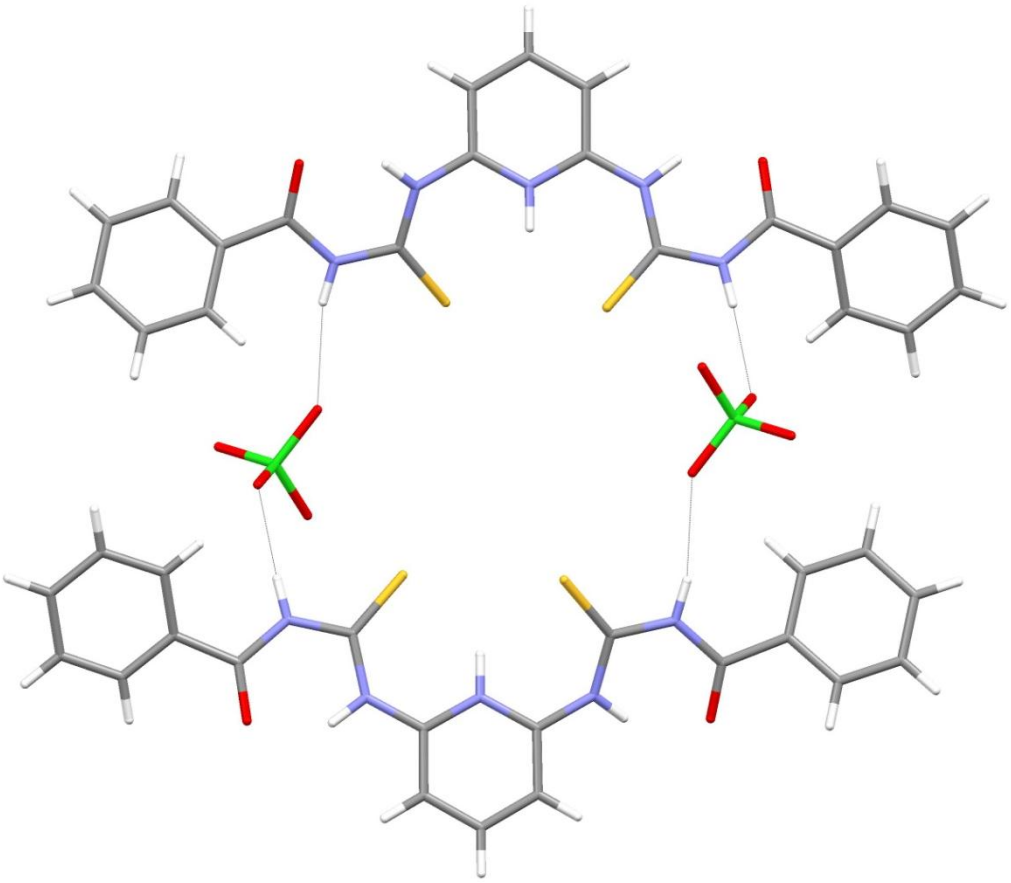

Fig. 135a: Di-ionic double stranded structure [($\mathbf{L^7}$)$_2$(ClO_4)$_2$].

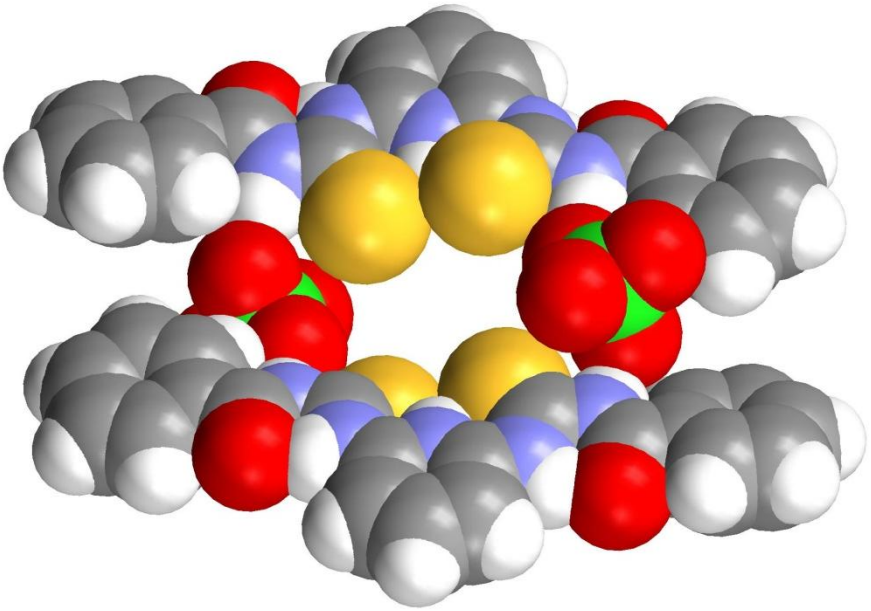

Fig. 135b: Space filling view of [($\mathbf{L^7}$)$_2$(ClO_4)$_2$].

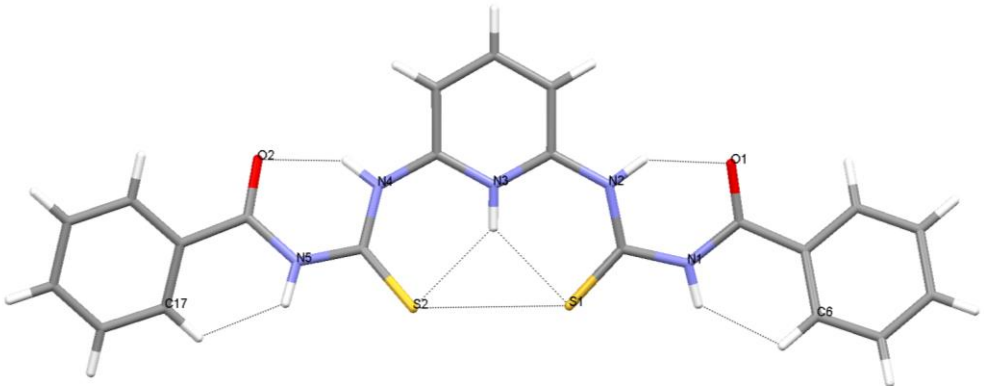

Fig. 136: Internal stabilizing interactions between the protonated pyridyl ring (N3) and sulphurs (S1 & S2) of the thiourea.

7.3 Summary:

Throughout this chapter a variety of self-assembled structures, based on a similar architecture have been shown. Modification of the central unit from a 1,3-diphenyl to a 1,3-dipyridyl has shown to have a direct impact on the overall self-assembly process (dinuclear double helicate to a mononuclear species). The modification of the central unit has not only altered the preference of the *N*-donor cation domains in the coordination of metal ions but has also impacted the ability of the complex to undergo hydrogen bonding interactions with anions.

In the case of the 1,3-phenyl centre a series of dinuclear double helicates with a cavity capable of hydrogen bonding anions have been formed ($Cu(BF_4)_2$, $Cu(ClO_4)_2$, $Bu_4(HSO_4)$ and 0.5 eq $H_2PO_4^-$). Coordination of **[L^5]** with a divalent metal ion and a trigonal planar anion (e.g. NO_3^-) in place of tetrahedral anions (e.g. ClO_4^-) gives a hexanuclear meso-circular helicate. Each ligand is coordinated by two bis-bidentate domains of separate ligands and two *O*-donors of a nitrate anion. Furthermore the complex forms a central cavity which is populated by two nitrate anions. A trinuclear triple helicate is formed with 1 eq of $H_2PO_4^-$ that then proceeds to dimerize with its own trinuclear oligomer via a cyclic array of six (···HO-P=O···) donor/acceptor units. Interestingly the difference between the last two structures is arguably attributable to the ability of the phosphate to undergo hydrogen bonding to itself.When the ligand contains a central 1,3-pyridyl unit a mononuclear species is formed as this unit can coordinate metal ions. This complex does not contain amine hydrogen atoms of sufficient geometry to form a cavity and no discrete binding of anions is observed.

Chapters 6-7 Experimental:

Synthesis of ligand [L^5]. To a 50 ml round bottom flask was added phenyl-1,3-dithiourea (0.30 g, 1.3 mmol) and 2-(α–bromoacetyl)pyridine (1.10 g, 3.9 mmol) and ethanol (25 mL) and the suspension heated at 80 °C for 12 hours during which time the reagents dissolved and a heavy yellow precipitate was formed. The yellow solid was isolated *via* filtration and washed with ethanol (2 x 5 mL) and ether (2 x 5 mL), giving the ligand as the hydrobromide salt. The salt was suspended in concentrated ammonia (10 mL) for 12 hours, filtered and washed with water (2 x 5 mL), ethanol (2 x 5 mL) and ether (2 x 5 mL), giving the free base ligand as a tan solid (0.50 g, 36%). ^{1}H NMR spectroscopy (400 MHz, d_6-DMSO) δ 10.38 (s, 2H, NH), δ 8.56 (d, 2H, py, *J* = 4.40), δ 8.28 (s, 1H, ph), δ 8.02 (d, 2H, py, *J* = 7.80), δ 7.76 (t, 2H, py, *J* = 5.4), δ 7.57 (s, 2H, tz), δ 7.31 (s, 3H, ph overlapping), δ 7.27 (dd, 2H, py, *J* = 5.1, 6.9 Hz) (Fig. 137). ^{13}C NMR spectroscopy (100 MHz d_6-DMSO) δ 163.9, 152.5, 150.9, 149.7, 142.2, 137.5, 130.0, 123.0, 121.1, 110.8, 107.2 and 160.0. ESI-MS *m/z* 429 ($[M+H]^+$), HR ESI-MS found 428.0875 $C_{22}H_{16}N_6S_2$ require 428.0878 (error 0.64 ppm).

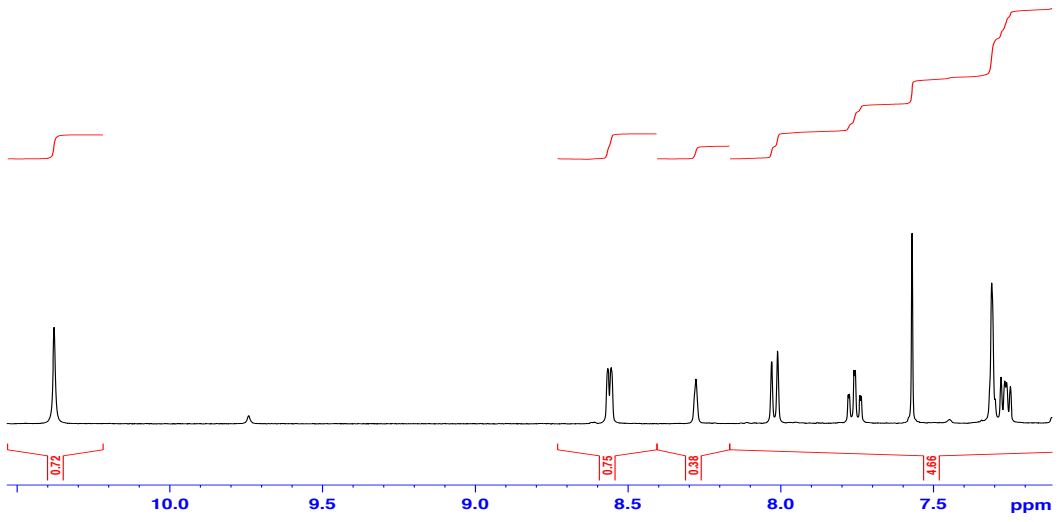

*Fig. 137: ^{1}H NMR spectrum of the aromatic region of **[L^5]**. (400MHz,* d_6-DMSO) signals of note include the amine and thiazole proton (δ 10.38 and 7.57 respectively).

Synthesis of $[Cu_2(L^5)_2](ClO_4)_4$. To a suspension of $Cu(ClO_4)_2{\cdot}6H_2O$ (9.5 mg, 0.026 mmol) in $MeNO_2$ (1 mL) was added a suspension of ligand **$[L^5]$** (11 mg, 0.026 mmol) in $MeNO_2$ and the reaction warmed and sonicated until a clear dark blue solution had formed. Diisopropyl ether was slowly allowed to diffuse into the solution resulting in blue plate-like crystals after several days. Filtration and washing with diisopropyl ether (1 mL) and diethyl ether (1 mL) gave blue crystals which lost solvent rapidly (yield = 68%). ESI-MS *m/z* 1281 corresponding to $\{(Cu_2(\mathbf{L^5})_2)(ClO_4)_3\}^+$. The tetrafluoroborate derivative was synthesised in an analogous fashion.

Synthesis of $[Cu_2(L^5)_2(SO_4)](CF_3SO_3)_3$. To a suspension of $Cu(CF_3SO_3)_2{\cdot}6H_2O$ (9.5 mg, 0.026 mmol) in $MeNO_2$ (1 mL) was added a suspension of ligand **$[L^5]$** (11 mg, 0.026 mmol) in $MeNO_2$ and the reaction warmed and sonicated until a clear dark blue solution had formed. To this was then added $Et_4N(HSO_4)$ (3.96 mg, 0.012 mmol) and a couple of drops of MeOH to aid dissolution. Ethyl acetate was slowly allowed to diffuse into the solution resulting in yellow-brown crystals. ESI-MS showed a mass ion at *m/z* 1229 which corresponds to $\{[Cu_2(\mathbf{L^5})_2](SO_4)(CF_3SO_3)\}^+$.

Synthesis of $[Cu_2(L^5)_2(OPO_3H_2)](CF_3SO_3)_3$. To a suspension of $Cu(CF_3SO_3)_2{\cdot}6H_2O$ (9.5 mg, 0.026 mmol) in $MeNO_2$ (1 mL) was added a suspension of ligand **$[L^5]$** (11 mg, 0.026 mmol) in $MeNO_2$ and the reaction warmed and sonicated until a clear dark blue solution had formed. To this was then added $Bu_4N(OPO_3H_2)$ (4.6 mg 0.013 mmol) and a couple of drops of MeOH to aid dissolution. Ethyl acetate was slowly allowed to diffuse into the solution resulting in a mixture of olive-green and blue crystals. ESI-MS *m/z* 1279 which corresponds to $\{[Cu_2(\mathbf{L^5})_2(OPO_3H_2)(ClO_4)_2]\}^+$.

Synthesis of **$([Cu_3(L^5)_3(OPO_3H_2)_3])_2(BF_4)_6$.** To a suspension of $Cu(ClO_4)_2{\cdot}6H_2O$ (9.5 mg. 0.026 mmol) in $MeNO_2$ (1 mL) was added a suspension of ligand **$[L^5]$** (11 mg, 0.026 mmol) in $MeNO_2$ and the reaction warmed and sonicated until a clear dark blue solution had formed. To this was then added $Bu_4N(OPO_3H_2)$ (9.2 mg 0.027 mmol) and a couple of drops of MeOH to aid dissolution. Diisopropyl ether was slowly allowed to diffuse into the solution resulting in a mixture of olive-green plate-like and brown needle-like crystals. ESI-MS *m/z* at 1966 which corresponds to $\{[Cu_3(\mathbf{L^5})_3(OPO_3H_2)_3](ClO)_2\}^+$ and an ion at *m/z* 4036 which corresponds to the dimer

$\{[Cu_3(\mathbf{L^5})_3(OPO_3H_2)_3]_2(ClO)_5\}^+$ as well as a peak at *m/z* 1279 which corresponds to $\{[Cu_2(\mathbf{L^5})_2(OPO_3H_2)(ClO_4)_2]^+$.

Synthesis of $[Cu_6(\mathbf{L^5})_6(NO_3)_6](NO_3)_2$: To a suspension of $Cu(NO_3)_2{\cdot}3H_2O$ (6.19 mg, 0.026 mmol) in $MeNO_2$ (1 mL) was added a suspension of ligand **$[\mathbf{L^5}]$** (11 mg, 0.026 mmol) in $MeNO_2$ and the reaction warmed and sonicated until a clear dark green solution had formed. Chloroform was slowly allowed to diffuse into the solution resulting in green crystals.

Collection and analysis of all crystallographic data was carried out by Prof. C. Rice.

Crystal data for $[Cu_2(\mathbf{L^5})_2](BF_4)_4$: $C_{49}H_{47}B_4Cu_2F_{16}N_{17}O_{10}S_4$, *M* = 1636.59*, monoclinic*, *a* = 15.7577 (8) Å, *b* = 24.3791 (12) Å, *c* = 18.1470 (9) Å, *β* = 112.7137 (17)˚, *V* = 6430.7 (6) Å^3, *T* = 150 K, space group *P21/n*, *Z* = 4, *μ(MoKα)* = 3.071 mm^{-1}, 40212 reflections measured, 11704 independant reflections (R_{int} = 0.0581). The final R_1 values were 0.0797 ($I > 2\sigma(I)$). The final $wR(F^2)$ values were 0.2179 ($I > 2\sigma(I)$). The final R_1 values were 0.0902 (all data). The final $wR(F^2)$ = 0.2299 (all data). The goodness of fit on F^2 was 1.028. CCDC 1014137. The structure contained both disordered tetrafluoroborate counter ions and nitromethane solvent molecules and these were modelled in two positions using the *PART* instruction. For all the disordered atoms/molecules the *DELU*, *SIMU* and *SADI* constrains were used in the least-squares refinement and for one nitromethane solvent molecule the *DIFX* instruction was used to restrain the bond lengths to a chemically reasonable value.

Crystal data for $[Cu_2(\mathbf{L^5})_2](ClO_4)_4$: $C_{47.76}H_{43.27}Cl_4Cu_2N_{15.76}O_{23.5}S_4$, *M* = 1611.07, monoclinic, *a* = 15.7956 (4) Å, *b* = 24.5518 (6) Å, *c* = 18.1885 (4) Å, *β* = 111.9649 (10)˚, *V* = 6541.7 (3) Å^3, *T* = 150 K, space group *P21/n*, *Z* = 4, *μ(MoKα)* = 4.279 mm^{-1}, 50983 reflections measured, 11860 independent reflections (R_{int} = 0.0587). The final R_1 values were 0.0687 ($I > 2\sigma(I)$). The final $wR(F^2)$ values were 0.2060 ($I > 2\sigma(I)$). The final R_1 values were 0.0866 (all data). The final $wR(F^2)$ = 0.2242 (all data). The goodness of fit on F^2 was 1.074. CCDC 1014138. The structure contained both disordered perchlorate counter ions and nitromethane solvent molecules and these were modelled in two positions using the *PART* instruction. In all cases of disordered atoms/molecules *DELU*,

SIMU, *SADI*, and in some cases *ISOR*, constraints were used in the lest-squares refinement.

Crystal data for $[Cu_2(L^5)_2(HSO_4)](ClO_4)_3$: $C_{46}H_{32}Cu_2F_6N_{12}O_{10}S_7$, M = 1378.39, triclinic, a = 12.9800 (5) Å, b = 16.3791 (6) Å, c = 16.5386 (6) Å, β =75.060 (2)˚, V = 2983.2 (2) Å^3, T = 150 K, space group *P21/n*, Z = 2, μ(MoKα) = 3.888 mm^{-1}, 32914 reflections measured, 10291 independent reflections (R_{int} = 0.1173). The final R_1 values were 0.1054 ($I > 2\sigma(I)$). The final $wR(F^2)$ values were 0.2739 ($I > 2\sigma(I)$). The final R_1 values were 0.1533 (all data). The final $wR(F^2)$ = 0.3165 (all data). The goodness of fit on F^2 was 1.0795.

Crystal data for $[Cu_2(L^5)_2(OPO_3H_2)](ClO_4)_3$: $C_{47.76}H_{43.93}Cl_3Cu_2N_{12.41}O_{19}PS_4$, M = 1488.46, monoclinic, a = 10.8777 (8) Å, b = 14.4583 (10) Å, c = 40.129 (3) Å, β = 93.474 (2)˚, V = 6299.5 (8) Å^3, T = 150 K, space group *P21/n*, Z = 4, μ(MoKα) = 1.039 mm^{-1}, 74826 reflections measured, 17704 independent reflections (R_{int} = 0.0391). The final R_1 values were 0.0649 ($I > 2\sigma(I)$). The final $wR(F^2)$ values were 0.1881 ($I > 2\sigma(I)$). The final R_1 values were 0.0930 (all data). The final $wR(F^2)$ = 0.2083 (all data). The goodness of fit on F^2 was 1.0708. CCDC 1014139. The structure contained a disordered perchlorate counter anion and a methanol solvent molecule and these were modelled in two positions using the *PART* instruction. In all cases of disordered atoms/molecules *DELU*, *SIMU*, *SADI*, and in some cases *ISOR*, constraints were used in the lest-squares refinement.

Crystal data for $([Cu_3(L^5)_3(OPO_3H_2)_3])_2(BF_4)_6$: $C_{76}H_{80}B_3Cu_3F_{12}N_{22}O_{21}P_3S_6$, M = 2374.03, monoclinic, a = 38.5799 (9) Å, b = 13.6472 (4) Å, c = 39.6602 (10) Å, β = 91.5678 (13)˚, V = 20873.6 (9) Å^3, T = 150 K, space group *C2/c*, Z = 8, μ(MoKα) = 3.106 mm^{-1}, 73045 reflections measured, 19060 independent reflections (R_{int} = 0.0769). The final R_1 values were 0.0782 ($I > 2\sigma(I)$). The final $wR(F^2)$ values were 0.2176 ($I > 2\sigma(I)$). The final R_1 values were 0.1166 (all data). The final $wR(F^2)$ = 0.2493 (all data). The goodness of fit on F^2 was 1.0614. CCDC 1014140. The structure contained a disordered tetrafluoroborate counter anion and a nitromethane solvent molecule and these were modelled in two positions using the *PART* instruction. In all cases of disordered atoms/molecules *DELU*, *SIMU*, *SADI*, and in some cases *ISOR*, constraints were used in the lest-squares refinement. Furthermore, the structure contained disorder that could

not be satisfactorily modelled and as a result the diffuse electron density was removed using the solvent mask facility in Olex2, resulting in voids in the crystal structure.[6] The solvent mask removed a total of 320.02 electrons in the unit cell which corresponds to four molecules of nitromethane and four molecules of diisopropyl ether in the unit cell.

Crystal data for $[Cu_6(L^5)_6(NO_3)_6](NO_3)_2$: $C_{138}H_{102}Cl_{18}Cu_6N_{44}O_{24}S_{12}$, M = 4164.76*, trigonal*, a = 34.1503 (13) Å, b = 34.1503 (13) Å, c = 16.9013 (7) Å, β = 90 °, V = 17070.2 (12) Å^3, T = 150 K, space group *R-3*, Z = 3, $\mu(MoK\alpha)$ = 0.931 mm^{-1}, 24312 reflections measured, 6478 independent reflections (R_{int} = 0.0493). The final R_1 values were 0.0835 (I >2σ(I)). The final $wR(F^2)$ values were 0.2727 (I > 2σ(I)). The final R_1 values were 0.1226 (all data). The final $wR(F^2)$ = 0.3116 (all data). The goodness of fit on F^2 was 1.0591.

Synthesis of ligand [L^6]. To a 50 ml round bottom flask was added benzoyl chloride (0.28 g, 2 mmol) and ammonium thiocyanate (0.15 g, 2 mmol) which was dissolved in an acetonitrile/pyridine solution (20:0.6 mL). The reaction was stirred at room temperature for 30 minutes before the addition of 2,6-diaminopyridine (0.10 g, 0.94 mmol). The suspension was allowed to react at room temperature for a further four hours, during which time the reagents dissolved and a thick yellow precipitate formed which was isolated via vacuum filtration and washed with water (2 x 5 mL), ethanol (2 x 5 mL) and ether (2 x 5 mL), giving pyridine aroyl-thiourea (0.21 g). A 50 mL round bottom flask was charged with pyridine aroyl-thiourea (0.50 g, 1.15 mmol), diH_2O (25 mL) and NaOH (0.03 g, 0.38 mmol). The reaction was sonicated until all the reagents had dissolved and then heated at 80 °C for four hours. The reaction was cooled and acetic acid (0.5 mL) added drop wise until a yellow precipitate formed. The solid was isolated *via* filtration and washed with water (2 x 5 mL), ethanol (2 x 5 mL) and ether (2 x 5 mL), giving the thioamide (0.30 g).

A 50 mL reaction vessel was charged with thioamide (0.30 g, 1.32 mmol) and a four-fold excess of 2-(α-bromoacetyl)pyridine (1.1 g, 3.9 mmol) in ethanol (25 mL), the reaction was sonicated until clear and yellow and heated at 80 °C for 12 hours. During which time a thick yellow precipitate formed which was then isolated *via* vacuum filtration and washed with ethanol (2 x 5 mL) and ether (2 x 5 mL), giving the ligand as the hydrobromide salt. The salt was suspended in concentrated ammonia (10 mL) for 12 hours, re-filtered and washed with water (2 x 5 mL), ethanol (2 x 5 mL) and ether (2 x 5 mL), giving the free base ligand as a tan solid (0.50 g, 36%). ^{1}H NMR spectroscopy (400 MHz, d_6-DMSO) δ 11.08 (s, 2H, NH), δ 8.60 (d, 2H, py, *J* = 4.4 Hz), δ 8.0 (d, 2H, py, *J* = 7.84 Hz), δ 7.90 (td, 2H, py, *J* = 1.64, 7.68 Hz), δ 7.75 (t, 1H, py, *J* = 8 Hz), δ 7.69 (s,2H, tz), δ 7.33 (t, 2H, py, *J* = 4.96, 6.64 Hz), δ 7.22 (d, 2H, py, *J* = 8 Hz) (Fig. 138). ^{13}C NMR spectroscopy (100 MHz d_6-DMSO) δ 207, 161.6, 152.9, 151.4, 149.9, 140.4, 137.8, 123, 120.6, 109.6 and 103.7. ESI-MS *m/z* 430 ($[M+H]^+$).

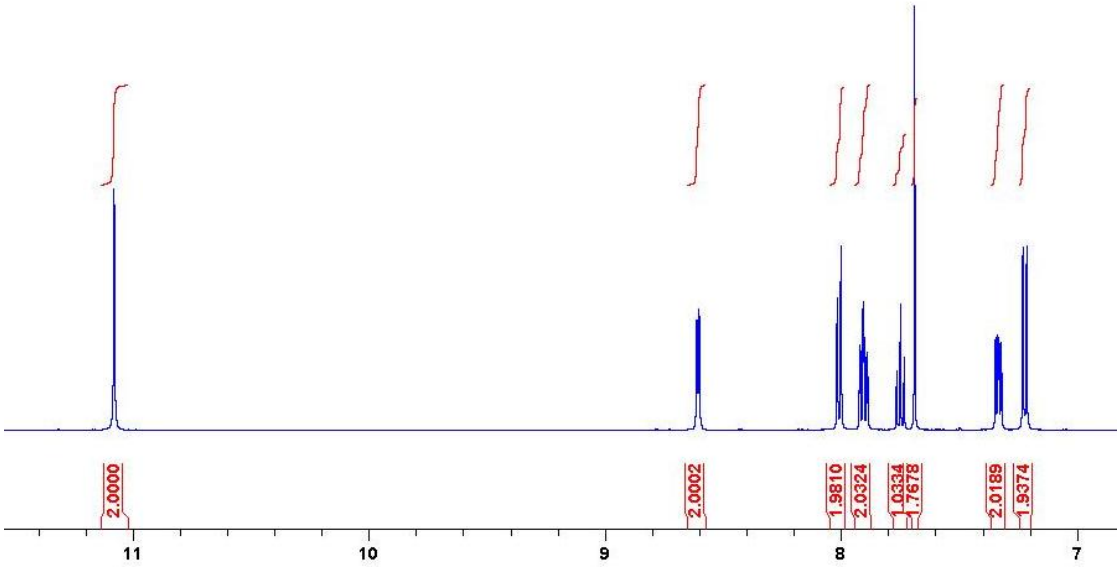

*Fig. 138: ^{1}H NMR spectrum of the aromatic region of **[L^{6}]**.* (400MHz, d_6-DMSO) signals of note include the amine and thiazole proton (δ 11.07 and 7.68 respectively).

Synthesis of [Cu(L^{6})](ClO$_4$)$_2$. To a suspension of $Cu(ClO_4)_2 \cdot 6H_2O$ (10 mg, 0.027 mmol) in $MeNO_2$ (1 mL) was added a suspension of ligand **[L^{6}]** (11 mg, 0.026 mmol) in $MeNO_2$ (1 mL) and the reaction warmed and sonicated until a clear green solution had formed. Diisopropyl ether was slowly allowed to diffuse into the solution resulting in green crystals. ESI-MS showed two mass ions at *m/z* 1082 and 1284 corresponding to $\{[Cu_2(\mathbf{L^6})_2(ClO_4)]\}^+$ and $\{[Cu_2(\mathbf{L^6})_2(ClO_4)_3]\}^+$ respectively.

Synthesis of [Cu(L^{6})](BF$_4$)$_2$. To a suspension of $Cu(BF_4)_2 \cdot 6H_2O$ (10 mg, 0.028 mmol) in $MeNO_2$ (1 mL) was added a suspension of ligand **[L^{6}]** (11 mg, 0.026 mmol) in $MeNO_2$ (1 mL) and the reaction warmed and sonicated until a clear yellow solution had formed. Diisopropyl ether was slowly allowed to diffuse into the solution resulting in yellow-brown crystals. ESI-MS showed an ion peak at *m/z* 1071 corresponding to $\{[Cu_2(\mathbf{L^6})_2(BF_4)]\}^+$.

Synthesis of [L^{7}(ClO$_4$)$_2$]$^{2-}$. To a suspension of $(Bu)_4NHClO_4$ (8.8 mg, 0.026 mmol) in DMF (1 mL) was added a suspension of ligand **[L^{7}]** (11 mg, 0.026 mmol) in DMF (1 mL) and the reaction warmed and sonicated until a pale yellow solution had formed. The DMF was slowly allowed to evaporate resulting in yellow crystals.

Collection and analysis of all crystallographic data was carried out by Prof. C. Rice.

Crystal data for $[Cu(L^6)](ClO_4)_2$: $C_{45}H_{33}Cl_{14}Cu_2N_{14}O_{17}S_4$, M = 1439.01, monoclinic, a = 25.6316 (12) Å, b = 11.2840 (5) Å, c = 19.1923 (11) Å, β =99.0757 (18)˚, V = 5481.4 (5) Å^3, T = 150 K, space group $C2/c$, Z = 4, $\mu(MoK\alpha)$ = 1.209 mm^{-1}, 63761 reflections measured, 8395 independent reflections (R_{int} = 0.0421). The final R_1 values were 0.0407 ($I > 2\sigma(I)$). The final $wR(F^2)$ values were 0.0923 ($I > 2\sigma(I)$). The final R_1 values were 0.0664 (all data). The final $wR(F^2)$ = 0.1059 (all data). The goodness of fit on F^2 was 1.0577.

Crystal data for $[Cu(L^6)](BF_4)_2$: $C_{45}H_{33}B_4Cu_2F_{16}N_{14}OS_4$ M = 1388.41, monoclinic, a = 25.3552 (15) Å, b = 11.2299 (6) Å, c = 19.0603 (11) Å, β =98.6572 (18)˚, V = 5365.3 Å^3, T = 150 K, space group $C2/c$, Z = 4, $\mu(MoK\alpha)$ = 1.057 mm^{-1}, 43753 reflections measured, 8199 independent reflections (R_{int} = 0.0743). The final R_1 values were 0.0589 ($I > 2\sigma(I)$). The final $wR(F^2)$ values were 0.1190 ($I > 2\sigma(I)$). The final R_1 values were 0.1190 (all data). The final $wR(F^2)$ = 0.1445 (all data). The goodness of fit on F^2 was 1.051.

Crystal data for $[L^7(ClO_4)_2]^{2-}$: $C_{21}H_{18}ClN_5O_6S_2$, M = 535.97, monoclinic, a = 10.2114 (3) Å, b = 20.5761 (6) Å, c = 10.8715 (3) Å, β =98.1720 (16)˚, V = 2261.02 Å^3, T = 150 K, space group $P21/n$, Z = 4, $\mu(MoK\alpha)$ = 3.674 mm^{-1}, 16288 reflections measured, 4221 independent reflections (R_{int} = 0.0624). The final R_1 values were 0.0486 ($I > 2\sigma(I)$). The final $wR(F^2)$ values were 0.1076 ($I > 2\sigma(I)$). The final R_1 values were 0.0781 (all data). The final $wR(F^2)$ = 0.1195 (all data). The goodness of fit on F^2 was 1.035.

Overall Conclusion & Future Work:

In conclusion, several multidentate *N*-donor ligands have been synthesized for the coordination of different d-block metal ions. In addition a variety of *NH*-donor domains have been incorporated within the ligand strand resulting in a series of interesting interactions of the resulting complexes with anions. Overall the results have shown that the addition of external *NH*-donor atoms on to the ligand strand (**L^1 – L^4**) produce complexes which are not affected by different anions and the self-assembly process is not governed by the presence of different anions regardless of their shape and charge. However we have shown that the addition of *NH*-donor groups *within* the ligand strand **[L^5]** produces a system that can be controlled by different anions and these can have a dramatic effect on the overall structure.

Reaction of the ligands containing *external NH*-donors (**L^1 – L^4**) and divalent cations (Cu(II) or Co(II)) mononuclear complexes are formed. However on reaction of the same ligands with monovalent cations (such as Cu(I)) dinuclear double helicates are formed. The formation of these contrasting complexes is entirely cation dependant, and no change in the self-assembly process is observed when different anions are used.

However, ligands containing *NH*-donors within the ligand chain **[L^5]** have been shown to exhibit excellent anion interaction properties on coordination with a variety of metal ions, particularly divalent cations. Coordination of **[L^5]** with Cu(II) gave a di-nuclear double helicate with a range of counter ions encapsulated within a *NH*-donor cavity.

Furthermore these complexes were shown to be anion dependant as the reaction of the original complex with varying stoichiometries of anions (SO_4^{2-}, $H_2PO_4^-$) resulted in anion directed assemblies, notably a phosphate dimer.

Reaction with **[L^5]** with $Cu(BF_4)_2$ or $Cu(ClO_4)_2$ gives a dinuclear double helicate with a cleft within the helicate assembly in which an anion is bound. However, reaction of this with half an equivalent of either sulphate (SO_4^{2-}) or dihydrogen phosphate ($H_2PO_4^-$) results in the formation of a different dinuclear double helicate whereby the cleft is

occupied by either a dihydrogen phosphate or sulphate anion which bridges the metal centres.

An addition of excess sulphate results in no change in the complex (*via* ESI-MS studies). However, addition of one equivalent of di-hydrogen phosphate leads to the formation of a pentanuclear circular helicate through a series of phosphate-ligand interactions, the inclusion of three dihydrogen phosphates into the centre of the assembly forces the dimerization of the circular helicate through a new series of phosphate-phosphate interactions.

Reaction of this dinuclear species with one equivalent of $(Bu_4N)NO_3$ resulted in the formation of a hexanuclear circular *meso*-helicate (or mesocate). In this structure each *N*-donor domain of a thiazole and pyridine ring coordinate two different Cu^{2+} metal centres. Each metal centre exhibits a distorted octahedral arrangement with two ligand strands completing 4 of its 6 coordination sites, the remaining sites are occupied by two *O*-donors of a nitrate anion. In addition an amine of each ligand strand points into on the centre of the complex creating a cavity capable of hosting two nitrate anions.

On reaction of **[L^6]** with a divalent metal ion (e.g. Cu(II)) a simple mono-nuclear structure is observed. Although a mono-nuclear assembly is expected, it is interesting that even a simple change in the ligand strand can have dramatic effects on the self-assembly process. When a central 1,3-phenylene spacer is employed (i.e. [L^5]) a dinuclear double helicate is formed, however, when a 1,3-pyridine unit is contained within the ligand strand (i.e. **[L^6]**) a simple mono-nuclear species is produced.

Although the initial aim to synthesis a series of multidentate ligands with the capacity for coordination of metal ions (through *N*-donor atoms) and the interaction with anions (via *NH* hydrogen bonding interactions) has been achieved, further work needs to be carried out in order to develop a greater understanding of anion control of the self-assembled process. This can be accomplished by using the pyridyl-thiazole amide unit by the incorporation of different spacer units separating the binding domains. Groups such as di-substituted naphthalene and phenanthrene may lead to a series of

different supramolecular species due to their increased size, conformational rigidity and steric bulk.

Addition of these spacer groups into the ligand strand could lead to a reduction in the ligands flexibility and steric interaction leading to a number of different supramolecular self-assemblies. One possibility is the self-assembly of an anion binding pocket which would be the correct size to incorporate two or more phosphate anions which would then undergo condensation to give diphosphate in a analogous way natural systems store chemical energy (i.e ATP).

However, no research can be exhaustive and these points only serve to prove this. The research detailed within this thesis has more than exceeded the initial experimental aims.

References:

1. Beer, P. D., Gale, P. A. and Smith, D. K., '*Supramolecular Chemistry'*, New York: Oxford University Press Inc, 1999.
2. Steed, K. E., Turner, D. R. and Wallace, K. J., '*Core Concepts in Supramolecular Chemistry and Nanochemistry',* John Wiley & Sons, Chichester, 2007.
3. 3a. Lehn, J. M., 'Cryptates: The Chemistry of Macropolycyclic Inclusion Complexes', *Am. Chem. Rev.,* 1978, **11**, 49-57. 3b. Pedersen, C. J., 'Cyclic Polyethers and Their Complexes with Metal Salts', *J. Am. Chem. Soc.,* 1967, **89**, 7017-7036.
4. Pedersen, C. J., 'Cyclic Polyethers and Their Complexes with Metal Salts', *J. Am. Chem. Soc.,* 1967, **89**, 7017-7036.
5. Cram, D. J., 'The Design of Molecular Hosts, Guests, and Their Complexes (Nobel Lectures)', *Angew. Chem.,* 1988, **27**, 1009-1112.
6. Gale, P. A., 'Supramolecular chemistry: from complexes to complexity', *Phil. Trans. R. Soc. Lond.,* 2000, **358**, 431-453.
7. Housecroft, C. E. and Constable, E. C., *Chemistry*, Harlow: Pearson Education Limited, 2006.
8. Schneider, H. J. and Yatsimirsky, A., '*Principles and Methods in Supramolecular Chemistry',* New York: John Wiley & Sons Inc, 1999.
9. Hasenknopf, B., Lehn, J., Boumediene, N., Dupont-gervais, A., Dorsselaer, A. Van, Kneisel, B. and Fenske, D., 'Self-Assembly of Tetra- and Hexanuclear Circular Helicates', *J. Am. Chem. Soc.,* 1997, **119**, 10956-10962.
10. Steed, J. A. and Atwood, J. L., '*Supramolecular Chemistry'*, West Sussex: John Wiley & Sons Ltd, 2000.
11. Tinko, J. M., Helegson, R. C. and Cram, D. J., 'Host-guest complexation. Designed chiral recognition in solution between carboxyl-containing macrocyclic polyethers and an α-amino acid', *J. Am. Chem. Soc.*, 1978, **100**, 2828-2834.
12. Anderson, S., Anderson, H. L. and Sanders, J. K. M., 'Expanding roles for templates in synthesis', *Acc. Chem. Res.* 1993, **26**, 469-475.

13. Fischer, E., *Berichte de Deutschen Chemischen Gasellschaft.*, 1894, **27**, 2985-2993.
14. Hasenknopf, B., Lehn, J. M., Boumediene, N., Dupont-Gervaid, A., Dorsselaer, A. V., and Fenske, D., 'Self-assembly of tetra- and hetranuclear circular helicates', *J. Am. Chem. Soc.,* 1997, **119**, 10956-10962.
15. Steel, P. J., 'Metallosupramolcular chemistry – What now', *Chem. In. New Zealand*., 2011, **75**, 194-197.
16. Lehn, J. M., Ruben, M., Rojo, J., Francisco, J., and Uppadine, L. H., 'Grid-type metal ion architectures: Functional metallosupramolecular arrays', *Angew. Chem. Int. Ed.,* 2004, **43,** 3644-3662.
17. Hanan, G. S., Arana, C. R., Lehn, J. M. and Fenske, D., 'Synthesis, structure, and properties of dinuclear and trinuclear rack-type Ru(II) complexes', *Angew. Chem.*, 1995, **34**, 1122-1124.
18. Baxter, P. N. W., Lehn, J. M., Kneisel, B. O., and Fenske, D., 'Self-assembly of a symmetric tetracopper box-grid with guest trapping in the solid state', *Chem. Commun*., 1997, 2231-2232.
19. Stadler, A. M., Burg, C., Ramirez, J., and Lehn, J. M., 'Grid-double-helicate interconversion', *Chem. Commun.,* 2013, **49,** 5733-5735.
20. Baxter, P. N. W., Hanan, S., and Lehn, J. M., 'Inorganic arrays *via* multicomponent self-assembly: the spontaneous generation of ladder architectures', *Chem. Commun.,* 1996, 2019-2020.
21. Leininger, S., Olenyuk, B., and Stang, P. J., 'Self-assembly of discrete cyclic nanostrucutres mediated by transition metals', *Chem. Rev.,* 2000, **100**, 853-908.
22. Vogtle, F., *Supramolecular Chemistry*, John Wiley & Sons Ltd., Chicester, 1991.
23. Lawrance, G. A., *Introduction to Coordination Chemistry*, John Wiley & Sons Ltd., Chicester, 2009.
24. Fujita, M., Nagao, S., and Ogura, K., 'Guest-induced organization of a three-dimensional palladium(II) cage-like complex. A prototype for "induced fit" molecular recognition', *J. Am. Chem. Soc.,* 1995, **117**, 1649-1650.
25. Yoshizawa, M., Kusukawa, T., Kawano, M., Ohhara, T., Tanaka, I., Kurihara, K., Nimura, N., and Fujita, M., 'Endohedral clusterizaion of ten water molecules

into a “Molecular Ice” within the hydrophobic pocket of a self-assembled cage’, *J. Am. Chem. Soc.,* 2005, **127,** 2798-2799.

26. Nakabayashi, K., Kawano, M., Yoshizawa, M., Ohkoshi, S. I. and Fujita, M., ‘Cavity-induced spin-spin interaction between organic radicals within a self-assembled coordination cage’, *J. Am. Chem. Soc.,* 2004, **126,** 16694-16695.
27. Kramer, R., Lehn, J. M. and Marquis-Rigault, M., ‘Self-recognition in helicate self-assembly: Spontaneous formation of helical metal complexes from mixtures of ligands and metal ions’, *Proc. Natl. Acad. Sci.,* 1993, **90,** 5394-5398.
28. Piguet, C., ‘Helicates and related metallosupramolecular assemblies: toward structurally controlled and functional devices’, *Journal of Inclusion Phenomena and Macrocyclic Chemistry.,* 1999, **34**, 361-391.
29. Allen, K. E., Faulkner, R. A., Harding, L. P., Rice, C. R., Johannessen, R. T., Voss, M. L. and Whitehead, M., ‘Head-To-Tail and heteroleptic pentanuclear circular helicates’, *Angew. Chem. Int. Ed.,* 2010, **49,** 6655-6658.
30. Piguet, C., Bernardinelli, G. and Hopfgartner, G., ‘Helicates as versatile supramolecular complexes’, *Chem. Rev.,* 1997, **97,** 2005-2062.
31. Greenwald, M., Wessely, D., Katz, E., Willner, I. and Cohen, Y., ‘From homoleptic to heteroleptic double stranded copper(I) helicates: The role of self-recognition in self-assembly processes’, *J. Org. Chem.,* 2000, **65,** 1050-1058.
32. Lehn, J. M., Rigault, A., Siegel, J., Harrowfield, J., Chevier, B. and Moras, D., ‘Spontaneous assembly of double-stranded helicates from oligobipyridine ligands and copper(I) cations: Structure of an inorganic double helix’, *Proc. Natl. Acad. Sci.,* 1987, **84,** 2565-2569.
33. Baylies, C. J., Harding, L. P., Jeffery, J. C., Moon, R., Rice, C. R. and Johannessen, T. R., ‘Electrostatic control of the formation of heteroleptic transition metal helicates’, *New J. Chem.,* 2007, **31,** 1525-1529.
34. Hasenknopf, B., Lehn, J. M., Baum, G. and Fenske, D., ‘Self-assembly of a heteroduplex helicate from two different ligand strands and Cu(II) cations’, *Proc. Natl. Acad. Sci.,* 1996, **93,** 1397-1400.
35. Constable, E. C., Heirtzler, F., Neuburger, M. and Zehnder, M., ‘Steric control of directional isomerism in dicopper(I) helicates of asymmetrically substituted

2,2’:6’,2’’:2’’,6’’’-Quaterpyridine derivatives’, *J. Am. Chem. Soc.*, 1997, **119,** 5606-5617.

36. Andre, N., Jensen, T. B., Scopelliti, R., Imbert, D., Elhabiri, M., Hopfgartner, G., Piguet, C. and Bunzil, J. C. G., ‘Supramolecular recognition of heteropairs of lanthanide ions: A step toward self-assembled bifunctional probes’, *Inorg. Chem.,* 2004, **43,** 515-529.
37. Piguet, C., Borkovec, M., Hamacek, J. and Zeckert, K., ‘Strict self-assembly of polymetallic helicates: The concepts behind the semantics’, *Coord. Chem. Rev.,* 2005, **249,** 705-726.
38. Barley, M., Constable, E. C., Corr, S., McQueen, R. C. S., Nutkins, J. C., Ward, M. D. and Drew, B., ‘Molecular helicity in inorganic complexes’, *J. Chem. Soc. Dalton Trans.*, 1988, 2655-2662.
39. Goodgame, D. M. L., Hill, S. P. W. and Williams, D. J., ‘Ligand-induced fomration of a triple helical bridge involving *O*-donor ligands in dimeric lanthanide complexes’, *J. Chem. Soc. Chem. Commun.,* 1993, 1019-1021.
40. Constable, E. C., Edwards, A, J., Raithby, P. R., Smith, D. R., Walker, J. V. and Whall, L., ‘Heterodimetallic double helicates from redistributed reactions’, *Chem. Commun.,* 1996, 2551-2552.
41. Constable, E. C., Edwards, D. J., Raithby, P. R. and Walker, J. V., ‘The first structurally characterized heterodinuclear double-helicate complex’, *Angew. Chem. Int. Ed.,* 1993, **32,** 1465-1467.
42. Cahn, R. S., Ingold, C. and Perlog, V., ‘Specification of molecular chemistry’, *Angew. Chem. Int. Ed.,* 1966, **5**, 385-415.
43. Mamula, O., Zelewsky, A. V., Brodard, P., Schlapfer, C. W., Bernardinelli, G. and Stoeckli-Evans, H., ‘Helicates of Chiragen-Type Ligands and Their Aptitude for Chiral Self-Recognition’, *Chem. Eur. J.,* 2005, **11,** 3049-3057.
44. Baum, G., Constable, E. C., Fenske, D. and Kulke, T., ‘Diastereoselective formation of disilver(I) double helicates with chiral 2,2’: 6’,2’’: 6’’,2’’’-qauterpyridines’, *Chem. Commun.,* 1997, 2043-2044.
45. Constable, E. C., Kulke, T., Baum, G. and Fenske, D., ‘Diastereoselective formation of chiral helicates’, *Inorg. Chem. Commun.,* 1998, **1,** 80-82.

46. Piguet, C., Bernardinelli, G., Bocquet, B., Schaad, O. and Williams , A. F., 'Cobalt (III) / cobalt(II) electrochemical potential controlled by steric constraints in self-assembled dinuclear triple-helical complxes', *Inorg. Chem.,* 1994, **33,** 4112-4121.
47. Bain, L., Bullock, S., Harding, L., Riss-Johannessen, T., Midgley, G., Rice, C. R. and Whitehead, M., 'Controlling the formation of metallosupramolecular assemblies by metal ionic radii', *Chem. Chommun.,* 2010, **46,** 3496-3498.
48. Allen, K. E., Faulkner, R. A., Harding, L. P., Rice, C. R., Riss-Johannessen, T., Voss, M. L. and Whitehead, M., 'Head-To-Tail and Heteroleptic Pentanuclear Circular Helicates', *Angew. Chem. Int. Ed.,* 2010, **49,** 6655-6658.
49. Hopfgartner, G., Piguet, C. and Henion, J. D., 'Ion spray-tandem mass spectrometry of supramolecular coordination complexes', *J. Am. Soc. Mass Spec.* 1994, **8,** 748-756.
50. Prasanna de Silva, A., Gunaratne, H. Q. N., McVeigh, C., Maguire, G. E. M., Maxwell, P. R. S. and O'Hanlon, E., 'Fluorescent signaling of the brain neurotransmitter ϒ-aminobutyric acid and related amino acid zwitterions', *Chem. Commun.,* 1996, 2191-2192.
51. Albrecht, M., Schmid, S., deGroot, M., Weis, P. and Frohlich, R., 'Self-assembly of an unpolar enantiomerically pure helicate-type metalla-cryptand', *Chem. Commun.* 2003, 2526-2527.
52. Beer, P. D. and Gale, P. A., 'Anion recognition and sensing: The state of the art and future perspectives', *Angew. Chem. Int. Ed.,* 2001, **40,** 486-516. WAS 53
53. Berg, J. M., 'Zinc finger domains: From predictions to design', *Acc. Chem. Res.,* 1995, **28,** 14-19.
54. Christianson, D. W., 'Carboxypeptidase A', *Acc. Chem. Res.,* 1989, **22,** 62-69.
55. Kraut, J. A. and Madias, E., 'Serum anion gap: Its uses and limitations in clinical medicine', *Clin. J. Am. Soc. Nephrol.,* 2007, **2,** 162-174.
56. Curley, E. M., O'Flynn, M. G. and McDonnell, K. P., 'Phosphorus loss in subsurface flow from agricultural lands after manure application to miscanthus x giganteus-impacts on groundwater quality', *Int. J. Agric. Res.,* 2010, **5,** 268-275.
57. C. Glidewell, *Chem. Br.* **1990**, *26*, 137.

58. Schmidtchen, F. P., 'Inclusion of anions in macrotricyclic quaternary ammonium salt', *Angew. Chem. Int. Ed.,* **16,** 720-721.
59. Schmidtchen, F. P., 'Synthese makrotricyclischer amine', *Eur. J. Inorg. Chem.,* 1980, **113,** 864-874.
60. Wenzel, M., Bruere, S. R., Knapp, Q. W., Tasker, P. A. and Plieger, P. G., 'Zwitterionic dicoper helicates: Anion encapsulation and binding studies', *Dalton Trans.,* 2010, 2936-2941.
61. Pascal, R. A., Spergel, J. and Van Engen, D., 'Synthesis and X-ray crystallography characterization of a (1,3,5) cyclophane with three amide N-H groups surrounding a central cavity. A neutral host for anion complexation', *Tetrahedron Letters.,* 1986, **27,** 4099-4102.
62. Amendola, V., Fabbrizzi, L. and Mosca, L., 'Anion recognition by hydrogen bonding: urea-based receptors', *Chem. Soc. Rev.,* 2010, **39,** 3889-3915.
63. Shriver, D. F. and Biallas, M. J., 'Observation of the chelate effect with a bidentate lewis acid', *J. Am. Chem. Soc.,* 1967, **89,** 1078-1081.
64. Galbraith, E. and James, T. D., 'Born based anion receptors as sensors', *Chem. Soc. Rev.,* 2010, **39,** 3831-3842.
65. Park, C. H., Simmons, H. E., 'Macrobicyclic Amines. III. Encapsulation of halide ions *in,in*-1,(k+2)-Diazabicyclo[*k.l.m*]alkane-ammonium ions', *J. Am. Chem. Soc.,* 1968, **90,** 2431-2432.
66. Antonisse, M. M. G. and Reinhoudt, D. N., 'Neutral anion receptors: design and application', *Chem. Commun.,* 1998, 443-448.
67. Beer, P. D., 'Anion selective recognition and optical/electrochemical sensing by novel transition-metal receptor systems', *Chem. Commun.,* 1996, 689-696.
68. Beer, P. D., 'Transition-metal receptor systems for the selective recognition and sensing of anionic guest species', *Acc. Chem. Res.,* 1998, **31,** 71-80.
69. Czarnik, A. W., 'Chemical communication in water using fluorescent chemosensors', *Acc. Chem. Res.,* 1994, **27,** 302-308.
70. Fabbrizzi, L., Francese, G., Licchelli, M., Perotti, A. and Taglietti, A., 'Fluorescent sensor of imidazole and histidine', *Chem. Commun.,* 1997, 581-582.

71. Balzani, V. and Juris, A., 'Photochemistry and photophysics of Ru(II)-polypyridine complexes in the Bologna group. From early studies to recent developments', *Coord. Chem. Rev.,* 2001, **211,** 97-115.
72. Xiao, K. P., Buhlmann, P., Nishizawa, S., Amemiya,S. and Umezawa, Y., 'A chloride ion-selective solvent polymeric membrane electrode based on a hydrogen bond forming ionophore', *Anal. Chem.,* 1997, **69,** 1038-1044.
73. Szemes, F., Hesek, D., Chen, Z., Dent, S. W., Drew, M. G. B., Goulden, A. J., Graydon, A. R., Grieve, A., Mortimer, R. J., Wear, T., Wightman, J. S. and Beer, P. D., 'Synthesis and characterization of novel acyclic, macrocyclic, and calyx[4]arene ruthenium(II) bipyridyl receptor molecules that recognize and sense anions', *Inorg. Chem.,* 1996, **35,** 5868-5879.
74. Beer, P. D., Dent, S. W. and Wear, T. J., 'Spectral and electrochemical recognition of halide anions by acyclic mononuclear ruthenium(II) bipyridyl molecules', *J. Chem. Soc., Dalton Trans.,* 1996, 2341-2346.
75. Sanchez-Quesada, J., Steel, C., Prados, P. and Mendoza, J., 'Anion helicates: Double strand helical self-assembly of chiral bicyclic guanidinium dimmers and tetramers around sulfate templates', *J. Am. Chem. Soc.,* 1996, **118,** 277-278.
76. Katz, H. E., 'Hydride Sponge: 1,8-Naphthalenediylbis(dimethylborane)', *J. Am. Chem. Soc.,* 1985, **107,** 1421-1423.
77. Keegan, J., Kruger, P. E., Neiuwenhuyzen, M., O'Brian, J. and Martin, N., 'Anion directed assembly of a dinuclear double helicate', *Chem. Commun.,* 2001, 2192-2193. WAS 79
78. Selvakumar, P. M., Jebaraj, P. Y., Sahoo, J., Suresh, E., Prathap, K. J., Kureshy, R. I. and Subramanian, P. S., 'The first bromide ion directed double helicate and its role in catalysis' , *RSC. Adv.,* 2012, **2,** 7689-7692.
79. Li, S., Jia, C., Wu, B., Luo, Q., Huang, X., Yang, Z., Li, Q. S. and Yang, X. J., 'A triple anion helicate assembled from a bis(biurea) ligand and phosphate ions', *Angew. Chem. Int. Ed.,* 2011, **50,** 5721-5724.
80. Beissel, T., Powers, P. E. and Raymond, K. N., 'Symmetry-based metal complex cluster formation', *Angew. Chem. Int. Ed. Engl.,* 1996, **35,** 1084-1086.

81. Saalfrank,R. W., Horner, B., Stalke, D. and Salbeck, J., 'The first neutral adamantanoid iron(III)-chelate complex: Spontaneous formation, structure, and electrochemistry', *Angew. Chem. Int. Ed. Engl.,* 1993, **32,** 1179-1182.
82. Paul, R. L., Bell, Z. R., Jeffery, J. C., McCleverty, J. A. and Ward, M. D., 'Anion-templated self-assembly of tetrahedral cage complexes of cobalt(II) with bridging ligands containing two bidentate pyrazolyl-pyridine binding sites', *PNAS.,* 2002, **99,** 4883-4888.
83. Wu, B., Cui, F., Lei, Y., Li, S., Amadeu, N. DS., Janiak, C., Lin, Y. J., Weng, L. H., Wang, Y. Y. Y. and Yang, X. J., 'Tetrahedral anion cage: Self-assembly of a $(PO_4)_4L_4$ complex from a tris(bisurea) ligand', *Angew. Chem. Int. Ed.,* 2013, **52,** 5096-5100.
84. Wang, J., Li, S., Yang, P., Huang, X., Yang, X. J. and Wu, B., 'From anion complexes to anion coordination polymers (ACPs): assembly with a 1,5-naphthylene bridged bis-bisurea ligand', *CrystEngComm.,* 2013, **15,** 4540-4548.
85. Schmidtchen, F. P., 'Reflections on the construction of anion receptors is there a sign to resign from design', *Coord. Chem. Rev.,* 2006, 250, 2918-2928.
86. Caltagirone, C. and Gale, P. A., 'Anion receptor chemistry: highlights from 2007', *Chem. Soc. Rev.,* 2009, **38**, 520-563.
87. Juwarker, H. and Jeong, K. S., 'Anion-controlled foldamers', *Chem. Soc. Rev.,* 2010, **39**, 3664-3674.
88. Gale, P. A., 'Anion receptor chemistry: highlights from 2008 and 2009', *Chem. Soc. Rev.,* 2010, **39,** 3746-3771.
89. Sessler, J. L., Cyr, M. J. and Lynch, V., 'Synthetic and structural studies of sapphyrin a 22-π-electron pentapyrrolic "expanded porphyrin"', *J. Am. Chem. Soc.,* 1990, **112,** 2810-2813.
90. Sessler, J. L., Weghorn, S. J., Lynch, V. and Fransson, K., '5,15,25-Tris-nor-hexapyrrin: the first structurally characterized linear hexapyrrin', *J. Chem. Soc., Chem. Commun.,* 1994, 1289-1290.
91. Gianelli. L., Amerndola. V., Fabbrizzi, L., Pallavicini, P. and Mellerio, G. G., 'Investigation of reduction of Cu(II) complexes in positive-ion mode electrospray mass spectrometry', *Rapid Commun. Mass Spectrom.,* 2001, **15**, 2347-2353.

92. Mohebat, R. and Mohammadian, G., 'An efficient one-pot synthesis of *bis*-1-(aroyl)-3-(aryl)thiourea', *J. Chem. Res.,* 2012, 626-628.
93. Comba, P., Jurisic, P., Lampeka, Y. D., Peters, A., Prikhod'ko, A. I. and Pritzkow, H., 'Axial bonds in copper(II) compounds', *Inorganica Chimica Acta.,* 2001, **324**, 99-107.
94. Feilden, J., Sprott, J., Long, DL., Kogerler, P. and Cronin, L., 'Controlling Aggregation of Copper(II)-Based Coordination Compounds: From Mononuclear to Dinuclear, Tetranuclear, and Polymeric Copper Complexes', *Inorg. Chem.,* 2006, **45**, 2886-2895.
95. Nieves corella Ochoa, M., Cooper, G. J. T., Newton, G. N., Long, DL., Seeber, G. and Cronin, L., 'Supramolecular Architectures of Copper(II) Perchlorate Complexes of *cis,trans*-1,3,5-Triaminocyclohexane Assembled Exploiting the Delicate Balance Between Weak and Strong Interactions', *Z. Naturforsch*., 2010m **65b**, 1-7.

Appendix: Publications

Circular Helicates

DOI: 10.1002/anie.201407645

Formation of a Dimer of Trinuclear Helicates which Encapsulates an Array of Six Hydrogen-Bonded Anions

Robert A. Faulkner, Lindsay P. Harding, Joshua Higginson, Craig R. Rice, and Christopher Slater*

Abstract: *The amine-containing ligand L, composed of two bidentate pyridyl-thiazole moieties linked by a 1,3-diaminophenylene unit, reacts with copper(II) ions to form a dinuclear double helicate $[Cu_2L_2]^{4+}$. Reaction of $[Cu_2L_2]^{4+}$ with dihydrogen phosphate (0.5 equivalents) gives the unsaturated dinuclear double helicate $[Cu_2L_2(OPO_3H_2)]^{3+}$. $[Cu_2L_2(OPO_3H_2)]^{3+}$ further reacts with another 0.5 equivalents of dihydrogen phosphate to give a trinuclear circular helicate which then self-assembles into a hexameric cluster $[\{Cu_3L_3(OPO_3H_2)_3\}]^{26+}$.*

Self-assembly is a process in which large and complex molecular species are spontaneously formed from small subunits which contain sufficient molecular information to assemble into complex architectures.[1] One area of metallo-supramolecular self-assembly that has received much attention is the design of polynuclear helicates.[2] These linear structures form by self-assembly and consist of two or more multidentate ligand strands which are helically wrapped around metal cations. Not only can polynuclear double-, triple-, and quadruple-stranded helicates now be made in a predictable fashion, they can also be programmed to express certain structural features of higher-order complexity.[2] Self-assembly of multidentate ligand strands can also result in the formation of cyclic helicate systems[3] which are similar to the linear helicates, that is, they retain the "over-and-under" ligand motif requisite of helical chirality. The cyclic oligomers, of general formula $[M_n(L)_n]$ ($n > 2$), can feature higher-order complexity giving head-to-tail and heteroleptic systems.[4]

Another area of self-assembly is the formation of hydrogen-bond-directed assemblies, which require molecules containing hydrogen-bond donor and acceptor groups resulting in the self-assembly of discrete molecular species.[5] For example, the capsules prepared by Rebek et al. are self-assembled species formed by dimerization of two imide-functionalized resorcinarenes by complimentary amide-carbonyl donor–acceptor interactions.[6] However, generally self-assembly relies on the use of one mechanism to express the chemical information (e.g. either a metallo-supramolecular or hydrogen-bond-directed mechanism). Herein, we demonstrate how a ligand (L), upon reaction with copper(II) ions and $OPO_3H_2^-$ ions, gives a trinuclear circular helicate $[Cu_3L_3(OPO_3H_2)_3]^{3+}$. The helicate then interacts with another trinuclear assembly through hydrogen-bonding interactions between the P–OH units to give the dimeric assembly $[Cu_3L_3(OPO_3H_2)_3]_2^{6+}$. The overall self-assembly process is driven by two orthogonal interactions, that is, metallo-supramolecular assembly to give the trinuclear species and subsequent hydrogen-bonding interactions which result in the formation of the dimer. Formations of synthetic supramolecular systems which contain hierarchical levels of self-assembly are rare, with a notable example described by Ward et al. where a Ag^+-containing dinuclear double helicate forms infinite chains through Ag···Ag interactions.[7] Three of these chains wrap around a central spine of anions (by hydrogen-bonding and CH···π interactions) giving a triple helix of double helicates.[7] Furthermore, metallo-supramolecular assemblies which form cages that encapsulate oxoanions have also been studied[8] as well as metal–organic frameworks that contain protonated water clusters.[9]

The ligand L (Figure 1), which contains two bidentate pyridyl-thiazole domains bridged by a 1,3-diaminophenylene unit, was prepared by reaction of phenyl-1,3-diurea and 2-(α-bromoacetyl)pyridine heating in ethanol at reflux. Reaction

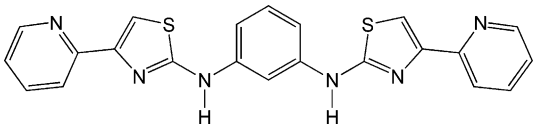

Figure 1. The structure of bis-bidentate ligand L.

of the ligand with $Cu(BF_4)_2$ in $MeNO_2$ gives a dark-blue solution from which dark-blue crystals are formed upon diffusion of diisopropyl ether into the solution. Analysis by single-crystal X-ray diffraction showed that in the solid state a dinuclear double helicate ($[Cu_2L_2]^{4+}$) is formed (Figure 2).

In the crystal, each of the copper ions adopts a distorted tetrahedral coordination geometry arising from coordination by two pyridyl-thiazole units, one from each ligand (Cu–N bond lengths 1.991 (4)–1.973 (4) Å). The ligands wrap around one another giving a twist indicative of a linear helicate. Self-assembly in such a manner creates a cavity which encapsulates a tetrafluoroborate anion which forms hydrogen bonds between the fluoride atoms and to two of the amines (average (av.) bond length: N···F 2.847 Å) and two phenyl hydrogen atoms (av. C···F 3.520 Å). As a result of the constraints of the

[*] R. A. Faulkner, Dr. L. P. Harding, J. Higginson, Prof. C. R. Rice, C. Slater
Department of Chemical and Biological Sciences
University of Huddersfield
Huddersfield HD1 3DH (UK)
E-mail: c.r.rice@hud.ac.uk

Supporting information for this article is available on the WWW under http://dx.doi.org/10.1002/anie.201407645.

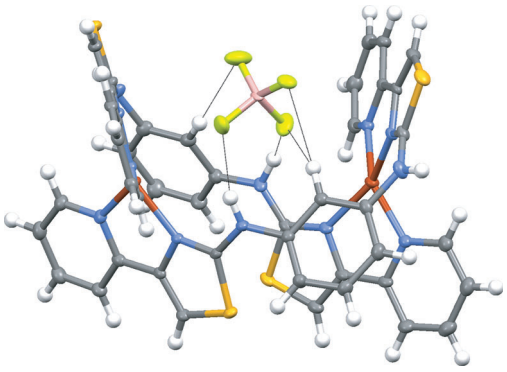

Figure 2. Molecular structure of $[Cu_2L_2](BF_4)^{3+}$. Thermal ellipsoids are set at 50% probability and the remaining anions have been omitted for clarity. Atom colors: C = gray; H = white; N = blue; S = yellow; Cu = red; F = green; B = pink.

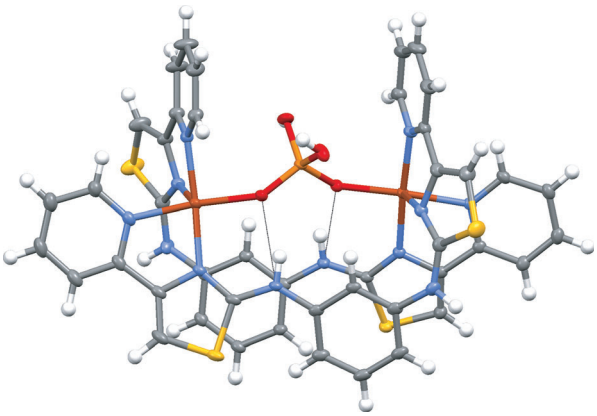

Figure 3. Molecular structure of $[Cu_2L_2(OPO_3H_2)]^{3+}$, showing one dihydrogen phosphate anion which bridges the two Cu centers. Thermal ellipsoids are set at 50% probability and the remaining anions have been omitted for clarity. Atom colors: C = gray; H = white; N = blue; S = yellow; Cu = dark orange; P = light orange; O = red.

geometry required to form the helicate, the two remaining amine units do not interact with the anion but point outwards from the complex forming hydrogen bonds with other tetrafluoroborate anions. An essentially isostructural assembly was obtained using $Cu(ClO_4)_2$ that is, a dinuclear double helicate that encapsulates a perchlorate anion. ESI-MS analysis gave an ion at *m*/*z* 1281 corresponding to the fragment $\{(Cu_2L_2)(ClO_4)_3\}^+$.

Reaction of $[Cu_2L_2](ClO_4)_4$ with $Bu_4N(OPO_3H_2)$ (0.5 equivalents) in nitromethane and a small amount of methanol (approximately 5% v/v) results in the color of the solution changing from dark blue to light brown. Slow diffusion of ethyl acetate into the solution gave olive-colored crystals which were analyzed by single-crystal diffraction. Examination of the solid-state data shows that a dinuclear double-helicate assembly is still present, for example, $[Cu_2L_2]^{4+}$ (Figure 3). In this structure, the ligand partitions into two bidentate pyridyl-thiazole domains, each of which coordinates a different metal ion (Cu–N bond lengths: 1.996(3)–2.357(3) Å). However, unlike the previous structure, the coordination geometry of the metal ions is completed by coordination of a dihydrogen phosphate anion which bridges the two metal ions (av. Cu–OP 1.979 Å).[10] The coordination sphere is supplemented by weak interactions with oxygen atoms from the perchlorate anions (av. Cu–OCl 2.763 Å) resulting in a pseudo-octahedral geometry. The dihydrogen phosphate ion also forms hydrogen bonds to two of the amines on the ligand unit (average N···O distance 2.745 Å) and, in an analogous fashion to $[Cu_2L_2]^{4+}$, the two remaining amines point away from the complex. As further ligands are present completing the coordination geometry of the metal ion, this species is termed an unsaturated helicate.

It is assumed that as there are three perchlorate anions present in the crystal structure, the dihydrogen phosphate is still only mono-anionic.[10] Analysis of the ESI-MS gave an ion at *m*/*z* 1279 which corresponds to $\{Cu_2L_2(OPO_3H_2)(ClO_4)_2\}^+$ and although the masses for $OPO_3H_2^-$ and ClO_4^- are similar, they are sufficiently different to differentiate between the fragments $\{Cu_2L_2(OPO_3H_2)(ClO_4)_2\}^+$ and $\{Cu_2L_2(ClO_4)_3\}^+$.

Reaction of either $[Cu_2L_2(OPO_3H_2)]^{3+}$ with 0.5 equivalents of the dihydrogen phosphate anion (or reaction of one equivalent of the same anion with $[Cu_2L_2]^{4+}$) in nitromethane and a small amount of methanol (approximately 5% v/v) upon slow diffusion of diisopropyl ether produced light-brown crystals. Single-crystal X-ray diffraction showed that in the solid state an unsaturated trinuclear triple helicate had formed (Figure 4 a).

In the solid state, each of the copper ions is pentacoordinate which arises from coordination of two bis-bidentate N-donor units from different ligands (Cu–N bond lengths 1.947(5)–49(5) Å) and a monodentate dihydrogen phosphate anion (Cu–OP 1.988(5)- 2.008(4) Å).[11] It is again assumed that the dihydrogen phosphate is mono-anionic as three tetrafluoroborate anions are present within the crystal structure (e.g. $[CuL(OPO_3H_2)]_3(BF_4)_3$).[11] The 1,3-diaminophenylene spacers bridge each of the bidentate domains in an "over-and-under" conformation giving rise to the helical cyclic oligomer. From each ligand, both of the amine units form a hydrogen bond to the dihydrogen phosphate anion through different types of interactions. It is not unusual for an anion to induce the change in formation of a linear helicate to its cyclic analogue through either templation[3b,c] or metal ion coordination.[3m] However, what is novel is the inclusion of three anions within the central core of the cyclic helicate (rather than a single anion which is usual for cyclic-helicate templation).

It is clear from the dihydrogen-phosphate-bridged double helicate $[Cu_2L_2(OPO_3H_2)]^{3+}$ that there is sufficient conformational flexibility to allow the additional dihydrogen phosphate ions in this structure to occupy the coordination sites previously occupied by the perchlorate anions. The coordination of the two dihydrogen phosphate anions to both metal ion centers does not necessitate the formation of the trinuclear oligomer.

This arrangement is presumably a consequence of hydrogen bonding between the amine NH···O and phenyl CH···O, hydrogen bonding between the ligand strands and the anions (N···O distances 2.890–3.053 Å; C···O distances 3.335–3.471 Å), as well as the H-bonding interactions within the

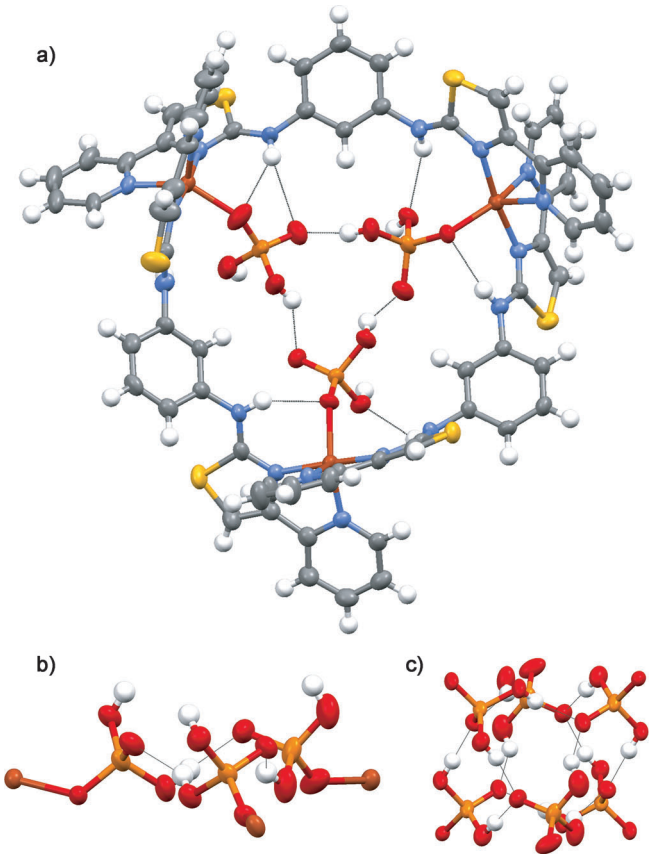

Figure 4. Crystal structure of $[Cu_3L_3(OPO_3H_2)_3]^{3+}$. a) Top view of the trinuclear circular triple helicate showing the intramolecular hydrogen bonding to three dihydrogen phosphate anions. b) View showing the H-bonding interactions within the cyclic trimer of the three dihydrogen phosphate anions. c) View of the six dihydrogen phosphate anions involved in both intra- and intermolecular hydrogen-bonding interactions. Thermal ellipsoids are set at 50% probability and the remaining anions have been omitted for clarity.

cyclic trimer of dihydrogen phosphate anions (P=O···O–P distances 2.603–2.680 Å).[12]

Furthermore, the remaining three P–OH bonds not involved in the intramolecular hydrogen bonding all point outwards from the core in the same direction (Figure 4b). The three hydrogen atoms interact with another three oxygen acceptor atoms from the P=O bonds encapsulated within another trinuclear oligomer, giving a cyclic array of six (··HO–P=O··) donor/acceptor units (Figure 4c). The intermolecular P–O···O=P distances are in the range 2.546–2.605 Å and are, on average, shorter than the intramolecular distances of the same type. This results in dimerization of the trinuclear circular helicates giving $[\{Cu_3L_3(OPO_3H_2)_3\}^{3+}]_2$ (Figure 5a–c). Thus a combination of Cu^{2+} and ligand interactions in the cyclic helicate and anion–ligand and anion–anion hydrogen bonds results in this unusual assembly which encapsulates six dihydrogen phosphate anions in a cylinder-like array. ESI-MS showed a signal m/z 1966 which corresponds to $\{[Cu_3L_3(OPO_3H_2)_3](ClO_4)_2\}^+$, a signal at m/z 4036 which corresponds to the dimer $\{[Cu_3L_3(OPO_3H_2)_3]_2(ClO_4)_5\}^+$, and a signal at m/z 1279 which corresponds to $\{[Cu_2L_2(OPO_3H_2)(ClO_4)_2]^+$.

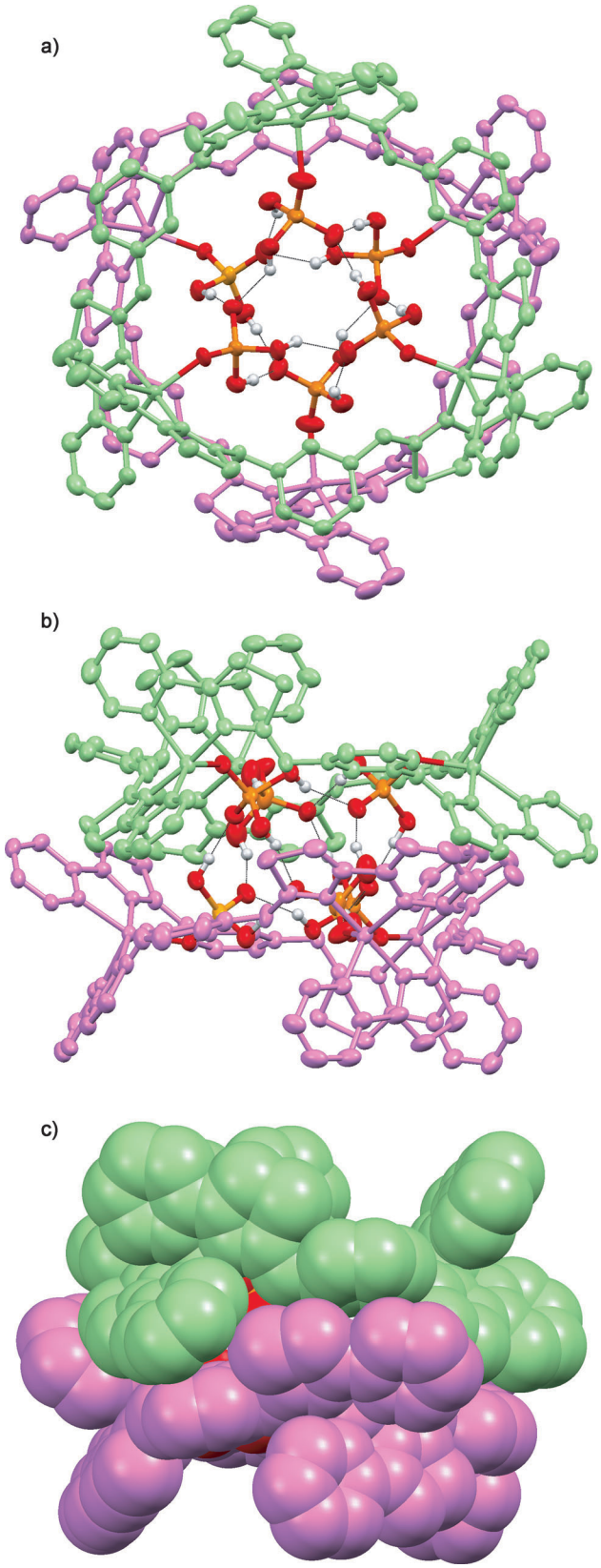

Figure 5. Crystal structure of $[\{Cu_3L_3(OPO_3H_2)_3\}]_2^{6+}$. a) Top view of the trinuclear circular helicate dimer showing the intramolecular hydrogen bonding. b) Side view of the dimer. c) Space-filling view of the dimer. Thermal ellipsoids are set at 50% probability and the remaining anions have been omitted for clarity. Colors: P = orange; O = red; H = white; one helicate is colored green, the other is colored purple.

It is clear that ligand L upon reaction with Cu^{2+} forms a dinuclear double helicate both in solution and the solid state and, upon reaction with dihydrogen phosphate (0.5 equivalents), an unsaturated dinuclear double helicate is formed. Furthermore, reaction with a further half equivalent of dihydrogen phosphate results in the formation of a trinuclear circular helicate which dimerizes by hydrogen bonding and is formed both in solution and the solid state. However, it is important to note that whilst crystallization of $[Cu_2L_2]^{4+}$ results in a homogeneous mass of dark-blue crystals, crystallization of $[Cu_2L_2(OPO_3H_2)]^{3+}$ produces both blue and olive green crystals (from X-ray analysis, the blue crystals correspond to $[Cu_2L_2]^{4+}$). Crystallization of $[\{Cu_3L_3(OPO_3H_2)_3\}]_2^{6+}$ produces olive and light-brown crystals (with the olive crystals composed of the $[Cu_2L_2(OPO_3H_2)]^{3+}$ complex). This mixture of species indicates that the unsaturated double helicate and the trinuclear circular helicate are in equilibrium and the formation is dependent on dihydrogen phosphate concentration. Regardless, the formation of the hydrogen-bonded dimer of the trinuclear circular helicate does occur both in solution and the solid state.[13]

Received: July 28, 2014
Revised: August 14, 2014
Published online: October 5, 2014

Keywords: copper · cyclic helicate · helical structures · self-assembly · X-ray diffraction

[1] a) J.-M. Lehn in *Supramolecular Chemistry*, VCH, Weinheim, **1995**; b) J. W. Steed, J. L. Atwood in *Supramolecular Chemistry*, Wiley, Chichester, **2000**; c) J. S. Lindsey, *New J. Chem.* **1991**, *15*, 153 – 180; d) D. B. Amabilino, J. F. Stoddart, *Chem. Rev.* **1995**, *95*, 2725 – 2828; e) J. E. D Davies, D. D. MacNicol, F. Vogtle, *Templating, Self-assembly and Self-organisation in Comprehensive Supramolecular Chemistry*, *Vol. 9* (Ed.: J. L. Atwood), Elsevier, Oxford, **1996**; f) L. R. Macgillivray, J. L. Atwood, *Nature* **1997**, *389*, 467 – 472; g) N. Branda, R. Wyler, J. Rebek, Jr., *Science.* **1994**, *263*, 1267 – 1268.

[2] a) M. J. Hannon, L. J. Childs, *Supramol. Chem.* **2004**, *16*, 7 – 22; b) M. Albrecht, *Chem. Rev.* **2001**, *101*, 3457 – 3497; c) M. Albrecht, *Chem. Soc. Rev.* **1998**, *27*, 281 – 287; d) C. Piguet, G. Bernardinelli, G. Hopfgartner, *Chem. Rev.* **1997**, *97*, 2005 – 2061; e) E. C. Constable in *Comprehensive Supramolecular Chemistry*, *Polynuclear Transition Metal Helicates*, *Vol. 9* (Ed.: J.-P. Sauvage), Elsevier, Oxford, pp. 213. **1996**.

[3] a) M. Albrecht, *Supramolecular templating in the formation of helicates*, *Vol. 248* of *Topics in Current Chemistry* (Eds.: C. A. Schalley, F. Vögtle, K.-H. Dötz), Springer, Berlin, **2004**, pp. 105 – 139; b) B. Hasenknopf, J.-M. Lehn, N. Boumediene, E. Leize, A. Van Dorsselaer, *Angew. Chem. Int. Ed.* **1998**, *37*, 3265 – 3268; *Angew. Chem.* **1998**, *110*, 3458 – 3460; c) B. Hasenknopf, J.-M. Lehn, N. Boumediene, A. Dupont-Gervais, A. Van Dorsselaer, B. Kneisel, D. Fenske, *J. Am. Chem. Soc.* **1997**, *119*, 10956 – 10962; d) S. P. Argent, H. Adams, T. Riis-Johannessen, J. C. Jeffery, L. P. Harding, O. Mamula, M. D. Ward, *Inorg. Chem.* **2006**, *45*, 3905 – 3919; e) J. Hamblin, F. Tuna, S. Bunce, L. J. Childs, A. Jackson, W. Errington, N. W. Alcock, H. Nierengarten, A. V. Dorsselaer, E. Leize-Wagner, M. J. Hannon, *Chem. Eur. J.* **2007**, *13*, 9286 – 9296; f) Y. Pang, S. Cui, B. Li, J. Zhang, Y. Wang, H. Zhang, *Inorg. Chem.* **2008**, *47*, 10317 – 10324; g) L. J. Childs, M. Pascu, A. J. Clarke, N. W. Alcock, M. J. Hannon, *Chem. Eur. J.* **2004**, *10*, 4291 – 4300; h) L. J. Childs, N. W. Alcock, M. J. Hannon, *Angew. Chem. Int. Ed.* **2002**, *41*, 4244 – 4247; *Angew. Chem.* **2002**, *114*, 4418 – 4421; i) G. Baum, E. C. Constable, D. Fenske, C. E. Housecroft, T. Kulke, *Chem. Commun.* **1999**, 195 – 196; j) L. Bain, S. Bullock, L. Harding, T. Riis-Johannessen, G. Midgley, C. R. Rice, M. Whitehead, *Chem. Commun.* **2010**, *46*, 3496 – 3498; k) R. Krämer, J.-M. Lehn, A. DeCian, J. Fischer, *Angew. Chem. Int. Ed. Engl.* **1993**, *32*, 703 – 706; *Angew. Chem.* **1993**, *105*, 764 – 767; l) B. Hasenknopf, J.-M. Lehn, B. O. Kneisel, G. Baum, D. Fenske, *Angew. Chem. Int. Ed. Engl.* **1996**, *35*, 1838 – 1840; *Angew. Chem.* **1996**, *108*, 1987 – 1990; m) H. B. T. Jeazet, K. Gloe, T. Doert, O. N. Kataeva, A. Jäger, G. Geipel, G. Bernhard, B. Büchner, K. Gloe, *Chem. Commun.* **2010**, *46*, 2373 – 2375.

[4] K. E. Allen, R. A. Faulkner, L. P. Harding, C. R. Rice, T. Riis-Johannessen, M. L. Voss, M. Whitehead, *Angew. Chem. Int. Ed.* **2010**, *49*, 6655 – 6658; *Angew. Chem.* **2010**, *122*, 6805 – 6808.

[5] a) W. Yi, W. Bei, Q. G. Wang, *J. Crystallogr. Spectrosc. Res.* **1990**, *20*, 79 – 84; b) G. M. Whitesides, E. E. Simanek, J. P. Mathias, C. T. Seto, D. H. Chin, M. Mammen, D. M. Gordon, *Acc. Chem. Res.* **1995**, *28*, 37 – 44.

[6] a) J. Rebek, Jr., *Acc. Chem. Res.* **2009**, *42*, 1660 – 1668; b) W. Jiang, D. Ajami, J. Rebek, Jr., *J. Am. Chem. Soc.* **2012**, *134*, 8070 – 8073.

[7] A. Stephenson, M. D. Ward, *Chem. Commun.* **2012**, *48*, 3605 – 3607.

[8] a) R. Custelcean, *Chem. Commun.* **2013**, *49*, 2173 – 2182; b) R. Custelcean, P. V. Bonnesen, N. C. Duncan, X. Zhang, L. A. Watson, G. V. Berkel, W. B. Parson, B. P. Hay, *J. Am. Chem. Soc.* **2012**, *134*, 8525 – 8534; c) R. Custelcean, J. Bosano, P. V. Bonnesen, V. Kertesz, B. P. Hay, *Angew. Chem. Int. Ed.* **2009**, *48*, 4025 – 4029; *Angew. Chem.* **2009**, *121*, 4085 – 4089.

[9] M. Wei, C. He, W. Hua, C. Duan, S. Li, Q. Meng, *J. Am. Chem. Soc.* **2006**, *128*, 13318 – 13319.

[10] The data was not of sufficient quality to locate the hydrogen atoms on the dihydrogen phosphate anion in the difference Fourier map and it was assumed that the noncoordinating oxygen atoms would bear the hydrogen atoms. The two bond lengths are larger (average P–OH 1.557 Å compared to an average P–O 1.512 Å) in agreement with their single-bond character and correlate well with the distances reported previously, see: A. D. Mighell, J. P. Smith, W. E. Brown, *Acta Crystallogr. Sect. B* **1969**, *B25*, 776 – 781.

[11] As with $[Cu_2\mathbf{L}_2(OPO_3H_2)]^{3+}$, the data was not of sufficient quality to locate the hydrogen atoms on the dihydrogen phosphate anion in the difference Fourier map and the two hydrogen atoms were placed on the longest two of the four bonds (average P–OH 1.557 Å, compared to an average bond length P–O 1.504 Å).

[12] For H-bonded assemblies of dihydrogen phosphate anions, see: M. E. Light, S. Camiolo, P. A. Gale, M. B. Hursthouse, *Acta Crystallogr. Sect. E* **2001**, *57*, o727.

[13] For all three species, the crystallizations were repeated several times and either a full data set or unit cell collected, each time giving the same cell parameters as those measured for the structures reported.

